Structural and Mechanistic Studies on Eukaryotic UDP-galactopyranose Mutases

Michelle Lynn Oppenheimer

Dissertation submitted to the faculty of the Virginia Polytechnic Institute and State University in partial fulfillment of the requirements for the degree of

Doctor of Philosophy
In
Biochemistry

Pablo Sobrado, Chair
Richard F. Helm
Marcy Hernick
Jianyong Li

March 21, 2012
Blacksburg, VA

Keywords: UDP-galactopyranose mutase, galactofuranose, flavoprotein, enzyme mechanism, X-ray crystallography

Structural and Mechanistic Studies on Eukaryotic UDP-galactopyranose Mutases

Michelle Lynn Oppenheimer

ABSTRACT

Galactofuranose (Gal*f*) is the five membered ring form of galactose. It is found on the cell wall and surface of many pathogens including *Mycobacterium tuberculosis*, *Aspergillus fumigatus*, *Leishmania major*, and *Trypanosoma cruzi*. Gal*f* has been implicated in pathogenesis in these organisms; thus the biosynthetic pathway of Gal*f* is a target for drug design. Gal*f* is synthesized by the enzyme UDP-galactopyranose mutase (UGM), which converts UDP-galactopyranose (UDP-Gal*p*) to UDP-galactofuranose (UDP-Gal*f*). Solving the mechanism and structure of UGMs will aid in the development of specific inhibitors against these enzymes. Herein we present the detailed functional analysis of UGMs from *A. fumigatus*, *T. cruzi*, and *L. major*. The mechamism and structure these eukaryotic UGMs were examined by steady-state kinetics, rapid-reaction kinetics, trapping of reaction intermediates, fluorescence anisotropy, and X-ray crystallography. The mechanism first involves reduction of the required flavin by NADPH, followed by UDP-Gal*p* binding and subsequent S_N2 attack by the flavin on galactose displacing UDP to form a flavin N5-C1 galactose adduct. Next, the galactose ring opens forming an iminium ion allowing isomerization to occur. Lastly, the product is released and UGM is available to bind another substrate or be reoxidized by molecular oxygen. The three-dimensional structure of *A. fumigatus* UGM was solved using X-ray crystallography in four conformations: oxidized in complex with sulfate ions, reduced, reduced in complex with UDP, and reduced in complex with UDP-Gal*p,* giving valuable information on the unique features of eukaryotic UGMs including features important for

oligomerization and for substrate binding. The novel mechanism and structure provide valuable information for the development of specific inhibitors of eukaryotic UGMs.

ACKNOWLEDGEMENTS

I would like to thank the many people who have helped me as I pursued my Ph.D. First, I would like to thank my advisor, Dr. Pablo Sobrado, who provided me with an excellent environment to conduct research and excellent guidance. I am grateful for all I have learned during my time in his lab. Also, I would like to thank the many lab members who contributed to my work and provided advice including, Wyatt Chocklett, Dr. Jun Qi, Dr. Karina Kizjakina, Reeder Robinson, Mike Fedkenheur, Ana Lisa Valenciano, Jacob Ellerbrock, Allison Blumer, Dr. Elvira Romero, and Dr. Nancy Vogelaar. I would also like to thank my committee members for their willingness to help including: Dr. Richard Helm, Dr. Marcy Hernick, and Dr. Jianyong Li. Thank you also to Dr. Mahaney for his help during my graduate career. My work could also not be completed without the help of our collaborators Dr. Jack Tanner, Dr. Todd Lowary, and Dr. Richard Helm and their lab members. I am appreciative for their generous contributions of their time and effort.

Graduate school would not have been possible without the support of my family and friends. I am grateful for my parents, Marc and Dorothy, who regularly provided encouragement and support. I am also thankful for my brother, Michael, for his help throughout the years. I cannot express enough gratitude to my fiancé, Robert Briggs, for his continual confidence in me and for all of his advice these last few years. I can't wait to enter the next step in life with him by my side. I am also thankful to numerous other friends and family for their inspiration and support, there are simply too many of you to list you by name.

TABLE OF CONTENTS

LIST OF FIGURES

LIST OF SCHEMES

LIST OF TABLES

LIST OF ABBREVIATIONS

AfUGM	UDP-galactopyranose mutase from *Aspergillus fumigatus*
$AfUGM_r$	Reduced form of UDP-galactopyranose mutase from *Aspergillus fumigatus*
CeUGM	UDP-galactopyranose mutase from *Caenorhabditis elegans*
DEAE	Diethyl amino ethyl
DrUGM	UDP-galactopyranose mutase from *Deinococcus radiodurans*
EcUGM	UDP-galactopyranose mutase from *Escherichia coli*
FAD	Flavin adenine dinucleotide
Gal	D-Galactose
GalE	UDP-galactose 4' epimerase
Gal*f*	D-Galactofuranose
GalfT	Galactofuranose transferase
Gal*p*	D-Galactopyranose
GalPUT	Galactose-1-phosphate uridyltransferase
Glc	D-Glucose
GIPL	Glycoinositolphospholipid
GIPC	Glycosylinositolphosphoceramide
Glc-6-P	Glucose-6-phosphate
GK	Galactokinase
GPI	Glycosylphophatidylinositol
HEPES	4-(2-hydroxyethyl)-1-piperazineethanesulfonic acid
HPLC	High pressure liquid chromatography
HRMS	High resolution mass spectrometry
IMAC	Immobilized metal affinity chromatography
IPTG	Isopropyl-β-thiogalactopyranoside
KpUGM	UDP-galactopyranose mutase from *Klebsiella pneumoniae*
LmUGM	UDP-galactopyranose mutase from *Leishmania major*
LPG	Lipophosphoglycan
LPGM	Lipophosphoglycomannan

LPPG	Lipopeditophosphoglycan
MBP	Maltose binding protein
MtUGM	UDP-galactopyranose mutase from *Mycobacterium tuberculosis*
NADH	Nicotinamide adenine dinucleotide reduced
NADPH	Nicotinamide adenine dinucleotide phosphate reduced
NMR	Nuclear magnetic resonance
PCR	Polymerase chain reaction
PEG	Polyethylene glycol
PDB	Protein Data Bank
PGM	Phosphoglucomutase
PG	Phosphoglycan
PMSF	Phenylmethylsulfonyl fluoride
SAXS	Small-angle X-ray scattering
SDS-PAGE	Sodium dodecyl polyacrylamide gel electrophoresis
TcUGM	UDP-galactopyranose mutase from *Trypanosoma cruzi*
Tev	Tobacco etch virus protease
TLC	Thin layer chromatography
UDP	Uridine diphosphate
UDP-Gal	UDP-α -D -galactose
UDP-Gal*f*	UDP- α-D- galactofuranose
UDP-Gal*p*	UDP- α-D- galactopyranose
UDP-Glc	UDP-D-glucose
UGM	UDP-galactopyranose mutase
UGT	UDP-galactofuranose transporter
USP	UDP-sugar pyrophosphorylase

ATTRIBUTIONS

Several chapters of this thesis were done in collaboration with others both in research and writing. The contributing coauthors include: Assistant Professor Pablo Sobrado, Associate Professor Richard Helm, Post-doctorate Jun Qi, Post-doctorate Karina Kizjakina, and Senior Research Associate Keith Ray from the Department of Biochemistry at Virginia Tech; Ana Lisa Valenciano from Department of Biochemistry at Virginia Tech and Instituto Tecnologico de Costa Rica; graduate student Myles Poulin and Professor Todd L. Lowary from Univeristy of Alberta; graduate student Richa Dhatwalia, graduate student Harkewal Singh, Dale B. Karr, Professor John J. Tanner from the Department of Chemistry at the University of Missouri-Columbia; Jay C. Nix from the Molecular Biology Consortium at the Lawrence Berkeley National Laboratory; and undergraduate student Joshua Crawford and Assistant Professor Brad Pierce from Department of Chemistry and Biochemistry at University of Texas Arlington. Each chapter/appendix explains the specific contributions of each collaborator for that section. Each published chapter has the original work cited and is used with permission of the publishers. All work on this thesis, unless noted, is my own.

CHAPTER 1

Introduction

Flavoproteins are most commonly known for their redox, oxidase, and monooxygenase activites [1]. However, new classes of flavoproteins have been identified to catalyze acid/base reactions and novel non-redox reactions [2]. The enzyme UDP-galactopyranose mutase (UGM) is a flavoprotein responsible for the isomerization of UDP-α-D-galactopyranose (UDP-Gal*p*) to UDP-α-D-galactofuranose (UDP-Gal*f*) [3]. UDP-Gal*f* serves as the precursor molecule for Gal*f* found on the cell wall and cell surface of many pathogens. UGM has been shown to be a good drug target for several pathogens including: *Mycobacterium tuberculosis*, *Leishmania major*, *Trypanosoma cruzi*, and *Aspergillus fumigatus* [4-7]. Prokaryotic UGMs have been studied in detail, however little has been known about eukaryotic UGMs. Also until recently the mechanism of UGM was controversial as the proposed role of the flavin acting as a nucleophile in the reaction was unprecedented. This thesis reviews the literature on Gal*f* and Gal*f* biosynthesis in *A. fumigatus*, *L. major*, and *T. cruzi* and presents our work on the UGMs from these species.

Gal*f* and proteins involved in Gal*f* biosynthesis have been shown to be important for virulence, host-pathogen interactions, and normal cellular morphology [8-10]. Chapter 2 reviews the literature on the biosynthesis of Gal*f*, structures of Gal*f* containing oligosaccharides, and the importance of Gal*f* and Gal*f* biosynthesis for survival of the kinetoplastids, *L. major* and *T. cruzi.* Similarly, chapter 3 focuses on Gal*f* and Gal*f* biosynthesis in the fungi *A. fumigatus* and *A. niger*.

The eukaryotic UGMs from *A. fumigatus* (AfUGM), *L. major* (LmUGM), and *T. cruzi* (TcUGM) have been recombinantly expressed, purified, and examined mechanistically and structurally. There have been two proposed mechanisms for UGM, both of which show the

required reduced flavin acting as a scaffold for isomerization by forming a flavin N5-C1 galactose adduct (Chapter 6, Scheme 2) [11, 12]. In one mechanism, the adduct is formed by a nucleophilic attack and in the second mechanism the adduct is formed by single electron transfer [11-14]. A summary of the previous studies conducted to determine the mechanism is outlined in Chapter 6 where a complete mechanism for eukaryotic UGMs is proposed using TcUGM as a prototype. The proposed mechanism shows the flavin attacking the C1 of galactose by an S_N2 reaction forming the flavin-galactose adduct which allows for ring opening and isomerization. AfUGM also is unique as it maintains a half-reduced state which allows it to remain active in oxidizing environments (Chapter 4).

The three-dimensional structure of eukaryotic UGMs was also solved. While the active site and core structure of UGMs are relatively conserved, there are several structural elements unique to eukaryotic UGMs which are important for activity and oligomerization as described in Chapter 7. The quaternary structure is also shown to differ between species: prokaryotic UGMs are dimers, while the eukaryotes *L. major* and *T. cruzi* posses monomeric UGMs (Chapters 5 & 6, respectively), *A. fumigatus* was found to be tetrameric (Chapters 4 & 7) [15].

The work presented here is important for developing our understanding of the unique chemistry of this new class of flavoproteins. This work will also aid in the development of specific inhibitors for eukaryotic UGMs, which will lead to treatments of the diseases aspergillosis, leishmaniasis, and Chagas' disease.

1. References

[1]. V. Joosten, W.J. van Berkel, "Flavoenzymes," *Curr Opin Chem Biol*, vol.11, pp. 195-202, 2007.

[2]. S. Bornemann, "Flavoenzymes that catalyse reactions with no net redox change," *Nat Prod Rep*, vol.19, pp. 761-772, 2002.

[3]. P.M. Nassau, S.L. Martin, R.E. Brown, A. Weston, D. Monsey, M.R. McNeil, K. Duncan, "Galactofuranose biosynthesis in *Escherichia coli* K-12: Identification and cloning of UDP-galactopyranose mutase," *J Bacteriol*, vol.178, pp. 1047-1052, 1996.

[4]. F. Pan, M. Jackson, Y. Ma, M. McNeil, "Cell wall core galactofuran synthesis is essential for growth of mycobacteria," *J Bacteriol*, vol.183, pp. 3991-3998, 2001.

[5]. B. Kleczka, A.C. Lamerz, G. van Zandbergen, A. Wenzel, R. Gerardy-Schahn, M. Wiese, F.H. Routier, "Targeted gene deletion of *Leishmania major* UDP-galactopyranose mutase leads to attenuated virulence," *J Biol Chem*, vol.282, pp. 10498-10505, 2007.

[6]. C. Lamarre, R. Beau, V. Balloy, T. Fontaine, J.W. Hoi, S. Guadagnini, N. Berkova, M. Chignard, A. Beauvais, J.P. Latge, "Galactofuranose attenuates cellular adhesion of *Aspergillus fumigatus*," *Cell Microbiol*, vol.11, pp. 1612-1623, 2009.

[7]. P.S. Schmalhorst, S. Krappmann, W. Vervecken, M. Rohde, M. Muller, G.H. Braus, R. Contreras, A. Braun, H. Bakker, F.H. Routier, "Contribution of galactofuranose to the virulence of the opportunistic pathogen *Aspergillus fumigatus*," *Eukaryot Cell*, vol.7, pp. 1268-1277, 2008.

[8]. M. Oppenheimer, A.L. Valenciano, P. Sobrado, "Biosynthesis of galactofuranose in kinetoplastids: Novel therapeutic targets for treating leishmaniasis and Chagas' disease," *Enzyme Res*, vol.2011, pp. 415976, 2011.

[9]. L.L. Pedersen, S.J. Turco, "Galactofuranose metabolism: A potential target for antimicrobial chemotherapy," *Cell Mol Life Sci*, vol.60, pp. 259-266, 2003.

[10]. B. Tefsen, A.F. Ram, I. van Die, F.H. Routier, "Galactofuranose in eukaryotes: Aspects of biosynthesis and functional impact," *Glycobiology*, pp., 2012.

[11]. M. Soltero-Higgin, E.E. Carlson, T.D. Gruber, L.L. Kiessling, "A unique catalytic mechanism for UDP-galactopyranose mutase," *Nat Struct Mol Biol*, vol.11, pp. 539-543, 2004.

[12]. T.D. Gruber, W.M. Westler, L.L. Kiessling, K.T. Forest, "X-ray crystallography reveals a reduced substrate complex of UDP-galactopyranose mutase poised for covalent catalysis by flavin," *Biochemistry*, vol.48, pp. 9171-9173, 2009.

[13]. Z.H. Huang, Q.B. Zhang, H.W. Liu, "Reconstitution of UDP-galactopyranose mutase with 1-Deaza-FAD and 5-Deaza-FAD: Analysis and mechanistic implications," *Bioorg Chem*, vol.31, pp. 494-502, 2003.

[14]. S.W.B. Fullerton, S. Daff, D.A.R. Sanders, W.J. Ingledew, C. Whitfield, S.K. Chapman, J.H. Naismith, "Potentiometric analysis of udp-galactopyranose mutase: Stabilization of the flavosemiquinone by substrate," *Biochemistry*, vol.42, pp. 2104-2109, 2003.

[15]. D.A.R. Sanders, A.G. Staines, S.A. McMahon, M.R. McNeil, C. Whitfield, J.H. Naismith, "UDP-galactopyranose mutase has a novel structure and mechanism," *Nat Struct Mol Biol*, vol.8, pp. 858-863, 2001.

CHAPTER 2

Biosynthesis of Galactofuranose in Kinetoplastids: Novel Therapeutic Targets for Treating Leishmaniasis and Chagas' Disease

Reproduced with permission from: Oppenheimer, M., Valenciano, A.L., and Sobrado, P., "Biosynthesis of Galactofuranose in Kinetoplastids: Novel Therapeutic Targets for Treating Leishmaniasis and Chagas' Disease," Enzyme Res, ID: 415976, 2011.

Author Contributions:
Michelle Oppenheimer researched the information and wrote the review article.

Ana L. Valenciano helped with background research and studies with LmUGM.

Pablo Sobrado oversaw, edited, and directed the writing of the review article.

Abstract

Cell surface proteins of parasites play a role in pathogenesis by modulating mammalian cell recognition and cell adhesion during infection. β-Galactofuranose (Gal*f*) is an important component of glycoproteins and glycolipids found on the cell surface of *Leishmania* spp. and *Trypanosoma cruzi*. β-Gal*f*-containing glycans have been shown to be important in parasite-cell interaction and protection against oxidative stress. Here, we discuss the role of β-Gal*f* in pathogenesis and recent studies on the Gal*f*-biosynthetic enzymes: UDP-galactose 4' epimerase (GalE), UDP-galactopyranose mutase (UGM), and UDP-galactofuranosyl transferase (GalfT). The central role in Gal*f* formation, its unique chemical mechanism, and the absence of a homologous enzyme in humans identifies UGM as the most attractive drug target in the β-Gal*f*-biosynthetic pathway in protozoan parasites.

1. D-Galactofuranose

D-Galactofuranose (β-Gal*f*) is the five-member ring isomer of galactose (Figure 1). This rare sugar was initially found in several human bacterial pathogens including *Mycobacterium tuberculosis, Escherichia coli, Salmonella typhimorium*, and *Klebsiella pneumoniae* [1-4]. In *M. tuberculosis*, β-Gal*f* is found in the arabinogalactan layer where it links the pepitidoglycan and mycolic acid layers [1]. In *E. coli* and *K. pneumoniae*, it is present in the O antigen, while in *S. typhimorium* it is found in the T antigen [2-4]. In all of these organisms, the enzyme UDP-galactopyranose mutase (UGM) serves as the sole biosynthetic source of β-Gal*f* as it is responsible for converting UDP-Gal*p* to UDP-Gal*f* (Figures 2 and 3) [5-10]. UDP-Gal*f* serves as the precursor molecule of β-Gal*f*, which is attached to the various components of the cell surface by galactofuranosyl transferases (GalfTs) (Figure 2) [11, 12]. UGMs and GalfTs are not found in humans, therefore, they have been examined as potential drug targets.

Deletion of the genes coding for UGM or GalfTs have shown that these proteins are essential in *M. tuberculosis,* highlighting the importance for Gal*f* in bacteria [13]. Studies have also been conducted to identify inhibitors for *M. tuberculosis* UGM [14-17]. These studies showed that specific inhibitors of *M. tuberculosis* UGM were able to prevent mycobacterium growth and, therefore, validated Gal*f* biosynthesis as a drug target against mycobacteria [14]. β-Gal*f* has also been shown to be present in fungi [18-21]. In the human pathogen *Aspergillus fumigatus*, it is found in four components of the cell wall: galactomannan, glycoprotein oligosacchrides, glycophosphoinositol (GPI) anchored lipophosphogalactomannan (LPGM), and sphingolipids [18, 22]. Deletion of the UGM and the Gal*f* transporter genes in *Aspergillus* spp. resulted in attenuated virulence, increased temperature sensitivity, and thinner cell walls [23, 24]. Gal*f* is also present in protozoan parasites and is a virulence factor [25]. In *Leishmania* spp., it is

present in the lipophosphoglycan (LPG) and in glycoinositolphospholipids (GIPLs). In *T. cruzi*, Gal*f* is found in the GIPLs and glycoprotein oligosaccharides [26, 27]. This review focuses on current knowledge on the biosynthetic pathway of β-Gal*f* and its role in the pathogenesis of *T. cruzi* and *Leishmania* spp.

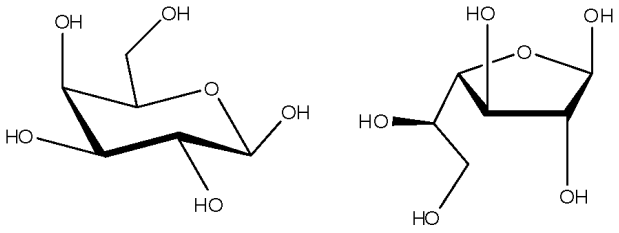

β-Galactopyranose β-Galactofuranose

Figure 2.1 Structures of β-D-Galactopyranose and β-D-Galactofuranose.

1.1 Overview of T. cruzi *and* Leishmania *spp.* *T. cruzi* is the causative agent of Chagas' disease, which often develops severe cardiac complications in patients with the chronic form of the disease [28]. In the *T. cruzi* life cycle, the parasite undergoes three developmental stages as it is transmitted from the insect vector (triatomine bug) to mammals: trypomastigote (vector feces and mammalian bloodstream), epimastigote (vector midgut), and amastigote (mammalian smooth muscle) [29]. *Leishmania* spp. are the causative agents of leishmaniasis, which can manifest in three forms--visceral, cutaneous, or mucocutaneous--depending on the speices [30]. In the *Leishmania* spp. lifecycle, there are two stages: the amastigote (mammalian host macrophages) and the promastigote stage (vector (sand fly) midgut) [30].

Current treatments are limited due to toxic side effects and cost, therefore new drugs are needed [31-33]. Lifecycle progression of both *T. cruzi* and *Leishmania* spp. is associated with changes in the carbohydrate composition on the cell surface. These changes are important for mediating host-pathogen interactions. Gal*f* levels and Gal*f*-containing glycans are shown to be modulated throughout the parasite life cycle and are important for pathogenesis [26, 34-36]. As

Gal*f* biosynthesis has been shown to be an attractive drug target for other pathogens, enzymes involved in this pathway may also prove to be ideal drug targets for the treatment of Chagas' disease and leishmaniasis.

2. Biosynthesis of Gal*f* in kinetoplastids

The biosynthesis of Gal*f* begins with the uptake and metabolism of D-galactose (Gal). Gal is an epimer of glucose that differs only by the orientation of the hydroxyl group at the carbon 4 position. Gal is a component of lactose in milk, is present in grains and beets, and can be utilized for energy after conversion to D-glucose (Glc). Gal is also a major component of glycans, present in proteins and lipids in most organisms, ranging from bacteria to mammals. The metabolism of Gal occurs via the Isselbacher or Leloir pathways (Figure 2). In the Leloir pathway, Gal is converted to glucose-6-phosphate (Glc-6-P), an intermediate in glycolysis (Figure 2A). After Gal is transported into the cytoplasm by hexose transporters it is phosphorylated by galactokinase (GalK). Phosphorylation of Gal prevents its transport out of the cell. Gal-1-phosphate (Gal-1-P) is then coupled to uridyl diphosphate by galactose-1-phosphate uridyltransferase (GalPUT) yielding two products, UDP-Gal and Glc-1-phosphate (Glc-1-P). UDP-Gal, is converted to UDP-glucose (UDP-Glc) by UDP-glucose-4-epimerase (GalE). Glc-1-P is isomerized to Glc-6-P by phosphoglucomutase (PGM) [37, 38]. In the Isselbacher pathway, Gal-1-P can be directly converted to UDP-Gal by the enzyme UDP-sugar-pyrophosphorylase (USP) (Figure 2B) [39]. These pathways contribute to the pool of UDP-Gal required for the biosynthesis of glycocalyx.

In *Leishmania* spp., galactose has been shown to be obtained from the environment by hexose transporters through radioactive labeling assays and both the Leloir and Isselbacher

pathways function to maintain proper levels of UDP-Gal in the cell [40]. The Isselbacher pathway is present in *L. major* due to the wide substrate specificity of USP, which can convert many sugars to the corresponding UDP-sugar including glucose, galactose, galacturonic acid, and arabinose [41]. The wide range of substrate specificity has been explored by crystallographic studies and has been attributed to a larger active site that can alter conformations of residues involved with sugar binding and the flexibility of the sugar-binding loop [42]. Deletion of the USP gene in *L. major* showed that the protein is nonessential and demonstrates that since the Leloir and Isselbacher pathways are redundant, proteins involved with the formation of UDP-Gal are not essential for *Leishmania* spp. survival [41, 43]. In *T. cruzi* and *Trypanosoma brucei,* galactose cannot be obtained from the environment because it is not recognized by the hexose transporters; therefore, these parasites rely on the action of GalE from the Leloir pathway for the direct conversion of UDP-Glc to UDP-Gal for galactose [37, 44, 45]. In both *T. cruzi* and *L. major*, UDP-Gal is converted to UDP-Gal*f* by UGM (Figure 2C and 3) [7]. UDP-Gal*f* is the substrate for several UDP-galactofuranosyl transferases, which decorate many glycoproteins and glycolipids on the cell surface of *T. cruzi* and *L. major*.

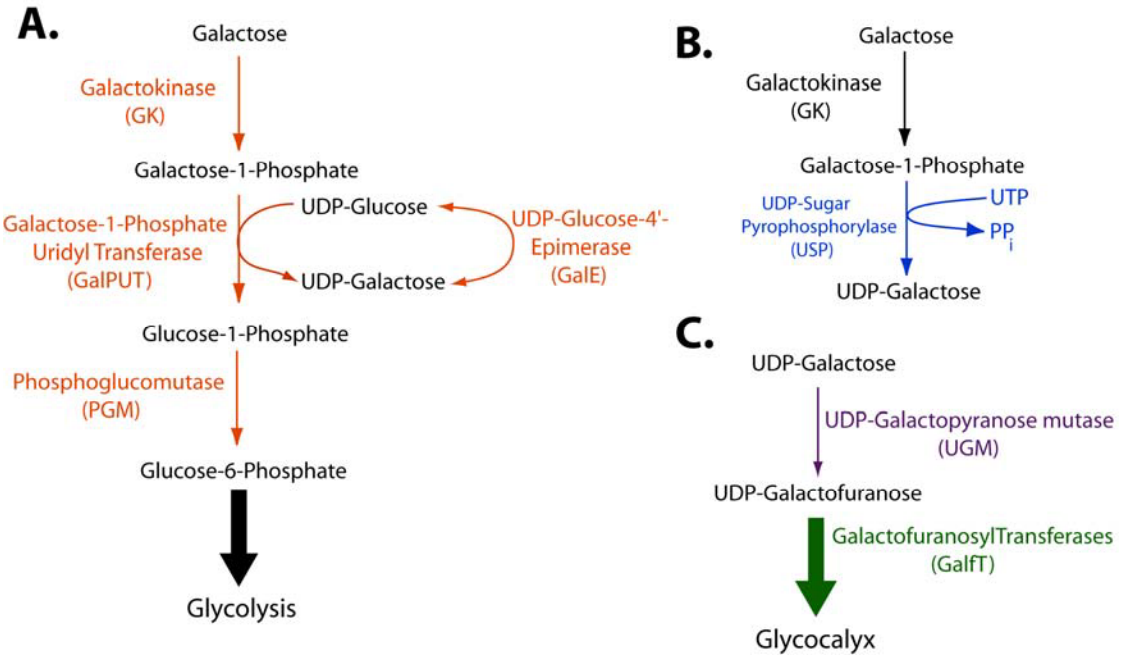

Figure 2.2 Biosynthetic pathways of Gal*f*. **A.** In the Leloir pathway, Gal is transported to the cytoplasm where it is converted to galactose-1-phosphate by galactokinase (GK). Galactose-1-phosphate uridyl tranferase (GalPUT) and UDP-Glc-4'-epimerase (GalE) are involved in the synthesis of UDP-galactose. **B.** Alternatively, galactose can be directly converted to UDP-galactose by the Isselbacher pathway by UDP-sugar pyrophosphorylase (USP). **C.** UDP-Galactose is then converted to UDP-Gal*f* by UDP-Galactopyranose mutase (UGM) and UDP-Gal*f* is subsequently added to the glycocalyx by Galactofuranosyl transferases (GalfT).

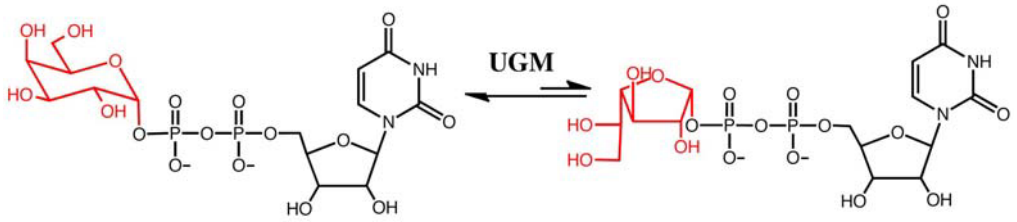

UDP-Galactopyranose UDP-Galactofuranose

Figure 2.3 Reaction catalyzed by UDP-Galactopyranose mutase (UGM).

2.1 Galactofuranose-containing proteins and lipids. Gal*f* is found in many major components of the glycocalyx of *Leishmania* spp. and *T. cruzi*. In *Leishmania* spp., Gal*f* is found in the lipophosphoglycan (LPG) and in glycoinositolphospholipids (GIPLs), while in *T. cruzi*, Gal*f* is found in the GIPLs and glycoprotein oligosaccharides (Figure 4) [26, 27]. In this section, we will describe the structure and role in pathogenesis of known Gal*f*-containing glycoconjugates.

2.1.1 Lipophosphoglycan (LPG) from Leishmania *spp.* LPG from *Leishmania* spp. has four components: a phosphoinositol lipid, a core oligosaccharide, phosphoglycan (PG) repeat units, and a cap (Figure 4A). β-Gal*f* is found in the core structure where it plays a role in connecting the PG repeat units to the phospholipid [35, 46]. LPG has been found to be important for adhesion to the sandfly midgut, resistance to the human complement C3b, protection from oxidative stress, and prevention from phagosomal transient fusion [47-50].

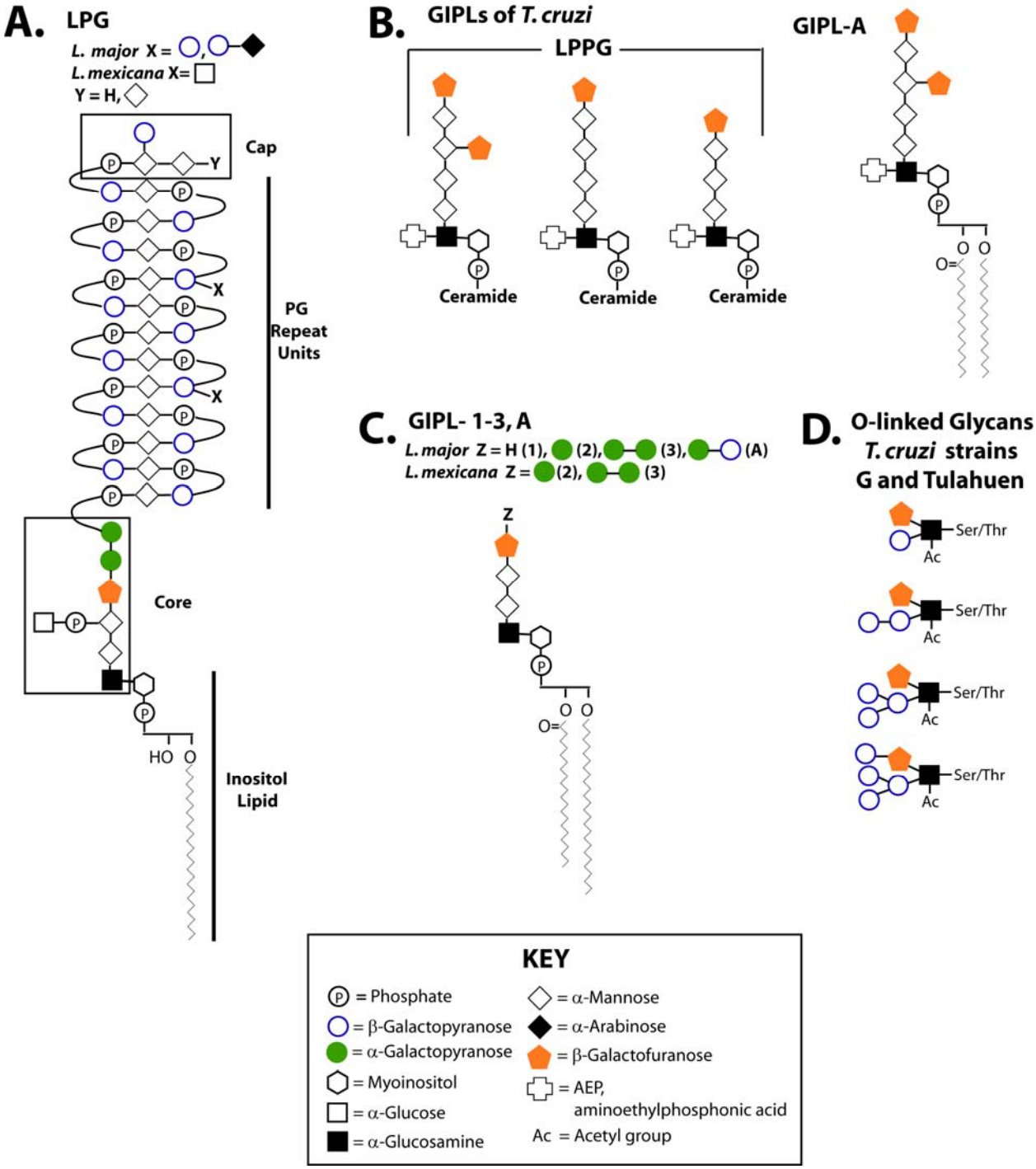

Figure 2.4 Structures of Gal*f* containing glycans of *Leishmania* spp. and *T. cruzi*. **A.** Structure of LPG from *Leishmania spp*. **B.** Structures of GIPLs from *T. cruzi*, including the previously annotated LPPG and GIPL-A **C.** Structures of GIPL-1-3, A from *L. major* and *L. mexicana*. **D.** Selected subset of structures of O-linked glycans found in both *T. cruzi* strains G and Tuhulan.

2.1.2 Glycoinositolphospholipids (GIPLs). GIPLs are free glycosylated phospholipids found in many kinetoplastids. Those found in *Leishmania* spp. and *T. cruzi* are considered unique due to the presence of β-Gal*f* (Figure 4B and C) [26, 51-54]. GIPL structure is species and strain dependent and varies in expression levels throughout the life stages of the parasite [55-58]. GIPLs from *Leishmania* spp. are thought to be precursor molecules for the synthesis of the LPG core structure [59]. *L. major* GIPL-1 has been shown to be involved in parasite-host interactions and is thought to play an important role in establishing infection [57, 60].

GIPLs from *T. cruzi* include a class of phospholipids previously identified as lipopeptidophosphoglycans (LPPGs) [61-63]. The LPPGs were originally considered a separate class from the GIPLs due to the presence of contaminating amino acids during their purification; these amino acids have since been identified as part of the NETNES (a glycoprotien composed of 13 amino acids with up to 5 post-translational modifications found on the cell surface of *T. cruzi*) [27, 64]. The importance of GIPLs in *T. cruzi* is revealed by studies that show it plays a role in antigenicity, both with rabbit and human sera [36, 53]. The antigenicity is thought to be primarily due to the terminal β-Gal*f* residues either from the GIPLs or the O-linked mucins, as removal of β-Gal*f* results in decreased levels of antigencity [36, 53, 65]. It has also been shown that GIPLs play a role in attachment of the parasite to the luminal midgut of the vector *Rhodnius prolixus* [55]. *T. cruzi* modulates this interaction by altering GIPL expression levels during its life cycle, as epimastigotes have much higher expression of GIPLs than trypomastigotes [55, 65, 66].

2.1.3 N- *linked glycans.* β-Gal*f* is found in mannose N-linked oligosaccharides in several species of trypanosomatid flagellates including *T. cruzi, Leptomanas samueli, Herpetomnas*

samuelpessoai, Crithidia fasciculate, and *Crithidia harmosa* [36, 67-70]. In *T. cruzi*, Gal*f* has been identified in the 80-90 kDa glycoproteins found in the trypomastigote [36]. The glycan structures have been solved for *L. samueli*, *C. fasciculate,* and *C. harmosa* and are shown to be species dependent [67, 69]. β- Gal*f* units are found as terminal sugars linked to mannose residues in high mannose type N-linked glycans [67, 69]. The role of N-linked glycans has currently not been largely explored for *T. cruzi.*

2.1.4 T. cruzi O- *linked glycans and mucins. T. cruzi* mucins are a family of GPI-linked glycoproteins with high levels of O-linked glycosylation [71]. Several studies have been conducted to determine the composition of the oligosaccharides bound to Thr and Ser residues in these glycoproteins [72-76]. In *T. cruzi*, the O-glycans are not linked to N-acetylgalactosamine as in mammals and other organisms; instead, they are linked to N-acetylglucosamine [77]. It has been demonstrated that these glycans vary highly among *T. cruzi* strains and β-Gal*f* is a component of the glycan structures of *T. cruzi* strains G, Tulahuen, and Dm28c; however, β-Gal*f* is not found in *T. cruzi* strains CL-Brener and Y (Figure 4E) [72-74, 78, 79]. These mucins play an important role in parasite-host interaction by both protecting against host defense mechanisms and ensuring targeting of specific cells and tissues [71, 77].

3. Galactofuranose is a virulence factor in kinetoplastids

It has been shown that incubation of *L. major* or *T. cruzi* with Gal*f*-specific antibodies block parasite binding to macrophages or mammalian cells, resulting in a 50-80% decrease in infection rates [60, 66, 80, 81]. It was further shown that the antibody specifically bound to the β-Gal*f* present in GIPLs of *T. cruzi* and GIPL-1 of *L. major* [60, 66]. This suggests that β-Gal*f*

and the GIPLs of *T. cruzi* and GIPL-1 of *L. major* play a role in cell adhesion and infection. Furthermore, it was shown that macrophages incubated with *p*-nitrophenol-β-Gal*f* were infected 80% less by *L. major*, while macrophages incubated with *p*-nitrophenol-β-Gal*p* saw no decrease in infectivity [60]. Together, these results confirm that β-Gal*f* plays an important role in parasite-host interaction and suggest that β-Gal*f* biosynthetic enzymes are potential drug targets.

3.1 UDP-glucose 4'-epimerase (GalE). In *T. cruzi*, GalE is the first protein required for Gal*f* biosynthesis [82]. GalE is classified as a short-chain dehydrogenase/reductase (SDR) with a conserved Tyr-X-X-X-Lys motif and a characteristic Rossmann fold structure for NAD^+ binding [38, 83]. GalE is a homodimer that consists of two domains, an N-terminal domain with the Rossmann fold, and a C-terminal domain that binds the substrate, UDP-Glc [84, 85]. The catalytic site is located in the cleft between the two domains [84, 85]. The mechanism is shown to be conserved across species and involves the deprotonation of the Glc O4' hydroxyl and hydride transfer from the C4 carbon of Gal to NAD^+ [84, 85]. The intermediate 4-keto sugar rotates in the active site and NADH transfers back the hydride to the opposite face forming UDP-Gal [84, 85].

Mutant strains of *T. brucei* and *T. cruzi* with deletion of the *galE* gene have not been obtained suggesting that Gal metabolism is essential for parasite survival [45, 82, 86, 87]. Conditional null mutants were created in *T. brucei* using tetracycline-regulated expression [45, 86]. Studies with this strain showed that removal of tetracycline from the trypomastigote parasite led to cell death and decreased Gal surface-expression levels by 30% [45, 86]. These studies showed that upon Gal starvation, Gal was eliminated from *T. brucei* variant surface

glycoprotein (VSG) and from poly-N-acetyllactosamine-containing glycoproteins causing cell growth to cease and differentiation to a stumpy-like form, ultimately leading to cell death [87]. Single *galE* knockout mutants of *T. cruzi* epimastigotes were also constructed [82]. These cell strains showed several phenotypic differences including shortened flagella and agglutination, which is thought to be the result of a lack of surface mucins [82]. Interestingly, these cell strains show a preference for expressing high levels of Gal*f* containing GIPLs over Gal*p* mucins, whose expression levels were reduced 6-9 fold, suggesting that levels of Gal*f* is preferentially maintained in the glycocalyx over Gal*p* [82]. In *Leishmania* spp., Gal can be obtained from extracellular sources, presumably by a family of hexose transporters [40, 88]. Thus, GalE is not essential in these parasites.

Studies have been undertaken to identify novel inhibitors that specifically target the GalE of *T. brucei* [89, 90]. Using high-throughput screens and computer modeling experiments, inhibitors that showed preference to *T. brucei* GalE over human GalE were identified [89, 90]. However, when these compounds were tested *in vitro* with *T. brucei* and either mammalian CHO cells or liver (MRC5) cells, these compounds either were cytotoxic to both the parasite and mammalian cells or that the compound was ineffective against *T. brucei* [89, 90]. These studies suggest that, while GalE remains a potential drug target, there will be many difficulties in designing specific inhibitors for the treatment of these diseases without unwanted side effects.

3.2 UDP-galactopyranose mutase (UGM). UGM is a flavo-dependent enzyme that catalyzes the conversion of UDP-Gal*p* to UDP-Gal*f*. UGM was first identified in *Escherichia coli* K-12 in 1996, and since then it has been identified in several other pathogenic microorganisms including *M. tuberculosis*, *L. major*, *T. cruzi*, and *A. fumigatus* [5-8]. Interestingly, while *T. cruzi* produces

UGM the related *T. brucei* does not and as a result, *T. brucei* does not produce Gal*f* [70]. UGM has been found to be the sole biosynthetic source of Gal*f* and, since it is not found in mammals it is considered an ideal drug target.

Deletion of the UGM gene in *L. major* shows that this enzyme plays an important role in pathogenesis [25]. In the absence of UGM, *L. major* mutants were completely depleted of Gal*f*, lacked LPG PG repeats, and contained truncated forms of GIPLs [25]. Furthermore, mice infection by *L. major* lacking Gal*f* was significantly attenuated [25]. As previously mentioned, deletion of UGM also showed that Gal*f* is a virulence factor in *A. fumigatus* and *Aspergillus nidulans* [23, 91]. These studies show the importance of UGM and validate this enzyme as a drug target in protozoan and other eukaryotic human pathogens.

Although the reaction catalyzed by UGM does not involve a net redox change for the conversion of UDP-Gal*p* to UDP-Gal*f*, the reaction requires the flavin cofactor to be in the reduced form [92, 93]. Structural and mechanistic studies of the prokaryotic UGM have led to two proposals for the ring contraction mechanism (Figure 5). One mechanism depicts the reduced flavin acting as a nucleophile, attacking the anomeric carbon (C1) of Gal to form a flavin N5-C1 Gal adduct [94]. This adduct has been isolated and characterized in the prokaryotic UGM from *K. pneumoniae* [94, 95]. The other proposed mechanism involves a single electron transfer from the reduced flavin to Gal, which then forms the sugar-flavin adduct [96].

Several structures have been solved for prokaryotic UGMs, in both oxidized and reduced states with and without substrate bound, providing excellent groundwork for the development of specific inhibitors [95, 97, 98]. The structure of prokaryotic UGMs show that it is a homodimer and a mixed α/β class protein with 3 domains: an FAD-binding domain with a typical Rossmann fold, a 5-helix bundle, and a 6-stranded anti-parallel β-sheet [98, 99]. The structures of the

reduced protein with substrate bound show that Gal is properly positioned for interaction with the flavin [95, 98].

Much less is known about the mechanism and structure of eukaryotic UGMs. These enzymes share low sequence identity and the presence of inserts in the primary structure predicts significant structural differences (Figure 6). In fact, comparison of the oligomeric states between prokaryotic and eukaryotic UGMs indicates that quaternary structures vary among species (Table 1) [100]. Furthermore, our group, as well as others, have demonstrated that known inhibitors of prokaryotic UGMs are not effective or have decreased potency against *L. major*, *A. fumigatus*, and *T. cruzi* UGMs [7, Appendix B]. Therefore, mechanistic and structural work is urgently needed on the eukaryotic enzymes.

Table 2.1 UDP-galactopyranose mutases

Species	Amino acids	% identity[a]	Oilgomeric state	Reference
E. coli	367	100	Dimer	[99]
M. tuberculosis	399	44	Dimer	[97]
L. major	491	15	Monomer	Chapter 5
T. cruzi	480	15	Monomer	Chapter 6
A. fumigatus	510	14	Tetramer	[100]

[a]Identity to the *E. coli* enzyme

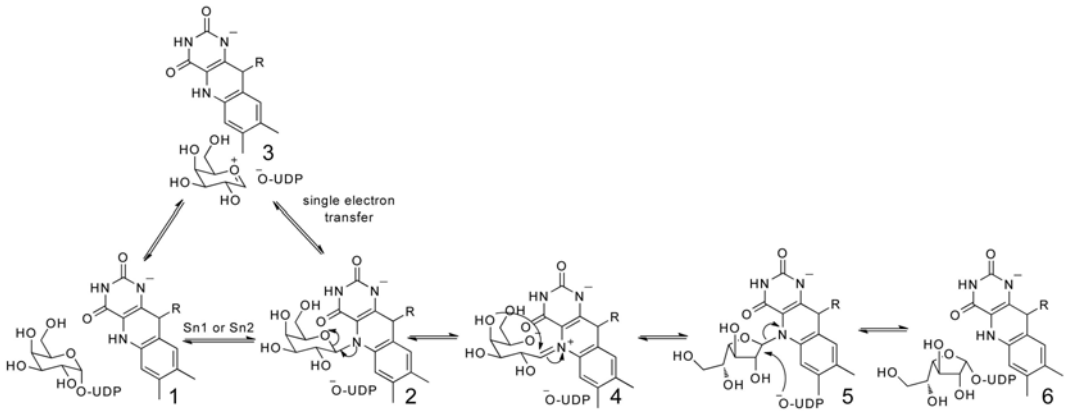

Figure 2.5 Proposed chemical mechanism for UGMs [92-96]. Nucleophilic attack by the reduced flavin (1) leads to a flavin-galactose adduct (2). This step can either occur via an S_N1 or S_N2 reaction. Alternatively, the flavin can transfer one electron to a galactose oxocarbenium ion, forming a sugar and flavin radical that can also form the flavin-galactose adduct. Formation of a flavin iminium ion leads to sugar ring opening (4). Sugar ring contraction occurs by attack of the C4 hydroxyl to the C1-carbon (5). The final step is the bond formation to UDP (6).

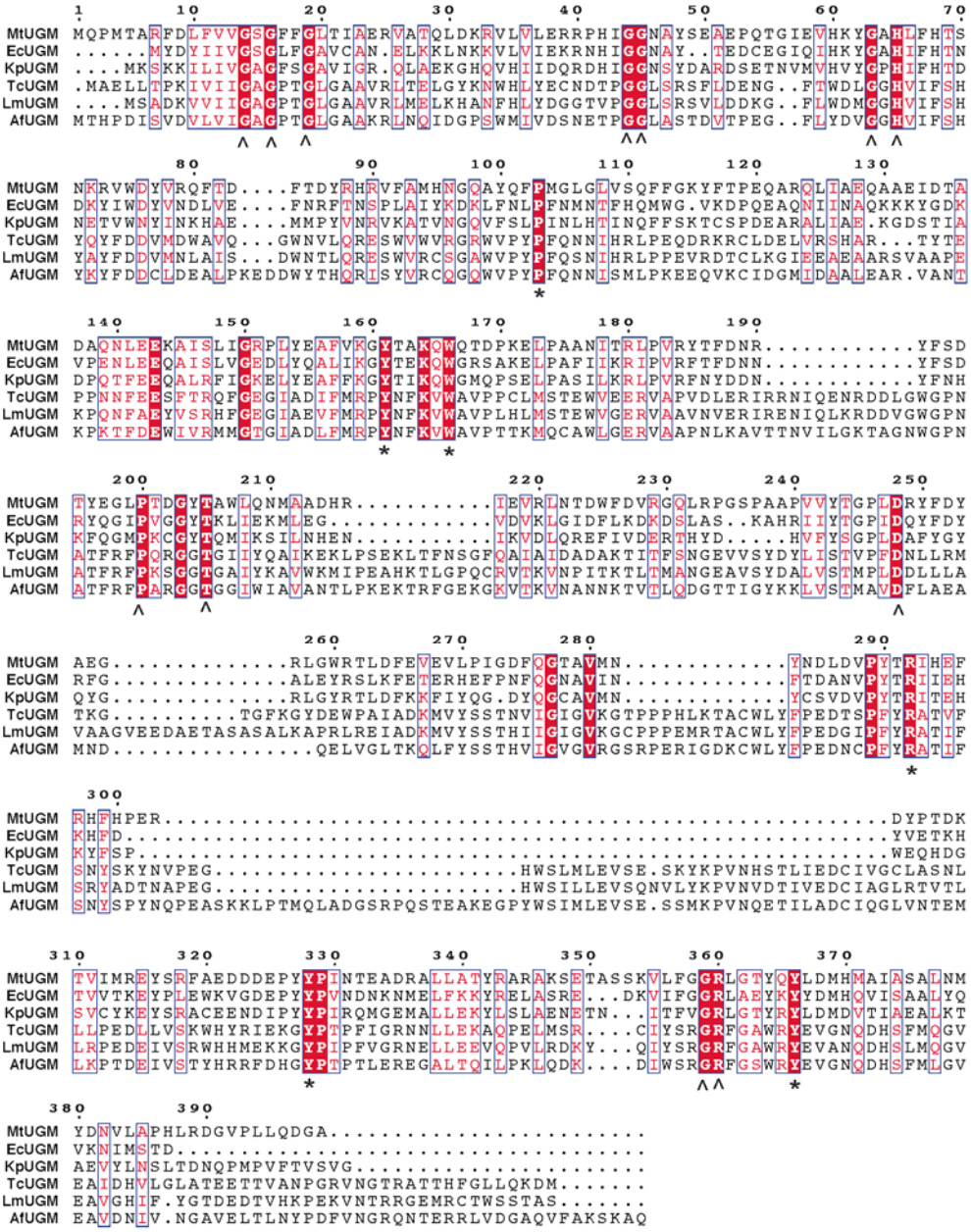

Figure 2.6 Multiple sequence alignment of UDP-galactopyranose mutases. Conserved amino acids found in the active site of bacterial UGM are marked with a star and those involved in flavin binding are marked with arrowheads. Abbreviations: Mt, *M. tuberculosis*, Ec, *E. coli*; Kp, *K. pneumoniae*; Tc, *T. cruzi*; Lm, *L. major*; Af, *A. fumigatus*; The program Clustal W was used to generate the alignment and Espript 2.2 to create the figure [109].

3.3 UDP-galactofuranose transferases. UDP-Gal*f* is synthesized in the cytosol by UGM and is transported into the Golgi where it is attached to the LPG and GIPLs by galactofuranosyl

transferases (GalfT) [101]. Currently, all known linkages of Gal*f* in *T. cruzi* and *Leishmania* spp. are in the β anomer configuration. The most extensively studied GalfT is LPG-1 from *L. major* and *L. donovani*. Studies on LPG-1 have revealed that it is localized to the Golgi apparatus, where it adds the β-Gal*f* to the core LPG structure [101, 102]. LPG-1 is a metal glycosyltranferase with typical conserved motifs including a cytoplasmic tail, a transmembrane domain, and a DXD metal-binding motif [103]. Mutants with the deletion of *lpg-1* gene in both *L. major* and *L. donovani* show LPG-1 to be important for LPG formation. These deletion studies show LPG-1 is responsible for the addition of Gal*f* to LPG and does not play a role in the addition of Gal*f* in the GIPLs [102, 104]. Due to the lack of LPG, this *lpg-1* deletion strain displayed attenuated virulence in *L. major* [102, 104]. These studies showed that LPG-1 could serve as a drug target in *L. major*.

There are no published studies on the GalfT from *T. cruzi*. In order to identify GalfTs in *T. cruzi*, a BLAST search was conducted using LPG-1 from *L. major* as a template, and more than 30 putative proteins annotated as β-GalfTs in the *T. cruzi* genome were identified [105, 106]. The top 10 putative GalfT sequences from the *T. cruzi* BLAST search were aligned with the *L. major* and *L. donovani* LPG-1 showing high sequence identity between these proteins (Figure 7). These sequences all contain the proposed catalytic site and demonstrate redundancy of the genes [103]. While only 10 sequences were analyzed here, the other sequences also showed high sequence identity and conservation of the proposed catalytic site. Redundancy of GalfTs are common in many different species, as often different transferases are used for each linkage type based on anomericity, bond linkage, and the substrate acceptors for Gal*f* [107]. Due to the high number of GalfTs in *T. cruzi*, targeting GalfTs for drug design most likely would not be effective.

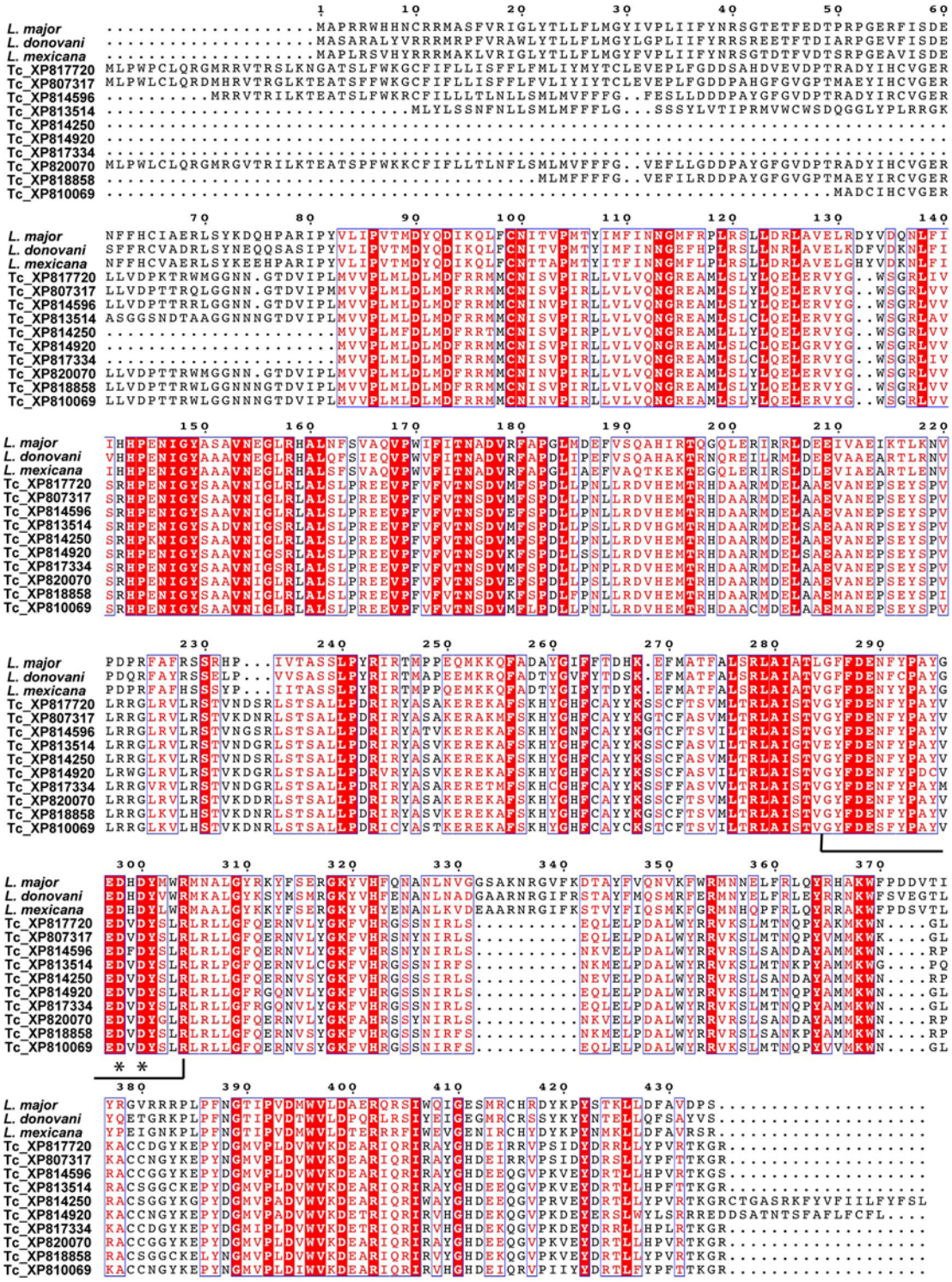

Figure 2.7 Alignment of *L. major* LPG-1 (XP001683753), *L. donovani* LPG-1 (ADG26596), *L. mexicana* LPG-1 (CAB6682), and ten putative *T. cruzi* GalfTs. Putative *T. cruzi* GalfTs were identified by BLAST search using *L. major* LPG-1 as the probe. The active site residues are shown in brackets and the metal binding motif is represented with asterisks. The alignment was created as indicated in Figure 6.

4. Concluding Remarks

To cause infection, protozoan parasites must recognize the mammalian host environment, bind and infect the target cells, and evade the immune system. Undoubtedly, the cell surface of these pathogens plays important roles in these processes. Current drugs are able to kill most of the parasites during treatment; however, these treatments do not eliminate all the parasites, presumably because they can "hide" in the intracellular forms. Modification of the cell surface sugar composition will alter the mechanism of infection. Enzymes involved in the biosynthesis of Gal*f* have been shown to play a role in parasite growth and pathogenesis. GalE is essential for growth in *T. cruzi* and *T. brucei*, while UGM and LPG-1 are important virulence factors in *L. major* [25, 82, 102]. Due to the presence of a GalE homolog in humans, compounds that inhibit this enzyme have toxic side effects. Furthermore, this enzyme is not important for virulence in *Leishmania* spp. UGM plays a central role in Gal*f* biosynthesis and is the only source of UDP-Gal*f*, which is the substrate for all the GalfT that attach Gal*f* to the final sugar-acceptor molecules. Consequently, UGM emerges as an attractive drug candidate, as no homolog is found in humans [108]. The unique chemical structure of UGM suggests that specific inhibitors can be identified. Targeting UGM in *T. cruzi* and *L. major* will affect their virulence in humans and perhaps allow the immune system to effectively clear the parasite. Alternatively, inhibition of UGM will enhance the activity of other anti-parasitic drugs. Such combination therapy might be necessary to combat these complex eukaryotic human pathogens.

5. Acknowledgements

This work was supported in part by NIH grants RO1 GM094469 (P. Sobrado, PI) and RO1 AI082542 (R. Tarleton, PI). M.O. was supported by a fellowship from the American Heart Association. A.L.V was supported by a fellowship from the Ministry of Science and Technology (MICIT) from Costa Rica.

6. References

[1]. D.C. Crick, S. Mahapatra, P.J. Brennan, "Biosynthesis of the arabinogalactan-peptidoglycan complex of *Mycobacterium tuberculosis*," *Glycobiology*, vol.11, pp. 107R-118R, 2001.

[2]. G. Stevenson, B. Neal, D. Liu, M. Hobbs, N.H. Packer, M. Batley, J.W. Redmond, L. Lindquist, P. Reeves, "Structure of the o antigen of *Escherichia coli* K-12 and the sequence of its rfb gene cluster," *J Bacteriol*, vol.176, pp. 4144-4156, 1994.

[3]. M. Berst, C.G. Hellerqvist, B. Lindberg, O. Luderitz, S. Svensson, O. Westphal, "Structural investigations on T1 lipopolysaccharides," *Eur J Biochem*, vol.11, pp. 353-359, 1969.

[4]. C. Whitfield, J.C. Richards, M.B. Perry, B.R. Clarke, L.L. MacLean, "Expression of two structurally distinct D-galactan O antigens in the lipopolysaccharide of *Klebsiella pneumoniae* Serotype O1," *J Bacteriol*, vol.173, pp. 1420-1431, 1991.

[5]. A. Weston, R.J. Stern, R.E. Lee, P.M. Nassau, D. Monsey, S.L. Martin, M.S. Scherman, G.S. Besra, K. Duncan, M.R. McNeil, "Biosynthetic origin of mycobacterial cell wall galactofuranosyl residues," *Tubercle and Lung Disease*, vol.78, pp. 123-131, 1998.

[6]. H. Bakker, B. Kleczka, R. Gerardy-Schahn, F.H. Routier, "Identification and partial characterization of two eukaryotic UDP-galactopyranose mutases," *Biol Chem*, vol.386, pp. 657-661, 2005.

[7]. S.M. Beverley, K.L. Owens, M. Showalter, C.L. Griffith, T.L. Doering, V.C. Jones, M.R. McNeil, "Eukaryotic UDP-galactopyranose mutase (GLF gene) in microbial and metazoal pathogens," *Eukaryot Cell*, vol.4, pp. 1147-1154, 2005.

[8]. P.M. Nassau, S.L. Martin, R.E. Brown, A. Weston, D. Monsey, M.R. McNeil, K. Duncan, "Galactofuranose biosynthesis in *Escherichia coli* K-12: Identification and cloning of UDP-galactopyranose mutase," *J Bacteriol*, vol.178, pp. 1047-1052, 1996.

[9]. R. Koplin, J.R. Brisson, C. Whitfield, "UDP-galactofuranose precursor required for formation of the lipopolysaccharide O antigen of *Klebsiella pneumoniae* Serotype O1 is synthesized by the product of the Rfbdkpo1 gene," *J Biol Chem*, vol.272, pp. 4121-4128, 1997.

[10]. M. Sarvas, H. Nikaido, "Biosynthesis of T1 antigen in *Salmonella*: Origin of D-galactofuranose and D-ribofuranose residues," *J Bacteriol*, vol.105, pp. 1063-1072, 1971.

[11]. M.R. Richards, T.L. Lowary, "Chemistry and biology of galactofuranose-containing polysaccharides," *Chembiochem*, vol.10, pp. 1920-1938, 2009.

[12]. L. Kremer, L.G. Dover, C. Morehouse, P. Hitchin, M. Everett, H.R. Morris, A. Dell, P.J. Brennan, M.R. McNeil, C. Flaherty, K. Duncan, G.S. Besra, "Galactan biosynthesis in *Mycobacterium tuberculosis*. Identification of a bifunctional UDP-galactofuranosyltransferase," *J Biol Chem*, vol.276, pp. 26430-26440, 2001.

[13]. F. Pan, M. Jackson, Y. Ma, M. McNeil, "Cell wall core galactofuran synthesis is essential for growth of mycobacteria," *J Bacteriol*, vol.183, pp. 3991-3998, 2001.

[14]. E.C. Dykhuizen, J.F. May, A. Tongpenyai, L.L. Kiessling, "Inhibitors of UDP-galactopyranose mutase thwart mycobacterial growth," *J Am Chem Soc*, vol.130, pp. 6706-6707, 2008.

[15]. E.C. Dykhuizen, L.L. Kiessling, "Potent ligands for prokaryotic UDP-galactopyranose mutase that exploit an enzyme subsite," *Org Lett*, vol.11, pp. 193-196, 2009.

[16]. M.S. Scherman, K.A. Winans, R.J. Stern, V. Jones, C.R. Bertozzi, M. McNeil, "Drug targeting mycobacterium tuberculosis cell wall synthesis: Development of a microtiter plate-

based screen for UDP-galactopyranose mutase and identification of an inhibitor from a uridine-based library," *Antimicrob Agents Chemother*, vol.47, pp. 378-382, 2003.
[17]. M. Soltero-Higgin, E.E. Carlson, J.H. Phillips, L.L. Kiessling, "Identification of inhibitors for UDP-galactopyranose mutase," *J Am Chem Soc*, vol.126, pp. 10532-10533, 2004.
[18]. J.P. Latge, "Galactofuranose containing molecules in *Aspergillus fumigatus*," *Med Mycol*, vol.47 Suppl 1, pp. S104-109, 2009.
[19]. K. Barr, R.A. Laine, R.L. Lester, "Carbohydrate structures of three novel phosphoinositol-containing sphingolipids from the yeast *Histoplasma capsulatum*," *Biochemistry*, vol.23, pp. 5589-5596, 1984.
[20]. V.V. Vaishnav, B.E. Bacon, M. O'Neill, R. Cherniak, "Structural characterization of the galactoxylomannan of *Cryptococcus neoformans* Cap67," *Carbohydr Res*, vol.306, pp. 315-330, 1998.
[21]. J.P. Latge, H. Kobayashi, J.P. Debeaupuis, M. Diaquin, J. Sarfati, J.M. Wieruszeski, E. Parra, J.P. Bouchara, B. Fournet, "Chemical and immunological characterization of the extracellular galactomannan of *Aspergillus fumigatus*," *Infect Immun*, vol.62, pp. 5424-5433, 1994.
[22]. M. Bernard, J.P. Latge, "*Aspergillus fumigatus* cell wall: Composition and biosynthesis," *Med Mycol*, vol.39 Suppl 1, pp. 9-17, 2001.
[23]. P.S. Schmalhorst, S. Krappmann, W. Vervecken, M. Rohde, M. Muller, G.H. Braus, R. Contreras, A. Braun, H. Bakker, F.H. Routier, "Contribution of galactofuranose to the virulence of the opportunistic pathogen *Aspergillus fumigatus*," *Eukaryot Cell*, vol.7, pp. 1268-1277, 2008.
[24]. J. Engel, P.S. Schmalhorst, T. Dork-Bousset, V. Ferrieres, F.H. Routier, "A single UDP-galactofuranose transporter is required for galactofuranosylation in *Aspergillus fumigatus*," *J Biol Chem*, pp., 2009.
[25]. B. Kleczka, A.C. Lamerz, G. van Zandbergen, A. Wenzel, R. Gerardy-Schahn, M. Wiese, F.H. Routier, "Targeted gene deletion of *Leishmania major* UDP-galactopyranose mutase leads to attenuated virulence," *J Biol Chem*, vol.282, pp. 10498-10505, 2007.
[26]. R.M. de Lederkremer, W. Colli, "Galactofuranose-containing glycoconjugates in trypanosomatids," *Glycobiology*, vol.5, pp. 547-552, 1995.
[27]. R.M. de Lederkremer, R. Agusti, "Glycobiology of *Trypanosoma cruzi*," *Adv Carbohydr Chem Biochem*, vol.62, pp. 311-366, 2009.
[28]. J.R. Coura, J. Borges-Pereira, "Chagas disease: 100 years after its discovery. A systemic review," *Acta Trop*, vol.115, pp. 5-13, 2010.
[29]. W. De Souza, "Basic cell biology of *Trypanosoma cruzi*," *Curr Pharm Des*, vol.8, pp. 269-285, 2002.
[30]. H. Kato, E.A. Gomez, A.G. Caceres, H. Uezato, T. Mimori, Y. Hashiguchi, "Molecular epidemiology for vector research on leishmaniasis," *Int J Environ Res Public Health*, vol.7, pp. 814-826, 2010.
[31]. J.A. Urbina, "Specific chemotherapy of chagas disease: Relevance, current limitations and new approaches," *Acta Trop*, vol.115, pp. 55-68, 2010.
[32]. L. Kedzierski, A. Sakthianandeswaren, J.M. Curtis, P.C. Andrews, P.C. Junk, K. Kedzierska, "Leishmaniasis: Current treatment and prospects for new drugs and vaccines," *Curr Med Chem*, vol.16, pp. 599-614, 2009.
[33]. J.V. Richard, K.A. Werbovetz, "New antileishmanial candidates and lead compounds," *Curr Opin Chem Biol*, vol.14, pp. 447-455, 2010.

[34]. M.A. Ferguson, "The surface glycoconjugates of trypanosomatid parasites," *Philos Trans R Soc Lond B Biol Sci*, vol.352, pp. 1295-1302, 1997.
[35]. S.J. Turco, A. Descoteaux, "The lipophosphoglycan of *Leishmania* parasites," *Annu Rev Microbiol*, vol.46, pp. 65-94, 1992.
[36]. D.B. Golgher, W. Colli, T. Souto-Padron, B. Zingales, "Galactofuranose-containing glycoconjugates of epimastigote and trypomastigote forms of *Trypanosoma cruzi*," *Mol Biochem Parasitol*, vol.60, pp. 249-264, 1993.
[37]. P.A. Frey, "The leloir pathway: A mechanistic imperative for three enzymes to change the stereochemical configuration of a single carbon in galactose," *FASEB J*, vol.10, pp. 461-470, 1996.
[38]. H.M. Holden, I. Rayment, J.B. Thoden, "Structure and function of enzymes of the leloir pathway for galactose metabolism," *J Biol Chem*, vol.278, pp. 43885-43888, 2003.
[39]. K.J. Isselbacher, "Evidence for accessory pathway of galactose metabolism in mammalian liver," *Science*, vol.126, pp. 652-654, 1957.
[40]. S.J. Turco, M.A. Wilkerson, D.R. Clawson, "Expression of an unusual acidic glycoconjugate in *Leishmania donovani*," *J Biol Chem*, vol.259, pp. 3883-3889, 1984.
[41]. S. Damerow, A.C. Lamerz, T. Haselhorst, J. Fuhring, P. Zarnovican, M. von Itzstein, F.H. Routier, "*Leishmania* UDP-sugar pyrophosphorylase: The missing link in galactose salvage?," *J Biol Chem*, vol.285, pp. 878-887, 2010.
[42]. A. Dickmanns, S. Damerow, P. Neumann, E.C. Schulz, A.C. Lamerz, F.H. Routier, R. Ficner, "Structural basis for the broad substrate range of the UDP-sugar pyrophosphorylase from *Leishmania major*," *J Mol Biol*, vol.405, pp. 461-478, 2011.
[43]. A.C. Lamerz, S. Damerow, B. Kleczka, M. Wiese, G. van Zandbergen, J. Lamerz, A. Wenzel, F.F. Hsu, J. Turk, S.M. Beverley, F.H. Routier, "Deletion of UDP-glucose pyrophosphorylase reveals a UDP-glucose independent UDP-galactose salvage pathway in *Leishmania major*," *Glycobiology*, vol.20, pp. 872-882, 2010.
[44]. R. Eisenthal, S. Game, G.D. Holman, "Specificity and kinetics of hexose transport in *Trypanosoma brucei*," *Biochim Biophys Acta*, vol.985, pp. 81-89, 1989.
[45]. J.R. Roper, M.L. Guther, K.G. Milne, M.A. Ferguson, "Galactose metabolism is essential for the african sleeping sickness parasite *Trypanosoma brucei*," *Proc Natl Acad Sci U S A*, vol.99, pp. 5884-5889, 2002.
[46]. M.A. Carver, S.J. Turco, "Cell-free biosynthesis of lipophosphoglycan from *Leishmania donovani*. Characterization of microsomal galactosyltransferase and mannosyltransferase activities," *J Biol Chem*, vol.266, pp. 10974-10981, 1991.
[47]. G.F. Spath, L.A. Garraway, S.J. Turco, S.M. Beverley, "The role(s) of lipophosphoglycan (lpg) in the establishment of *Leishmania major* infections in mammalian hosts," *Proc Natl Acad Sci U S A*, vol.100, pp. 9536-9541, 2003.
[48]. S.J. Turco, G.F. Spath, S.M. Beverley, "Is lipophosphoglycan a virulence factor? A surprising diversity between *Leishmania* species," *Trends Parasitol*, vol.17, pp. 223-226, 2001.
[49]. A. Svarovska, T.H. Ant, V. Seblova, L. Jecna, S.M. Beverley, P. Volf, "*Leishmania major* glycosylation mutants require phosphoglycans (lpg2-) but not lipophosphoglycan (lpg1-) for survival in permissive sand fly vectors," *PLoS Negl Trop Dis*, vol.4, pp. e580, 2010.
[50]. B.A. Butcher, S.J. Turco, B.A. Hilty, P.F. Pimenta, M. Panunzio, D.L. Sacks, "Deficiency in beta1,3-galactosyltransferase of a *Leishmania major* lipophosphoglycan mutant adversely

influences the *Leishmania*-sand fly interaction," *J Biol Chem*, vol.271, pp. 20573-20579, 1996.
[51]. M.J. McConville, S.W. Homans, J.E. Thomas-Oates, A. Dell, A. Bacic, "Structures of the glycoinositolphospholipids from *Leishmania major*. A family of novel galactofuranose-containing glycolipids," *J Biol Chem*, vol.265, pp. 7385-7394, 1990.
[52]. R.M. de Lederkremer, O.L. Casal, A.M. Alves, W. Colli, "Evidence for the presence of D-galacofuranose in the lipopetidophosphoglycan from *Trypanosoma cruzi*," *FEBS Letters*, vol.116, pp. 25-29, 1980.
[53]. L. Mendonca-Previato, P.A. Gorin, A.F. Braga, J. Scharfstein, J.O. Previato, "Chemical structure and antigenic aspects of complexes obtained from epimastigotes of *Trypanosoma cruzi*," *Biochemistry*, vol.22, pp. 4980-4987, 1983.
[54]. R.M. de Lederkremer, C. Lima, M.I. Ramirez, M.A. Ferguson, S.W. Homans, J. Thomas-Oates, "Complete structure of the glycan of lipopeptidophosphoglycan from *Trypanosoma cruzi* epimastigotes," *J Biol Chem*, vol.266, pp. 23670-23675, 1991.
[55]. N.F. Nogueira, M.S. Gonzalez, J.E. Gomes, W. de Souza, E.S. Garcia, P. Azambuja, L.L. Nohara, I.C. Almeida, B. Zingales, W. Colli, "*Trypanosoma cruzi*: Involvement of glycoinositolphospholipids in the attachment to the luminal midgut surface of *Rhodnius prolixus*," *Exp Parasitol*, vol.116, pp. 120-128, 2007.
[56]. M.A. Ferguson, "The structure, biosynthesis and functions of glycosylphosphatidylinositol anchors, and the contributions of trypanosome research," *J Cell Sci*, vol.112 (Pt 17), pp. 2799-2809, 1999.
[57]. E. Suzuki, A.K. Tanaka, M.S. Toledo, S.B. Levery, A.H. Straus, H.K. Takahashi, "Trypanosomatid and fungal glycolipids and sphingolipids as infectivity factors and potential targets for development of new therapeutic strategies," *Biochim Biophys Acta*, vol.1780, pp. 362-369, 2008.
[58]. J.C. Carreira, C. Jones, R. Wait, J.O. Previato, L. Mendonca-Previato, "Structural variation in the glycoinositolphospholipids of different strains of *Trypanosoma cruzi*," *Glycoconj J*, vol.13, pp. 955-966, 1996.
[59]. M.J. McConville, M.A. Ferguson, "The structure, biosynthesis and function of glycosylated phosphatidylinositols in the parasitic protozoa and higher eukaryotes," *Biochem J*, vol.294 (Pt 2), pp. 305-324, 1993.
[60]. E. Suzuki, A.K. Tanaka, M.S. Toledo, H.K. Takahashi, A.H. Straus, "Role of Beta-D-galactofuranose in leishmania major macrophage invasion," *Infect Immun*, vol.70, pp. 6592-6596, 2002.
[61]. R.M. de Lederkremer, C.E. Lima, M.I. Ramirez, M.F. Goncalvez, W. Colli, "Hexadecylpalmitoylglycerol or ceramide is linked to similar glycophosphoinositol anchor-like structures in *Trypanosoma cruzi*," *Eur J Biochem*, vol.218, pp. 929-936, 1993.
[62]. R.M. de Lederkremer, "Free and protein-linked glycoinositolphospholipids in *Trypanosoma cruzi*," *Braz J Med Biol Res*, vol.27, pp. 239-242, 1994.
[63]. J.O. Previato, R. Wait, C. Jones, G.A. DosReis, A.R. Todeschini, N. Heise, L.M. Previato, "Glycoinositolphospholipid from *Trypanosoma cruzi*: Structure, biosynthesis and immunobiology," *Adv Parasitol*, vol.56, pp. 1-41, 2004.
[64]. J.I. Macrae, A. Acosta-Serrano, N.A. Morrice, A. Mehlert, M.A. Ferguson, "Structural characterization of NETNES, a novel glycoconjugate in *Trypanosoma cruzi* epimastigotes," *J Biol Chem*, vol.280, pp. 12201-12211, 2005.

[65]. V.L. Pereira-Chioccola, A. Acosta-Serrano, I. Correia de Almeida, M.A. Ferguson, T. Souto-Padron, M.M. Rodrigues, L.R. Travassos, S. Schenkman, "Mucin-like molecules form a negatively charged coat that protects *Trypanosoma cruzi* trypomastigotes from killing by human anti-alpha-galactosyl antibodies," *J Cell Sci*, vol.113 (Pt 7), pp. 1299-1307, 2000.
[66]. E. Suzuki, R.A. Mortara, H.K. Takahashi, A.H. Straus, "Reactivity of MEST-1 (antigalactofuranose) with *Trypanosoma cruzi* glycosylinositol phosphorylceramides (GIPCs): Immunolocalization of GIPCs in acidic vesicles of epimastigotes," *Clin Diagn Lab Immunol*, vol.8, pp. 1031-1035, 2001.
[67]. C.T. Moraes, M. Bosch, A.J. Parodi, "Structural characterization of several galactofuranose-containing, high-mannose-type oligosaccharides present in glycoproteins of the trypanosomatid *Leptomonas samueli*," *Biochemistry*, vol.27, pp. 1543-1549, 1988.
[68]. D.H. Mendelzon, J.O. Previato, A.J. Parodi, "Characterization of protein-linked oligosaccharides in trypanosomatid flagellates," *Mol Biochem Parasitol*, vol.18, pp. 355-367, 1986.
[69]. D.H. Mendelzon, A.J. Parodi, "N-linked high mannose-type oligosaccharides in the protozoa *Crithidia fasciculata* and *Crithidia harmosa* contain galactofuranose residues," *J Biol Chem*, vol.261, pp. 2129-2133, 1986.
[70]. D.C. Turnock, M.A. Ferguson, "Sugar nucleotide pools of *Trypanosoma brucei*, *Trypanosoma cruzi*, and *Leishmania major*," *Eukaryot Cell*, vol.6, pp. 1450-1463, 2007.
[71]. C.A. Buscaglia, V.A. Campo, A.C. Frasch, J.M. Di Noia, "*Trypanosoma cruzi* surface mucins: Host-dependent coat diversity," *Nat Rev Microbiol*, vol.4, pp. 229-236, 2006.
[72]. C. Jones, A.R. Todeschini, O.A. Agrellos, J.O. Previato, L. Mendonca-Previato, "Heterogeneity in the biosynthesis of mucin o-glycans from *Trypanosoma cruzi* Tulahuen strain with the expression of novel galactofuranosyl-containing oligosaccharides," *Biochemistry*, vol.43, pp. 11889-11897, 2004.
[73]. O.A. Agrellos, C. Jones, A.R. Todeschini, J.O. Previato, L. Mendonca-Previato, "A novel sialylated and galactofuranose-containing O-linked glycan, Neu5Acalpha2-->3Gal*p*beta1-->6(Gal*f*beta1-->4)GlcNac, is expressed on the sialoglycoprotein of *Trypanosoma cruzi* Dm28c," *Mol Biochem Parasitol*, vol.126, pp. 93-96, 2003.
[74]. J.O. Previato, C. Jones, L.P. Goncalves, R. Wait, L.R. Travassos, L. Mendonca-Previato, "O-glycosidically linked N-acetylglucosamine-bound oligosaccharides from glycoproteins of *Trypanosoma cruzi*," *Biochem J*, vol.301 (Pt 1), pp. 151-159, 1994.
[75]. A.A. Serrano, S. Schenkman, N. Yoshida, A. Mehlert, J.M. Richardson, M.A. Ferguson, "The lipid structure of the glycosylphosphatidylinositol-anchored mucin-like sialic acid acceptors of *Trypanosoma cruzi* changes during parasite differentiation from epimastigotes to infective metacyclic trypomastigote forms," *J Biol Chem*, vol.270, pp. 27244-27253, 1995.
[76]. I.C. Almeida, M.A. Ferguson, S. Schenkman, L.R. Travassos, "Lytic anti-alpha-galactosyl antibodies from patients with chronic Chagas' disease recognize novel O-linked oligosaccharides on mucin-like glycosyl-phosphatidylinositol-anchored glycoproteins of *Trypanosoma cruzi*," *Biochem J*, vol.304 (Pt 3), pp. 793-802, 1994.
[77]. A. Acosta-Serrano, I.C. Almeida, L.H. Freitas-Junior, N. Yoshida, S. Schenkman, "The mucin-like glycoprotein super-family of *Trypanosoma cruzi*: Structure and biological roles," *Mol Biochem Parasitol*, vol.114, pp. 143-150, 2001.

[78]. A.R. Todeschini, E.X. da Silveira, C. Jones, R. Wait, J.O. Previato, L. Mendonca-Previato, "Structure of O-glycosidically linked oligosaccharides from glycoproteins of *Trypanosoma cruzi* CL-brener strain: Evidence for the presence of O-linked sialyl-oligosaccharides," *Glycobiology*, vol.11, pp. 47-55, 2001.
[79]. J.O. Previato, C. Jones, M.T. Xavier, R. Wait, L.R. Travassos, A.J. Parodi, L. Mendonca-Previato, "Structural characterization of the major glycosylphosphatidylinositol membrane-anchored glycoprotein from epimastigote forms of *Trypanosoma cruzi* Y-strain," *J Biol Chem*, vol.270, pp. 7241-7250, 1995.
[80]. E. Suzuki, M.S. Toledo, H.K. Takahashi, A.H. Straus, "A monoclonal antibody directed to terminal residue of beta-galactofuranose of a glycolipid antigen isolated from *Paracoccidioides brasiliensis*: Cross-reactivity with *Leishmania major* and *Trypanosoma cruzi*," *Glycobiology*, vol.7, pp. 463-468, 1997.
[81]. M.V. De Arruda, W. Colli, B. Zingales, "Terminal beta-D-galactofuranosyl epitopes recognized by antibodies that inhibit *Trypanosoma cruzi* internalization into mammalian cells," *Eur J Biochem*, vol.182, pp. 413-421, 1989.
[82]. J.I. MacRae, S.O. Obado, D.C. Turnock, J.R. Roper, M. Kierans, J.M. Kelly, M.A. Ferguson, "The suppression of galactose metabolism in *Trypanosoma cruzi* epimastigotes causes changes in cell surface molecular architecture and cell morphology," *Mol Biochem Parasitol*, vol.147, pp. 126-136, 2006.
[83]. U. Oppermann, C. Filling, M. Hult, N. Shafqat, X. Wu, M. Lindh, J. Shafqat, E. Nordling, Y. Kallberg, B. Persson, H. Jörnvall, "Short-chain dehydrogenases/reductases (SDR): The 2002 update," *Chemico-Biological Interactions*, vol.143-144, pp. 247-253, 2003.
[84]. M.P. Shaw, C.S. Bond, J.R. Roper, D.G. Gourley, M.A. Ferguson, W.N. Hunter, "High-resolution crystal structure of *Trypanosoma brucei* UDP-galactose 4'-epimerase: A potential target for structure-based development of novel trypanocides," *Mol Biochem Parasitol*, vol.126, pp. 173-180, 2003.
[85]. M.S. Alphey, A. Burton, M.D. Urbaniak, G.J. Boons, M.A. Ferguson, W.N. Hunter, "*Trypanosoma brucei* UDP-galactose-4'-epimerase in ternary complex with NAD+ and the substrate analogue UDP-4-deoxy-4-fluoro-alpha-d-galactose," *Acta Crystallogr Sect F Struct Biol Cryst Commun*, vol.62, pp. 829-834, 2006.
[86]. J.R. Roper, M.L. Guther, J.I. Macrae, A.R. Prescott, I. Hallyburton, A. Acosta-Serrano, M.A. Ferguson, "The suppression of galactose metabolism in procylic form *Trypanosoma brucei* causes cessation of cell growth and alters procyclin glycoprotein structure and copy number," *J Biol Chem*, vol.280, pp. 19728-19736, 2005.
[87]. M.D. Urbaniak, D.C. Turnock, M.A. Ferguson, "Galactose starvation in a bloodstream form *Trypanosoma brucei* UDP-glucose 4'-epimerase conditional null mutant," *Eukaryot Cell*, vol.5, pp. 1906-1913, 2006.
[88]. R.J. Burchmore, D. Rodriguez-Contreras, K. McBride, P. Merkel, M.P. Barrett, G. Modi, D. Sacks, S.M. Landfear, "Genetic characterization of glucose transporter function in *Leishmania mexicana*," *Proc Natl Acad Sci U S A*, vol.100, pp. 3901-3906, 2003.
[89]. M.D. Urbaniak, J.N. Tabudravu, A. Msaki, K.M. Matera, R. Brenk, M. Jaspars, M.A. Ferguson, "Identification of novel inhibitors of UDP-Glc 4'-epimerase, a validated drug target for African Sleeping sickness," *Bioorg Med Chem Lett*, vol.16, pp. 5744-5747, 2006.
[90]. J.D. Durrant, M.D. Urbaniak, M.A. Ferguson, J.A. McCammon, "Computer-aided identification of *Trypanosoma brucei* uridine diphosphate galactose 4'-epimerase inhibitors:

Toward the development of novel therapies for African Sleeping sickness," *J Med Chem*, vol.53, pp. 5025-5032
[91]. A.M. El-Ganiny, D.A. Sanders, S.G. Kaminskyj, "*Aspergillus nidulans* UDP-galactopyranose mutase, encoded by UgmA plays key roles in colony growth, hyphal morphogenesis, and conidiation," *Fungal Genet Biol*, vol.45, pp. 1533-1542, 2008.
[92]. Q. Zhang, H.W. Liu, "Studies of UDP-galactopyranose mutase from *Escherichia coli*: An unusual role of reduced FAD in catalysis," *J Am Chem Soc*, vol.122, pp. 6, 2000.
[93]. D.A.R. Sanders, A.G. Staines, S.A. McMahon, M.R. McNeil, C. Whitfield, J.H. Naismith, "UDP-galactopyranose mutase has a novel structure and mechanism," *Nature Structural Biology*, vol.8, pp. 858-863, 2001.
[94]. M. Soltero-Higgin, E.E. Carlson, T.D. Gruber, L.L. Kiessling, "A unique catalytic mechanism for UDP-galactopyranose mutase," *Nat Struct Mol Biol*, vol.11, pp. 539-543, 2004.
[95]. T.D. Gruber, W.M. Westler, L.L. Kiessling, K.T. Forest, "X-ray crystallography reveals a reduced substrate complex of UDP-galactopyranose mutase poised for covalent catalysis by flavin," *Biochemistry*, vol.48, pp. 9171-9173, 2009.
[96]. Z.H. Huang, Q.B. Zhang, H.W. Liu, "Reconstitution of UDP-galactopyranose mutase with 1-deaza-FAD and 5-deaza-FAD: Analysis and mechanistic implications," *Bioorganic Chemistry*, vol.31, pp. 494-502, 2003.
[97]. K. Beis, V. Srikannathasan, H. Liu, S.W. Fullerton, V.A. Bamford, D.A. Sanders, C. Whitfield, M.R. McNeil, J.H. Naismith, "Crystal structures of *Mycobacteria tuberculosis* and *Klebsiella pneumoniae* UDP-galactopyranose mutase in the oxidised state and *Klebsiella pneumoniae* UDP-galactopyranose mutase in the (active) reduced state," *J Mol Biol*, vol.348, pp. 971-982, 2005.
[98]. S. Karunan Partha, K.E. van Straaten, D.A. Sanders, "Structural basis of substrate binding to UDP-galactopyranose mutase: Crystal structures in the reduced and oxidized state complexed with UDP-galactopyranose and UDP," *J Mol Biol*, pp., 2009.
[99]. D.A. Sanders, S.A. McMahon, G.L. Leonard, J.H. Naismith, "Molecular placement of experimental electron density: A case study on UDP-galactopyranose mutase," *Acta Crystallogr D Biol Crystallogr*, vol.57, pp. 1415-1420, 2001.
[100]. M. Oppenheimer, M.B. Poulin, T.L. Lowary, R.F. Helm, P. Sobrado, "Characterization of recombinant UDP-galactopyranose mutase from *Aspergillus fumigatus*," *Arch Biochem Biophys*, vol.502, pp. 31-38, 2010.
[101]. D.S. Ha, J.K. Schwarz, S.J. Turco, S.M. Beverley, "Use of the green fluorescent protein as a marker in transfected *Leishmania*," *Mol Biochem Parasitol*, vol.77, pp. 57-64, 1996.
[102]. G.F. Spath, L. Epstein, B. Leader, S.M. Singer, H.A. Avila, S.J. Turco, S.M. Beverley, "Lipophosphoglycan is a virulence factor distinct from related glycoconjugates in the protozoan parasite *Leishmania major*," *Proc Natl Acad Sci U S A*, vol.97, pp. 9258-9263, 2000.
[103]. K. Zhang, T. Barron, S.J. Turco, S.M. Beverley, "The Lpg1 gene family of *Leishmania major*," *Mol Biochem Parasitol*, vol.136, pp. 11-23, 2004.
[104]. K.A. Ryan, L.A. Garraway, A. Descoteaux, S.J. Turco, S.M. Beverley, "Isolation of virulence genes directing surface glycosyl-phosphatidylinositol synthesis by functional complementation of *Leishmania*," *Proc Natl Acad Sci U S A*, vol.90, pp. 8609-8613, 1993.
[105]. N.M. El-Sayed, P.J. Myler, D.C. Bartholomeu, D. Nilsson, G. Aggarwal, A.N. Tran, E. Ghedin, E.A. Worthey, A.L. Delcher, G. Blandin, S.J. Westenberger, E. Caler, G.C.

Cerqueira, C. Branche, B. Haas, A. Anupama, E. Arner, L. Aslund, P. Attipoe, E. Bontempi, F. Bringaud, P. Burton, E. Cadag, D.A. Campbell, M. Carrington, J. Crabtree, H. Darban, J.F. da Silveira, P. de Jong, K. Edwards, P.T. Englund, G. Fazelina, T. Feldblyum, M. Ferella, A.C. Frasch, K. Gull, D. Horn, L. Hou, Y. Huang, E. Kindlund, M. Klingbeil, S. Kluge, H. Koo, D. Lacerda, M.J. Levin, H. Lorenzi, T. Louie, C.R. Machado, R. McCulloch, A. McKenna, Y. Mizuno, J.C. Mottram, S. Nelson, S. Ochaya, K. Osoegawa, G. Pai, M. Parsons, M. Pentony, U. Pettersson, M. Pop, J.L. Ramirez, J. Rinta, L. Robertson, S.L. Salzberg, D.O. Sanchez, A. Seyler, R. Sharma, J. Shetty, A.J. Simpson, E. Sisk, M.T. Tammi, R. Tarleton, S. Teixeira, S. Van Aken, C. Vogt, P.N. Ward, B. Wickstead, J. Wortman, O. White, C.M. Fraser, K.D. Stuart, B. Andersson, "The genome sequence of *Trypanosoma cruzi*, etiologic agent of Chagas disease," *Science*, vol.309, pp. 409-415, 2005.

[106]. N.M. El-Sayed, P.J. Myler, G. Blandin, M. Berriman, J. Crabtree, G. Aggarwal, E. Caler, H. Renauld, E.A. Worthey, C. Hertz-Fowler, E. Ghedin, C. Peacock, D.C. Bartholomeu, B.J. Haas, A.N. Tran, J.R. Wortman, U.C. Alsmark, S. Angiuoli, A. Anupama, J. Badger, F. Bringaud, E. Cadag, J.M. Carlton, G.C. Cerqueira, T. Creasy, A.L. Delcher, A. Djikeng, T.M. Embley, C. Hauser, A.C. Ivens, S.K. Kummerfeld, J.B. Pereira-Leal, D. Nilsson, J. Peterson, S.L. Salzberg, J. Shallom, J.C. Silva, J. Sundaram, S. Westenberger, O. White, S.E. Melville, J.E. Donelson, B. Andersson, K.D. Stuart, N. Hall, "Comparative genomics of trypanosomatid parasitic protozoa," *Science*, vol.309, pp. 404-409, 2005.

[107]. D. Kapitonov, R.K. Yu, "Conserved domains of glycosyltransferases," *Glycobiology*, vol.9, pp. 961-978, 1999.

[108]. L.L. Pedersen, S.J. Turco, "Galactofuranose metabolism: A potential target for antimicrobial chemotherapy," *Cell Mol Life Sci*, vol.60, pp. 259-266, 2003.

[109]. P. Gouet, E. Courcelle, D.I. Stuart, F. Metoz, "Espript: Analysis of multiple sequence alignments in postscript," *Bioinformatics*, vol.15, pp. 305-308, 1999.

CHAPTER 3

D-Galactofuranose in *Aspergillus* spp.

Abstract

Aspergillosis is caused by the fungus *Aspergillus fumigatus* and includes both allergic bronchopulmonnary aspergillosis (ABPA) and invasive pulmonary aspergillosis (IPA) [1]. These diseases affect immuno-compromised patients including those with organ transplants, AIDS, and cystic fibrosis [2, 3]. These infections require early detection and treatment as they are associated with a high mortality rate [4]. New drugs are currently needed as treatments are limited and often ineffective [1]. D-galactofuranose (Gal*f*) biosynthesis has become an attractive drug target for *A. fumigatus* as Gal*f* has been shown to be important for virulence, normal conidiation, and normal cellular morphology [5-7]. The role of Gal*f* and the identification of Gal*f* in the cell wall of *A. fumigatus* and the closely related *Aspergillus niger* has become an area of interest for drug discovery to help develop new drugs for the treatment of aspergillosis. This chapter will explore the biosynthesis of Gal*f* and the localization and physiological role of Gal*f* in fungi.

1. Gal*f* Biosynthesis in *Aspergillus* spp.

Gal*f* biosynthesis in *Aspergillus* spp. is initiated by the uptake of galactose by hexose transporters (Figure 1). Galactose is then converted to UDP-galactopyranose (UDP-Gal*p*) by galactokinase (GK) and galactose-1-phosphate uridyl transferase (GalPUT) [8]. UDP-Gal*p* can also be obtained by directly converting UDP-glucose (UDP-Glc) to UDP-Gal*p* by the enzyme UDP-glucose-4'-epimerase (GalE) [8, 9]. UDP-Gal*p* is then converted to UDP-Gal*f* by UDP-galactopyranose mutase (UGM) [10-12]. As UDP-Gal*f* is made in the cytosol by UGM, it must

be transported to the Golgi by the UDP-Gal*f* transporter (UGT) where it then is transferred to different oligosaccharides found on the cell surface by Gal*f* transferases (GalfTs) [7, 13]. Lastly, the Gal*f* containing oliogosacchrides are transported to the cell surface by vesicle transport.

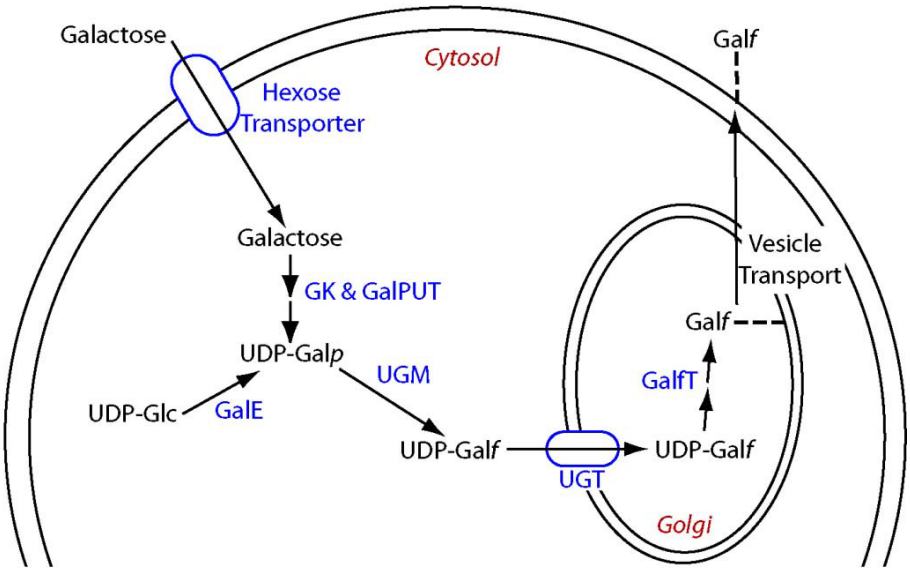

Figure 3.1 Overview of Gal*f* biosynthesis in *Aspergillus* spp. Galactose is uptaken from the environment by hexose transporters and converted to UDP-Gal*p* by galactokinase (GK) and galactose 1- phosphate uridyl transferase (GalPUT). UDP-Gal*p* can also be obtained by converting UDP-Glc to UDP-Gal*p* by UDP-glucose-4'-epimerase (GalE). The pool of UDP-Gal*p* is then isomerized to UDP-Gal*f* by UDP-galactopyranose mutase (UGM). UDP-Gal*f* is transported into the Golgi by UDP-Gal*f* transporter (UGT), where it is then transferred to various oligosaccharides (shown as dashed line) by galactofuranosyltransferases (GalfTs). The Gal*f*-oligosaccharides are then transported to the cell surface by vesicle transport.

2. Gal*f* in *A. fumigatus* and *A. niger*

In *A. fumigatus* and *A. niger* Gal*f* is found in the galactomannan, N-linked and O-linked glycoprotein oligosaccharides, and glycosylinositolphosphoceramides (GIPCs) [14-16]. This section presents the structure of Gal*f*-containing oligosaccharides and the role of Gal*f* in these olgiosaccharides (Figure 2).

2.1 Galactomannan. Galactomannan is a polysaccharide produced by *Aspergillus* spp. which is widely present on the cell wall as a structural support [17, 18]. It is found soluble in media, glycosylphosphatidylinositol (GPI) anchored, or covalently linked to the cell wall β1-3 glucan network [17, 19]. Galactomannan is composed an α-(1→2)-linked mannopyranose dimer with branches at the 6 position containing 4-5 β-Gal*f* residues linked β-(1→5), although differences in branching patterns of the mannose and Gal*f* have been reported (Figure 2A) [20]. These variations are commonly attributed to differences in strains and growth media of the *Aspergillus* [14, 18, 20, 21]. Galactomannan is found to be immunogenic due to the presence of the β-Gal*f* residues. Several monocolonial antibodies from sera have been identified to recognize the Gal*f* residues suggesting the importance for Gal*f* in host-pathogen interactions [19, 20]. These monocolonial antibodies have been shown to be specific for Gal*f* and are used as the primary means of detection of *A. fumigatus* infections in patients [19, 20, 22, 23].

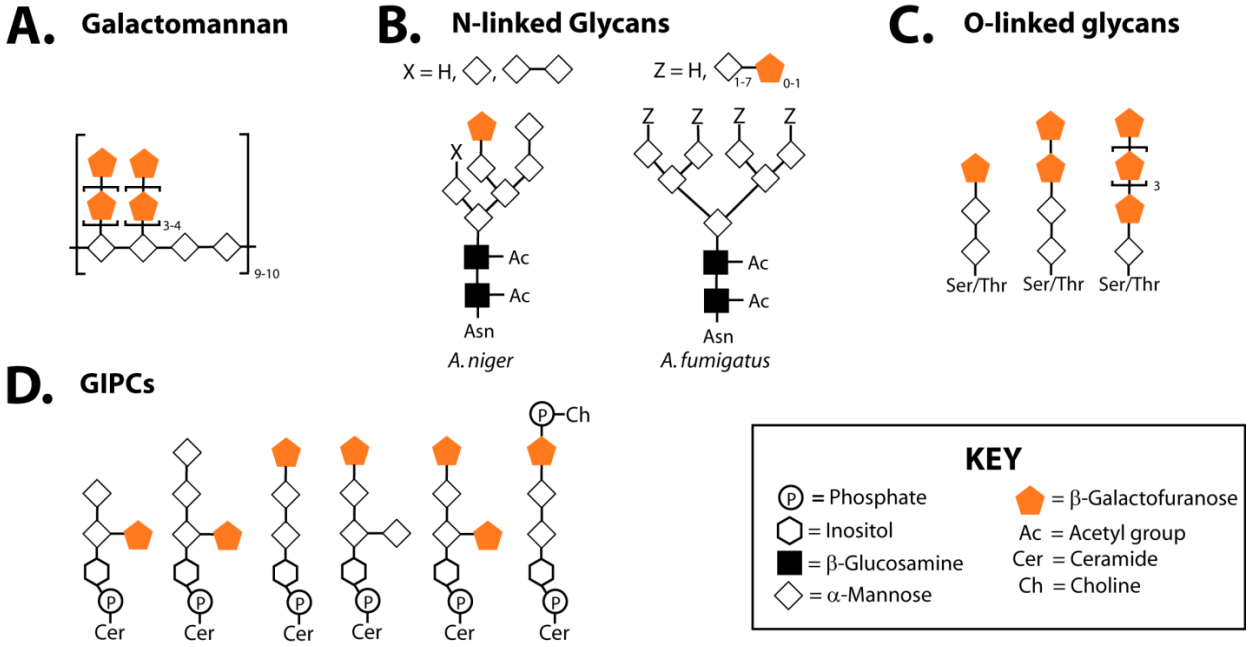

Figure 3.2 Structures of oligosaccharides containing Gal*f* in *A. fumigatus* and *A. niger*. A) Galactomannan of *A. fumigatus*. B) N-linked glycans found in either *A. niger* (left) or *A. fumigatus* (right). C) O-linked glycans from *A. fumigatus*. D) Selected GIPCs containing Gal*f* from *A. fumigatus*.

2.2 N-*linked glycans.* N-linked glycans are present on many glycoproteins secreted by both *A. fumigatus* and *A. niger* [6, 21]. The structures of N-linked glycans have been solved for two proteins (phospholipase C and phytase) in *A. fumigatus* and for a common N-linked glycan in *A. niger* (Figure 2B) [6, 21]. In all of these structures, Gal*f* is found linked at the terminal non-reducing end of a mannose and N-acetylglucosamine core [6, 21]. The Gal*f* of the N-linked glycans is found to be important for recognition of *A. fumigatus* by human sera and is shown to be antigenic [21].

2.3 O-*linked glycans.* The structures of the O-linked glycans found in *A. fumigatus* include α-(1→6) manosyl chains that can be capped with various lengths of Gal*f* residues (Figure 2C) [24]. These glycans are found to be antigenic, with the strongest affect attributed to the Gal*f* component [24]. It was found that de-O-glycosylation of *A. fumigatus* decreased human sera reactivity by 50% [24]. It was also shown that incubating free oligosaccharides of the same structure of the O-glycans with human sera and *A. fumigatus* resulted in 65% decrease in recognition of phosphoglycomannan by human sera. Both of these results show O-glycans are important for host-pathogen interactions [24].

2.4 Glycosylinositolphosphoceramides. Glycosylinositolphosphoceramides (GIPCs) are acidic glycosphingolipids with an inositol phosphoceramide core [25]. GIPCs are known to play roles in cell regulation, polarity, trafficking, stress response, and cell wall integrity [26]. GIPC chains are rich in mannose residues and can have short branches [25]. There have been several GIPCs identified that contain terminal Gal*f* units (Figure 2D) [25, 27]. The terminal Gal*f* residues are recognized by antibodies, however the role of GIPCs in immunity is currently unknown [25].

3. Importance Gal*f* Biosynthesis in *A. fumigatus* and *A. niger*

Gal*f* is expressed primarily in swollen mature conidia, germ tubes, and phialides in both *A. fumigatus* and *A. niger* [28, 29]. The importance of Gal*f* in virulence, cell morphology, and in temperature and fungicide sensitivities has been explored by the deleting either the UGM or UGT gene in both *A. fumigatus* and *A. niger*.

The importance of UGM has been examined in detail. UGM localization and expression studies showed UGM is cytosolic and highly expressed during germ tube formation by Q-RTPCR [5, 13]. UGM was also shown to be activated during the cell wall stress response pathway by complementation studies [12]. Deletion of UGM in both *A. niger* and *A. fumigatus* show the importance for Gal*f* as lack of UGM activity resulted in compact colony growth and wide highly branched hyphae [5, 6, 28, 30]. The cell walls were shown to have abnormal architecture; in *A. niger* there was an increased cell wall thickness, while in *A. fumigatus* the cell walls were reported to be thinner [6, 28, 30]. In all studies with the UGM deletion strains in *A. fumigatus* and *A. niger*, the colonies also showed decreased and delayed conidiation (slowed reproduction and growth cycle) [5, 6, 28, 30]. These studies also showed an increased sensitivity to temperature [6, 12]. One study with the *A. fumigatus* deletion strain showed attenuated virulence and increased sensitivities to the fungal drugs, voriconazole and nikkomycin Z [6].

UGT transports UDP-Gal*f* from the cytosol to the Golgi in exchange for UDP [7]. Deletion strains of UGT were made for both *A. niger* and *A. fumigatus*. The studies of the UGT deletion strains reported similar results to the studies done on the UGM deletion strains [7, 13]. It was found that the deletion strains had compact colonies, wide highly branched hyphae, reduced conidiation, and increased sensitivity to temperature stress [7, 13]. The *A. niger* UGT

deletion strain also had increased cell wall thickness, attenuated virulence, and increased sensitivity to the fungal drug, caspofugin [13].

These studies show both of the proteins UGM and UGT are important for normal fungal morphology and growth verifying the importance for Gal*f* biosynthesis in *A. fumigatus* and *A. niger* and verifying these proteins are potential drug targets.

4. Summary

Gal*f* has been found to be incorporated into several oligosaccharides located on the cell wall of *A. fumigatus* and *A. niger*. Gal*f* is shown to interact with specific antibodies isolated from sera demonstrating Gal*f* plays a role in infection. The protein UGM is central to Gal*f* biosynthesis and has been shown to be a virulence factor in *A. fumigatus* and *A. niger* proving UGM is an ideal drug target for fungi. Developing an understanding of the structure and mechanism of UGM from *Aspergillus* will lead to design of new inhibitors for the treatment of aspergillosis. The UGM from *A. fumigatus* is examined in detail in Chapters 4 and 7.

5. References

[1]. B.H. Segal, "Aspergillosis," *N Engl J Med*, vol.360, pp. 1870-1884, 2009.

[2]. C. Virnig, R.K. Bush, "Allergic bronchopulmonary aspergillosis: A US perspective," *Curr Opin Pulm Med*, vol.13, pp. 67-71, 2007.

[3]. S. Chong, T.S. Kim, W.J. Koh, E.Y. Cho, K. Kim, "Case report: Invasive pulmonary aspergillosis complicated by pulmonary artery occlusion in an immunocompetent patient," *Clin Radiol*, vol.61, pp. 287-290, 2006.

[4]. G. Chamilos, M. Luna, R.E. Lewis, G.P. Bodey, R. Chemaly, J.J. Tarrand, A. Safdar, Raad, II, D.P. Kontoyiannis, "Invasive fungal infections in patients with hematologic malignancies in a tertiary care cancer center: An autopsy study over a 15-year period (1989-2003)," *Haematologica*, vol.91, pp. 986-989, 2006.

[5]. C. Lamarre, R. Beau, V. Balloy, T. Fontaine, J.W. Hoi, S. Guadagnini, N. Berkova, M. Chignard, A. Beauvais, J.P. Latge, "Galactofuranose attenuates cellular adhesion of *Aspergillus fumigatus*," *Cell Microbiol*, vol.11, pp. 1612-1623, 2009.

[6]. P.S. Schmalhorst, S. Krappmann, W. Vervecken, M. Rohde, M. Muller, G.H. Braus, R. Contreras, A. Braun, H. Bakker, F.H. Routier, "Contribution of galactofuranose to the virulence of the opportunistic pathogen *Aspergillus fumigatus*," *Eukaryot Cell*, vol.7, pp. 1268-1277, 2008.

[7]. J. Engel, P.S. Schmalhorst, T. Dork-Bousset, V. Ferrieres, F.H. Routier, "A single UDP-galactofuranose transporter is required for galactofuranosylation in *Aspergillus fumigatus*," *J Biol Chem*, pp., 2009.

[8]. P.A. Frey, "The Leloir pathway: A mechanistic imperative for three enzymes to change the stereochemical configuration of a single carbon in galactose," *FASEB J*, vol.10, pp. 461-470, 1996.

[9]. H.M. Holden, I. Rayment, J.B. Thoden, "Structure and function of enzymes of the Leloir pathway for galactose metabolism," *J Biol Chem*, vol.278, pp. 43885-43888, 2003.

[10]. S.M. Beverley, K.L. Owens, M. Showalter, C.L. Griffith, T.L. Doering, V.C. Jones, M.R. McNeil, "Eukaryotic UDP-galactopyranose mutase (Glf gene) in microbial and metazoal pathogens," *Eukaryot Cell*, vol.4, pp. 1147-1154, 2005.

[11]. P.M. Nassau, S.L. Martin, R.E. Brown, A. Weston, D. Monsey, M.R. McNeil, K. Duncan, "Galactofuranose biosynthesis in *Escherichia coli* K-12: Identification and cloning of UDP-galactopyranose mutase," *J Bacteriol*, vol.178, pp. 1047-1052, 1996.

[12]. R.A. Damveld, A. Franken, M. Arentshorst, P.J. Punt, F.M. Klis, C.A. van den Hondel, A.F. Ram, "A novel screening method for cell wall mutants in *Aspergillus niger* identifies UDP-galactopyranose mutase as an important protein in fungal cell wall biosynthesis," *Genetics*, vol.178, pp. 873-881, 2008.

[13]. S. Afroz, A.M. El-Ganiny, D.A. Sanders, S.G. Kaminskyj, "Roles of the *Aspergillus nidulans* UDP-galactofuranose transporter, UgtA in hyphal morphogenesis, cell wall architecture, conidiation, and drug sensitivity," *Fungal Genet Biol*, vol.48, pp. 896-903, 2011.

[14]. B. Tefsen, A.F. Ram, I. van Die, F.H. Routier, "Galactofuranose in eukaryotes: Aspects of biosynthesis and functional impact," *Glycobiology*, pp., 2012.

[15]. J.P. Latge, "Galactofuranose containing molecules in *Aspergillus fumigatus*," *Med Mycol*, vol.47 Suppl 1, pp. S104-109, 2009.

[16]. M. Bernard, J.P. Latge, "*Aspergillus fumigatus* cell wall: Composition and biosynthesis," *Med Mycol*, vol.39 Suppl 1, pp. 9-17, 2001.
[17]. C. Costachel, B. Coddeville, J.P. Latge, T. Fontaine, "Glycosylphosphatidylinositol-anchored fungal polysaccharide in *Aspergillus fumigatus*," *J Biol Chem*, vol.280, pp. 39835-39842, 2005.
[18]. T. Fontaine, C. Simenel, G. Dubreucq, O. Adam, M. Delepierre, J. Lemoine, C.E. Vorgias, M. Diaquin, J.P. Latge, "Molecular organization of the alkali-insoluble fraction of *Aspergillus fumigatus* cell wall," *J Biol Chem*, vol.275, pp. 27594- 27607, 2000.
[19]. E. Reiss, P.F. Lehmann, "Galactomannan antigenemia in invasive aspergillosis," *Infect Immun*, vol.25, pp. 357-365, 1979.
[20]. J.P. Latge, H. Kobayashi, J.P. Debeaupuis, M. Diaquin, J. Sarfati, J.M. Wieruszeski, E. Parra, J.P. Bouchara, B. Fournet, "Chemical and immunological characterization of the extracellular galactomannan of *Aspergillus fumigatus*," *Infect Immun*, vol.62, pp. 5424-5433, 1994.
[21]. W. Morelle, M. Bernard, J.P. Debeaupuis, M. Buitrago, M. Tabouret, J.P. Latge, "Galactomannoproteins of *Aspergillus fumigatus*," *Eukaryot Cell*, vol.4, pp. 1308-1316, 2005.
[22]. M.A.S.H. Mennink-Kersten, D. Ruegebrink, R.R. Klont, A. Warris, N.M.A. Blijlevens, J.P. Donnelly, P.E. Verweij, "Improved detection of circulating aspergillus antigen by use of a modified pretreatment procedure," *J Clin Microbiol*, vol.46, pp. 1391-1397, 2008.
[23]. D. Stynen, J. Sarfati, A. Goris, M.C. Prevost, M. Lesourd, H. Kamphuis, V. Darras, J.P. Latge, "Rat monoclonal antibodies against aspergillus galactomannan," *Infect Immun*, vol.60, pp. 2237-2245, 1992.
[24]. E.A. Leitao, V.C. Bittencourt, R.M. Haido, A.P. Valente, J. Peter-Katalinic, M. Letzel, L.M. de Souza, E. Barreto-Bergter, "Beta-galactofuranose-containing O-linked oligosaccharides present in the cell wall peptidogalactomannan of *Aspergillus fumigatus* contain immunodominant epitopes," *Glycobiology*, vol.13, pp. 681-692, 2003.
[25]. C. Simenel, B. Coddeville, M. Delepierre, J.P. Latge, T. Fontaine, "Glycosylinositolphosphoceramides in *Aspergillus fumigatus*," *Glycobiology*, vol.18, pp. 84-96, 2008.
[26]. R.C. Dickson, C. Sumanasekera, R.L. Lester, "Functions and metabolism of sphingolipids in *Saccharomyces cerevisiae*," *Prog Lipid Res*, vol.45, pp. 447-465, 2006.
[27]. M.S. Toledo, S.B. Levery, B. Bennion, L.L. Guimaraes, S.A. Castle, R. Lindsey, M. Momany, C. Park, A.H. Straus, H.K. Takahashi, "Analysis of glycosylinositol phosphorylceramides expressed by the opportunistic mycopathogen *Aspergillus fumigatus*," *J Lipid Res*, vol.48, pp. 1801-1824, 2007.
[28]. A.M. El-Ganiny, D.A. Sanders, S.G. Kaminskyj, "*Aspergillus nidulans* UDP-galactopyranose mutase, encoded by UgmA plays key roles in colony growth, hyphal morphogenesis, and conidiation," *Fungal Genet Biol*, vol.45, pp. 1533-1542, 2008.
[29]. L. Heesemann, A. Kotz, B. Echtenacher, M. Broniszewska, F.O. Routier, P. Hoffmann, F. Ebel, "Studies on galactofuranose-containing glycostructures of the pathogenic mold *Aspergillus fumigatus*," *International Journal of Medical Microbiology*, vol.301, pp. 523-530, 2011.
[30]. B.C. Paul, A.M. El-Ganiny, M. Abbas, S.G. Kaminskyj, T.E. Dahms, "Quantifying the importance of galactofuranose in *Aspergillus nidulans* hyphal wall surface organization by atomic force microscopy," *Eukaryot Cell*, vol.10, pp. 646-653, 2011.

CHAPTER 4

Characterization of recombinant UDP-galactopyranose mutase from *Aspergillus fumigatus*

Reprinted from Archives of Biochemistry and Biophysics, Vol 502 (1) Oppenheimer, M., Poulin, M.B., Lowary, T.L., Helm, R.F., and Sobrado, P. "Characterization of recombinant UDP-galactopyranose mutase from *Aspergillus fumigatus*," pp. 31-38, Copyright (2010), with permission from Elsevier.

Author Contributions:
Michelle Oppenheimer performed all the research except the experiments mentioned below and helped write the article.

Myles Poulin and Todd Lowary provided the UDP-Gal*f* for the activity assay.

Richard Helm performed the mass spectrometry analysis and helped with UDP-Gal*f* synthesis.

Pablo Sobrado oversaw and directed the research, and helped write the article.

Abstract

UDP-Galactopyranose mutase (UGM) is a flavin-containing enzyme that catalyzes the conversion of UDP-galactopyranose to UDP-galactofuranose, the precursor of galactofuranose, which is an important cell wall component in *Aspergillus fumigatus* and other pathogenic microbes. *A. fumigatus* UGM (AfUGM) was expressed in *Escherichia coli* and purified to homogeneity. The enzyme was shown to function as a homotetramer by size exclusion chromatography and to contain ~50% of the flavin in the active reduced form. A k_{cat} value of 72 ± 4 s^{-1} and a K_M value of 110 ± 15 μM were determined with UDP-galactofuranose as substrate. In the oxidized state, AfUGM does not bind UDP-galactopyranose, while UDP and UDP-glucose bind with K_d values of 33 ± 9 μM and 90 ± 30 μM, respectively. Functional and structural differences between the bacterial and eukaryotic UGMs are discussed.

1. Introduction

Human pathogenic fungi of the genus *Aspergillus* are responsible for severe human diseases ranging from allergic reactions and lung infections to sepsis and death [1]. There are hundreds of members of the *Aspergillus* genus, but only a few have been identified as pathogenic to humans, with *A. fumigatus* and *A. niger* being the most common [1, 2]. Among the diseases related to *Aspergillus* infection, allergic bronchopulmonary aspergillosis (ABPA) and invasive pulmonary aspergillosis (IPA) represent significant health threats to immunocompetent and immunocompromised persons [3, 4]. IPA infections are commonly observed in patients receiving chemotherapy, organ transplants, and in late-stage AIDS [4]. A 0.3% to 5.8% increase in IPA infections in patients admitted to intensive care units (ICUs) has been reported in recent years and IPA infections are accompanied by a high mortality rate (50-70%) [5].

Chemotherapeutic treatments against *Aspergillus* spp. include compounds that inhibit the biosynthesis of cell wall components such as β-1, 3-glucan. Inhibition of cell wall biosynthesis renders the fungi more susceptible to osmotic stress, leading to cell lysis [6]. Cell wall biosynthesis in *Aspergillus* spp. is an attractive target for chemical intervention since enzymes in this biosynthetic pathway are absent in humans [7]. A major component of the cell wall of *A. fumigatus* is galactofuranose (Gal*f*), the 5-membered ring form of galactose [8]. The presence of Gal*f* in *A. fumigatus* has been known for many years and was first identified as a component of galactomannan by immunodetection in patients suffering from IPA [9]. Gal*f* has also been shown to be a major component of saccharide structures in secreted molecules, membrane lipids, and glycosyl phosphoinositol (GPI)-anchored lipophosphogalactomannan in *Aspergillus* spp. [9]. In bacteria, the biosynthesis of Gal*f* has been well characterized and involves the action of UDP-galactopyranose mutase (UGM), a flavin-dependent enzyme that catalyzes the conversion of

UDP-galactopyranose (UDP-Gal*p*) to UDP-galactofuranose (UDP-Gal*f*) (Scheme 1) [10]. UGM homologues have been identified in eukaryotic organisms such as *A. fumigatus, A. niger, Leishmania major*, and *Trypanosoma cruzi* [11-13]. *A. fumigatus* UGM (AfUGM) has been shown to be an important virulence factor. Screening for genes involved in cell wall biosynthesis in *A. niger* identified UGM activity as important in cell wall biogenesis [14]. Deletion of the AfUGM gene leads to attenuated virulence, diminished cell wall thickness, and increased sensitivity to antifungal agents [13]. These results clearly indicate that AfUGM is an attractive target for the identification of new antifungal drugs. Here, we report the functional expression and characterization of the recombinant AfUGM enzyme.

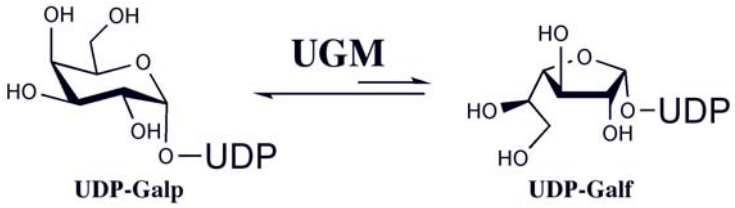

Scheme 4.1 Reaction catalyzed by AfUGM

2. Materials and Methods

2.1 Materials. UDP and UDP-galactopyranose were purchased from Sigma (St Louis, MO). Accuprime polymerase, TOP-10, and BL21TI^{R} chemical competent cells were obtained from Invitrogen (Carlsbad, CA). The restriction endonucleases *Sgf*I and *Pme*I were obtained from Promega (Madison, WI) and plasmid miniprep and PCR purification kits were from Qiagen (Valencia, CA). All other buffers and chemicals were purchased from Fisher Scientific (Pittsburgh, PA). Expression plasmids, pVP55A and pVP56K, were obtained from the Center for Eukaryotic Structural Genomics, University of Wisconsin, Madison [15].

2.2 Subcloning. The gene coding for *A. fumigatus* UGM cloned into pET21 was obtained from Dr. Françoise H. Routier (Hannover Medical School, Hannover, Germany). The gene was amplified by PCR using 5'-ggttgcgatcgccatgacccaccccgatatctccg-3'(*Sgf*I site is underlined) as the forward primer and 5'-aaaagtttaaacttactgggccttgctcttggc-3' (*Pme*I site is underlined) as the reverse primer. After electrophoreses in a 0.8% agarose gel, the PCR product was excised and purified using a Qiagen PCR clean-up kit. The purified product was digested with the restriction enzymes *Sgf*I and *Pme*I for 40 min at 37 °C. The product of this reaction was ligated into the plasmids pVP55A and pVP56K, which were previously treated with *Sgf*I and *Pme*I. The AfUGM gene cloned in pVP55A was expressed as a fusion protein to an 8x-His tag. In pVP56K, the gene was cloned for expression as a fusion protein to an 8x-His-maltose binding protein (8x-His-MBP) [16]. In both plasmids, the gene was under control of the T5 promoter and could be induced by addition of isopropyl-β-thiogalactopyranoside (IPTG). pVP55A provides resistance to ampicillin and pVP56K provides resistance to kanamycin [15].

2.3 Protein Expression. Cell growth was performed in media containing either 25 μg/ml kanamycin or 100 μg/mL ampicillin, depending on whether the cells were transformed with pVP56K or pVP55A, respectively. Plasmids containing the AfUGM gene were transformed into chemically competent BL21T1^{R} cells and plated onto Luria-Bertani (LB) agar plates supplemented with the appropriate antibiotic and incubated overnight at 37 °C. A 60 ml LB/antibiotic culture was inoculated with a single colony and incubated at 37 °C with agitation (250 rpm) overnight. The next day, 6 flasks each containing 1.5 L of LB/antibiotic were inoculated with 10 mL of overnight culture and incubated at 37 °C with agitation (250 rpm). Cell growth was monitored by measuring the optical density at 600 nm (OD_{600}) until a value of 0.6

was reached, at which point IPTG was added to a final concentration of 0.200 mM to induce the expression of the recombinant AfUGM enzyme. Cells were harvested by centrifugation at 5000*g* for 20 min after 4 h induction at 20 °C. The final cell pellet was stored at -80 °C. This procedure typically yielded ~ 30 g of cell paste. Expression of AfUGM cloned in pVP56K was also done using auto-induction medium following previously published protocols [17]. Using auto-induction, the final yield of cell paste was ~60 g from 6 L of auto-induction medium.

2.4 Protein purification. Cell pellets (~30 g) were resuspended in 150 ml of 25 mM HEPES, 300 mM NaCl, and 20 mM imidazole at pH 7.5 containing 25 µg/mL each of lysozyme, DNase, and RNase, and 1 mM phenylmethylsulfonyl fluoride (PMSF) and stirred for 30 min at 4 °C. Resuspended cells were disrupted by sonication with pulse-rest cycles, 5s on-10 s off, for a total of 3 min. During sonication the solution was kept on ice. Unlysed cells and insoluble proteins were precipitated by centrifugation at 30,000*g* for 45 min at 4 °C. The resulting supernatant was loaded onto a nickel immobilized affinity chromatography (IMAC) column previously equilibrated in 20 mM HEPES, 300 mM NaCl, and 20 mM imidazole at pH 7.5. Three column volumes of the same buffer were used as a wash step. Bound proteins were eluted with an imidazole gradient from 20 to 300 mM in the same buffer. Fractions that contained AfUGM were easily identified due to the bright yellow color characteristic of flavoproteins and by SDS-PAGE analysis. To remove the fusion tags, 8x-His-MBP-AfUGM or 8x-His-AfUGM were treated with 6x-His-tobacco etch virus (6x-His-Tev) protease (1:20 ratio) overnight at 4 °C with slow stirring. The resulting sample was centrifuged at 30,000*g* for 20 min to pellet denatured proteins. The supernatant was diluted 4-fold and loaded back onto the IMAC, and the flow-through containing AfUGM was collected. This sample was concentrated and diluted by addition

of 25 mM HEPES, pH 7.5, to decrease the NaCl concentration to less than 30 mM, and loaded onto an diethyl amino ethyl (DEAE) ion exchange chromatography column equilibrated with 25 mM HEPES, pH 7.5. A gradient from 0 to 400 mM NaCl was used to elute the bound proteins; *Af*UGM eluted early in the gradient (~80 mM). Fractions containing AfUGM were pooled, concentrated, and stored at -80 °C.

2.5 UV-visible spectrophotometry. The spectrum of recombinant AfUGM was recorded using an Agilent 8453 UV-visible spectrophotometer. The spectrum shows peaks at 278 nm, 373 nm, and 450 nm with a shoulder at 470 nm (Figure 1).

2.6 Flavin oxidation/reduction studies. AfUGM (10-15 μM) was reduced by addition of excess dithionite and spectra were monitored until all excess dithionite was consumed. The cuvette was exposed to air to allow the reduced enzyme to react with molecular oxygen. The spectra were recorded for at least 30 min. After no further flavin oxidation was observed, 0.5 mM UDP or UDP-Gal*p* was added to the reaction and monitored for 15 min until no further changes in the flavin spectrum were observed. To determine the extinction coefficient, protein was heat denatured at 95 ^{o}C for 10 min and centrifuged in a table top centrifuge for 10 min to pellet the precipitated protein. A spectrum of the resulting solution was recorded.

2.7 Activity Assay. The activity of recombinant AfUGM was tested by monitoring the formation of UDP-Gal*f* from UDP-Gal*p* by HPLC. The assay was performed in 0.1 mL of 25 mM HEPES, 125 mM NaCl, 20 mM dithionite, 0.5 mM UDP-Gal*p* at pH 7.5, and the reaction was initiated by addition of 50 nM AfUGM. Concentration of AfUGM was determined using the flavin

extinction coefficient at 450 nm, ε_{450}= 10.6 $mM^{-1}cm^{-1}$. The reaction was incubated at 37 °C for 10 min and terminated by heat denaturation, 95 ^{o}C for 5 min, in a DNA engine thermo cycler (BioRad, Hercules, CA) . The resulting mixture was injected on a PA-100 (Dionex) HPLC column on a Shimadzu Prominence UFLC with a flow rate of 0.8 mL/min. The sample was eluted isocratically with 75 mM KH_2PO_4, pH 4.5. Absorbance at 262 nm was monitored to identify fractions containing substrate and product. Under these conditions, UDP-Gal*p* eluted at 24.8 min and UDP-Gal*f* at 31.5 min. The extent of conversion was determined by comparing the integration of the substrate and product peaks (as the extinction coefficients for both the product and substrate are the same at 262 nm). Activity of AfUGM was also monitored in the reverse direction, monitoring UDP-Gal*f* isomerization to UDP-Gal*p*. UDP-Gal*f* was synthesized using published protocols [18, 19]. Increasing amounts of UDP-Gal*f* (20- 800 μM) were incubated with 50 nM AfUGM for 1 min at 37 ^{o}C, then the reaction was stopped by heat denaturation at 95 ^{o}C for 5 min. The formation of UDP-Gal*p* was determined by HPLC as indicated above.

2.8 Determination of active redox state. To determine if AfUGM was active in the oxidized or reduced state, the enzyme was assayed with 0.5 mM UDP-Gal*p* in the presence or absence of 20 mM dithionite as described above. To ensure that AfUGM was completely oxidized, the enzyme was reacted with 0.5 mM of cytochrome c, ferricyanide, or dichloroindophenol (DCIP) before the activity was measured.

2. 9 Molecular weight determination. The molecular mass of the recombinant AfUGM in solution was determined using size-exclusion chromatography. The purified AfUGM was loaded onto a Superdex 200 column (GE Healthcare) equilibrated with 25 mM HEPES at pH 7.5

containing 125mM NaCl. Using a set of protein standards (aproprotein (6.5 kDa), ribonuclease (13 kDa), carbonic anhydrase (29 kDa), ovalbumin (43 kDa), canolbumin (75 kDa), aldolase (158 kDa), and ferritin (440 kDa)), a standard curve was obtained by plotting the log of molecular weight versus K_{av} for the standards [20]. The molecular weight of AfUGM was determined to be 275,000 ± 20,000 Da, suggesting that in solution AfUGM functions as a tetramer (57,152 Da per monomer).

2.10 Fluorescence Assay. Fluorescence of AfUGM (20 μM) was measured with a SpectraMax M5e plate reader (Molecular Devices) using 450 nm as the excitation wavelength and the fluorescence spectrum was obtained from 500 nm to 700 nm. Ligand binding was monitored by measuring the changes in fluorescence at 520 nm upon addition of UDP, UDP-Gal*p*, or UDP-Glucose (UDP-Glc). The data were analyzed by subtracting the fluorescence value at 520 nm in the absence of ligand (S), and dividing this value by the maximum fluorescence value (S_{max}). The data were fit to $S= (S_{max}*[Ligand])/(K_d + [Ligand])$ where K_d is the dissociation constant.

2.11 Circular Dichroism Spectroscopy. Circular dichroism (CD) spectra were recorded on a Jasco J-815 spectropolarimeter. For acquisition of far-UV CD spectra, AfUGM (1.1 μM) was placed in a buffer consisting of 10 mM potassium phosphate, pH 7.5, and 50 mM KF. Experiments were performed in a 1-mm path length quartz cell at room temperature. The CD spectra was obtained from the average of five scans from 190 to 250 nm using a bandwidth of 1-nm and a response time of 1 s at a scan speed of 20 nm/min. Buffer backgrounds were subtracted from the protein spectra. Spectra were deconvoluted to estimate secondary structure content with the online server DichroWeb [21].

2.12 Mass spectrum analysis. Purified AfUGM was precipitated by addition of equal volumes of methanol and precipitated by centrifugation at 10,000*g*. The denatured protein was washed with methanol to remove excess buffer and salt. The sample was analyzed using a liquid chromatography electrospray ionization-mass spectrometer (LC-MS). To determine the type of flavin bound to AfUGM, the cofactor was removed by heating the protein at 95 °C for 5 min and precipitating the denatured protein by centrifugation for 10 min at 10,000*g*. The supernatant was analyzed by matrix-assisted laser desorption/ionization time of flight (MALDI-TOF) mass spectrometry.

3. Results

3.1 Expression and purification of recombinant AfUGM. The gene coding for AfUGM was cloned into two plasmids, pVP55A and pVP56K, for the expression of the recombinant protein with two fusion tags, an 8x-His and an 8x-His-MBP, respectively. Expression was done either using LB or auto-induction media [17]. When AfUGM was expressed as a fusion to 8x-His, the protein was soluble. However, the solubility was enhanced by expression of the protein as a fusion to 8x-His-MBP. Recombinant AfUGM was isolated using a nickel IMAC, followed by removal of the fusion tag by treatment with Tev protease, which also contained an 6x-His tag. This allowed for the isolation of free AfUGM from the Tev and 8x-His tag by loading the sample back onto an IMAC and collecting the yellow flow-through. A final step using a DEAE column was needed to obtain highly pure AfUGM (Figure 1). In general, the purification of 8x-His-*Af*UGM yielded 2 mg of protein per gram of cell paste and a 2-fold increase was obtained with

8x-His-MBP-AfUGM. We generally obtained twice the amount of cell mass and purified protein using the auto-induction method.

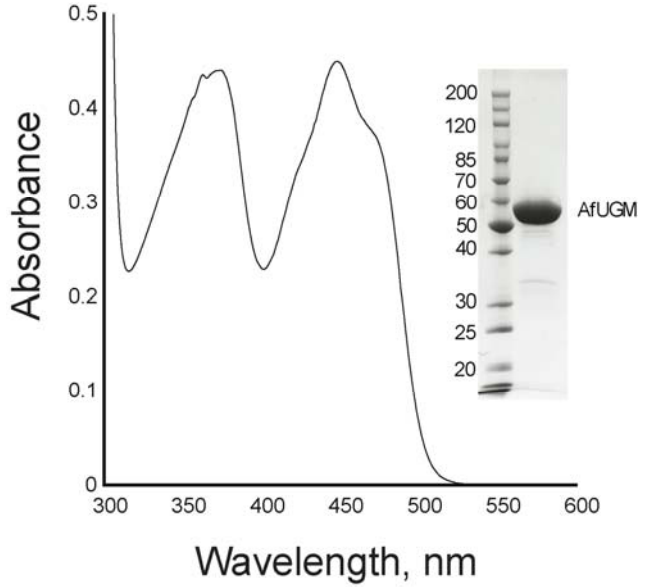

Figure 4.1 Spectrum of the flavin cofactor in recombinant AfUGM. The insert shows a coomasie stained SDS-PAGE of the purified enzyme.

3.2 Redox active form of AfUGM. Initial characterization of bacterial UGM reported that the recombinant enzyme from *E. coli* was active in the oxidized state [22]. Later, it was shown that bacterial UGMs are two orders of magnitude more active in the reduced form, demonstrating that this is the active state [23]. Our initial activity assays with recombinant AfUGM showed very surprising results. The enzyme was active in the oxidized state, only being 2-3 fold less active than in the reduced state, and the activity varied significantly from each protein preparation. We tested the possibility that a fraction of AfUGM was partially reduced by treating the enzyme with the common electron acceptors ferricyanide, DCIP, or cytochrome c and then testing the activity after oxidation by these compounds. Results are shown in Figure 2. In the oxidized state, AfUGM was 30-50 % as active as in the reduced state. Upon incubating AfUGM with cytochrome c, the activity remained at levels similar to those in the oxidized state, indicating that cytochrome c does not interact with AfUGM. In contrast, upon treatment with either ferricyanide

or DCIP, no activity was observed with AfUGM, suggesting that these small molecules can accept electrons from the flavin cofactor in AfUGM, a feature observed in many flavoenzymes [24, 25]. AfUGM treated with either ferricyanide or DCIP is not inactivated, since the enzyme is active upon reduction by addition of excess dithionite (not shown). Thus, the active form of AfUGM is the reduced state.

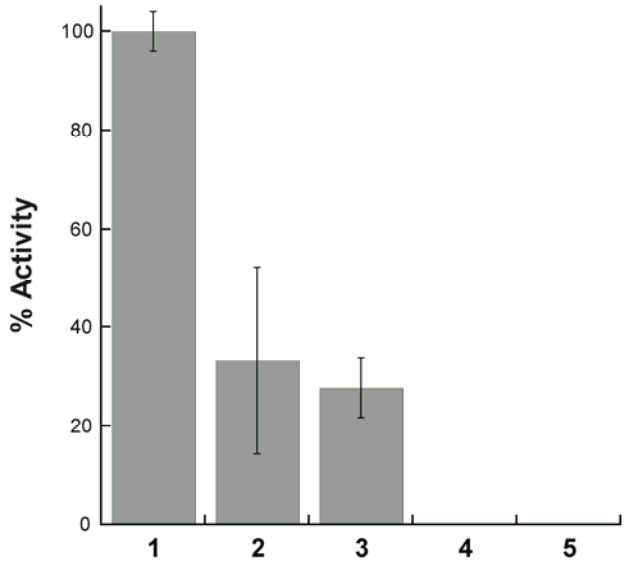

Figure 4.2 Determination of the active redox state of AfUGM. UDP-Gal*p* (0.5 mM) was incubated with AfUGM and 20 mM dithionite (1), AfUGM as purified (2), after reacting with 0.5 mM cytochrome c (3), 0.5 mM $[Fe(CN)_6]^{-3}$ (4), or 0.5 mM DCIP (5). The samples were incubated for one minute and the product analyzed by HPLC as described in the Materials and Methods.

3.3 Redox state of recombinant AfUGM. As indicated in the previous section, AfUGM is active when the flavin cofactor is in the reduced state. Interestingly, even though the recombinant enzyme is isolated under aerobic conditions the enzyme is ~50% as active as the fully reduced enzyme. Upon addition of dithionite, a spectrum corresponding to fully reduced flavin is obtained. Upon exposure to air, oxidation of the cofactor back to the initial oxidized state is observed. Surprisingly, if the concentration of the bound flavin is measured after heat denaturation is performed, approximately 50% more flavin is observed (Figure 3A). These

results suggest that even in the presence of oxygen AfUGM is capable of stabilizing ~50 % of the flavin in the reduced state. Complete oxidation of the enzyme was achieved by addition of UDP. Binding of UDP was accompanied by changes in the flavin spectrum and oxidation of the total flavin bound to AfUGM (Figure 3B). Addition of substrate also leads to oxidation AfUGM, however, binding of UDP-Gal*p* did not cause changes in the flavin spectrum and the rate of oxidation was ~10 fold lower than with UDP. Furthermore, complete oxidation of the flavin was not achieved even after 20 min incubation. The ability of AfUGM to stabilize the reduced form of the flavin is a unique feature not previously reported in UGM enzymes.

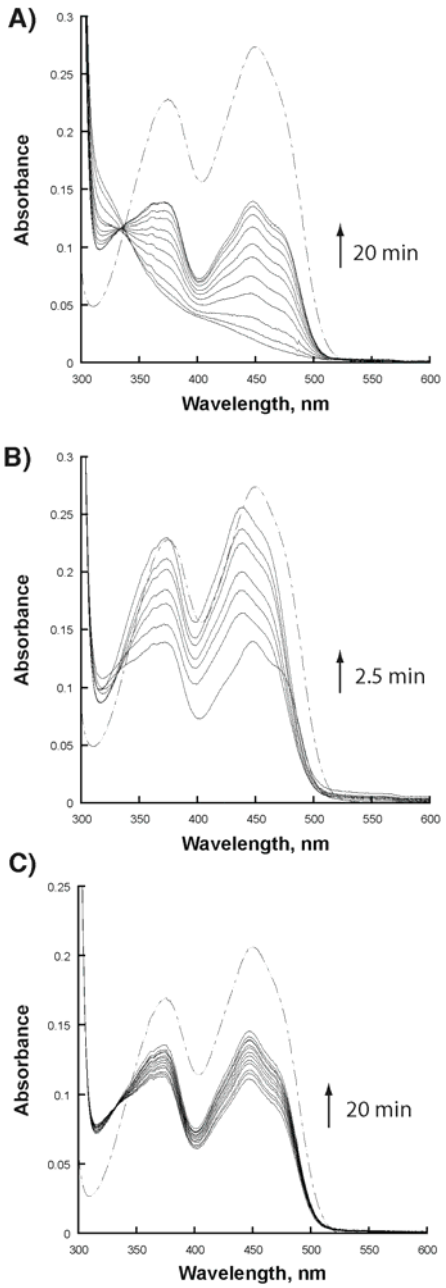

Figure 4.3 Examining the oxidation state of native AfUGM. A) Spectral changes associated with the oxidation of reduced AfUGM. After exposing the protein to air for 20 min, an oxidized flavin spectrum is observed. This spectrum is identical to the initial spectrum before reduction by dithionite. The total amount of bound flavin is approximately 2-fold higher than the observed oxidized flavin in AfUGM. B) Effect of UDP binding to AfUGM. Upon addition of 0.5 mM UDP, the spectrum of the flavin changes and oxidation occurs in 2.5 min. The total oxidized bound flavin is similar in concentration to the total free flavin. C) Slow partial oxidation of bound flavin is observed upon addition of 0.5 mM UDP-Gal*p*. The rate of oxidation was ~10-fold slower than with UDP. In all three experiments, the total bound flavin was obtained by heat denaturation of the enzyme and analysis of the supernatant after centrifugation (broken lines).

3.4 Enzyme activity. The activity of recombinant AfUGM was determined with UDP-Gal*f* to accurately measure the initial rates at various substrate concentrations. The activity of AfUGM follows a saturation kinetic behavior and the data was fit to the Michaelis-Menten equation (Figure 4). Kinetic parameters are summarized in Table 1. Although there are some differences in the k_{cat} and K_M values, the catalytic efficiencies of this eukaryotic UGM is within 5-fold of the values reported for other prokaryotic UGMs.

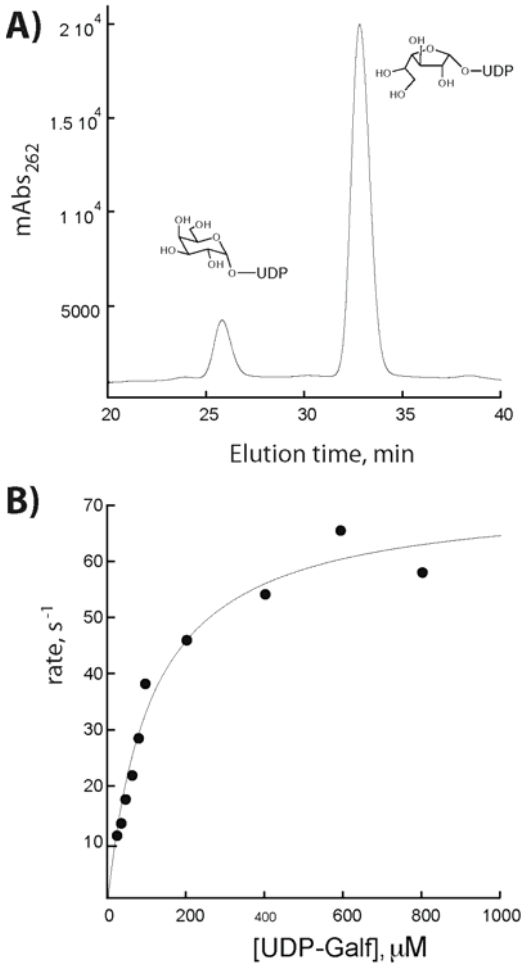

Figure 4.4 Steady-state kinetic characterization of AfUGM. Activity determined by monitoring the formation UDP-Gal*p* from UDP-Gal*f*. A) Chromatogram of the HPLC trace at 262 nm showing the elution times of UDP-Gal*f* (31.5 min) and UDP-Gal*p* (24.8 min). B) Initial rates of the formation of UDP-Gal*p* as a function of UDP-Gal*f*. The line is fit to the Michaelis-Menten equation.

Table 4.1 Kinetic parameters of UDP-galactopyranose mutases[a].

Species	k_{cat}, s^{-1}	K_M, μM	k_{cat}/K_M, $\mu M^{-1} s^{-1}$	Ref.
A. fumigatus	72 ± 4	110 ± 15	0.65 ± 0.09	This work
E. coli	27	22	1.22	[38]
K. pneumoniae	5.5 ± 0.66	43 ± 6	0.12 ± 0.02	[44]
D. radiodurans	66 ± 2.4	55 ± 7.0	1.18	[34]

[a]All the kinetic parameters are with UDP-galactofuranose as substrate in the presence of 5-20 mM dithionite.

3.5 Oligomeric state of eukaryotic AfUGM. The molecular weight of AfUGM was determined by size exclusion chromatography. Our analysis shows that this protein appears to be active as a tetramer (Figure 5 and Table 2). For comparison, we also determined the molecular weight of *Mycobacterium tuberculosis* UGM (MtUGM). It was determined that in solution MtUGM functions as a dimer. This is consistent with the X-ray crystallography data showing homodimeric structures for MtUGM and other bacterial UGMs [23, 26]. Thus, bacterial and eukaryotic UGMs appear to differ in their quaternary structure.

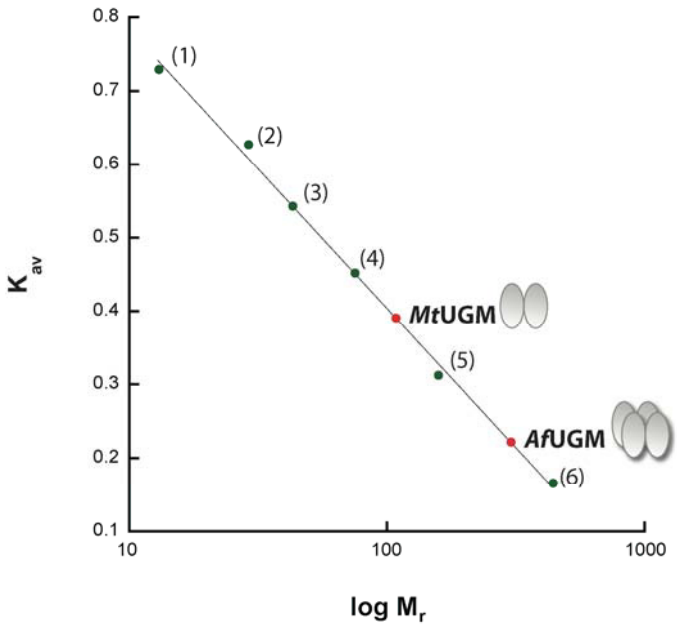

Figure 4.5 Size exclusion chromatography. The elution volumes for aprotinin (1), ribonuclease (2), ovalbumin (3), conoalbumin (4), aldolase (5), and ferritin (6) were used to calculate the K_{av} values ($K_{av} = (V_e - V_o)/ (V_t V_o)$, where V_o is the void volume of the column, V_t is the total volume of the column, and V_e is the elution volume of the protein). The K_{av} values for MtUGM and AfUGM are also plotted.

Table 4.2 Molecular weight analysis.

Method	Sample	Expected Molecular Weight (Da)	Observed Molecular Weight (Da)
SDS-PAGE	AfUGM	57,152	55,000
ESI-MS	AfUGM	57,152	57,174
MALDI	FAD	785.55	786
Size exclusion	AfUGM	228,608 (tetramer)	275,000 ± 20,000
Size exclusion	MtUGM	91,600 (dimer)	108,000 ± 14,000

3.6 Primary and secondary structures. Among the UGM from *A. fumigatus*, *L. major*, and *T. cruzi*, the sequence identity is between 35-50 %. In contrast, between the bacterial and eukaryotic enzymes the identity is less than 15%. Some of the conserved residues are those predicted to be in the FAD binding domain and those found to be in the active site of bacterial

UGMs (Figure 6). We measured the CD spectrum to obtain information about the secondary structure of AfUGM (Figure 7). The spectrum shows characteristic features of folded proteins containing high α-helix content, with a positive band at 193 nm and negative bands at 208 nm and 222 nm [27]. Analysis of the spectrum predicts that the protein contains 42% helix, 13% strand, and 45% coil. These values are similar to the secondary structure content determined from known structures of bacterial UGMs (Table 3).

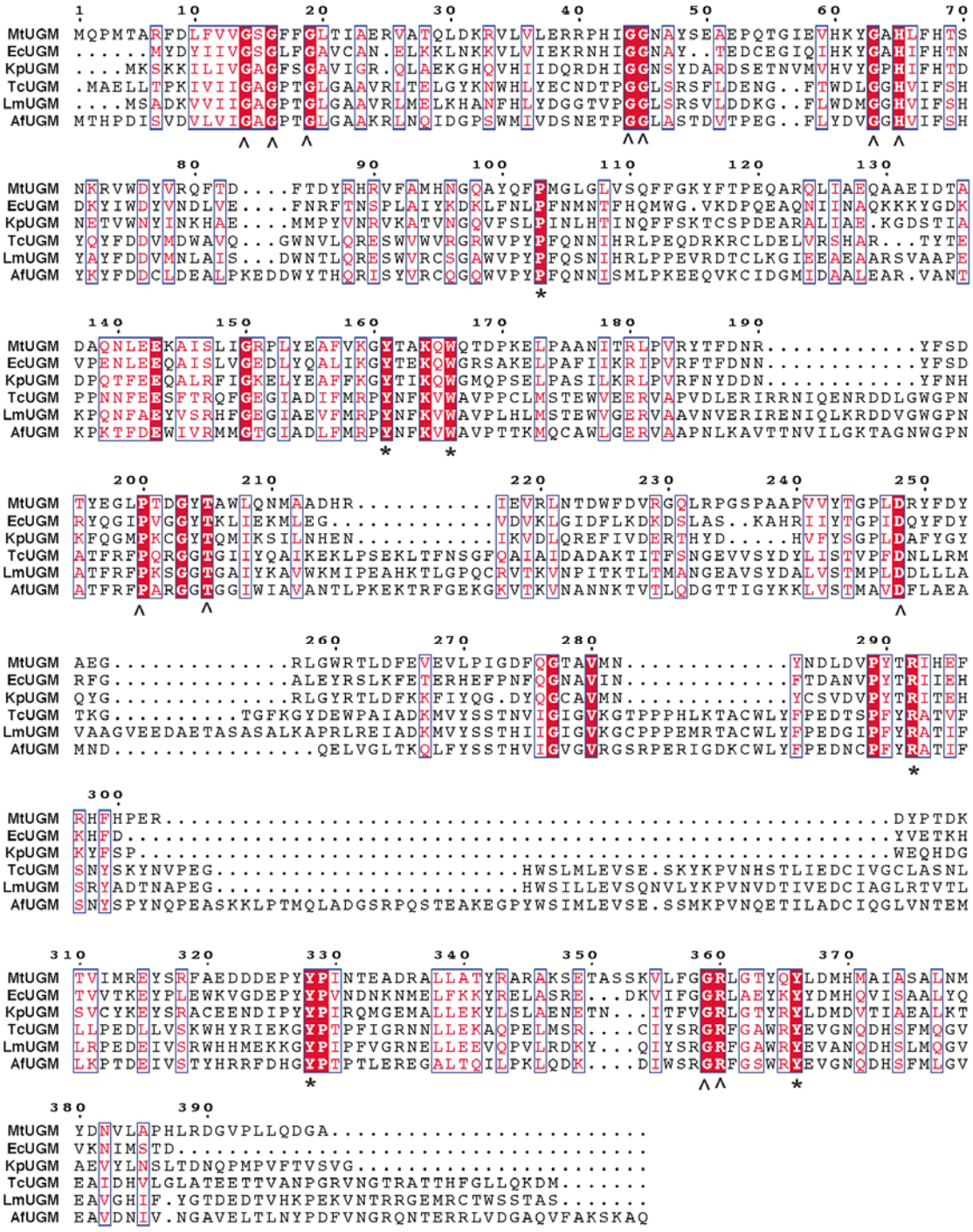

Figure 4.6 Multiple sequence alignment of UDP-galactopyranose mutases. Conserved amino acids found in the active site of bacterial UGM are marked with an asterisk and those involved in flavin binding are marked with arrowheads. Abbreviations: Mt, *M. tuberculosis*, Ec, *E. coli*; Kp, *K. pneumoniae*; Tc, *T. cruzi*; Lm, *L. major*; Af, *A. fumigatus*; The program Clustal W was used to generate the alignment and Espript 2.2 to create the figure [43].

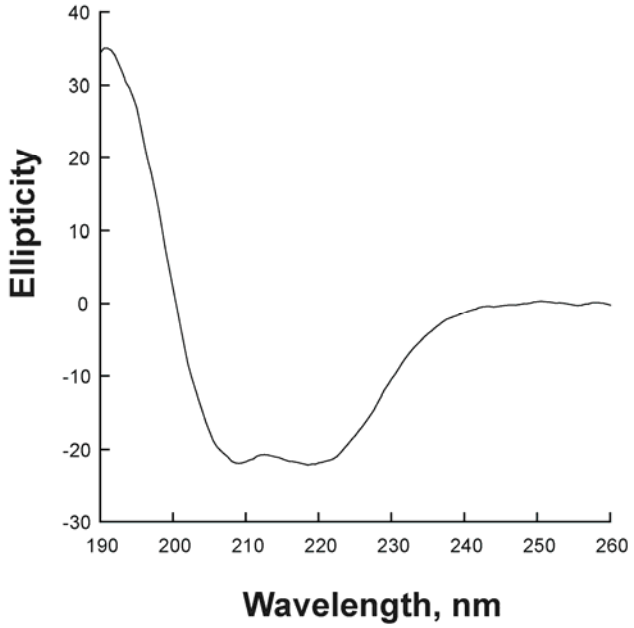

Figure 4.7 Far-UV circular dichroism spectrum of oxidized AfUGM.

Table 4.3 Secondary structure analysis of UDP-galactopyranose mutases.

Species	% Helix	% Strand	% Coil
A. fumigatus	42	13	45
E. coli	34	21	45
K. pneumoniae	34	22	44
M. tuberculosis	36	18	45

3.7 Ligand Binding. To determine the affinity of AfUGM to various ligands, we monitored changes in flavin fluorescence upon substrate binding at 520 nm (excitation at 450 nm). Upon ligand binding to oxidized AfUGM, the flavin fluorescence increased (Figure 8). This allowed us to calculate a K_d value for UDP and UDP-Glc (Table 4). Binding of UDP-Gal*p* to oxidized AfUGM could not be measured by monitoring flavin fluorescence as no in change fluorescence could be observed.

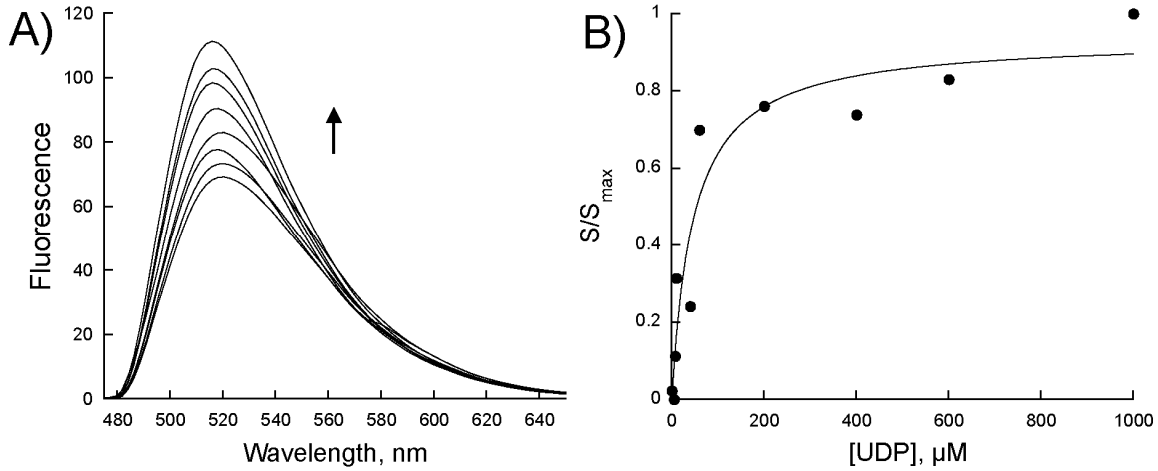

Figure 4.8 Flavin fluorescence changes upon ligand binding. A) Enhancement in the AfUGM flavin fluorescence (excitation at 450 nm) upon UDP binding. B) Binding isotherm derived from the ratio of flavin emission at 520 nm (S) at each UDP concentration divided by the maximum fluorescence (S_{max}) of the free AfUGM. Similar results were obtained with UDP-Glc (not shown).

Table 4.4 K_d values determined by fluorescence studies of UGMs in the oxidized state[a].

Species	UDP-Gal*p*	UDP	UDP-Glc	Ref.
A. fumigatus	ND.	33 ± 9	90 ± 35	This work
K. pneumoniae	220 ± 10	28 ± 5	500 ± 100	[36]

[a]All the K_d values are in μM.

4. Discussion

UGM catalyzes the conversion of UDP-Gal*p* to UDP-Gal*f*, the only source of galactofuranose *in vivo* [14]. This rare sugar is not found in humans and is present in many pathogenic bacteria, parasites, and fungi. In *M. tuberculosis*, the activity of the UGM has been shown to be essential [28]. Similarly, deletion of the UGM gene in *A. fumigatus* and *L. major* leads to severely attenuated virulence [13, 14, 29]. In *A. fumigatus*, Gal*f* deficiency leads to a decrease in cell wall thickness and increased sensitivity to antifungal drugs [30]. These results clearly suggest that UGM is an attractive drug target against several human pathogens, from bacteria to fungi and protozoa. The bacterial enzyme has been studied in detail. Although the

reaction does not involve a net redox change, the prokaryotic UGMs have been shown to be active only in the reduced form [23]. Purified recombinant AfUGM is active, however, it was demonstrated that this activity originated from AfUGM that was partially reduced by some endogenous bacterial enzyme (Figures 1-3). Alternatively, the enzyme might be partially reduced by light during the purification procedure.

The kinetic parameters for AfUGM determined under steady-state conditions showed that the activity of AfUGM is similar to previously reported values for prokaryotic UGMs (Table 1). The structure of the bacterial enzyme has been solved in both the inactive (oxidized) and active (reduced) states [23, 26]. The enzyme is a member of the α/β family and is composed of two domains, a classic FAD Rossmann fold and a novel 5-helical domain [23]. Comparison of the predicted secondary structure of AfUGM with known secondary structure of bacterial UGMs suggests that these enzymes are structurally related (Table 2, Figure 7). However, significant structural differences might be present between the bacterial and eukaryotic UGMs. Size exclusion chromatography results indicate that AfUGM functions as a homotetramer while all the prokaryotic enzymes have been shown to function as dimers (Figure 5) [23, 26, 31]. Primary sequence alignments show low amino acid sequence identity between the prokaryotic and eukaryotic UGMs (less than 15% identity). Furthermore, large amino acid inserts are present in the eukaryotic UGMs (Figure 6). These additional sequences might be involved in modulating subunit interactions.

In the bacterial UGMs, the interaction between UDP-Gal*p* and other ligands have been investigated by fluorescence, saturation transfer difference-NMR (STD-NMR), and recently by X-ray crystallography studies [32-35]. Binding assays following changes in the fluorescence of the oxidized flavin in the *Klebsiella pneumoniae* UGM (KpUGM) have shown that binding

affinity for UDP is similar to the value for Af UGM, while for UDP-Glc, the affinity for the bacterial enzyme is only 5-fold tighter, suggesting that the mode of binding for these substrates is somewhat similar between the bacterial and eukaryotic UGMs. While binding of UDP-Gal*p* to oxidized KpUGM was measured by monitoring changes in the flavin fluorescence, no changes with AfUGM upon binding of UDP-Gal*p* were observed (Table 4). It was also observed that UDP binding causes changes in the spectra of the oxidized flavin and triggers the oxidation of the reduced flavin. In contrast, changes in the flavin spectra are not observed upon binding of UDP-Gal*p* (Figure 3). Thus, this ligand either has a very low affinity or binds to AfUGM in a conformation that does not affect the fluorescence of the flavin.

Thus, a different mechanism of substrate binding is employed in the eukaryotic enzymes. Furthermore, increase in tryptophan fluorescence upon UDP and UDP-Gal*p* binding were also reported for KpUGM [36]. These changes were not observed in AfUGM, further demonstrating differences in the mechanism of binding/structure between the bacterial and eukaryotic enzymes (not shown).

Our results clearly show that the reduced enzyme is the active form of the enzyme and that AfUGM can stabilize ~50% of bound flavin in the reduced form. These results suggest a half-site reactivity for this unique tetrameric enzyme, where the active reduced monomers are protected from oxidation. UDP binding induces relatively rapid oxidation of the reduced flavin; however, in the presence of UDP-Gal*p* the oxidation is ~10-fold slower and does not reach 100% of the total flavin. Thus, during catalysis, even under aerobic conditions, AfUGM stabilizes the reduced form of the flavin, which is essential for activity. The slow oxidation observed in the presence of UDP-Gal*p* might be compensated by reduction by the still unknown electron transfer partner in vivo.

The mechanism by which UGM catalyses the conversion of UDP-Gal*p* to UDP-Gal*f* is not well understood. Using oxygen positional isotope exchange (PIX), it was demonstrated that the glycosidic bond is broken during catalysis [37, 38]. Potentiometry studies suggest that the semiquinone form of the flavin is formed and stabilized by substrate binding [39]. It was also shown that 5-deaza-flavin substituted prokaryotic UGM is inactive, indicating that an electron transfer step was necessary for catalysis [40]. Recently, it was demonstrated that a covalent substrate-FAD adduct is formed between the anomeric carbon and the N5 atom of the flavin [41, 42]. These data have led to two proposals describing the mechanism by which UGM catalyzes the FAD-dependent ring contraction to form UDP-Gal*f* [10]. One mechanism invokes the flavin as a nucleophile that attacks the anomeric carbon to displace UDP [41]. The other mechanism involves a single electron transfer from the reduced flavin to a postulated oxocarbenium sugar intermediate followed by the formation of a flavin-sugar adduct [39, 40]. Availability of high levels of active AfUGM provides the opportunity to test the role of the flavin cofactor in this novel enzyme. These results will be important for the development of novel antifungal agents.

5. Acknowledgments

This work was supported in part by funds from the Fralin Life Science Institute (PS), and the Alberta Ingenuity Centre for Carbohydrate Science and The National Sciences and Engineering Research Council of Canada (TL). MBP is the recipient of a Studentship Award from Alberta Ingenuity.

6. References

[1] R.L. Kradin, E.J. Mark, Arch. Pathol. Lab. Med. 132 (2008) 606-614.
[2] R.J. Trof, A. Beishuizen, Y.J. Debets-Ossenkopp, A.R. Girbes, A.B. Groeneveld, Intensive Care Med. 33 (2007) 1694-1703.
[3] C. Virnig, R.K. Bush, Curr. Opin. Pulm. Med. 13 (2007) 67-71.
[4] S. Chong, K.S. Lee, C.A. Yi, M.J. Chung, T.S. Kim, J. Han, Eur. J. Radiol. 59 (2006) 371-383.
[5] G. Chamilos, M. Luna, R.E. Lewis, G.P. Bodey, R. Chemaly, J.J. Tarrand, A. Safdar, Raad, II, D.P. Kontoyiannis, Haematologica 91 (2006) 986-989.
[6] D.W. Denning, J Antimicrob. Chemother. 49 (2002) 889-891.
[7] T.F. Patterson, Current infectious disease reports 8 (2006) 442-448.
[8] J.P. Latge, Med. Mycol. (2009) S104-109.
[9] C. Lamarre, R. Beau, V. Balloy, T. Fontaine, J.W. Hoi, S. Guadagnini, N. Berkova, M. Chignard, A. Beauvais, J.P. Latge, Cell Microbiol. (2009).
[10] M.R. Richards, T.L. Lowary, Chembiochem 10 (2009) 1920-1938.
[11] S.M. Beverley, K.L. Owens, M. Showalter, C.L. Griffith, T.L. Doering, V.C. Jones, M.R. McNeil, Eukaryotic Cell 4 (2005) 1147-1154.
[12] H. Bakker, B. Kleczka, R. Gerardy-Schahn, F.H. Routier, Biol. Chem. 386 (2005) 657-661.
[13] B. Kleczka, A.C. Lamerz, G. van Zandbergen, A. Wenzel, R. Gerardy-Schahn, M. Wiese, F.H. Routier, J. Biol. Chem. 282 (2007) 10498-10505.
[14] R.A. Damveld, A. Franken, M. Arentshorst, P.J. Punt, F.M. Klis, C.A. van den Hondel, A.F. Ram, Genetics 178 (2008) 873-881.
[15] P.G. Blommel, P.A. Martin, R.L. Wrobel, E. Steffen, B.G. Fox, Protein Expr. Purif. 47 (2006) 562-570.
[16] P. Sobrado, M.A. Goren, D. James, C.K. Amundson, B.G. Fox, Protein Expr. Purif. 58 (2008) 229-241.
[17] P.G. Blommel, K.J. Becker, P. Duvnjak, B.G. Fox, Biotechnol. Prog. 23 (2007) 585-598.
[18] N.L. Rose, R.B. Zheng, J. Pearcey, R. Zhou, G.C. Completo, T.L. Lowary, Carbohydr. Res. 343 (2008) 2130-2139.
[19] J.C. Errey, M.C. Mann, S.A. Fairhurst, L. Hill, M.R. McNeil, J.H. Naismith, J.M. Percy, C. Whitfield, R.A. Field, Org. Biomol. Chem. 7 (2009) 1009-1016.
[20] P. Andrews, The Biochemical Journal 91 (1964) 222-233.
[21] L. Whitmore, B.A. Wallace, Nucleic Acids Res. 32 (2004) W668-673.
[22] Q. Zhang, Liu, H.W., J. Am. Chem. Soc. 122 (2000) 9065-9070.
[23] D.A. Sanders, A.G. Staines, S.A. McMahon, M.R. McNeil, C. Whitfield, J.H. Naismith, Nat. Struct. Biol. 8 (2001) 858-863.
[24] E. Pessione, S. Divari, E. Griva, M. Cavaletto, G.L. Rossi, G. Gilardi, C. Giunta, Eur. J. Biochem. 265 (1999) 549-555.
[25] P. Sobrado, S.C. Daubner, P.F. Fitzpatrick, Biochemistry 40 (2001) 994-1001.
[26] K. Beis, V. Srikannathasan, H. Liu, S.W. Fullerton, V.A. Bamford, D.A. Sanders, C. Whitfield, M.R. McNeil, J.H. Naismith, J. Mol. Biol. 348 (2005) 971-982.
[27] N.J. Greenfield, Nat. Protoc. 1 (2006) 2876-2890.
[28] F. Pan, M. Jackson, Y. Ma, M. McNeil, J. Bacteriol. 183 (2001) 3991-3998.

[29] A.M. El-Ganiny, D.A. Sanders, S.G. Kaminskyj, Fungal Genet. Biol. 45 (2008) 1533-1542.
[30] P.S. Schmalhorst, S. Krappmann, W. Vervecken, M. Rohde, M. Muller, G.H. Braus, R. Contreras, A. Braun, H. Bakker, F.H. Routier, Eukaryotic Cell 7 (2008) 1268-1277.
[31] S.A. McMahon, G.A. Leonard, L.V. Buchanan, M.F. Giraud, J.H. Naismith, Acta Crystallogr. 55 (1999) 399-402.
[32] Y. Yuan, X. Wen, D.A. Sanders, B.M. Pinto, Biochemistry 44 (2005) 14080-14089.
[33] Y. Yuan, D.W. Bleile, X. Wen, D.A. Sanders, K. Itoh, H.W. Liu, B.M. Pinto, J. Am. Chem. Soc. 130 (2008) 3157-3168.
[34] S.K. Partha, K.E. van Straaten, D.A. Sanders, J. Mol. Biol. 394 (2009) 864-877.
[35] X. Yao, D.W. Bleile, Y. Yuan, J. Chao, K.P. Sarathy, D.A. Sanders, B.M. Pinto, M.A. O'Neill, Proteins 74 (2008) 972-979.
[36] X. Yao, D.W. Bleile, Y. Yuan, J. Chao, K.P. Sarathy, D.A. Sanders, B.M. Pinto, M.A. O'Neill, Proteins 74 (2009) 972-979.
[37] J.N. Barlow, Girvin, M.E., Blanchard, J.S, J. Am. Chem. Soc. 121 (1999).
[38] Q. Zhang, H. Liu, J. Am. Chem. Soc.123 (2001) 6756-6766.
[39] S.W. Fullerton, S. Daff, D.A. Sanders, W.J. Ingledew, C. Whitfield, S.K. Chapman, J.H. Naismith, Biochemistry 42 (2003) 2104-2109.
[40] Z. Huang, Q. Zhang, H.W. Liu, Bioorg. Chem. 31 (2003) 494-502.
[41] M. Soltero-Higgin, E.E. Carlson, T.D. Gruber, L.L. Kiessling, Nat. Struct. Mol. Biol. 11 (2004) 539-543.
[42] T.D. Gruber, W.M. Westler, L.L. Kiessling, K.T. Forest, Biochemistry (2009).
[43] P. Gouet, E. Courcelle, D.I. Stuart, F. Metoz, Bioinformatics (Oxford, England) 15 (1999) 305-308.
[44] J.M. Chad, K.P. Sarathy, T.D. Gruber, E. Addala, L.L. Kiessling, D.A. Sanders, Biochemistry 46 (2007) 6723-6732.

CHAPTER 5

Isolation and characterization of functional *Leishmania major* virulence factor UDP-galactopyranose mutase

Reprinted from Biochemical and Biophysical Research Communications, Vol 407, Oppenheimer, M., Valenciano, A.L., and Sobrado, P. "Isolation and characterization of functional *Leishmania major* virulence factor UDP-galactopyranose mutase," pp. 552-556, Copyright (2011), with permission from Elsevier.

Author Contributions:
Michelle Oppenheimer wrote the article and performed all the research except the experiments mentioned below.

Ana Lisa Valenciano cloned, expressed, and purified LmUGM in pF18K. She also obtained the solution molecular weight of LmUGM.

Pablo Sobrado oversaw and directed the research, and helped write the article.

Abstract

Human parasitic pathogens of the genus *Leishmania* are the causative agents of cutaneous, mucocutaneous, and visceral leishmaniasis. Currently, there are millions of people infected with these diseases and over 50,000 deaths occur annually. Recently, it was shown that the flavin-dependent enzyme UDP-galactopyranose mutase (UGM) is a virulence factor in *Leishmania major*. UGM catalyzes the conversion of UDP-galactopyranose to UDP-galactofuranose. The product, UDP-galactofuranose, is the only source of galactofuranose present on the cell surface of this parasite and has been implicated to be important for host-parasite interactions. The recombinant form of this enzyme was obtained in a soluble and active form. The enzyme was shown to be active only in the reduced state. A k_{cat} value of 5 ± 0.2 s^{-1} and a K_M value of 87 ± 11 μM were determined with UDP-galactofuranose as substrate.

Different from the dimeric bacterial and tetrameric fungal UGMs, this parasitic enzyme functions as a monomer.

1. Introduction

Leishmaniasis constitutes a group of diseases caused by infection of parasites from the genus *Leishmania,* which are present in more than 80 countries worldwide [1, 2]. There are three major forms of leishmaniasis: cutaneous, mucocutaneous, and visceral [1]. Symptoms of these diseases range from self-healing sores, as observed in cutaneous leishmaniasis, to infection of the liver, spleen, and lymph nodes, as observed in visceral leishmaniasis [3, 4]. If untreated, leishmaniasis can lead to severe scarring, disfigurement, and in severe cases it leads to death [3, 4]. The World Health Organization estimates that >2 million people are infected with these parasites, resulting in ~50,000 annual deaths [2]. Despite the significant health threat posed by these diseases, there are no efficacious drug treatments or vaccinations to prevent infection by *Leishmania* spp. [5].

The cell surface has been shown to play a role in host-pathogen interactions and aids in the ability of the pathogen to evade the host immune system. Previous research has shown that galactofuranose (Gal*f*) found on the cell surface of *L. major* plays a role in pathogenesis and in pathogen-host interactions [6]. Gal*f* is a unique sugar; it is only found in parasites and other human pathogens and is present in cell surface lipids and proteins. Specifically, in *Leishmania* spp., Gal*f* is found in lipophosphoglycan (LPG) and glycoinositolphospholipids (GIPLs) [7]. LPGs are essential for adhesion of the parasite to the midgut of the insect and, therefore, are important for transmission of the parasite to the human host [8, 9]. Deletion of LPG in *L. major* suggests that these glycosylated structures are involved in resistance to oxidative stress and the

human immune system [10, 11]. While Gal*f* containing GIPLs (specifically GIPL-1 from *L. major*) are shown to aid in establishing host infection [6, 12]. These results suggest that Gal*f* plays an important role in host specific cell recognition, parasitic growth, and pathogenesis. Since Gal*f* is not present in humans, the Gal*f* biosynthetic pathway is an attractive target for the development of novel anti-parasitic drugs [13, 14]. In this pathway, UDP-galactopyranose mutase (UGM) catalyzes the conversion of UDP-galactopyranose (UDP-Gal*p*) to form UDP-Gal*f*, which serves as the precursor for all the Gal*f* found on the cell surface [15]. Deletion of the UGM gene in *L. major* (LmUGM) leads to attenuated virulence, suggesting that UGM is a virulence factor and a potential drug target [16, 17]. We present the functional expression and characterization of recombinant LmUGM, which will allow further mechanistic and structural studies that might lead to the identification of specific inhibitors of this enzyme.

2. Materials and Methods

2.1 Materials. UDP and UDP-Gal*p* were purchased from Sigma (St. Louis, MO). Accuprime polymerase, TOP-10, and BL21T1^{R} chemical competent cells were obtained from Invitrogen (Carlsbad, CA). Restriction endonucleases *Sgf*I and *Pme*I, plasmid pFN18K, chemical competent cells BL21(DE3), and HaloLink Resin were obtained from Promega (Madison, WI). The plasmid miniprep and PCR purification kits were from Qiagen (Valencia, CA). All other buffers and chemicals were purchased from Fisher Scientific (Pittsburgh, PA). Expression plasmids, pVP55A and pVP56K, were obtained from the Center for Eukaryotic Structural Genomics, University of Wisconsin, Madison [18].

2.2 Cloning. The LmUGM gene was provided by Dr. Françoise Routier (Medizinische Hochschule, Hannover, Germany) cloned into the pET22 plasmid. In this plasmid, the gene product appears to be toxic to BL21(DE3) cells. Therefore, the LmUGM gene was amplified by PCR using the forward primer '5-ggttgcgatcgccatgagcgctgacaaggtggtc-3' (*Sgf*I site underlined) and the reverse primer 5'- ggtcgtcgacggcctcgtaggtttaaacttttt-3' (*Pme*I site underlined). After running the resulting PCR product on a 0.8% agarose gel electrophoresis, the DNA was excised and purified using a Qiagen PCR clean up kit. This was followed by digestion with the restriction enzymes *Sgf*I and *Pme*I for 40 min at 37 ^{o}C, then heat inactivation for 25 min at 65 ^{o}C. The digested PCR product was then ligated into the plasmids pVP55A, pVP56K, and pFN18K, which were previously treated with *Sgf*I and *Pme*I. Cloning was designed for the expression of an N-terminus tagged fusion protein. In pVP55A, the gene was expressed with an 8x-His tag, in pVP56K, the gene was expressed with an 8x-His tagged maltose binding protein (MBP), and in pFN18K, the gene was expressed with a HaloTag [19, 20]. In the vectors pVP55A and pVP56K, the inserted gene was under the control of the T5 promoter and in pFN18K, the inserted gene was under control of the T7 promoter. Both promoters can be induced by the addition of isopropyl-β-thiogalactopyranoside (IPTG). pVP55A provides resistance to ampicillin and both pVP56K and pFN18K provide resistance to kanamycin.

2.3 Protein expression. Cell growth was done in the presence of either 25 μg/mL kanamycin or 100 μg/mL ampillicin depending on whether the cells contained pVP56K, pFN18K, or pVP55A. BL21T1^{R} cells were transformed with pVP55A and pVP56K containing the LmUGM gene, while BL21(DE3) cells were transformed with the plasmid pFN18K containing the LmUGM gene. The transformed cells were plated onto Luria-Bertani (LB) agar plates with the appropriate

antibiotic. A single colony was used to inoculate a 50 mL LB culture containing the appropriate antibiotic and incubated at 37 ^{o}C with agitation at 250 rpm overnight. The next morning, 15 mL of the overnight culture was used to inoculate each of 3 flasks containing 1 L of LB. The flasks were incubated at 37 ^{o}C with 250 rpm agitation until the optical density at 600 nm (OD_{600}) reached a value of 0.6, at which point 1 mM IPTG was added to each culture to induce the expression of the recombinant LmUGM enzyme. The temperature was reduced to 15 ^{o}C to increase solubility of the LmUGM enzyme. Four hours after induction, the cells were harvested by centrifugation at 5000*g* for 15 min and the resulting cell pellets (~4.5 g) were stored at -80 ^{o}C until purification. LmUGM expressed in pVP55A and pVP56K was found to be insoluble. Expression of LmUGM in pVP56K was also performed using auto-induction medium to test if protein solubility was increased [21]. Using auto-induction medium, the yield of cell paste was ~60 g from 6 L of medium.

2.4 Protein purification by metal affinity chromatography. Cell pellets from auto-induction (~60 g) were resuspended in 150 mL 25 mM HEPES, 300 mM NaCl, 5 mM Imidazole, pH 7.5 containing 25 μg/mL each of lysozyme, DNase, and RNase. The resuspended cells were mixed for 30 min at 4 ^{o}C and cells were disrupted by homogenization (Nano DeBEE, BEE International) at 16,000 psi. The resulting lysate was then centrifuged at 30,000*g* for 30 min at 4 ^{o}C to remove the unlysed cells and insoluble proteins. The supernatant was collected and loaded onto a 5 mL nickel immobilized metal affinity chromatography (IMAC) column (GE Healthcare) previously equilibrated with buffer A (25 mM HEPES, 300 mM NaCl, 5 mM Imidazole, pH 7.5). The column was washed with three column volumes of buffer A and LmUGM was eluted with buffer A containing 300 mM imidazole. The 8x-His tag and MBP were removed by treating the

fusion protein with 6x-His- tobacco etch virus (6x-His-Tev) protease (1:20 ratio LmUGM:Tev) overnight with slow stirring at 4 ^{o}C. The resulting sample was centrifuged at 30,000*g* for 20 min to pellet small amounts of denatured proteins. The supernatant was diluted 4-fold and loaded onto a nickel IMAC. The 8x-His-MBP and 6x-His-Tev remained bound to the column, and the flow-through containing LmUGM was collected. This sample was concentrated and diluted by addition of 25 mM HEPES, pH 7.5, to decrease the NaCl concentration to less than 30 mM, and loaded onto a diethyl amino ethyl (DEAE) ion exchange chromatography column (GE Healthcare) equilibrated with 25 mM HEPES, pH 7.5. A gradient from 0 to 400 mM NaCl was used to elute the bound proteins; LmUGM eluted later in the gradient (~250 mM NaCl). Fractions containing LmUGM were pooled, concentrated, and stored at -80 ^{o}C.

2.5 Protein purification with HaloTag. Cell pellets (~4.5 g) were resuspended in 20 ml of 25 mM HEPES, 125 mM NaCl, pH 7.5, containing 25 µg/mL each of lysozyme, DNase, and RNase. The resuspended cells were lysed and a total volume of 75 mL of supernatant was obtained as indicated above. Approximately 30 mL of supernatant were mixed with 5 mL HaloLink resin for 1 h at room temperature. The resin was then precipitated by centrifuging at 1,000*g* for 5 min at 4 ^{o}C and supernatant was removed. The resin was then washed three times with 10 mL of 50 mM HEPES, 150 mM NaCl, pH 7.5. The resulting resin was resuspended with 2.5 mL of 50 mM HEPES, 150 mM NaCl, pH 7.5 and LmUGM was cleaved from the HaloTag by addition of 5 mg 6x-His-Tev protease. After incubation for 2 h at room temperature, the resin was precipitated by centrifugation at 2,500*g* for 5 min and the resulting supernatant containing free LmUGM was saved. The resin was washed with 1 mL 50 mM HEPES, 150 mM NaCl, pH 7.5 and the supernatant was also saved. 6x-His-Tev was removed by passing the supernatant on a 1 mL

nickel IMAC (GE Healthcare) column. Since LmUGM does not contain a His-tag it is collected in the flow through and TEV remains bound to the column. Analysis of the final product by sodium dodecyl sulfate polyacrylamide gel electrophoresis (SDS-PAGE) indicated that the LmUGM sample was homogeneous. The sample was concentrated and stored at -80 ^{o}C.

2.6 UV-visible spectrophotometry. The spectrum of recombinant LmUGM was recorded using an Agilent 8453 UV–visible spectrophotometer. The spectrum shows similar features to other UGM proteins with a bound flavin cofactor, with peaks at 276, 377, and 448 nm with a shoulder at 474 nm [22].

2.7 Activity Assay. The activity of recombinant LmUGM was tested with UDP-Gal*f* as the substrate following procedures previously described [22]. The protein concentration was calculated using the LmUGM flavin extinction coefficient at 450 nm (ε_{450} = 10 mM^{-1} cm^{-1}).

2.8 Molecular weight determination. The solution molecular weight was determined using size-exclusion chromatography. Purified LmUGM (10 μg) was loaded onto a Superdex 200 column (GE Healthcare) equilibrated with 50 mM phosphate buffer at pH 7.2 with 150 mM NaCl. Using a set of protein standards (aproprotein (6.5 kDa), ribonuclease (13 kDa), carbonic anhydrase (29 kDa), ovalbumin (43 kDa), canolbumin (75 kDa), aldolase (158 kDa), and ferritin (440 kDa)), a standard curve was obtained by plotting the log of molecular weight versus K_{av} for the standards [23].

3. Results and Discussion

3.1 Expression and Purification of LmUGM. LmUGM was expressed using three plasmids: pVP55A, pVP56K, and pFN18K. It was found that expression of LmUGM in pVP55A with only an 8x-His tag led to completely insoluble protein whether expressed in LB or auto-induction media. However, when expressed by auto-induction as an N-terminal fusion to MBP in pVP56K it was partially soluble. The protein was purified first using nickel IMAC as affinity chromatography for the 8x-His Tag on the N-terminus of the MBP. The resulting protein was treated with 6x-His-Tev to remove the 8x-His-MBP tag. The protein was loaded back over a nickel IMAC to remove both the 8x-His-MBP and 6x-His-Tev. LmUGM eluted in the flow through and was further purified by passing over a DEAE column. The resulting protein was only ~70-80% pure, and the amount of protein recovered from 6 L auto-induction media (60 g cell paste) was only 3-4 mg.

To increase protein solubility, recovery, and purity, LmUGM was expressed as a Halo-tagged protein in the pFN18K plasmid. This system expresses the protein of interest as a fusion to a catalytically inactive derivative of *Rhodococcocus* haloalkane dehalogenase (DhaA) [20]. This protein has been modified to form covalent bonds to chloroalkane-conjugated resins [20]. In addition, the 35-kDa DhaA protein was engineered to enhance the solubility of the fused protein [20]. LmUGM was found to be partially soluble when expressed as an N-terminal fusion to HaloTag in LB media. Halo-LmUGM was isolated using the HaloTag affinity resin. Since the fusion protein becomes covalently linked to the resin, this permits numerous washes to remove other contaminants. LmUGM can then be removed from the HaloTag and resin using 6x-His-Tev. LmUGM was isolated from 6x-His-Tev and other contaminants by loading the solution onto a nickel IMAC to remove the 6x-His-Tev yielding 3 mg of highly pure protein (~95%)

(Figure 1). In summary, 4.5 g of cell paste yielded 3 mg of homogeneous LmUGM using the HaloTag system. This is a ~ 20 fold increase in yield as compared to the expression of LmUGM as a fusion to MBP using auto-induction media (4 mg/60 g cell paste). The purified LmUGM contained a noncovalently bound flavin cofactor (50% incorporation), which was identified by mass spec analysis as FAD (data not shown). The UV/Vis spectrum displayed similar spectral characteristics to other flavoproteins with peaks at 377 nm and 448 nm and a shoulder at 474 nm (Figure 2).

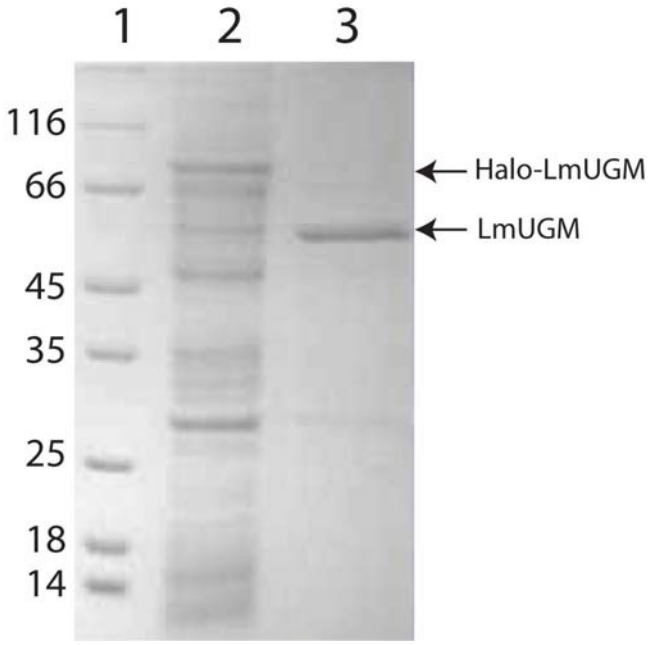

Figure 5.1 SDS-PAGE gel of LmUGM protein purified by HaloTag using HaloTag resin. Lane 1. Molecular weight marker, Lane 2. Complete lysate supernatant, Lane 3. Supernatant after cleavage with Tev protease and after nickel IMAC to remove the Tev protease.

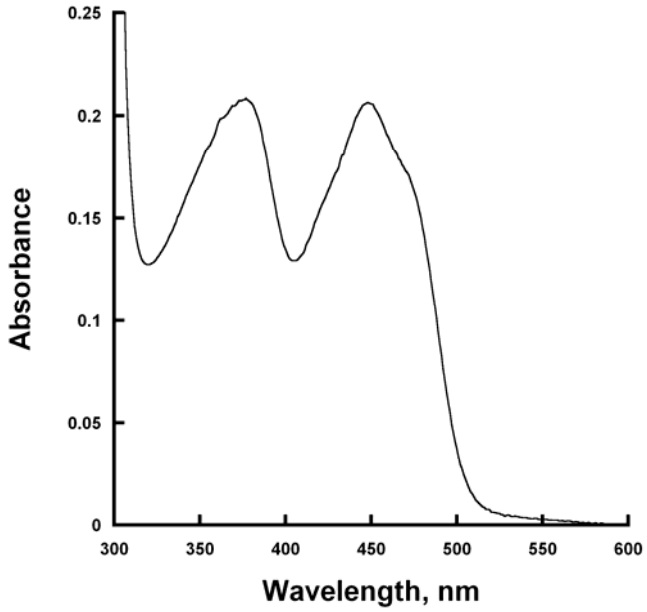

Figure 5.2 UV-Visible spectrum of the purified LmUGM.

3.2 Molecular weight determination. The molecular weight for LmUGM of 55 kDa calculated by SDS-PAGE analysis is consistent with the predicted value of 54,960 Da based on amino acid composition, suggesting that the protein was not subjected to major modifications by *E. coli* proteases during purification. The solution molecular weight of 57,400 ± 500 Da was determined by size exclusion chromatography (Figure 3). This value closely matches the predicted mass of a monomer of LmUGM. Interestingly, the oligomeric state of bacterial enzymes has been shown to be dimeric, while the eukaryotic UGM from *Aspergillus fumigatus* functions as a tetramer [22].

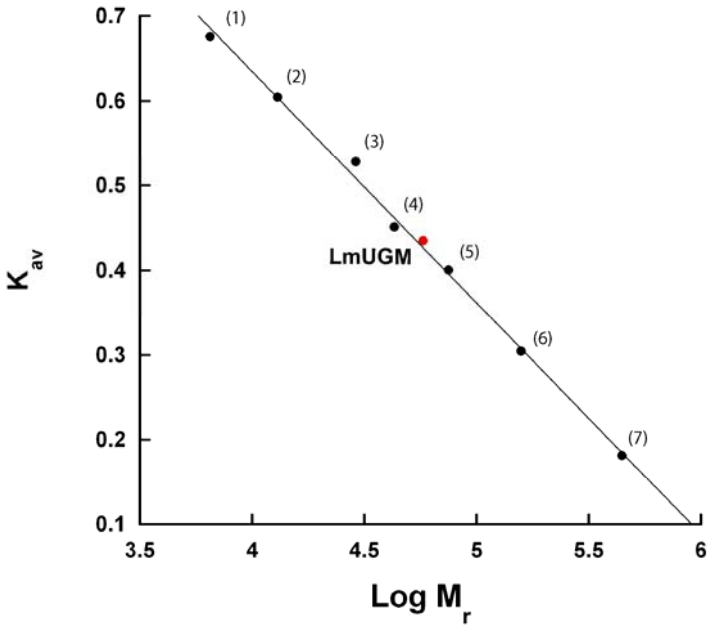

Figure 5.3 Solution molecular weight determination of LmUGM using size exclusion chromatography. The elution volumes for aprotinin (1), ribonuclease (2), carbonic anhydrase (3), ovalbumin (4), conalbumin (5), aldolase (6), and ferritin (7) were used to calculate the K_{av} values ($K_{av} = (V_e-V_o)/ (V_t V_o)$, where V_o is the void volume of the column, V_t is the total volume of the column, and V_e is the elution volume of the protein. The K_{av} value for LmUGM is also plotted).

3.3 Activity. We tested the activity of recombinant LmUGM with UDP-Gal*p* as substrate in the presence or absence of dithionite as a source of reducing equivalents. Consistent with published work on bacterial UGM and more recently on a eukaryotic UGM from the fungus *A. fumigatus*, the enzyme was active only when the flavin cofactor is in the reduced form [22, 24]. Since the equilibrium of the reaction favors the formation of UDP-Gal*p*, it is necessary to measure the activity in the reverse direction. Thus, the activity of LmUGM was measured as a function of UDP-Gal*f* concentration. As shown in Figure 4, the activity of LmUGM follows typical saturation kinetics that can be analyzed using the Michaelis-Menten equation. The kinetic values obtained from the fit are summarized on Table 1. The k_{cat} values for some UGMs are more than 10-fold higher; however, it is clear that these enzymes have similar K_M values. The differences in

the k_{cat} values might originate from the primary and quaternary structure variability between the members of this family of enzymes.

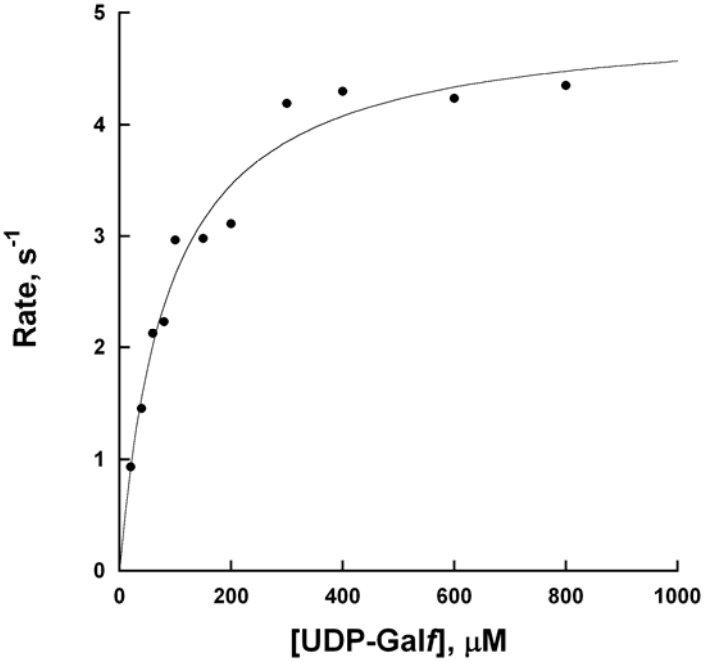

Figure 5.4 Activity of LmUGM as a function of UDP-Gal*f*. The line is a fit to the Michaelis-Menten equation.

Table 5.1 Kinetic parameters of UDP-galactopyranose mutases[a].

Species	k_{cat}, s^{-1}	K_M, μM	k_{cat}/K_M, μM^{-1} s^{-1}	Ref.
L. major	5 ± 0.2	87 ± 11	0.057 ± 0.006	This work
A. fumigatus	72 ± 4	110 ± 15	0.65 ± 0.09	[22]
E. coli	27	22	1.22	[28]
K. pneumoniae	5.5 ± 0.66	43 ± 6	0.12 ± 0.02	[29]
D. radiodurans	66 ± 2.4	55 ± 7	1.18	[30]

[a]All the kinetic parameters are with UDP-Gal*f* as substrate in the presence of 5-20 mM dithionite.

3.4 Concluding Remarks. In mycobacteria, UGM has been validated as a drug target, because this enzyme is essential for mycobacterial survival [25]. Similarly, the role of UGM in the virulence of eukaryotic pathogens has also been shown. In *A. fumigatus* and *L. major*, deletion of the UGM gene leads to attenuated virulence [16, 26]. Thus, inhibition of UGM might lead to the

identification of novel anti-fungal and anti-leishmanial drugs. Here, we report the functional expression of *L. major* UGM. The enzyme was expressed in a soluble form and the isolated enzyme contained the flavin cofactor. The enzyme was shown to be active in the reduced form and functions as a monomeric enzyme, which is different from the *A. fumigatus* and bacterial enzymes. Although, inhibitors of bacterial UGM have been identified, some are not active towards eukaryotic UGM [27, Appendix B]. This might be due the fact that bacterial and eukaryotic UGMs share less than 18% identity. Our results provide the opportunity for the screening of inhibitors specific to parasitic UGMs.

4. Acknowledgments

We would like to thank Prof. Françoise Routier for providing us with the pET22 plasmid containing the LmUGM gene. This work was supported by NIH grant RO1-GM094468 (P. Sobrado, PI). M.O. was supported by a fellowship from the American Heart Association. A.L.V was supported by a fellowship from the Ministry of Science and Technology of Costa Rica.

5. References

[1] H. Kato, E.A. Gomez, A.G. Caceres, H. Uezato, T. Mimori, and Y. Hashiguchi, Molecular epidemiology for vector research on leishmaniasis. Int J Environ Res Public Health 7 (2010) 814-26.

[2] WHO, World Health Report. (World Health Organization, Geneva, 2002) (2002).

[3] B.L. Herwaldt, Leishmaniasis. Lancet 354 (1999) 1191-9.

[4] M.S. Bailey, and D.N. Lockwood, Cutaneous leishmaniasis. Clin Dermatol 25 (2007) 203-11.

[5] L. Kedzierski, A. Sakthianandeswaren, J.M. Curtis, P.C. Andrews, P.C. Junk, and K. Kedzierska, Leishmaniasis: current treatment and prospects for new drugs and vaccines. Curr Med Chem 16 (2009) 599-614.

[6] E. Suzuki, A.K. Tanaka, M.S. Toledo, H.K. Takahashi, and A.H. Straus, Role of beta-D-galactofuranose in *Leishmania major* macrophage invasion. Infect Immun 70 (2002) 6592-6.

[7] R.M. de Lederkremer, and W. Colli, Galactofuranose-containing glycoconjugates in trypanosomatids. Glycobiology 5 (1995) 547-52.

[8] B.A. Butcher, S.J. Turco, B.A. Hilty, P.F. Pimenta, M. Panunzio, and D.L. Sacks, Deficiency in beta1,3-galactosyltransferase of a *Leishmania major* lipophosphoglycan mutant adversely influences the *Leishmania*-sand fly interaction. J Biol Chem 271 (1996) 20573-9.

[9] A. Svarovska, T.H. Ant, V. Seblova, L. Jecna, S.M. Beverley, and P. Volf, *Leishmania major* glycosylation mutants require phosphoglycans (lpg2-) but not lipophosphoglycan (lpg1-) for survival in permissive sand fly vectors. PLoS Negl Trop Dis 4 e580.

[10] G.F. Spath, L.A. Garraway, S.J. Turco, and S.M. Beverley, The role(s) of lipophosphoglycan (LPG) in the establishment of *Leishmania major* infections in mammalian hosts. Proc Natl Acad Sci U S A 100 (2003) 9536-41.

[11] S.J. Turco, G.F. Spath, and S.M. Beverley, Is lipophosphoglycan a virulence factor? A surprising diversity between *Leishmania* species. Trends Parasitol 17 (2001) 223-6.

[12] E. Suzuki, A.K. Tanaka, M.S. Toledo, S.B. Levery, A.H. Straus, and H.K. Takahashi, Trypanosomatid and fungal glycolipids and sphingolipids as infectivity factors and potential targets for development of new therapeutic strategies. Biochim Biophys Acta 1780 (2008) 362-9.

[13] S.M. Beverley, K.L. Owens, M. Showalter, C.L. Griffith, T.L. Doering, V.C. Jones, and M.R. McNeil, Eukaryotic UDP-galactopyranose mutase (GLF gene) in microbial and metazoal pathogens. Eukaryot Cell 4 (2005) 1147-54.

[14] H. Bakker, B. Kleczka, R. Gerardy-Schahn, and F.H. Routier, Identification and partial characterization of two eukaryotic UDP-galactopyranose mutases. Biol Chem 386 (2005) 657-61.

[15] P.M. Nassau, S.L. Martin, R.E. Brown, A. Weston, D. Monsey, M.R. McNeil, and K. Duncan, Galactofuranose biosynthesis in *Escherichia coli* K-12: identification and cloning of UDP-galactopyranose mutase. J Bacteriol 178 (1996) 1047-52.

[16] B. Kleczka, A.C. Lamerz, G. van Zandbergen, A. Wenzel, R. Gerardy-Schahn, M. Wiese, and F.H. Routier, Targeted gene deletion of *Leishmania major* UDP-galactopyranose mutase leads to attenuated virulence. J Biol Chem 282 (2007) 10498-505.

[17] L. Madeira da Silva, K.L. Owens, S.M. Murta, and S.M. Beverley, Regulated expression of the *Leishmania major* surface virulence factor lipophosphoglycan using conditionally destabilized fusion proteins. Proc Natl Acad Sci U S A 106 (2009) 7583-8.
[18] P.G. Blommel, P.A. Martin, R.L. Wrobel, E. Steffen, and B.G. Fox, High efficiency single step production of expression plasmids from cDNA clones using the Flexi Vector cloning system. Protein Expr Purif 47 (2006) 562-70.
[19] P. Sobrado, M.A. Goren, D. James, C.K. Amundson, and B.G. Fox, A Protein Structure Initiative approach to expression, purification, and in situ delivery of human cytochrome b5 to membrane vesicles. Protein Expr Purif 58 (2008) 229-41.
[20] R.F. Ohana, L.P. Encell, K. Zhao, D. Simpson, M.R. Slater, M. Urh, and K.V. Wood, HaloTag7: a genetically engineered tag that enhances bacterial expression of soluble proteins and improves protein purification. Protein Expr Purif 68 (2009) 110-20.
[21] P.G. Blommel, K.J. Becker, P. Duvnjak, and B.G. Fox, Enhanced bacterial protein expression during auto-induction obtained by alteration of lac repressor dosage and medium composition. Biotechnol Prog 23 (2007) 585-98.
[22] M. Oppenheimer, M.B. Poulin, T.L. Lowary, R.F. Helm, and P. Sobrado, Characterization of recombinant UDP-galactopyranose mutase from *Aspergillus fumigatus*. Arch Biochem Biophys 502 (2010) 31-8.
[23] P. Andrews, Estimation of the molecular weights of proteins by Sephadex gel-filtration. Biochem J 91 (1964) 222-33.
[24] D.A.R. Sanders, A.G. Staines, S.A. McMahon, M.R. McNeil, C. Whitfield, and J.H. Naismith, UDP-galactopyranose mutase has a novel structure and mechanism. Nature Structural Biology 8 (2001) 858-863.
[25] F. Pan, M. Jackson, Y. Ma, and M. McNeil, Cell wall core galactofuran synthesis is essential for growth of mycobacteria. J Bacteriol 183 (2001) 3991-8.
[26] P.S. Schmalhorst, S. Krappmann, W. Vervecken, M. Rohde, M. Muller, G.H. Braus, R. Contreras, A. Braun, H. Bakker, and F.H. Routier, Contribution of galactofuranose to the virulence of the opportunistic pathogen *Aspergillus fumigatus*. Eukaryot Cell 7 (2008) 1268-77.
[27] M. Soltero-Higgin, E.E. Carlson, J.H. Phillips, and L.L. Kiessling, Identification of inhibitors for UDP-galactopyranose mutase. J Am Chem Soc 126 (2004) 10532-3.
[28] Q. Zhang, and H. Liu, Mechanistic investigation of UDP-galactopyranose mutase from Escherichia coli using 2- and 3-fluorinated UDP-galactofuranose as probes. J Am Chem Soc 123 (2001) 6756-66.
[29] J.M. Chad, K.P. Sarathy, T.D. Gruber, E. Addala, L.L. Kiessling, and D.A. Sanders, Site-directed mutagenesis of UDP-galactopyranose mutase reveals a critical role for the active-site, conserved arginine residues. Biochemistry 46 (2007) 6723-32.
[30] S.K. Partha, K.E. van Straaten, and D.A. Sanders, Structural basis of substrate binding to UDP-galactopyranose mutase: crystal structures in the reduced and oxidized state complexed with UDP-galactopyranose and UDP. J Mol Biol 394 (2009) 864-77.

CHAPTER 6

Chemical mechanism of UDP-galactopyranose mutase from *Trypanosoma cruzi*: a potential drug target against Chagas' disease

Reproduced with permission from: Oppenheimer, M., Valenciano, A.L., Kizjakina, K., Qi, J., and Sobrado, P., "Chemical mechanism of UDP-galactopyranose mutase from *Trypanosoma cruzi*: a potential drug target against Chagas' disease," PLoS ONE 7(3): e32918, 2012. Under the Creative Commons Atribution Licence.

Author Contributions:
Michelle Oppenheimer performed all the research except the experiments mentioned below and wrote the article.

Ana Lisa Valenciano performed the oxidase assays.

Karina Kizjakina synthesized the Gal*f*-1-Phosphate and the UDP-Gal*f* with help from Michelle Oppenheimer.

Jun Qi trapped the iminium ion and performed the fluorescence anisotropy.

Pablo Sobrado oversaw and directed the research and helped write the article.

Abstract

UDP-galactopyranose mutase (UGM) is a flavoenzyme that catalyzes the conversion of UDP-galactopyranose to UDP-galactofuranose, the precursor of galactofuranose (Gal*f*). Gal*f* is found in several pathogenic organisms, including the parasite *Trypanosoma cruzi*, the causative agent of Chagas' disease. Gal*f* is important for virulence and is not present in humans, making its biosynthetic pathway an attractive target for the development of new drugs against *T. cruzi*. Although UGMs catalyze a non-redox reaction, the flavin must be in the reduced state for activity and the exact role of the flavin in this reaction is controversial. The kinetic and chemical mechanism of TcUGM was probed using steady state kinetics, trapping of reaction intermediates, rapid reaction kinetics, and fluorescence anisotropy. It was shown for the first

time that NADPH is an effective redox partner of TcUGM. The substrate, UDP-galactopyranose, protects the enzyme from reacting with molecular oxygen allowing TcUGM to turnover ~1000 times for every NADPH oxidized. Spectral changes consistent with a flavin iminium ion, without the formation of a flavin semiquinone, were observed under rapid reaction conditions. These data support the proposal of the flavin acting as a nucleophile. In support of this role, a flavin-galactose adduct was isolated and characterized. A detailed kinetic and chemical mechanism for the unique non-redox reaction of UGM is presented.

1. Introduction

The protozoan parasite *Trypanosoma cruzi* is the etiological agent of American trypanosomiasis or Chagas'disease. The World Health Organization estimates that 8-11 million people are infected with this disease in South and Central America [1]. Transmission occurs when a triatomine insect feeds on a human subject and defecates at the bite site [2]. Through rubbing, infected feces enter the bite wound, mouth, eyes, or open cuts. Transmission by blood transfusion, organ transplant, oral contamination, and congenital routes has also been reported [3-7]. *T. cruzi* has a dynamic life cycle, involving several morphological changes as the parasites travel from the insect vector to humans [8]. This is accompanied by several changes in cell surface sugar composition, which plays an important role in infection and resistance to the host immune system [9, 10]. Targeting the enzymes involved in biosynthesis of cell surface glycans may lead to the identification of new inhibitors that function as novel antiparasitic drugs for the treatment of Chagas' disease [11]. One unique sugar found on the cell surface of *T. cruzi* is galactofuranose (Gal*f*) [11].

Gal*f*, the five-membered ring form of galactose, is a component of the cell wall, glycolipids, and glycoproteins on the cell surface of many human pathogens including bacteria, fungi, and parasites [11-14]. In *T. cruzi*, Gal*f* is found in glycoprotein oligosaccharides and glycoinositolphospholipids, which are involved in parasite pathogenesis [11, 15, 16]. Additionally, Gal*f* is not present in humans. Thus, the biosynthetic pathway of Gal*f* is an attractive drug target for *T. cruzi* and other eukaryotic pathogens including *A. fumigatus* and *L. major* [11, 17]. UDP-galactopyranose mutase (UGM) catalyzes the conversion of UDP-galactopyranose (UDP-Gal*p*) to UDP-galactofuranose (UDP-Gal*f*), the precursor of Gal*f* found on the cell surface (Scheme 1) [18]. UGM is a unique flavoprotein, as it requires the flavin to be reduced in order to catalyze a non-redox reaction (Scheme 2) [19, 20]. The role of the flavin cofactor in catalysis is controversial. Experimental and structural data supports the role of the flavin acting as a nucleophile [21, 22]. Similarly, studies with flavin analogs and potentiometry experiments suggest that a single electron transfer step is necessary for catalysis [23, 24]. Here, we present a complete characterization of the recombinant form of UGM from *T. cruzi* (TcUGM). We utilize steady state kinetics, fluorescence anisotropy, rapid reaction kinetics, and the trapping of reaction intermediates to provide a clear view of the kinetic and chemical mechanisms employed by this unique enzyme. We also identify NAD(P)H as an effective electron donor to TcUGM, a function that is unique to eukaryotic UGMs.

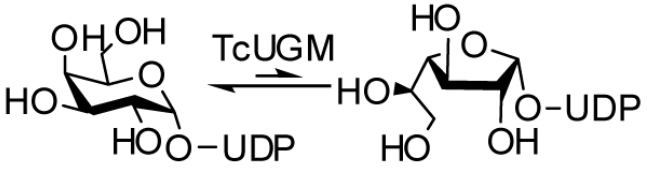

Scheme 6.1 Reaction catalyzed by TcUGM.

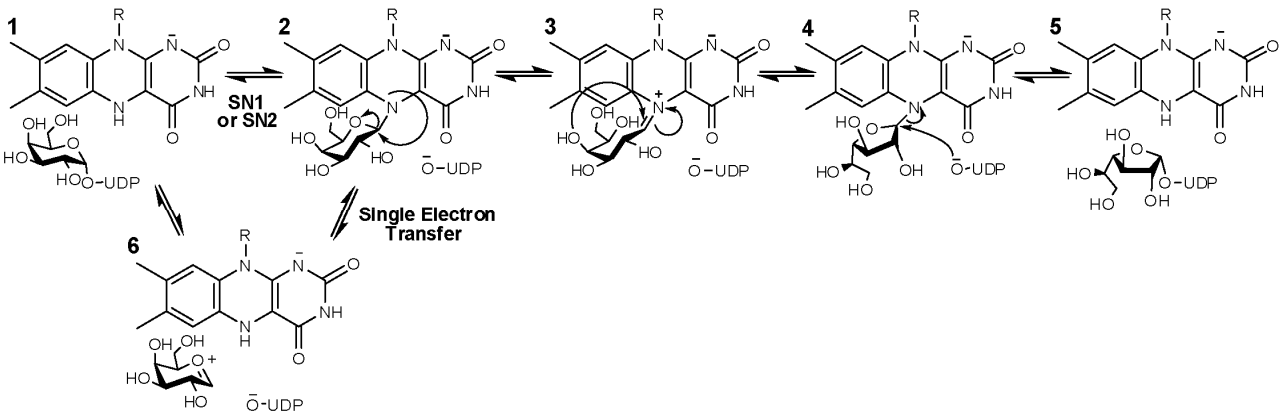

Scheme 6.2 The two proposed chemical mechanisms for UGMs. In one mechanism the reduced FAD (**1**) is depicted to act as a nucleophile forming a flavin-galactose adduct (either via S_N1 or S_N2) (**2**) and a subsequent iminium ion (**3**). These steps are followed by ring contraction forming the galactofuranose (**4**). An alternative mechanism predicts an electron transfer step, in which one electron is transferred from $FADH^-$ to an oxocarbenium ion intermediate (**6**) creating a flavin and a sugar radical, which react and form the galactose-FAD adduct (**2**), followed by ring contraction.

2. Materials and Methods

2.1 Materials. UDP, UDP-galactopyranose, and BL21T1^R chemical competent cells were purchased from Sigma (St. Louis, MO). Accuprime polymerase and TOP-10 chemical competent cells were obtained from Invitrogen (Carlsbad, CA). The restriction endonucleases *Sgf*I and *Pme*I were obtained from Promega (Madison, WI). Plasmid miniprep and PCR purification kits were from Qiagen (Valencia, CA). All other buffers and chemicals for biochemical studies were purchased from Fisher Scientific (Pittsburgh, PA). Expression plasmids, pVP55A and pVP56K, were obtained from the Center for Eukaryotic Structural Genomics, University of Wisconsin, Madison [25]. All reagents and solvents used in the synthesis of UDP-Gal*f*, if not specified otherwise, were obtained from Sigma-Aldrich (St. Louis, MO) or Fisher Scientific (Pittsburgh, PA) and were used without further purification. All the synthetic reactions were monitored to completion using thin layer chromatography (TLC) with *p*-anisaldehyde staining for visualizing carbohydrates along with UV detection when possible. ^1H and ^{13}C NMR were recorded on a

400MR Varian-400 MHz spectrometer. $CHCl_3$ (7.27 ppm) or HOD (4.79 ppm) were used as an internal reference.

2.2 Cloning. T. cruzi UGM (TcUGM) was amplified by PCR from genomic DNA using 5'-GGTTGCGATCGCCATGGCAGAATTATTGACACC -3' (*Sgf*I site is underlined) as the forward primer and 5'- CCAAGTTTAAACCATATCCTTCTGCAGTAGTC -3' (*Pme*I site is underlined) as the reverse primer. The TcUGM gene was inserted into the pVP55A and pVP56K vectors as previously described [17].

2.3 Protein expression and purification. Protein expression and purification of TcUGM was performed following methods previously described for *A. fumigatus* UGM with an additional final step of size exclusion chromatography in 25 mM HEPES, 125 mM NaCl, pH 7.5 (S-75, GE Healthcare, Piscataway, NJ) [17]. Purified TcUGM was concentrated, flash frozen in liquid N_2, and stored at -80 ^{o}C.

2.4 UV–visible absorbance spectrophotometry. The spectrum of recombinant TcUGM was recorded using an Agilent 8453 UV–visible spectrophotometer. The extinction coefficient was determined by dividing the absorbance value at 450 nm of the bound flavin in TcUGM by the absorbance value at 450 nm of free flavin (obtained by heat denaturation and centrifugation of the recombinant enzyme) and multiplying this value by the known extinction coefficient for FAD (ε_{FAD}= 11.3 $mM^{-1}cm^{-1}$) [26].

2.5 Solution molecular weight determination. The molecular weight of TcUGM was determined using size exclusion chromatography as previously described [17, 27].

2.6 NAD(P)H oxidation assays. Oxidation of NAD(P)H was monitored at 340 nm for 5 min. Reactions were performed at room temperature with air saturated 50 mM sodium phosphate buffer, pH 7.0, with various concentrations of NAD(P)H, in the presence or absence of 0.5 mM UDP-Gal*p*. The reaction was initiated by addition of 1 μM enzyme.

2.7 Flavin reduction by NAD(P)H. Flavin reduction by NAD(P)H was performed anaerobically in a glove box (Coy, Grass Lake, MI) using an Applied Photophysics Stopped Flow SX20 (Leatherhead, UK). Reactions were performed at 15 ^{o}C. Buffer (50 mM sodium phosphate pH 7.0) was made anaerobic by eight cycles of vacuum and argon flushing, each for 45 minutes. After this procedure, protocatechuate (400 μM) and protocatechuate dioxygenase (10 μg/mL) were added to the buffer to function as an oxygen scavenging system. All the solutions were prepared with the anaerobic buffer in the glove box. NAD(P)H solutions were prepared by dissolving the appropriate amounts in anaerobic buffer and concentrations were verified spectroscopically. The enzyme solution was made anaerobic by degassing with six 15 min cycles of vacuum and flushing with anaerobic argon. To ensure complete anaerobiosis, the solution was passed through a 2 mL desalting column previously equilibrated with anaerobic buffer. Enzyme with a final concentration of ~ 7.5 μM (after mixing) was mixed with various concentrations of NAD(P)H and the reaction was monitored with a photodiode array spectrophotometer until complete reduction was achieved. Identical experiments were performed in the presence of 0.5 mM UDP-Gal*p*. Change in absorbance at 452 nm was fitted to a

single exponential equation and the resulting k_{obs} values were plotted as a function of NAD(P)H concentration. These data was fit with equation 1 to obtain the rate constant for reduction (k_{red}) and the K_d value.

$$k_{obs} = \frac{k_{red} * [S]}{K_d + [S]} \qquad (1)$$

2.8 Synthesis of UDP-Galf. Synthesis of α-D-Galactofuranosyl bis(triethylammonium) phosphate (Gal*f*-1-phosphate) was performed over a series of three steps with methods adapted from previously published protocols [28-34]. Details of the synthesis and NMR data are outlined in the supplementary material found at the end of this chapter. UDP-Gal*f* was synthesized following published method reported by Poulin and coworkers [35].

2.9 Activity assay. The activity of recombinant TcUGM was tested with UDP-Gal*f* as the substrate following procedures previously described [17]. Concentration of TcUGM was determined based on bound flavin. TcUGM (100 nM) was reduced with either 20 mM dithionite, 500 μM NADPH, or 2.5 mM NADH for each activity assay.

2.10 Viscosity Effects. Viscosity effects were determined using the activity assay as described above. Reactions were done in the presence of 0, 5, 10, 20, and 30% glycerol, 800 μM UDP-Gal*f*, 20 mM dithionite, and 200 nM TcUGM. The relative viscosity (η_{rel}) of the reaction was determined using a reference table for different percentages of glycerol in solution [36].

2.11 Fluorescence anisotropy. Synthesis of UDP-rhodamine was performed as previously described [37]. The optimal concentration of TcUGM (30 μM) and UDP-rhodamine (30 nM) for

the binding assays was determined following procedures established in our laboratory for a related UGM enzyme from *Aspergillus fumigatus* [37]. Binding of UDP-Gal*p* to TcUGM was monitored in the presence and absence of 10 mM sodium dithionite by measuring the changes in anisotropy [37]. The K_d values were obtained using the equation 2, where m_1 and m_2 are the minimum and maximum anisotropy, respectively; m_3 is the slope, and m_4 is the K_d.

$$y = m_1 + \frac{(m_2 - m_1)x^{m_3}}{m_4^{m_3} + x^{m_3}} \qquad (2)$$

2.12 Trapping of the flavin-galactose adduct. The procedure was adapted from Gruber *et al*. and optimized for trapping and isolation of the adduct in TcUGM [22]. Reactions were prepared using 1 mM TcUGM, 200 mM UDP-Gal*p*, 1 M sodium cyanoborohyride, and 100 mM sodium dithionite in a final volume of 15 µL with 100 mM sodium phosphate buffer at pH 7.0. Reactions were incubated for 45 min at room temperature then terminated with addition of 6 M HCl and neutralized with 1 M sodium phosphate buffer at pH 7.0. A final concentration of 200 mM NaCl was added. The sample was then centrifuged to precipitate denatured protein from the yellow solution containing the free flavin. The adduct was isolated using HPLC (Shimadzu) by injecting the yellow solution onto a reverse phase C18 column (Phenomenex Luna C18 5 microns, 250 x 4.6 mm) equilibrated with 5% B (A: Water, B: 100% acetonitrile). The column was washed for 5 min with 5% B, then a 15 min linear gradient to 15% B, followed by 20 min linear gradient to 75% B. The flavin species were eluted at ~20-24 minutes and were characterized by high-resolution mass spectrometry (Virginia Tech Mass Spectrometry incubator).

*2.13 Reaction of reduced TcUGM with UDP-Gal*p*, UDP, and UDP-glucose.* Rapid reaction kinetics were done using the methods described for the TcUGM reduction studies. However, reduced TcUGM was prepared by addition of 20 mM sodium dithionite. Excess dithionite was removed using a 2 mL desalting column. Reduced TcUGM (~15 μM final concentration) was mixed with buffer alone for a final concentration of 0.15 mM UDP-Gal*f*, 0.25 mM UDP-Gal*p*, 0.25 mM UDP, and 0.25 mM UDP-glucose (UDP-Glc). Spectra were collected on a logarithmic time base from 1.3 ms to 2 s using a photodiode array. The rate of the intermediate formation was calculated by fitting the change in absorbance at 452 nm to a double exponential equation 3.

$$\upsilon = c + a_1 e^{-(k_1 * t)} + a_2 e^{-(k_2 * t)} \qquad (3)$$

3. Results

3.1 Expression and Purification. Successful expression of soluble TcUGM was accomplished in the pVP56K vector [17]. The protein was expressed as an N-terminal fusion to maltose binding protein (MBP) with an 8x-His tag, which aids in purification. BL21T1^R cells containing the pVP56K-TcUGM plasmid were grown in auto-induction medium for 8 h at 37 ^oC followed by overnight incubation at 25 ^oC [38]. Approximately 9 g of cell paste per liter of media was obtained and 1 mg of purified TcUGM was isolated for each g of cell paste. Recombinant TcUGM contained noncovalently bound flavin cofactor, which had a typical flavin spectrum with peaks at 376 nm and 448 nm with a shoulder at 468 nm (Figure 1). The extinction coefficient was determined to be 10.8 mM^{-1} cm^{-1} at 450 nm.

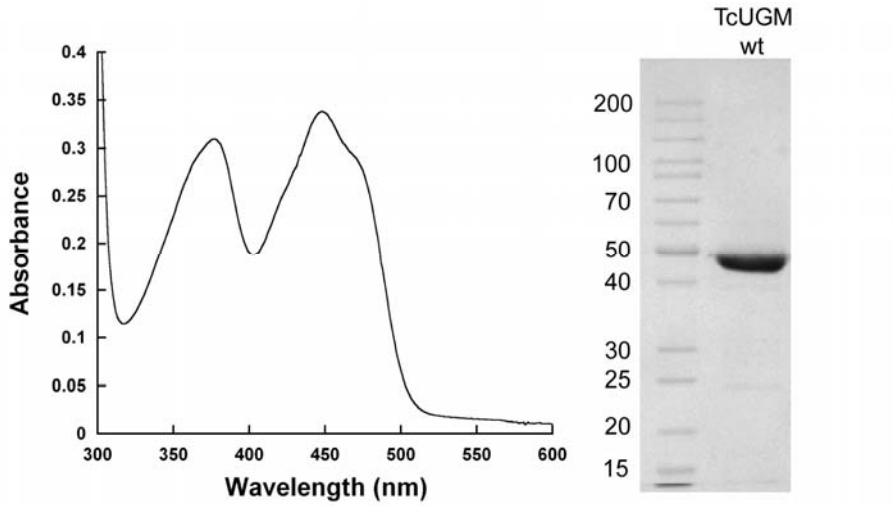

Figure 6.1 Flavin spectrum and SDS-PAGE of purified TcUGM.

3.2 Determination of the oligomeric state. Size exclusion chromatography was used to calculate a molecular weight of 67,800 ± 10,000 Da for the recombinant TcUGM (Figure 2). This value is consistent with the molecular weight predicted for a single polypeptide (54,700 Da).

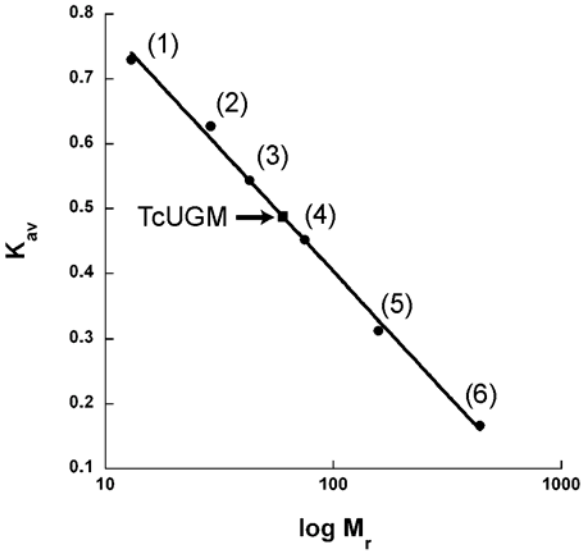

Figure 6.2 Size exclusion chromatography of TcUGM. The standards aprotinin (1, 6.5 kDa), ribonuclease (2, 13 kDa), ovalbumin (3, 43 kDa), conoalbumin (4, 75 kDa), aldolase (5, 158 kDa), and ferritin (6, 440 kDa) were used to calculate the K_{av} values using the equation, $\left(K_{av} = \frac{V_e - V_o}{V_t * V_o} \right)$, where V_o is the void volume of the column; V_t is the total volume of the column and V_e is the elution volume of the protein). TcUGM is shown on the plot as a black square (■).

3.3 Oxidase activity with NADPH and NADH. The activity of all UGMs requires the flavin to be in the reduced state. Although the prokaryotic enzymes have been extensively studied, the mechanism of reduction is yet to be determined [20, 39]. Even though an NAD(P)H binding domain was not found in the primary sequence of TcUGM, we tested whether this enzyme was capable of reacting with reduced dinucleotides. The oxidation of either NADH or NADPH was monitored in the presence and absence of UDP-Gal*p* under aerobic conditions. Under these conditions, no mutase activity is measured, instead what is measured is the steady-state reduction of the flavin cofactor in TcUGM, which is slowly oxidized by molecular oxygen (Figure 3A). In the absence of UDP-Gal*p,* a slow oxidase activity, k_{ox}, was observed for both coenzymes, while a 6-fold lower K_M value was measured for NADPH (Figure 3B). In the presence of UDP-Gal*p,* a minor decrease in k_{ox} was measured (Table 1). In contrast, when the same activity was measured with recombinant *M. tuberculosis* UGM (MtUGM), there was no measurable NAD(P)H oxidation (Table 1). *E. coli* UGM has also been shown to be unable to react with NAD(P)H [20,39].

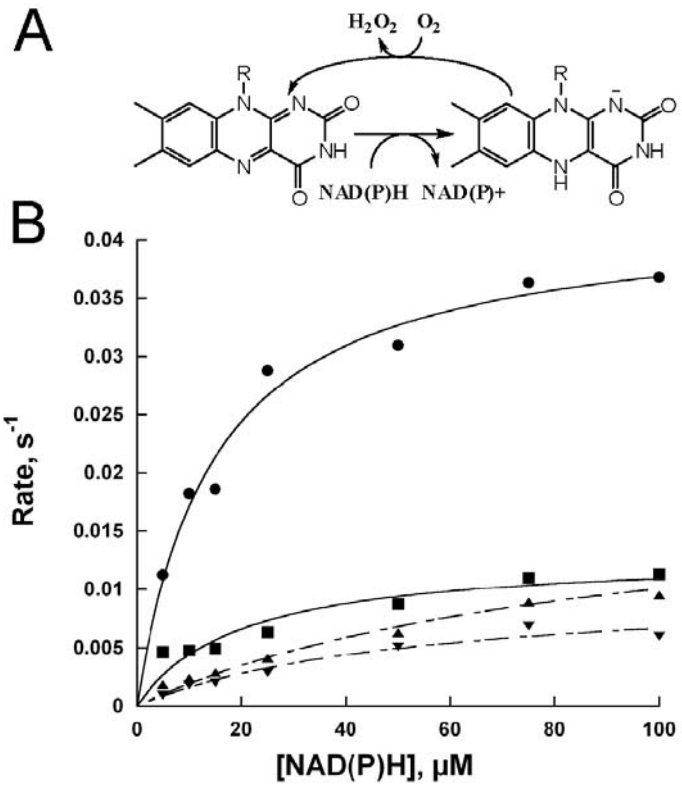

Figure 6.3 Oxidase activity of TcUGM with NAD(P)H. A) Scheme representing the oxidase activity of TcUGM measured in this assay. B) Activity of TcUGM measured in the presence and absence of saturating concentration of UDP-Gal*p* (0.5 mM) under air saturating conditions at room temperature (NADPH (●), NADH (▲), NADPH + UDP-Gal*p* (■), and with NADH + UDP-Gal*p* (▼)).

Table 6.1 Kinetic parameters of NAD(P)H oxidation reactions[a]

	NADH		NADPH	
	k_{ox}, s^{-1}	**K_M, µM**	**k_{ox}, s^{-1}**	**K_M, µM**
TcUGM	0.015 ± 0.002	90 ± 20	0.030 ± 0.002	15 ± 2
TcUGM + UDP-Gal*p* [b]	0.010 ± 0.002	50 ± 20	0.0099 ± 0.001	19 ± 5
MtUGM	1.8×10^{-6}	-	1.1×10^{-6}	-
NAD(P)H alone	1.8×10^{-7}	-	4.7×10^{-7}	-

[a] All reactions were done at room temperature with air saturated buffer (50 mM phosphate buffer pH 7.0).
[b] In the presence of 0.5 mM UDP-Gal*p*.

3.4 Flavin reduction monitored by rapid reaction kinetics. The decrease in absorbance at 450 nm under anaerobic conditions was measured in a stopped flow spectrophotometer to determine the

rate constant of flavin reduction of TcUGM by the reduced coenzyme (Figure 4A, B). The observed rate constant of flavin reduction, k_{red}, with NADPH was seven-fold faster than with NADH (Table 2, Figure 4C). Furthermore, the K_d value for NADPH was five-fold lower than for NADH. These results suggest that NADPH is the preferred coenzyme. Reduction of TcUGM with NADPH was also tested in the presence of saturating UDP-Gal*p*. Under this condition, the k_{red} value did not change, demonstrating reduction is unaffected by the presence of UDP-Gal*p* (0.57 ± 0.01 s^{-1} in the absence of UDP-Gal*p* versus 0.57 ± 0.04 s^{-1} in the presence of UDP-Gal*p*).

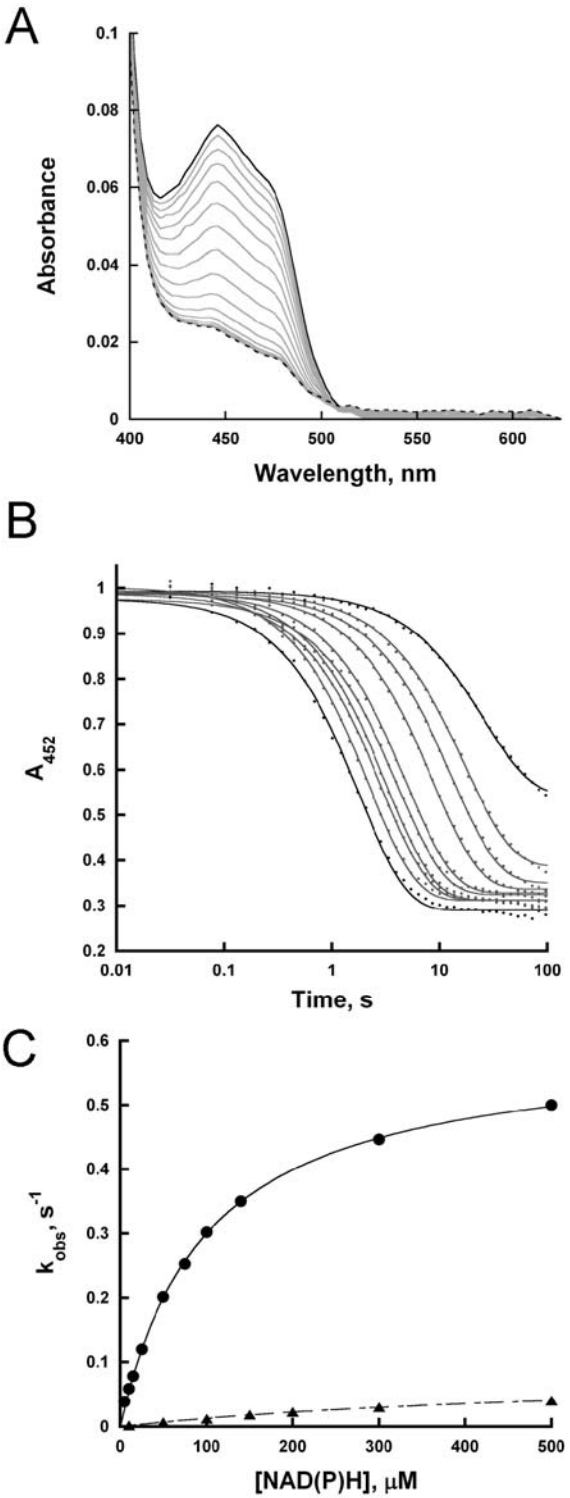

Figure 6.4 Anaerobic reduction of TcUGM with NAD(P)H. Reduction was done using the stopped flow spectrophotometer at 15 ^{o}C, data was collected from 2 ms to 100 s on a logarithmic timescale. A) Changes in the spectra of oxidized TcUGM after mixing with 0.5 mM NADPH over 23 s. B) Flavin reduction by NADPH for varying concentrations of NADPH. The data were fit to a single exponential decay equation. C) The k_{obs} values were plotted as a function NADPH (●) and NADH (▲) concentrations and fitted using the equation 2.

Table 6.2 TcUGM Reduction by NAD(P)H[a]

	k_{red}, s^{-1}	K_d, μM	k_{red}/K_d, μM^{-1} s^{-1}
NADPH	0.60 ± 0.006	98 ± 3	0.0061 ± 0.0001
NADH	0.085 ± 0.0006	550 ± 10	0.00015 ± 0.000002

[a] Reactions were measured under anaerobic conditions at 15 °C in 50 mM phosphate buffer pH 7.0.

3.5 Mutase activity. The activity of TcUGM reduced with NADPH and NADH was measured and compared to the values obtained with dithionite reduced enzyme (Table 3, Figure 5). The reverse reaction was monitored to allow significant accumulation of product, as equilibrium favors UDP-Gal*p* over UDP-Gal*f* (93% to 7%). Saturation kinetics were observed as a function of UDP-Gal*f* concentration. Data were fit to the Michaelis-Menten equation and very similar k_{cat} values were obtained independent of the source of reducing equivalents (Table 3). The K_M values were also very similar when the enzyme was reduced with NADPH or dithionite. In contrast, a higher K_M value was measured with NADH as the reductant, which we attributed to the slower rate of reduction by NADH (Table 3).

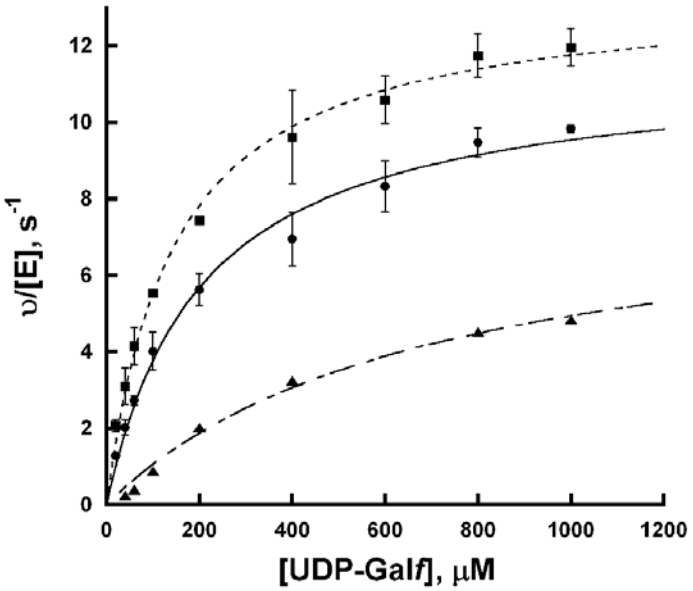

Figure 6.5 TcUGM activity with UDP-Gal*f*. TcUGM was reduced with either 20 mM dithionite (■), 0.5 mM NADPH (●), or 2.5 mM NADH (▲). Reactions were performed with 200 nM TcUGM incubated with varying concentrations of substrate for 1 min at 37 ^{o}C. The data was fit to the Michaelis-Menten equation. Summary of data is presented in Table 3.

Table 6.3 Steady state kinetics of TcUGM[a]

Reductant	**k_{cat}, s^{-1}**	**K_M, μM**	**k_{cat}/K_M, μM^{-1} s^{-1}**
Dithionite	13.4 ± 0.3	140 ± 10	0.093 ± 0.006
NADPH	11.5 ± 0.4	200 ± 20	0.056 ± 0.005
NADH	8.4 ± 0.9	690 ± 150	0.012 ± 0.001

[a] Reactions were incubated at 37 ^{o}C for 1 min in 25 mM Hepes, 125 mM NaCl pH 7.5, and terminated by heat denaturation at 95 ^{o}C. Reactions were performed using saturating amounts of reductant (20 mM dithionite, 0.5 mM NADPH, and 2.5 mM NADH).

3.6 Viscosity effects. To determine if product release is the rate-limiting step, the effect of viscosity on k_{cat} was measured. This was done by determining the activity of TcUGM at different concentrations of glycerol. If product release was the rate-limiting step, a decrease in the k_{cat} value would be observed as the viscosity of the medium increased. A plot of the ratio of the k_{cat} values in water, $(k_{cat})_0$, and at each concentration of viscogen, $(k_{cat})_\eta$, should yield a straight line with a positive slope. A slope of 1 is expected if product release is the rate-liming step. With TcUGM, a slope of zero was observed, indicating that product release is not the rate

determining step in the reaction (Figure 6). Therefore we concluded the k_{cat} is attributed to a chemical step in the reaction.

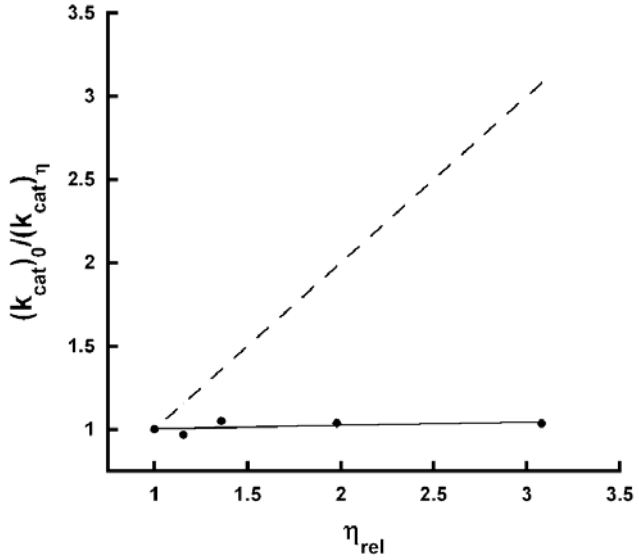

Figure 6.6 Effects of viscosity on the rate of the reaction. The effect of viscosity was determined by measuring the activity of TcUGM as a function of increasing concentrations of glycerol. The data was fit to a linear equation; the dashed line depicts the results of a diffusion controlled reaction. This line has a slope of 1.

*3.7 Determination of the binding affinity of UDP-Gal*p *to TcUGM.* To determine if UDP-Gal*p* binds to oxidized or reduced TcUGM, we synthesized UDP-rhodamine to measure binding of the substrate. Fluorescence anisotropy changes induced by release of the bound chromophore to TcUGM upon binding of the substrate can be used to calculate the dissociation constant (Figure 7A) [37].UDP-Gal*p* was found to have very weak affinity to oxidized TcUGM. We tested concentrations of substrate as high as 100 mM and were unable to measure binding. However, when TcUGM was reduced with dithionite, a K_d of 70 ± 40 μM was determined demonstrating UDP-Gal*p* only binds to the reduced state of TcUGM (Figure 7B).

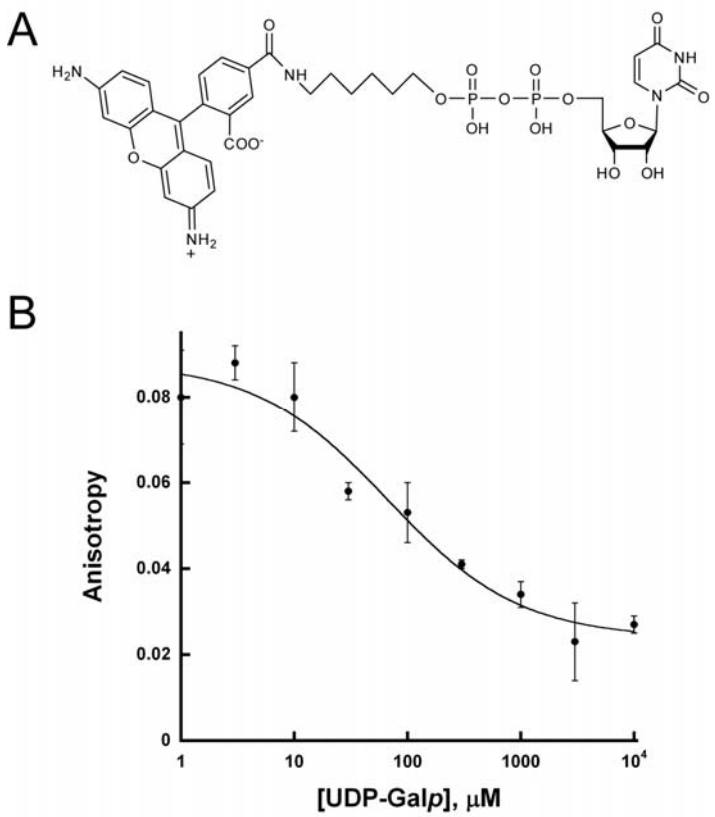

Figure 6.7 Fluorescence anisotropy assay to measure the affinity of UDP-Gal*p* to TcUGM. A) UDP-rhodamine chromophore used in the fluorescence anisotropy experiments. B) Fluorescence polarization binding assay. The binding of UDP-Gal*p* to chemically reduced TcUGM (30 μM) was monitored by measuring the changes in anisotropy as it displaces UDP-rhodamine (30 nM) from the active site. The concentrations of chromophore and enzyme were chosed based upon conditions that resulted in half-maximal anisotropy. The K_d values were obtained using equation 3.

3.8 Isolation of the flavin-galactose adduct. In the UGM reaction, a novel role for the flavin cofactor has been proposed. It was suggested that the flavin could attack UDP-Gal*p* at the anomeric carbon, leading to cleavage of the C-O bond (Scheme 2, **2**). In the bacterial enzymes a flavin-galactose adduct was isolated and characterized, supporting this role for the flavin cofactor [21, 22]. Involvement of such an adduct in the reaction of eukaryotic UGMs was investigated. The adduct was trapped by performing activity assays in the presence of sodium cyanoborohydride, which reduces the iminium ion during turnover. The flavin was extracted and then isolated by HPLC (Figure 8A). Two major peaks were observed, one corresponding to

native FAD, while the other had spectral peaks at 230 nm, 315 nm, and 378 nm (Figure 8B). This flavin spectrum is consistent with previous published spectra for the N5-flavin adduct however the peak at 378 nm is indicative of a C4a-oxygen-flavin adduct [21, 40]. This compound was characterized by high resolution mass spectrometry (HRMS) and shown to have a mass of 966.1946 Da (Figure 8C). This mass corresponds to the expected mass of the FAD-galactose adduct (950.2340 Da) with the addition of a hydroxyl group (16 Da) to give an expected mass of 966.2 Da. We propose that the flavin was hydroxylated at the C_{4a} position during the trapping and isolation process, which agrees with the observed spectrum.

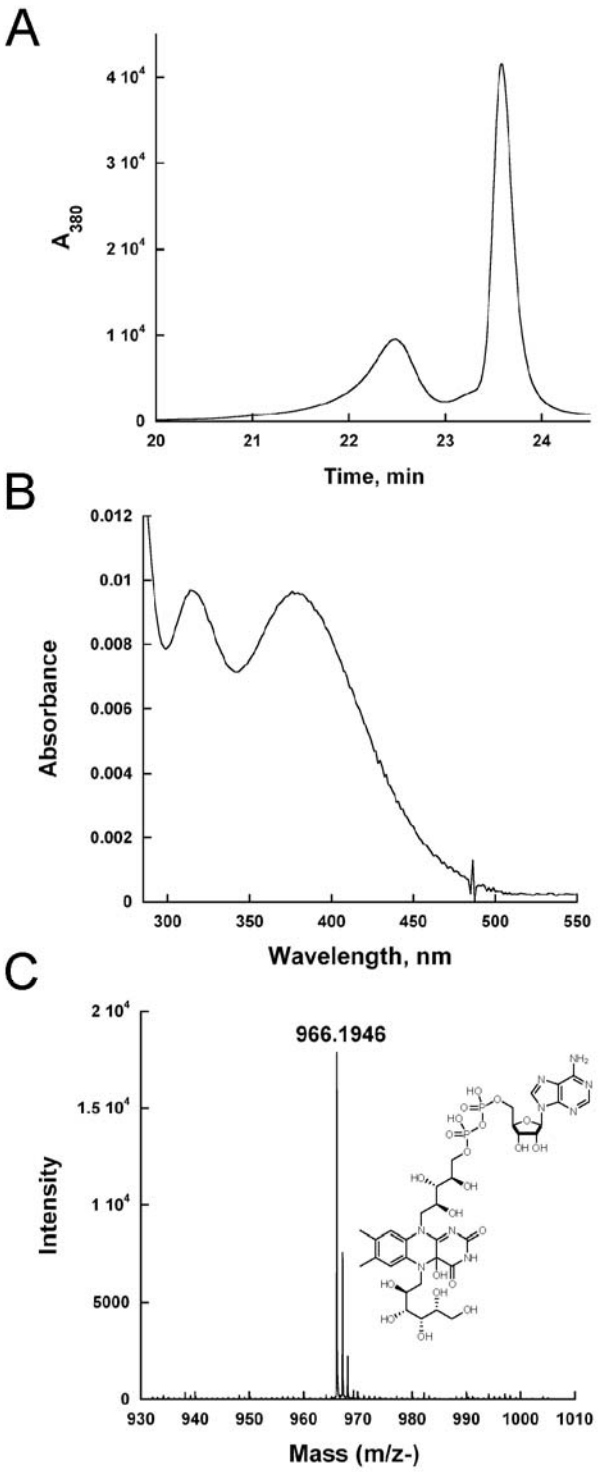

Figure 6.8 Trapping of a covalent flavin intermediate. A) Separation of the FAD and the adduct by HPLC. The peak eluding at 22.5 min is the adduct (~5% of the FAD species), while the second peak at 23.6 min is FAD(~95% of the flavin species). B) Spectrum of the TcUGM FAD-galactose adduct showing a spectrum indicative of a hydroxyl located at the C_{4a} position. C) High resolution mass spectrometry (negative ion mode) results of the peak eluding at 22.5 min. The inset shows the structure of the adduct with a hydroxyl group at the flavin C_{4a} position.

*3.9 Monitoring the reaction of reduced TcUGM with UDP-Gal*p*, UDP-Gal*f*, UDP, and UDP-Glc.* As the results obtained supported a flavin-galactose adduct, we next sought to establish how the flavin-galactose adduct is formed in the UGM reaction. However, the mechanism leading to the formation of this intermediate can occur via the formation of a flavin and sugar radical (Scheme 2, **6**-**2**) or by a direct nucleophilic attack by the flavin (Scheme 2, **1**-**2**). Since a flavin semiquinone has distinct spectroscopic characteristics, we used rapid reaction kinetics to monitor the reaction at early time points. In this experiment, anaerobically reduced TcUGM was mixed with either buffer alone, UDP, UDP-glucose (UDP-Glc), UDP-Gal*p*, or UDP-Gal*f* in the stopped-flow spectrophotometer and complete spectra were collected between 350 nm and 700 nm (Figure 9). When the enzyme was mixed with buffer alone or with UDP, no major spectral changes were detected (Figure 9A, buffer alone not shown). Difference spectra of TcUGM after mixing with UDP-Glc showed a slight decrease in absorbance at ~ 415 nm, which agrees with previous data with UDP-Glc binding to *Klebsiella pneumoniae* UGM (KpUGM) (Figure 10) [21,41]. TcUGM mixed with either UDP-Gal*p* or UDP-Gal*f* showed the same spectral changes with a decrease at ~ 405 nm, an isosbestic point at ~ 425 nm (red shifted 10 nm with UDP-Gal*p*), and a peak at ~ 460 nm (Figure 9B, C). Equilibrium binding of UDP-Gal*p* to KpUGM showed similar flavin spectral changes, however, it was red shifted by ~ 50 nm [21]. The change in absorbance at the higher wavelengths was attributed to the formation of the iminium ion intermediate [21]. As the change at higher wavelengths does not occur upon binding of the known ligand UDP-Glc, but only upon substrate binding, we propose that these spectral changes correspond to the formation of the iminium ion in TcUGM (Scheme 2, **3**). A k_1 value of 310 ± 40 s^{-1} and a k_2 value of 7.9 ± 0.7 s^{-1} were obtained from fitting the absorbance changes at 452 nm to a double exponential equation (Figure 9D). We attributed the fast rate to the formation of the

iminium ion. Since the rate of k_2 closely matches the value of k_{cat}, we concluded that it is associated with the rate limiting step, which could be either ring closing or reattachment of UDP. More importantly, upon mixing reduced TcUGM and substrate, a flavin semiquinone was not observed, suggesting either the semiquinone does not form or that the rate of decay is faster than the rate formation.

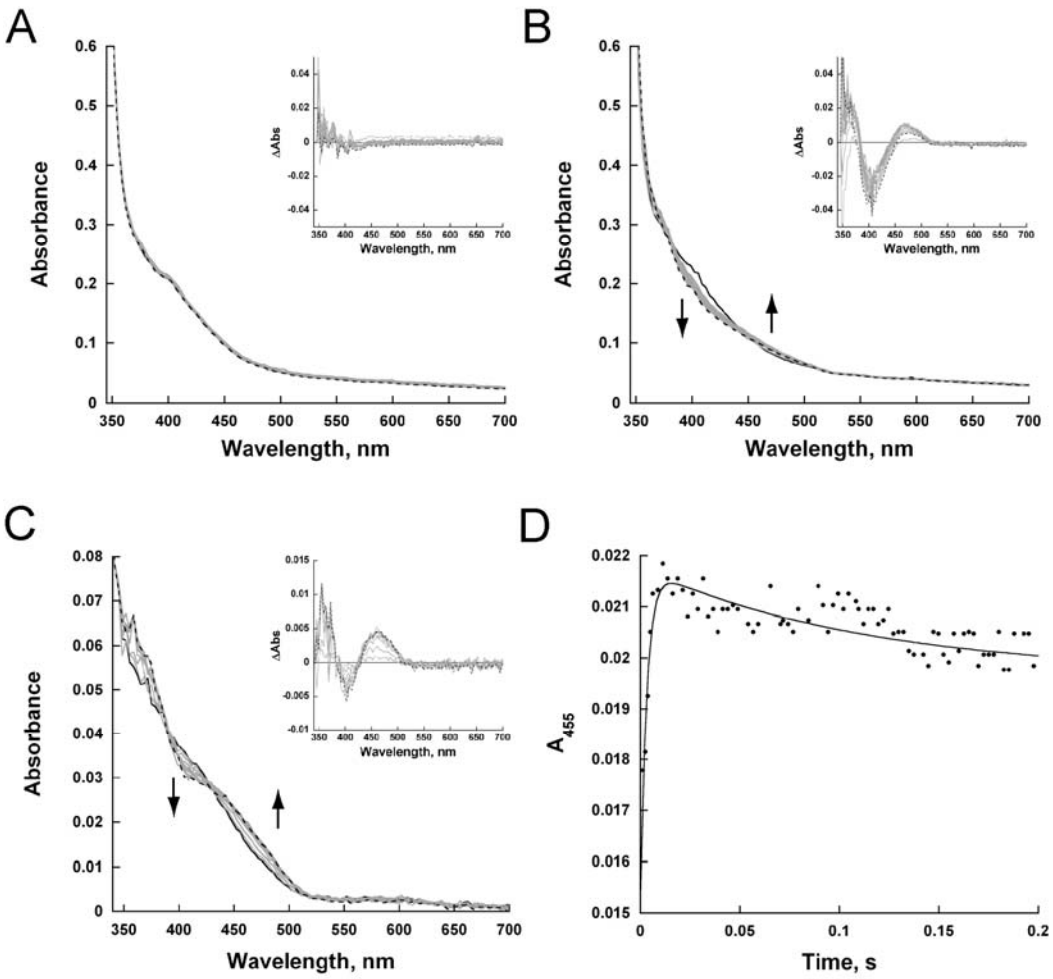

Figure 6.9 Rapid reaction kinetics with reduced TcUGM mixed with substrate and substrate analogs. The initial spectrum (1.2 ms) is shown as a solid line, the final spectrum (14 ms for UDP-Gal*f* and 1.5 s for all other analogs) as a dashed line, and intermediate time points as gray lines (spectra every 1.26 ms for UDP-Gal*f* and every tenth spectrum collected of 400 points on logarithmic time scale over 2s for all other analogs). Reduced TcUGM mixed with 0.25 mM UDP (A), 0.25 mM UDP-Gal*p* (B), 0.15 mM UDP-Gal*f* (C), and formation of the iminium ion monitored at 455 nm (D). The data shown in panel D is one example of many plots obtained monitoring the formation of the intermediates and was fit to equation 3 (D). Insets in A-C are difference spectra of each plot.

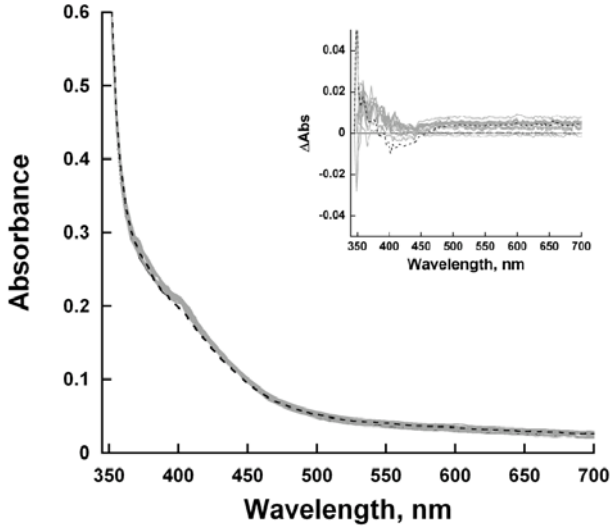

Figure 6.10 Rapid reaction kinetics with reduced TcUGM mixed with 0.25 mM UDP-Glc. Inset shows the difference spectra.

4. Discussion

UGM belongs to a growing group of flavoproteins where the protein environment modulates the reactivity of the flavin to perform novel non-redox chemistries [42, 43]. There are two proposed mechanisms for UGM. The proposed mechanisms differ on the steps leading to the formation of the flavin galactose adduct. In one mechanism, the flavin acts as a nucleophile and attacks the anomeric carbon leading to the formation of the flavin-galactose adduct intermediate, which can either occur via a direct attack on UDP-Gal*p* (S_N2) or on a postulated oxocarbenium ion intermediate (S_N1)(Scheme 2, **1**-**2**). In the other mechanism, elimination of UDP leads to the formation of an oxocarbenium ion followed by a single electron transfer from the reduced flavin (Scheme 2, **6**), forming a flavin seminquinone and sugar radical. Radical rearrangement of the N5 of the flavin and subsequent recombination leads to the formation of the flavin-galactose adduct (Scheme 2, **2**). Once the adduct is formed, the galactose ring opens leading to the formation of a sugar-flavin iminium ion (Scheme 2, **3**) [21, 22]. After

recyclization, the final step in the reaction involves an attack on the anomeric carbon by UDP, leading to the formation of UDP-Gal*f* (Scheme 2, **4-5**).

These mechanisms were developed and supported by data obtained entirely from studies on prokaryotic UGMs with several aspects of the proposed mechanisms not completely understood. It was shown by position isotope effects (PIX) that the glycosidic bond between galactose and UDP was broken during catalysis [44]. Later studies demonstrated that the semiquinone of the flavin is stabilized in the presence of UDP and UDP-Gal*p* and that UGM is inactive with 5-dezaflavin, supporting the single electron transfer mechanism [23, 24]. The formation of a flavin N5-C1 galactose adduct was then demonstrated by trapping the immium ion with $NaCNBH_3$ [21, 22]. This result supports a mechanism in which the flavin acts as a nucleophile. Furthermore, the structure of bacterial enzymes in complex with UDP-Gal*p*, show proper binding conformation for nucleophilic attack by the flavin cofactor [22, 45]. Also in support of the nucleophilic mechanism, it was also shown that the flavin was present as in the anionic hydroquinone form, a feature that is indicative of the N5 being a good nucleophile [21, 24].

Here, we expressed and purified the eukaryotic UGM from the parasite *T. cruzi*. Recombinant TcUGM was found to function as a monomer in solution, which differs from both the dimeric prokaryotic UGMs, and the tetrameric fungal UGM (AfUGM) [17, 20]. However, it is similar to the parasitic UGM from *L. major* (LmUGM), which is also a monomer [27]. This suggests that TcUGM and LmUGM are closely related, which agrees with their higher percent amino acid identity (60% with LmUGM, compared to 40% with AfUGM and 15% with EcUGM and MtUGM). TcUGM was found to be active only in the reduced form. Chemically reduced

TcUGM has similar kinetic parameters with UDP-Gal*f* as substrate as other UGMs [17, 27, 28, 45, 46].

Having stable and active TcUGM, a series of experiments were performed to address several unanswered questions about the chemical mechanism. We sought to determine the source of the reducing equivalents required for catalysis. *In vivo*, a common source of reducing equivalents for flavoenzymes is NAD(P)H. It was determined that recombinant TcUGM could be reduced by NADPH or NADH in the absence of UDP-Gal*p*, and was oxidized very slowly by molecular oxygen. In the presence of substrate, the reaction with oxygen was decreased. Thus, substrate binding protects the enzyme from oxidation, which is essential for activity since TcUGM is active only in the reduced form. There is no canonical NADPH binding domain in the primary sequence of TcUGM, thus the binding site of NADPH remains to be identified. The reactivity of TcUGM with NAD(P)H is unique since prokaryotic UGMs are unable to react with reduced coenzymes. Perhaps the bacterial enzymes have specific redox partners in the cell.

The rate of flavin reduction by NAD(P)H was directly monitored in the stopped-flow spectrophotometer. It was shown that the rate constant of flavin reduction and the affinity for NADPH was higher than for NADH. These results showed a 40-fold higher k_{red}/K_d value for NADPH over NADH, suggesting that NADPH is the preferred coenzyme. Our results clearly show, TcUGM can use either coenzyme *in vivo* depending on the cellular availability of NADPH and NADH, which is shown to vary based upon cellular environments [47-49].

The rate of flavin reduction was not affected by the presence of UDP-Gal*p*, indicating that binding of UDP-Gal*p* is not a prerequisite for reduction. Furthermore, UDP-Gal*p* only binds to the reduced form of TcUGM, indicating that UDP-Gal*p* binds after flavin reduction. The K_d value of UDP-Gal*p* for the reduced UGM was determined to be 70 ± 40 μM by fluorescence

anisotropy. Thus, the kinetic mechanism is initiated with binding of NADPH followed by hydride transfer and UDP-Gal*p* binding, with UDP-Gal*p* protecting the enzyme from reacting with molecular oxygen. It can be estimated from the k_{cat} value (~12 s^{-1}) and the rate of oxidation, (0.01 s^{-1}) that for every NADPH oxidized the enzyme can turn over ~1000 times.

When reduced TcUGM was mixed with UDP-Gal*p* or UDP-Gal*f* using stopped-flow spectroscopy only a small decrease in absorbance at 415 nm and an increase at 460 nm was observed. These changes were not observed when the enzyme was mixed with either UDP or UDP-Glc, ligands that do not turn over. Therefore, we assigned the spectral changes to the formation of the iminium ion. Similar spectral changes have been reported with bacteria UGM under equilibrium conditions, which are consistent with our conclusion [21]. Interestingly, the flavin semiquinone was not observed suggesting either it does not occur or it decays rapidly preventing detection. By addition of sodium cyanoborohydride into the reaction mixture, a flavin-sugar adduct was trapped and was isolated and characterized by mass spectrometry. This result validates the assignment of the iminium ion intermediate observed in the stopped-flow experiments. This adduct has also been characterized in KpUGM as a flavin N5-C1 galactose intermediate by HRMS and ^{1}H NMR [21, 22]. From our rapid reaction kinetics data, the changes in flavin absorbance best fit a double exponential equation with a fast and slow rate. We assigned the fast rate to the formation of the iminium ion, which occurs at 310 ± 42 s^{-1}. While the slow rate occurred at 7.9 ± 0.7 s^{-1}, and as it closely matches the k_{cat} value (~12 s^{-1}), we propose that this corresponds to the rate-limiting step. One possibility is that the rate constant that controls k_{cat} corresponds to product release. To determine if product release is the rate-limiting step in the reaction, viscosity effects studies on k_{cat} were performed. If product release is the slow step that determines the k_{cat} value, a linear decrease in the k_{cat} value should be observed

as a function of increasing concentrations of viscogen. Using glycerol as a viscogen, no changes in the k_{cat} value was observed, clearly indicating that product release is not the rate-limiting step in the reaction of TcUGM. Therefore, we conclude that the rate-limiting step must be ring closing or UDP reattachment. Further studies are needed to elucidate between the two.

Our results from the rapid reaction kinetic analysis show that a flavin iminium ion is formed and suggest that a flavin semiquinone does not play a role in catalysis. Furthermore, we were able to trap and characterize a flavin-galactose adduct. These data strongly supports the role of the flavin as a nucleophile. We proposed that the formation of this adduct occurs via a direct attack of the flavin (S_N2 mechanism) rather than formation of an oxocarbenium ion, followed by flavin attack (S_N1 mechanism). Our conclusion is supported by data from Sun et al. where linear free energy relationship (LFER) studies using various FAD analogs show changes in k_{cat} values that correlate linearly with changes in the nucleophilicity of the flavin N5 (ρ value of -2.4), which is consistent with an S_N2 mechanism [50]. Also, previous studies with *E. coli* UGM (EcUGM), it was shown that UDP-[2-deoxy-2-fluoro]-Gal*f* functions as a substrate with a k_{cat} value 10^3 slower than the reported k_{cat} with UDP-Gal*f* [28]. In contrast, in studies with glycosyltransferases, where the formation of an oxocarbenium ion is known to occur, it has been shown that substrates with fluorine at the C2 position destabilize the formation of the oxocarbenium ion preventing the reaction from occurring [51-54]. Therefore, if the UGM reaction proceeded by an oxocarbenium ion, UDP-[2-deoxy-2-fluoro]-Gal*f* should act as an inhibitor instead of as a slow substrate.

Together, the data presented here provides a detailed description of the mechanism of the parasitic TcUGM, which is summarized in Scheme 3. We show that TcUGM first binds to NADPH (Scheme 3, **b**), and after hydride transfer (Scheme 3, **c**), UDP-Gal*p* binds (Scheme 3,

d). We propose that an adduct forms by direct attack of the flavin to the C1 position of galactose (Scheme 3, **e**), without the formation of a flavin semiquinone or oxocarbenium ion. Ring opening leads to the rapid formation of an iminium ion (Scheme 3, **f**). Product release was determined not to be rate limiting, therefore, ring closing or formation of the glycosidic bond between Gal*f* and UDP represent the rate determining step(s) in this reaction. Since UDP is predicted to remain bound in the active site, we believe that formation of the anomeric bond will be fast, therefore, the slow step is most probably the isomerization step (Scheme 3, **f** to **g**). The mechanism of TcUGM clearly shows a unique mode of action for the flavin cofactor, where it functions as a nucleophile and a scaffold for holding the reaction intermediates. These results will aid in the development of new drugs against human pathogens such as *T. cruzi*, *A. fumigatus*, and *L. major*.

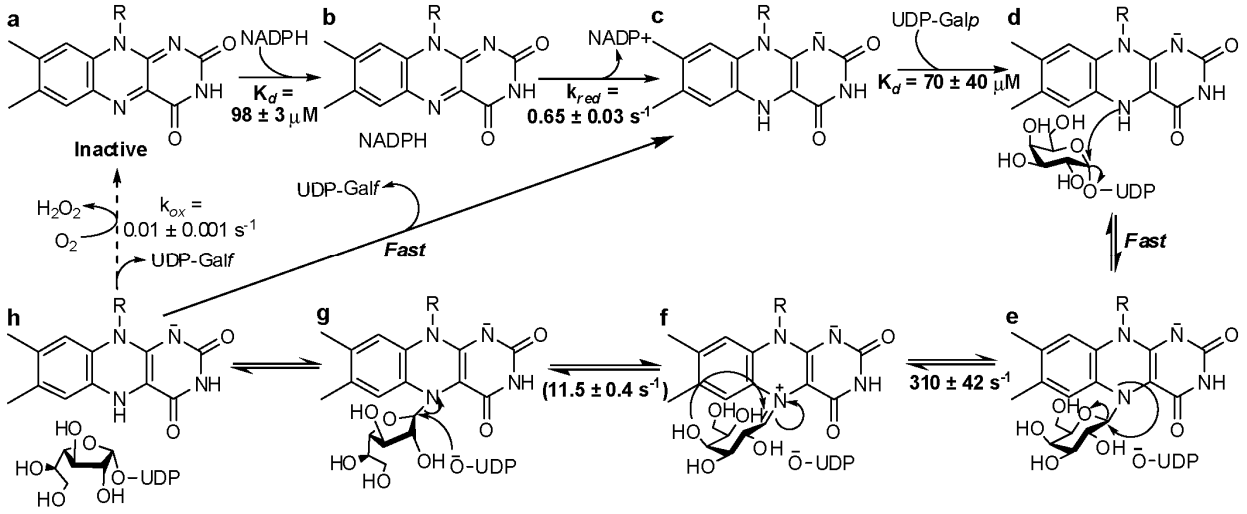

Scheme 6.3 Chemical mechanism of TcUGM. The reaction requires the oxidized flavin cofactor (**a**) to be reduced for activity. First, NADPH binds to the oxidized enzyme (**b**), and only after the flavin is reduced (**c**) will UDP-Gal*p* bind (**d**). The flavin then acts as a nucleophile attacking the C1 of galactose and forming a flavin sugar adduct (**e**), which occurs rapidly (**f**). This is followed by ring opening and recyclization (**g**). The rate limiting step in the reaction corresponds to either galactose isomerization or reattachment of the UDP (**f** to **g**). We postulate that the rate limiting step is the isomerization step. The final step is release of UDP-Gal*f*, which occurs rapidly. The flavin can proceed to the next reaction cycle or be slowly oxidized by molecular oxygen (**h** to **a**).

5. Acknowledgments

We thank Dr. Janet Webster for critical reading of the manuscript

6. References

1. WHO (2002) World Health Report. (World Health Organization, Geneva, 2002).
2. Bern C, Montgomery SP, Herwaldt BL, Rassi A, Jr., Marin-Neto JA, et al. (2007) Evaluation and treatment of Chagas disease in the United States: a systematic review. J Am Med Assoc 298: 2171-2181.
3. Dorn PL, Perniciaro L, Yabsley MJ, Roellig DM, Balsamo G, et al. (2007) Autochthonous transmission of *Trypanosoma cruzi,* Louisiana. Emerg Infect Dis 13: 605-607.
4. Buekens P, Almendares O, Carlier Y, Dumonteil E, Eberhard M, et al. (2008) Mother-to-Child Transmission of Chagas' Disease in North America: Why Don't We Do More? Matern Child Health J 12: 283-286.
5. Hanford EJ, Zhan FB, Lu Y, Giordano A (2007) Chagas disease in Texas: recognizing the significance and implications of evidence in the literature. Soc Sci Med 65: 60-79.
6. De Souza W (2002) Basic cell biology of *Trypanosoma cruzi*. Curr Pharm Des 8: 269-285.
7. Coura JR, Borges-Pereira J (2010) Chagas disease: 100 years after its discovery. A systemic review. Acta Trop 115: 5-13.
8. Prata A (1999) Evolution of the clinical and epidemiological knowledge about Chagas disease 90 years after its discovery. Mem Inst Oswaldo Cruz 94 Suppl 1: 81-88.
9. Buscaglia CA, Campo VA, Frasch AC, Di Noia JM (2006) *Trypanosoma cruzi* surface mucins: host-dependent coat diversity. Nat Rev Microbiol 4: 229-236.
10. Roper JR, Guther ML, Milne KG, Ferguson MA (2002) Galactose metabolism is essential for the African sleeping sickness parasite *Trypanosoma brucei*. Proc Natl Acad Sci U S A 99: 5884-5889.
11. Oppenheimer M, Valenciano AL, Sobrado P (2011) Biosynthesis of galactofuranose in kinetoplastids: novel therapeutic targets for treating leishmaniasis and Chagas' disease. Enzyme Res 2011: 415976.
12. Crick DC, Mahapatra S, Brennan PJ (2001) Biosynthesis of the arabinogalactan-peptidoglycan complex of *Mycobacterium tuberculosis*. Glycobiology 11: 107R-118R.
13. Stevenson G, Neal B, Liu D, Hobbs M, Packer NH, et al. (1994) Structure of the O antigen of *Escherichia coli* K-12 and the sequence of its rfb gene cluster. J Bacteriol 176: 4144-4156.
14. Latge JP (2009) Galactofuranose containing molecules in *Aspergillus fumigatus*. Med Mycol 47 Suppl 1: S104-109.
15. Pereira-Chioccola VL, Acosta-Serrano A, Correia de Almeida I, Ferguson MA, Souto-Padron T, et al. (2000) Mucin-like molecules form a negatively charged coat that protects *Trypanosoma cruzi* trypomastigotes from killing by human anti-alpha-galactosyl antibodies. J Cell Sci 113: 1299-1307.
16. Suzuki E, Mortara RA, Takahashi HK, Straus AH (2001) Reactivity of MEST-1 (antigalactofuranose) with *Trypanosoma cruzi* glycosylinositol phosphorylceramides (GIPCs): immunolocalization of GIPCs in acidic vesicles of epimastigotes. Clin Diagn Lab Immunol 8: 1031-1035.
17. Oppenheimer M, Poulin MB, Lowary TL, Helm RF, Sobrado P (2010) Characterization of recombinant UDP-galactopyranose mutase from *Aspergillus fumigatus*. Arch Biochem Biophys 502: 31-38.

18. Nassau PM, Martin SL, Brown RE, Weston A, Monsey D, et al. (1996) Galactofuranose biosynthesis in *Escherichia coli* K-12: identification and cloning of UDP-galactopyranose mutase. J Bacteriol 178: 1047-1052.
19. Zhang Q, Liu HW (2000) Studies of UDP-Galactopyranose Mutase from *Escherichia coli*: An Unusual Role of Reduced FAD in Catalysis. J Am Chem Soc 122: 6.
20. Sanders DAR, Staines AG, McMahon SA, McNeil MR, Whitfield C, et al. (2001) UDP-galactopyranose mutase has a novel structure and mechanism. Nat Struct Mol Biol 8: 858-863.
21. Soltero-Higgin M, Carlson EE, Gruber TD, Kiessling LL (2004) A unique catalytic mechanism for UDP-galactopyranose mutase. Nat Struct Mol Biol 11: 539-543.
22. Gruber TD, Westler WM, Kiessling LL, Forest KT (2009) X-ray crystallography reveals a reduced substrate complex of UDP-galactopyranose mutase poised for covalent catalysis by flavin. Biochemistry 48: 9171-9173.
23. Huang ZH, Zhang QB, Liu HW (2003) Reconstitution of UDP-galactopyranose mutase with 1-deaza-FAD and 5-deaza-FAD: analysis and mechanistic implications. Bioorg Chem 31: 494-502.
24. Fullerton SWB, Daff S, Sanders DAR, Ingledew WJ, Whitfield C, et al. (2003) Potentiometric analysis of UDP-galactopyranose mutase: Stabilization of the flavosemiquinone by substrate. Biochemistry 42: 2104-2109.
25. Blommel PG, Martin PA, Wrobel RL, Steffen E, Fox BG (2006) High efficiency single step production of expression plasmids from cDNA clones using the Flexi Vector cloning system. Protein Expr Purif 47: 562-570.
26. Macheroux P (1999) UV-visible spectroscopy as a tool to study flavoproteins. Methods Mol Biol 131: 1-7.
27. Oppenheimer M, Valenciano AL, Sobrado P (2011) Isolation and characterization of functional *Leishmania major* virulence factor UDP-galactopyranose mutase. Biochem Biophys Res Commun 407: 552-556.
28. Zhang Q, Liu H (2001) Mechanistic investigation of UDP-galactopyranose mutase from *Escherichia coli* using 2- and 3-fluorinated UDP-galactofuranose as probes. J Am Chem Soc 123: 6756-6766.
29. Cattiaux L, Sendid B, Collot M, Machez E, Poulain D, et al. (2011) Synthetic biotinylated tetra beta(1-->5) galactofuranoside for in vitro aspergillosis diagnosis. Bioorg Med Chem 19: 547-555.
30. D'Accorso N, Thiel IME, Schüller M (1983) Proton and C-13 nuclear magnetic resonance spectra of some benzoylated aldohexoses. Carbohydr Res 124: 177-184.
31. Davis CB (2006) Development of Novel Carbohydrate-Based Anti-Bacterial Agents, QLD, Australia: Griffith University.
32. Ness RK, Fletcher HG, Hudson CS (1951) 1,4-Anhydro-D-galactitol. J Am Chem Soc 73: 3742-3744.
33. Tsvetkov YE, Nikolaev AV (2000) The chemical synthesis of UDP-a-D-galactofuranose. J Chem Soc, Perkin Transactions 1: 889-891.
34. de Lederkremer RM, Nahmad VB, Varela O (1994) Synthesis of a-D-Galactofuranosyl Phosphate. J Org Chem 59: 690-692.
35. Poulin MB, Lowary TL (2010) Chapter Nineteen - Methods to Study the Biosynthesis of Bacterial Furanosides. In: Minoru F, editor. Methods in Enzymology: Academic Press. pp. 389-411.

36. Lide DR (2000) Handbook of Chemistry and Physics 2000-2001. Boca Raton, FL: CRC Press.
37. Qi J, Oppenheimer M, Sobrado P (2011) Fluorescence Polarization Binding Assay for *Aspergillus fumigatus* Virulence Factor UDP-Galactopyranose Mutase. Enzyme Res 2011: 513905.
38. Blommel PG, Becker KJ, Duvnjak P, Fox BG (2007) Enhanced bacterial protein expression during auto-induction obtained by alteration of lac repressor dosage and medium composition. Biotechnol Prog 23: 585-598.
39. Barlow JN, Marcinkevicience, J, Blanchard, JS (1999) The Enzymatic Conversion of UDP-galactopyranose to UDP-galactopyranose. In: Frey PA, Northrop, D.B., editor. Enzymatic Mechanisms. Amsterdam: IOS Press.
40. Chocklett SW, Sobrado P (2010) *Aspergillus fumigatus* SidA is a highly specific ornithine hydroxylase with bound flavin cofactor. Biochemistry 49: 6777-6783.
41. Gruber TD, Borrok MJ, Westler WM, Forest KT, Kiessling LL (2009) Ligand binding and substrate discrimination by UDP-galactopyranose mutase. J Mol Biol 391: 327-340.
42. Miller SM (2004) A new role for an old cofactor. Nat Struct Mol Biol 11: 497-498.
43. Bornemann S (2002) Flavoenzymes that catalyse reactions with no net redox change. Nat Prod Rep 19: 761-772.
44. Barlow JN, Girvin, ME, Blanchard, JS (1999) Positional Isotope Exchage Catalyzed by UDP-Galactopyranose Mutase. J Am Chem Soc 121: 12.
45. Partha SK, van Straaten KE, Sanders DA (2009) Structural basis of substrate binding to UDP-galactopyranose mutase: crystal structures in the reduced and oxidized state complexed with UDP-galactopyranose and UDP. J Mol Biol 394: 864-877.
46. Chad JM, Sarathy KP, Gruber TD, Addala E, Kiessling LL, et al. (2007) Site-directed mutagenesis of UDP-galactopyranose mutase reveals a critical role for the active-site, conserved arginine residues. Biochemistry 46: 6723-6732.
47. Greenbaum AL, Clark JB, McLean P (1965) The Estimation of the Oxidized and Reduced Forms of the Nicotinamide Nucleotides. Biochem J 95: 161-166.
48. Pinkas-Sarafova A, Markova NG, Simon M (2005) Dynamic changes in nicotinamide pyridine dinucleotide content in normal human epidermal keratinocytes and their effect on retinoic acid biosynthesis. Biochem Biophys Res Commun 336: 554-564.
49. London J, Knight M (1966) Concentrations of nicotinamide nucleotide coenzymes in micro-organisms. J Gen Microbiol 44: 241-254.
50. Sun HG, Ruszczycky MW, Chang WC, Thibodeaux CJ, Liu HW (2012) Nucleophilic participation of the reduced flavin coenzyme in the mechanism of UDP-Galactopyranose mutase. J Biol Chem. 287:4602-4608.
51. Eppe G, Peltier P, Daniellou R, Nugier-Chauvin C, Ferrieres V, et al. (2009) Probing UDP-galactopyranose mutase binding pocket: a dramatic effect on substitution of the 6-position of UDP-galactofuranose. Bioorg Med Chem Lett 19: 814-816.
52. Lai EC, Morris SA, Street IP, Withers SG (1996) Substituted glycals as probes of glycosidase mechanisms. Bioorg Med Chem 4: 1929-1937.
53. Gordon RD, Sivarajah P, Satkunarajah M, Ma D, Tarling CA, et al. (2006) X-ray crystal structures of rabbit N-acetylglucosaminyltransferase I (GnT I) in complex with donor substrate analogues. J Mol Biol 360: 67-79.

54. Tarling CA, Withers SG (2004) The synthesis of a series of modified mannotrisaccharides as probes of the enzymes involved in the early stages of mammalian complex N-glycan formation. Carbohydr Res 339: 2487-2497.

7. Supplementary Material- Synthesis of UDP-Gal*f*

7.1 Materials. All reagents and solvents used in the synthesis, if not specified otherwise, were obtained from Sigma-Aldrich (St. Louis, MO) or Fisher Scientific (Pittsburgh, PA) and were used without further purification. All reactions were monitored to completion using thin layer chromatography (TLC) with *p*-anisaldehyde staining for visualizing carbohydrates along with UV detection when possible. ^{1}H and ^{13}C NMR were recorded on a 400MR Varian 400 MHz spectrometer. $CHCl_3$ (7.27 ppm) or HOD (4.79 ppm) were used as an internal reference.

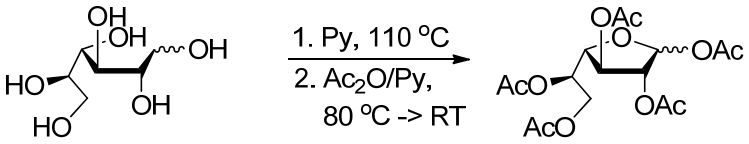

1 **2**

7.2 Step 1: Synthesis of 1,2,3,5,6-Penta-O-Acetyl-α/β-D-Galactofuranoside (2). The method was adapted with slight modifications from previously published protocols [1-3]. D-galactose (**1**) (10.0 g, 55 mmol) was dissolved in anhydrous pyridine (200 mL) and stirred at 110 °C for 2 h. Then, acetic anhydride was added in one portion (60 mL) through the condenser, the temperature was slowly lowered to room temperature, and the reaction continued stirring overnight. The dark reaction mixture was poured on ice (700 g) while stirring and when the ice melted, the oily residue was extracted with methylene chloride (3 × 300 mL), dried with anhydrous sodium sulfate, and concentrated to yield a crude mixture of galactopyranosides and galactofuranosides as a yellow oil. Most of the galactopyranose products (8.9 g, 23%) were precipitated out of the crude mixture as a white solid by crystallizing the crude oil from ethanol. The filtrate was concentrated to yield oily residue that consisted of a mixture of protected *α*- and *β*-galactofuranosides (**2**) (*α*/*β*:1/1, 5.2 g, 13%). A repeated crystallization was needed if galactopyranose products were still detected in the filtrate. NMR data were in agreement with previously published data [4, 5]. ^{1}H-NMR ($CDCl_3$, 400 MHz, *α* and *β* isomers): δ = 2.04-2.16

(m, 30H, CH_3CO), 4.13-4.24 (m, 2H), 4.29-4.38 (m, 4H), 5.10 (d, J = 5.4 Hz, 1H), 5.18 (bs, 1H), 5.25-5.38 (m, 2H), 5.34-5.39 (m, 1H), 5.56 (t, J = 6.5 Hz, 1H), 6.19 (s, 1H, 1-H$^{\beta}$), 6.33 (d, J = 4.1 Hz, 1H, 1-H$^{\alpha}$). ^{13}C-NMR ($CDCl_3$, 400 MHz, α and β isomers): δ = 20.47, 20.64, 20.67, 20.70, 20.79, 20.82, 21.00, 21.04, 62.11, 62.57, 69.25, 70.34, 73.41, 75.31, 76.33, 79.09, 80.60, 82.14, 93.09$^{\alpha}$, 99.12$^{\beta}$, 169.04, 169.41, 169.77, 170.01, 170.53.

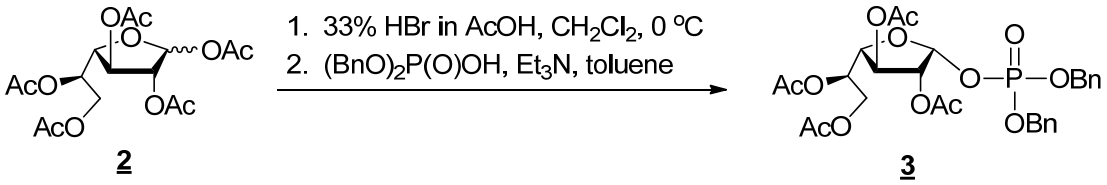

2 **3**

7.3 Step 2: Synthesis of Dibenzyl 2,3,5,6-tetra-O-Acetyl-α-D-Galactofuranosyl Phosphate (3).

The method was adapted with slight modifications from previously published protocols [3, 6]. The solution of peracetylated α-Gal*f* (**2**) (α/β mixture, 1.0 g, 2.6 mmol) in anhydrous dichloromethane (10 mL) was cooled to 0 °C in an ice bath followed by the addition of 33% HBr in glacial acetic acid (2.0 mL). The resulting reddish solution was stirred for 2 h maintaining 0 °C temperature until TLC analysis (ethyl acetate/hexane – 1/1, stained with p-anisaldehyde) showed the absence of the starting material. The solvent and residual acids were removed by repeatedly co-evaporating the mixture with anhydrous toluene. The residue was re-dissolved in 20 mL of toluene, followed by the addition of triethylamine (0.8 mL, d = 0.72 g/mL, 7.8 mmol) and dibenzyl phosphate (1.0 g, 3.6 mmol), and the resulting mixture was stirred for 1 h at 0 °C and overnight at room temperature. The white precipitate of triethylammonium bromide was filtered off and the filtrate concentrated and purified by flash column chromatography (eluent: ethyl acetate/hexane – 1/1). The product, α-Gal*f* 1-phosphate (**3**) was found in the last fractions and upon concentration yielded a yellowish oil (0.6 g, 40%). ^{1}H-NMR ($CDCl_3$, 400 MHz): δ = 1.93 (s, 3H, COCH_3), 1.96 (s, 3H, COCH_3), 2.01 (s, 3H, COCH_3), 2.06 (s, 3H, COCH_3), 4.10

(dd, J = 6.3, 11.9 Hz, 1H), 4.21 (dd, J = 4.4, 7.1 Hz, 1H), 4.28 (dd, J = 4.7, 11.9 Hz, 1H), 5.05 (d, J = 7.6, 4H, CH_2Bn), 5.14-5.26 (m, 2H), 5.44-5.58 (m, 1H), 5.97 (dd, J = 4.4, 5.6 Hz, 1H), 7.28-7.36 (m, 10H, arom.).

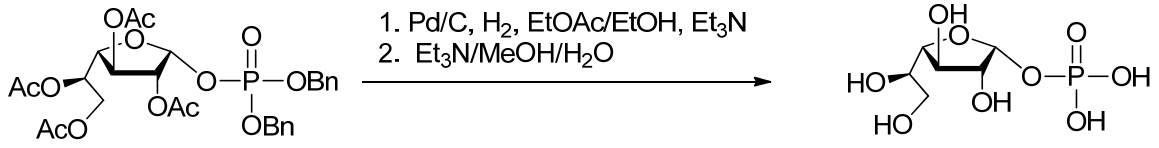

3 **4**

7.4 Step 3. Synthesis of α-D-Galactofuranosyl bis(triethylammonium) phosphate (4). The method was adapted with slight modifications from previously published protocols [3, 6, 7]. To the solution of peracetylated *α*-Gal*f* 1-phosphate (**3**) (240 mg, 0.395 mmol) in ethyl acetate/ethanol (1/1, 4 mL) triethylamine (0.4 mL) and Pd/C (10_{wt}%) (40 mg) were added, and the reaction was hydrogenated at room temperature and atmospheric pressure for 24 h. The mixture was filtered through the celite plug and concentrated to yield a yellowish oil. Debenzylated product, without further purification, was dissolved in methanol/water/triethylamine (2 mL/0.8 mL/0.4 mL) and the resulting solution was stirred at room temperature overnight, then concentrated to yield slightly yellowish oil, which was pure *α*-Gal*f* 1-phosphate **4** as a bis(triethylammonium) salt (158 mg, 86%). ^{1}H-NMR (D_2O, 400 MHz): δ = 1.29 (t, J = 7.3 Hz, 18H, CH_3CH_2N), 3.09 (q, J = 7.3 Hz, 12H, CH_3CH_2N), 3.59-3.83 (m, 4H), 4.04-4.15 (m, 1H), 4.17-4.25 (m, 1H), 5.50 (t, J = 4.7 Hz, 1H). NMR data were in agreement with those published [6, 7].

7.5 Step 4: Chemienzymatic coupling of UDP to α-Galf-1-Phosphate. UDP-Gal*f* was synthesized using the previously published chemienzymatic method as reported by the Lowary lab without modification [8]. ^{1}H-NMR (D_2O, 400 MHz): δ = 3.63-3.70 (m, 1H), 3.72-3.77 (m,

1H), 3.78-3.83 (m, 1H), 3.84-3.88 (m, 1H), 4.16-4.33 (m, 4H), 4.38-4.44 (m, 2H), 5.65-5.69 (m, 1H), 5.96-6.06 (m, 2H), 7.98 (d, J = 8.1 Hz, 1H).

8. Supplementary Material- References

[1]. L. Cattiaux, B. Sendid, M. Collot, E. Machez, D. Poulain, J.M. Mallet, "Synthetic biotinylated tetra beta(1-->5) galactofuranoside for in vitro aspergillosis diagnosis," *Bioorg Med Chem*, vol.19, pp. 547-555, 2011.
[2]. N. D'Accorso, I.M.E. Thiel, M. Schüller, "Proton and c-13 nuclear magnetic resonance spectra of some benzoylated aldohexoses," *Carbohydr Res*, vol.124, pp. 177-184, 1983.
[3]. Q. Zhang, H. Liu, "Mechanistic investigation of UDP-galactopyranose mutase from *Escherichia coli* using 2- and 3-fluorinated UDP-galactofuranose as probes," *J Am Chem Soc*, vol.123, pp. 6756-6766, 2001.
[4]. C.B. Davis, Development of novel carbohydrate-based anti-bacterial agents, Griffith University, QLD, Australia, 2006.
[5]. R.K. Ness, H.G. Fletcher, C.S. Hudson, "1,4-anhydro-D-galactitol," *J Am Chem Soc*, vol.73, pp. 3742-3744, 1951.
[6]. Y.E. Tsvetkov, A.V. Nikolaev, "The chemical synthesis of udp-α–D-galactofuranose," *J Chem Soc, Perkin Transactions 1*, pp. 889-891, 2000.
[7]. R.M. de Lederkremer, V.B. Nahmad, O. Varela, "Synthesis of α-D-galactofuranosyl phosphate," *J Org Chem*, vol.59, pp. 690-692., 1994.
[8]. M.B. Poulin, T.L. Lowary, "Methods to study the biosynthesis of bacterial furanosides," *Methods Enzymol*, vol.478, pp. 389-411

CHAPTER 7

Crystal structures of UDP-galactopyranose mutase from the pathogenic fungus *Aspergillus fumigatus*

This chapter was adapted from the article below:
This research was originally published in Journal of Biological Chemistry. Dhatwalia, R., Singh, H., Oppenheimer, M., Karr, D.B., Nix, J.C., Sobrado, P., and Tanner, J.J. "Crystal structures and small-angle X-ray scattering analysis of UDP-galactopyranose mutase from the pathogenic fungus Aspergillus fumigatus." *J Biol Chem*. 2012; (ID M111.327536) Vol 287: 9041-9051. © the American Society for Biochemistry and Molecular Biology.

Author Contributions:
Michelle Oppenheimer and Pablo Sobrado designed AfUGM mutants for crystallizations trials, purified all proteins used for these studies, and performed the activity assays. Michelle Oppenheimer also adapted the article for the purpose of this chapter.

Richa Dhatwalia, Harkewal Singh, Dale B. Karr, Jay C. Nix, and John J. Tanner worked on the crystallization trials of AfUGM, solved the crystal structure of AfUGM, performed data analysis, and wrote the original paper.

Abstract

UDP-galactopyranose mutase (UGM) is a flavoenzyme that catalyzes the conversion of UDP-galactopyranose to UDP-galactofuranose, which is a central reaction in galactofuranose biosynthesis. Galactofuranose has never been found in humans but is an essential building block of the cell wall and extracellular matrix of many bacteria, fungi, and protozoa. The importance of UGM for the viability of many pathogens and its absence in humans makes UGM a potential drug target. Here we report crystal structures in four comformational states for UGM from the fungus *Aspergillus fumigatus*, the causative agent of aspergillosis. The structures reveal that *A. fumigatus* UGM has several extra secondary and tertiary structural elements that are not found in bacterial UGMs yet are important for substrate recognition and oligomerization. *A. fumigatus* UGM forms a homotetramer in solution, which is unprecedented for UGMs. The binding of UDP

or the substrate induces profound conformational changes in the enzyme. Two loops on opposite sides of the active site move toward each other by over 10 Å to cover the substrate and create a closed active site. The amount of substrate-induced conformational change exceeds that of bacterial UGMs and is a direct consequence of the unique quaternary structure of *A. fumigatus* UGM. Galactopyranose binds at the *re* face of the FAD isoalloxazine with the anomeric carbon atom poised for nucleophilic attack by the FAD N5 atom. The structural data provide new insight into substrate recognition and the catalytic mechanism and thus will aid inhibitor design.

1. Introduction

UDP-galactopyranose mutase (UGM) is a unique flavoenzyme that catalyzes the reversible conversion of UDP-galactopyranose (UDP-Gal*p*) to UDP-galactofuranose (UDP-Gal*f*) (Fig. 1). Unlike flavin-dependent oxidoreductases, the redox state of the flavin in UGM is unchanged upon product formation (1). Although it is known that the FAD must be reduced for maximal catalytic activity, the precise role that the flavin plays in catalysis remains controversial.

UGM is also an attractive target for drug design. The carbohydrate moiety of the product of the reaction, galactofuranose (Gal*f*), is the five-membered ring form of the common monosaccharide galactose. Gal*f* has never been found in mammals and higher plants but is an essential building block of the cell wall and extracellular matrix of many bacteria, fungi, and protozoa (2). The UGM reaction is central to Gal*f* biosynthesis. Gene deletion studies have shown that UGM is essential for mycobacterial growth (3) and contributes to the virulence of the pathogenic fungus *Aspergillus fumigatus* (4) and the protozoan parasite *Leishmania major* (5). In summary, the importance of UGM for the viability of many pathogens and its absence in humans makes UGM a potential drug target.

This study focuses on the UGM from the *A. fumigatus*. *Aspergillus* spp. are ubiquitous fungi that cause diseases ranging from allergic reactions and lung infections to sepsis and death (6). Acquired by inhalation of airborne spores, *Aspergillus* infections (mainly *A. fumigatus*) can lead to invasive pulmonary aspergillosis, particularly in immunocompromised persons (6-8). Invasive pulmonary aspergillosis is also an emerging serious infection in patients with chronic obstructive pulmonary disease (9). The overall case-fatality rate associated with invasive aspergillosis is 58% (10). Also, bronchial colonization by *A. fumigatus* in people with asthma or cystic fibrosis causes allergic bronchopulmonary aspergillosis, a hypersensitivity lung disease that can lead to airway destruction and widening, and scarring of the lung, resulting in significant morbidity and mortality (11). The ubiquity of the fungus, the increasing occurrence of *Aspergillus* infections in humans, and the high mortality rate associated with invasive pulmonary aspergillosis demonstrate the need for new anti-*Aspergillus* drugs.

Inhibition of *A. fumigatus* UGM (AfUGM) is a potential strategy for the development of new drugs to treat patients with aspergillosis. In *Aspergillus*, Gal*f* is present in the galactomannan fraction of the cell wall, N- and O-glycans of secreted glycoproteins, glycosylphosphatidylinositol-anchored lipophosphogalactomannan, and sphingolipids (12). It is estimated that Gal*f* constitutes 5% of the dry weight of *A. fumigatus* (12). Deletion of the UGM gene in *A. fumigatus* results in a thinner cell wall and increased susceptibility to drugs (4). Furthermore, the mutated strain exhibits attenuated virulence in a low-dose mouse model of invasive aspergillosis (4). In another study, deletion of the UGM gene resulted in a reduced growth phenotype but virulence as measured in a higher-dose mouse model was unimpaired (13). The different outcomes of the two deletion studies may reflect the different doses used, with the low-dose model generally considered to mimic more closely the *in vivo* situation (2). Because of

the importance of UGM for the fitness of *A. fumigatus*, UGM is a promising target for the development of new drugs for adjunctive treatment for aspergillosis (2, 4).

The AfUGM structure has been solved in four conformations using X-ray crystallography including, the inactive oxidized form, the active reduced form, reduced form with UDP bound, and the reduced form with the substrate, UDP-Gal*p* bound. The data reveal interesting differences from bacterial UGMs, including additional secondary structure elements, unique mode of oligomerization, and profound conformational changes induced by substrate binding. The structures should aid inhibitor design efforts.

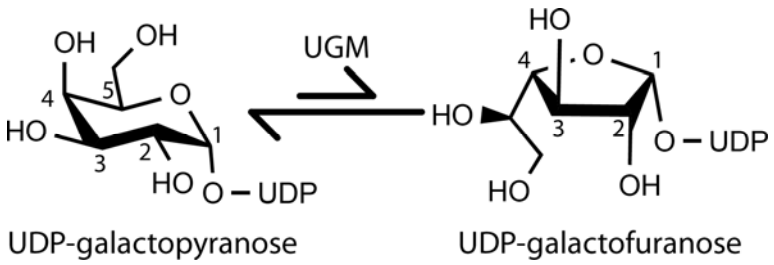

Figure 7.1 Reaction catalyzed by UGM.

2. Materials and Methods

2.1 Site-directed mutagenesis and design of AfUGM mutants. Site-directed mutagenesis was performed using the QuikChange protocol (Stratagene, CA). In order to select amino acids for mutation to aid in crystallization of AfUGM, a structural model was created using Phyre (14). Mutations were designed to be both in the active site and surface of AfUGM. Active site residues were identified using an alignment of AfUGM to prokaryotic UGMs and were based upon conserved active site residues in prokaryotic UGMs. These active site residues were also verified in the model (Fig. 2A). Residues at the protein surface were selected for mutation based upon their high entropic properties, which can impede crystal formation. Residues were

identified either examining the model or using the surface entropy reduction server (SERp) (Fig. 2A) (15). A summary of all the mutations made and tested for crystallization is found in Table 2.

2.2 Expression and purification of native AfUGM. Both AfUGM wildtype and mutants were expressed in the vector pVP55A or pVP56K using auto-induction media. Se-Met AfUGM was produced using the metabolic inhibition method (16). The metabolic inhibiton method works by growing *E. coli* with on minimal media and half hour before induction of AfUGM with IPTG, methonine biosynthesis is blocked and selenomethionine is put in the media. All AfUGM isoforms were purified following methods previously described (17).

2.3 Crystallization. Details on the methods of crystallization are outlined in reference (18). The surface lysine mutant AfUGM K344A K345A was used to solve the structure as native AfUGM and other mutants had translational pseudosymmetry.

2.4 Crystal soaking. Crystals of reduced AfUGM with and without bound active site ligands were prepared by soaking the aforementioned crystals with dithionite for reduction, and with ligands, either UDP or UDP-Gal*p*, details are outlined in the reference (18).

2.5 X-ray diffraction data collection, phasing, and refinement. Crystals were analyzed at beamlines 19ID and 24-ID-C of the Advanced Photon Source and beamline 8.2.2 of the Advanced Light Source. The first structure of AfUGM was determined using single-wavelength anomalous diffraction (SAD) phasing based on data collected at 19ID from Se-Met AfUGM crystals (Table 1). The resulting structure provided the starting coordinates for the refinements

of the other structures reported here. Details on the method of structure determination are found in the reference (18). A complete summary of the data collection and refinement statistics is also found in the reference (Table 1) (18).

Table 7.1 X-ray diffraction data collection and refinement[a]

	Se-Met	Sulfate complex	$AfUGM_r$	$AfUGM_r$-UDP	$AfUGM_r$-UDP-Gal*p*
Beamline	APS 19ID	APS 19ID	ALS 8.2.2	ALS 8.2.2	APS 24-ID-C
Active site ligand	sulfate	sulfate	None	UDP	UDP-Gal*p*
Resolution (Å)	55.00-2.65 (2.74-2.65)	50.0-2.35 (2.43-2.35)	48.6-2.20 (2.37-2.25)	48.6-2.25 (2.37-2.25)	48.8-2.25 (2.37-2.25)
$R_{merge}(I)$	0.087 (0.351)	0.086 (0.568)	0.097 (0.599)	0.086 (0.676)	0.097 (0.599)
Completeness (%)	99.0 (99.6)	90.5 (91.1)	99.8 (100.0)	97.9 (99.7)	97.3 (97.6)
No. of protein chains		4	4	4	4
No. of protein residues		2018	2020	2019	2019
No. of protein atoms		15597	15580	15551	15562
No. of FAD atoms		212	212	212	212
No. of ligand atoms		0	0	50	72
No. of water molecules		516	813	657	659
PDB code		3UTE	3UTF	3UTG	3UTH

[a]Values for the outer resolution shell of data are given in parenthesis.

2.6 Kinetics. The mutase activity was tested with UDP-Gal*f* as the substrate following procedures previously described (17). The enzyme concentration was determined using the flavin extinction coefficient at 450 nm of 10.6 $mM^{-1}cm^{-1}$.

2.7 Structure analysis. SSM (19) was used for structure superposition. The PDBePISA server was used to analyze protein interfaces in crystal lattices (20). COOT and PyMol (21) were used to analyze noncovalent interactions.

3. Results

3.1 Generation of mutants. Crystallization of native AfUGM proved difficult as crystals displayed translational pseudosymmetry, therefore several active site and surface mutations were made in order to aid in crystal formation (Table 2). The amino acids selected to mutate were chosen based upon an alignment with prokaryotic UGMs, an AfUGM model, or the SERp server. The surface amino acids were chosen in order to eliminate residues with polar, long side chains, which can impede the formation of a crystal lattice. These residues include: lysine, glutamic acid, and glutamine. The surface mutant, AfUGM K344A K345A was identified to generate crystals with good pathology and was used to solve for the AfUGM structure. The lysine residues were verified to be located on the surface of the AfUGM structure and away from the active site and oligomerization interfaces (Fig. 2). The kinetic parameters of AfUGM K344A K345A were also the same as native AfUGM (Table 3). These results show the mutation did not significantly alter the crystal structure or activity of AfUGM, as a result AfUGM K344A K345A was used for these studies and for the purpose of this paper AfUGM will refer to the AfUGM K344A K345A mutant.

Table 7.2 Summary of AfUGM mutants

Mutation	Type of mutation	Method used to identify residue
W167A	Active Site	Alignment
W204A	Active Site	Alignment
R211A	Active Site	Alignment
R327A	Active Site	Alignment
K231A K233A	Surface	Model
K239A K241A	Surface	SERp
K344A K345A	Surface	Model
K363A E364A	Surface	SERp
K231A K233A K344A K345A	Surface	Model

Table 7.3 Steady state kinetics of AfUGM and AfUGM K344A K345A

	k_{cat}, s^{-1}	K_M, μM	k_{cat}/K_M, μM^{-1} s^{-1}
Native	60 ± 3	70 ± 10	0.84 ± 0.13
K344A/K345A	55 ± 2	70 ± 9	0.75 ± 0.07

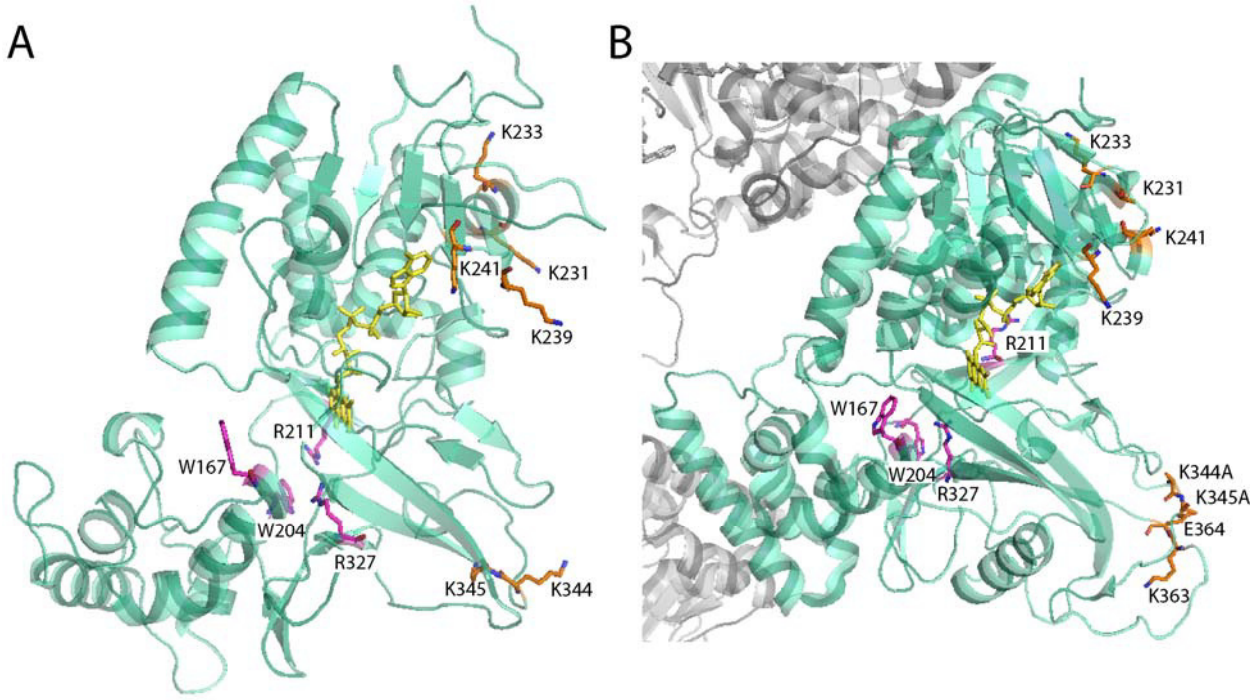

Figure 7.2 Ribbon diagram of AfUGM showing active site and surface residues chosen for mutation. (A) Model of AfUGM made using Phyre which threaded the sequence on the known three dimensional structure of oxidized *Mycobacterium tuberculosis* UGM (PDB code, 1VOJ) (14). (B) Crystal structure of oxidized AfUGM highlighting one subunit of the tetramer in cyan with the other subunits in light gray. The active site residues, W167, W204, and R327 (magenta) are shown to be in a similar orientation in both the model and crystal structure. However, the residue R211 is shown to be in a different location and orientation. The surface residues (orange) are shown to be in similar locations in both the model and structure, however, there are significant differences in the fold and orientation. (Note, residues K363 and E364 are not seen on the model as the model does not include random coils and loops.) The residues K344 and K345 were mutated to alanines to solve the crystal structure. This figure and others were prepared with PyMol.

3.2 Overall fold and flavin binding site. The AfUGM protomer has a mixed α/β fold (Fig. 3) and exhibits the same 3-domain architecture that was first identified in the structure of *E. coli* UGM (22). Domain 1 is the largest of the three domains. It is a tripartite unit consisting of residues 3-

90, 205-291, and 421-507, and includes a Rossmann fold core that binds the FAD. Domain 2 is a bundle of α-helices (residues 105-204). This domain mediates one of the major interfaces of the tetramer. Domain 3 (residues 91-104, 292-420) is situated between the other two domains and features a twisted, 7-stranded β-sheet. This domain participates in substrate binding. The FAD isoalloxazine binds in a crevice between domains 1 and 3.

AfUGM is about 100 residues longer than bacterial UGMs, and the extra residues form several structural elements that appear to be important for catalysis and oligomerization (red sections in Fig. 3A). The first of these extra elements is a 4-stranded β-sheet in domain 1 formed by residues 6-8 and 243-262. This β-sheet is located near the adenine of the FAD. Domain 2 has an extra helix (residues 188-197) not found in bacterial UGMs. This helix is situated between two mobile flaps that close and open in response to substrate binding and product release, respectively (Fig. 3A). Also, the second helix of the domain (residues 115-134) is about seven residues longer in AfUGM and rotated by about 90° from the corresponding helix in bacterial UGMs. The 115-134 and 188-197 helices form a 4-helix bundle in one of the dimer interfaces of the UGM tetramer (see below). Domain 3 of AfUGM has two large inserts compared to bacterial UGMs. The first is a long loop formed by residues 335-366. The second consists of residues 378-418, which fold into an α-helix followed by a β-strand. Because of the latter secondary structure element, the sheet of domain 3 has 7 strands rather than 6 as in bacterial UGMs. Finally, AfUGM has ~30 extra residues at the C-terminus. These residues form a U-shaped substructure that packs against domain 1 and features two α-helices. This extra structural element is involved in oligomerization (see below).

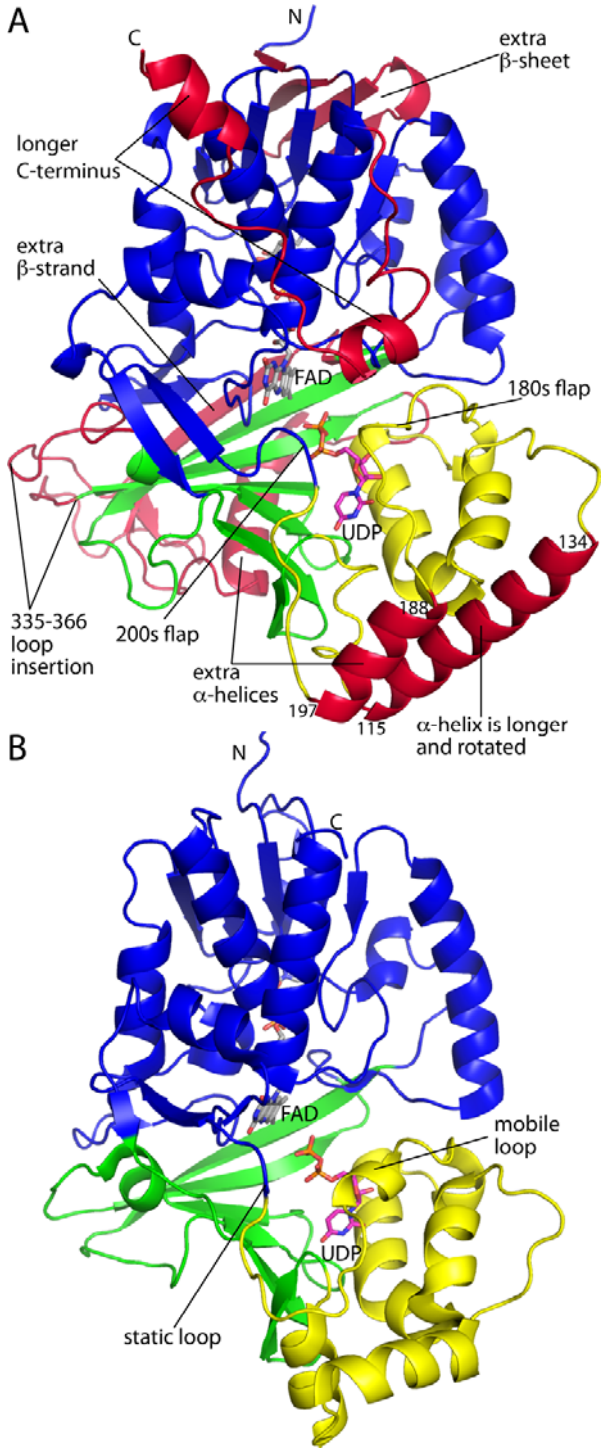

Figure 7.3 Overall fold of AfUGM. (A) Structure of the AfUGM protomer. Domains 1, 2, and 3 are colored blue, yellow, and green, respectively. Features that distinguish AfUGM from bacterial UGMs are colored red. (B) Protomer structure of a bacterial UGM (*Deinococcus radiodurans* UGM, PDB code 3HE3).

3.3 Quaternary structure. AfUGM had previously been identified as a tetramer in solution, the crystal structure and small angle X-ray scattering (SAXS) studies also confirmed AfUGM was a tetramer (for SAXS data see (18)). AfUGM is a dimer of dimers with symmetry that can be described with three mutually orthogonal 2-fold axes, denoted *P*, *Q*, and *R* that intersect at the center of the tetramer (Fig. 4). The *P*-, *Q*-, and *R*-axes relate protomer O to protomers P, Q, and R, respectively. The axes define three potential dimer interfaces corresponding to protomer O contacting the other three protomers. Only the OP and OQ interfaces are significant.

The OP interface buries 5000 $Å^2$ of area and is primarily hydrophilic, featuring 10 intersubunit hydrogen bonds. The interface is noncontiguous. The major part of the interface consists of the C-terminal residues 468-502 of two P-related chains interacting across the *P*-axis at the distal ends of the tetramer. Two such interfaces are located at opposite ends of the tetramer (Fig. 4). The minor part of the OP interface is located at the intersection of the 2-fold axes and involves just the guanidinium of Arg133 forming a hydrogen bond with the carbonyl of Val134 of the *P*-related chain (Fig. 4A, boxed inset). Thus, there are four of these intersubunit hydrogen bonds located in the center of the tetramer.

The OQ interface is located in the middle of the tetramer and buries 4600 $Å^2$ of contiguous surface area. Two helices (residues 115-134, and 188-197) from domain 2 of *Q*-related chains interact to form a 4-helix bundle oriented parallel to the Q-axis (Fig. 4). Note that these two helices are unique to AfUGM (Fig. 3A). The tetramer has two of these bundles. The 4-helix bundle has a hydrophobic interior featuring Val, Leu, and Ile side chains.

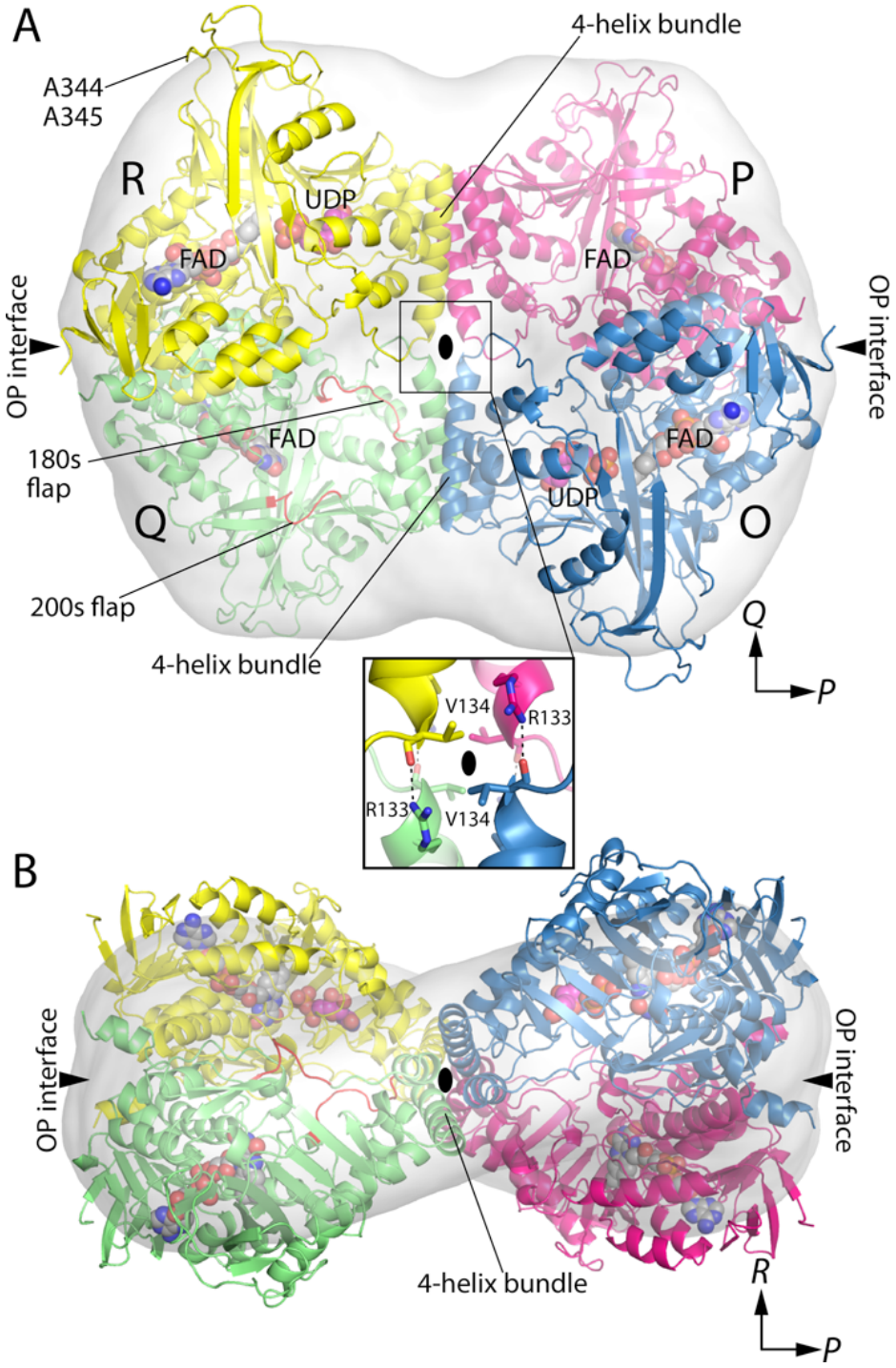

Figure 7.4 Quaternary structure of AfUGM. (A) The tetramer is viewed down the *R* molecular 2-fold axis. Each chain has a different color. The active site flaps of chain Q are colored red. The surface represents the SAXS shape reconstruction. Inset: Intersubunit hydrogen bonds at the intersection of molecular 2-fold axes. Chains related by the *P*-axis engage in hydrogen bonding. The oval represents the *R* two-fold molecular axis. (B) The tetramer is viewed down the *Q*-axis.

3.4 Active site of the sulfate complex. The crystals used for structure determination were grown in 1.5 M ammonium sulfate, and as crystallized, two sulfate ions are bound in the active site (Fig. 5A). The ions bind on the *re* side of the isoalloxazine. One of the ions binds next to the center ring of the isoalloxazine, which is the binding site for the Gal*p* moiety of the substrate. His63 – an absolutely conserved residue in UGMs - is likewise located on the *re* face and interacts with both sulfate ions. The location of the conserved histidine at the *re* face is unprecedented and likely a crystallization artifact.

The isoalloxazine is planar, which is consistent with the FAD being oxidized. It is noted that the crystals are yellow, which is also indicative of the oxidized state.

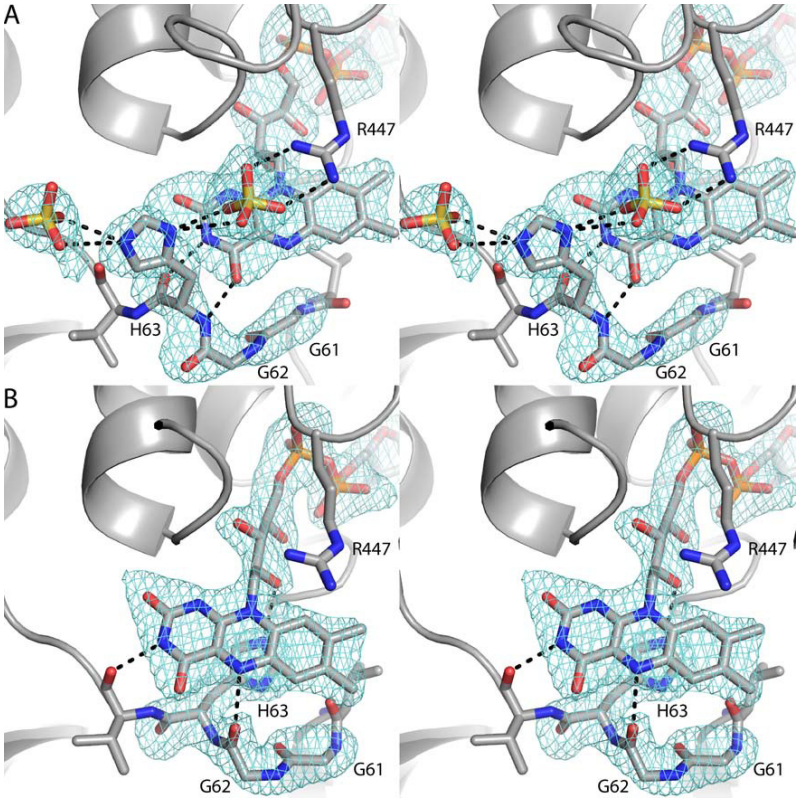

Figure 7.5 Stereographic views of histidine loop in the (A) sulfate complex and (B) AfUGM$_r$. In both panels, the cage represents a simulated annealing σ_A-weighted F_o - F_c omit map contoured at 3.0 σ.

3.5 The histidine loop of reduced AfUGM. The structure of the reduced enzyme ($AfUGM_r$) was determined from a crystal that was soaked in 80 mM sodium dithionite. The crystal changed from yellow to colorless, which indicated that the FAD was reduced.

Soaking with dithionite causes significant changes in the active site, which occur in all four chains. Electron density features for the sulfate ions are absent, and the conformation of the histidine loop is dramatically different (Fig. 5B). In particular, His63 has moved to the *si* face of the FAD where it stacks in parallel with the middle ring of the isoalloxazine and forms a hydrogen bond with the FAD 2'-OH. Furthermore, the carbonyl of Gly62 forms a hydrogen bond with the FAD N5. This conformational change in the protein is accompanied by a 3-Å shift in the FMN part of the FAD. This shift brings the N1 atom of the FAD within hydrogen-bonding distance of the backbone N-H group of Gln-458, which is consistent with the FAD adopting the anionic hydroquinone state.

The conformation of the histidine loop in $AfUGM_r$ is very similar to those of bacterial UGMs. In particular, in all other structures, the conserved histidine is located at the *si* face as in $AfUGM_r$. Furthermore, in all other UGMs, the carbonyl of the residue preceding the conserved His accepts a hydrogen bond from the N5 of reduced FAD. The carbonyl-N5 interaction is important for stabilizing the reduced state of FAD, a necessity for activity. As mentioned, Gly62 forms this critical hydrogen bond in $AfUGM_r$. It is concluded that the dithionite-reduced AfUGM structure represents the active, substrate-free form of the enzyme.

3.6 FAD conformation and binding site. The FAD of $AfUGM_r$ binds primarily to domain 1 (Fig. 3A). The conformation of the FAD is nearly identical to those of bacterial UGMs, and the flavin-protein interactions are highly conserved (Fig. 6). In particular, there are several

interactions with the protein backbone (Fig. 6B); these are conserved, as one would expect. Asp38 forms two hydrogen bonds with the ribose. This interaction appears to be universal in UGM. Some of the side chain interactions with the FAD in AfUGM are found in other bacterial UGMs. For example, Ser461 and Thr18, which interact with the ribityl 3'-OH and pyrophosphate, respectively, are analogous to Thr355 and Ser14 of *Klebsiella pneumoniae* UGM (KpUGM).

The FAD of $AfUGM_r$ exhibits a butterfly-like distortion of the isoalloxazine in which the pyrimidine ring bends 7° out of the plane such that the *si* face is concave (Fig. 6C). The direction of the bending is the same as that of *Deinococcus radiodurans* UGM (DrUGM) (23) and opposite to that of KpUGM (24). The angle is close to that of DrUGM and about half that of KpUGM (~13°).

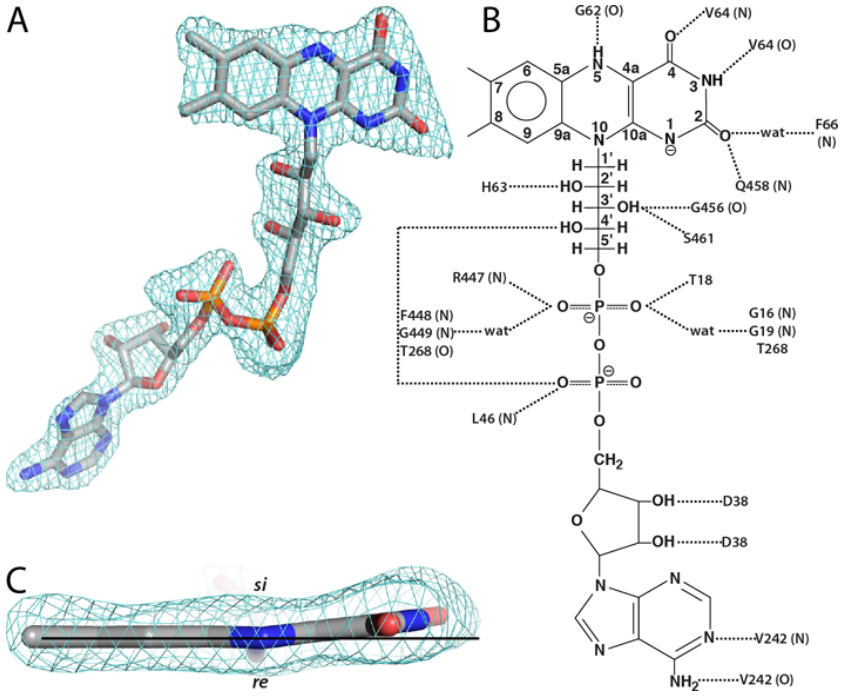

Figure 7.6 Electron density and interactions for the FAD in $AfUGM_r$. (A) View of the FAD oriented with the *re* side of the isoalloxazine system facing the viewer. The cage represents a simulated annealing σ_A-weighted F_o - F_c omit map contoured at 3.0 σ. (B) Schematic diagram of protein-FAD interactions in $AfUGM_r$. Backbone interactions are indicated by N or O in parentheses. (C) Edge-on view of the isoalloxazine. The horizontal line assists in seeing the 7° butterfly-like bend angle.

3.7 Structure of AfUGM$_r$ complexed with UDP. The structure of AfUGM$_r$ complexed with UDP was determined from a crystal that had been soaked in sodium dithionite and UDP. Electron density maps clearly indicated that UDP is bound in two of the four active sites of the tetramer (Fig. 7). The occupancy of UDP is estimated to be 0.9, which indicates essentially full occupancy and thus tight binding.

The binding of UDP induces profound conformational changes in the enzyme (Fig. 8). The largest of these changes involves residues 179-187 and 203-209. In the absence of UDP, these loops reside on the periphery of the enzyme, and thus the active site is open. Upon binding, the loops move toward each other like the flaps of a box top to create a closed active site. The conformational changes are substantial. For example, the middle residues of the two loops, Val183 and Pro206, move by 11 Å and 13 Å, respectively, upon ligand binding. One consequence of the flaps folding inward is that the side chain of Phe66 swings into the active site to avoid a clash with Pro206 (Fig. 8). As shown below, Phe66 contacts the Gal*p* moiety of the substrate.

The closing of the flaps is accompanied by smaller conformational changes in residues 104-107 and 146-161 that fine-tune the uridine binding pocket. Tyr104 and Phe158 move apart from each other by 3 Å to create space for the incoming uridine. Phe106 and Gln107 shift by 1.0 and 2.0 Å, respectively, to form three hydrogen bonds with the base (interactions are shown in Fig. 7). Finally, movements of ~1.0 Å bring Asn163, Trp167, Tyr317, Arg327, and Tyr453 into contact distance of the ribose and pyrophosphate (Fig. 7).

The dramatic closing of the flaps also results in the formation of new protein-protein interactions that stabilize the closed active site conformation (Fig. 8). In particular, Glu181 and Arg182 of the 180s flap interact with His68 and Asn457, respectively, in the closed state,

whereas in the open state, the interacting partners are separated by 17 - 19 Å. Another interaction that stabilizes the closed state involves Arg91, whose side chain moves to make four hydrogen bonds with the 200s flap.

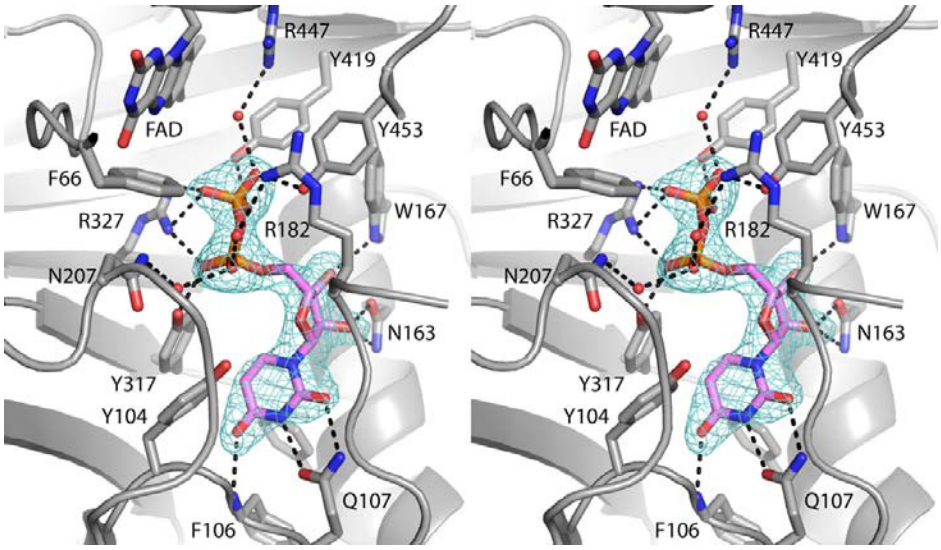

Figure 7.7 Electron density map for UDP bound to AfUGM$_r$ (stereographic view). The cage represents a simulated annealing σ_A-weighted F_o - F_c omit maps contoured at 3.0 σ.

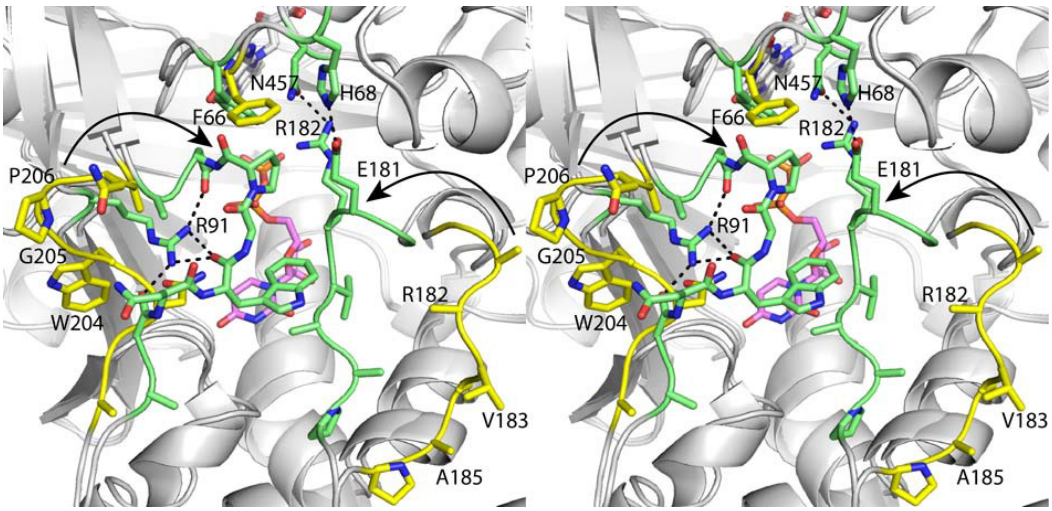

Figure 7.8 Comparison of the open and closed forms of AfUGM$_r$ (stereographic view). AfUGM$_r$ is shown in yellow. The AfUGM$_r$-UDP complex structure is shown in green. UDP is colored pink. Selected interactions in the closed state are indicated by dashed lines. The arrows denote the direction of flap closure.

*3.8 Structure of AfUGM$_r$ complexed with UDP-Gal*p. The structure of AfUGM$_r$ complexed with the substrate UDP-Gal*p* was determined from a crystal that was soaked in sodium dithionite and UDP-Gal*p*. As with the UDP complex, electron density maps indicated binding in two of the four active sites (Fig. 9A). The occupancy of UDP-Gal*p* is estimated to be 0.8. Electron density is weak for the O5 atom of the Gal*p* moiety, suggesting the possibility of conformational disorder in this part of the ring. We note that conformational disorder of the Gal*p* moiety has been observed previously ((24), PDB code 3INT). As seen with UDP, the substrate induces closure of both flaps.

The conformation and interactions of the UDP moiety of the substrate are essentially identical to those of the AfUGM$_r$-UDP complex, so we will focus on the Gal*p* moiety. Gal*p* binds at the *re* face of the FAD isoalloxazine with the anomeric carbon atom (C1) poised 3.4 Å from the FAD N5 atom (Fig. 9A, red dashes). The hydroxyl groups of Gal*p* make direct hydrogen bonds with Arg182, Asn207, and Asn457 (Fig. 9B). Water-mediated interactions are formed with Thr329, Tyr334, and Arg447. Also, the O4 hydroxyl forms a hydrogen bond with the FAD O4 carbonyl. In addition to these electrostatic interactions, nonpolar contacts are formed with Phe66 and Trp315. These steric interactions presumably help enforce specificity for Gal*p* and orient the carbohydrate for catalysis.

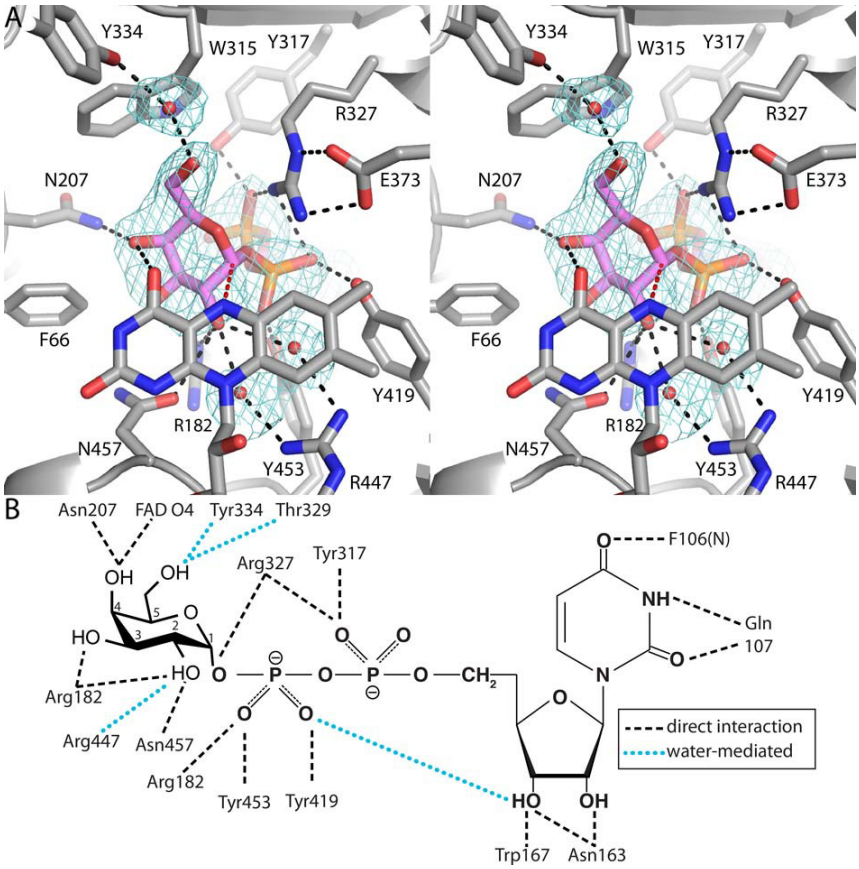

Figure 7.9 Electron density map (stereographic view) and interaction diagram for UDP-Gal*p* bound to AfUGM$_r$. (A) The cages represent a simulated annealing σ_A-weighted F_o - F_c omit map contoured at 2.5 σ. The red dashes indicate the 3.4 Å separation between the anomeric C atom of Gal*p* and the FAD N5. (B) Schematic diagram of noncovalent electrostatic interactions.

*3.9 Comparison of UDP-Gal*p *interactions in AfUGM and bacterial UGMs.* The structures of the UDP-Gal*p* complexes of AfUGM, KpUGM, and DrUGM were compared to identify similarities and differences in substrate recognition (Fig. 10). In all three structures, the substrate adopts an extended conformation, the O4 hydroxyl of Gal*p* forms a hydrogen bond to the FAD O4, and the anomeric C atom is near the FAD N5. Several conserved residues participate in substrate recognition, including Arg182, Arg327, Trp167, Tyr419, and Tyr453 (AfUGM numbering).

Differences between the two classes of UGM are also evident (Fig. 9). In particular, the UMP moiety of AfUGM is displaced by 3-5 Å compared to the bacterial enzymes. The uridine

ring is shifted by ~4 Å and rotated by almost 90°. This difference allows the uridine to form two hydrogen bonds with Asn107, a residue without a counterpart in bacterial UGMs. Displacement of the UMP also reflects a different arrangement of Tyr residues that interact with the pyrophosphate (Tyr317 in AfUGM, Tyr185 in KpUGM, Tyr209 in DrUGM). Finally, the O6 hydroxyl of Gal*p* in AfUGM is rotated by 110° from that in the bacterial enzymes. This difference is due to the potential for steric clash with Trp315.

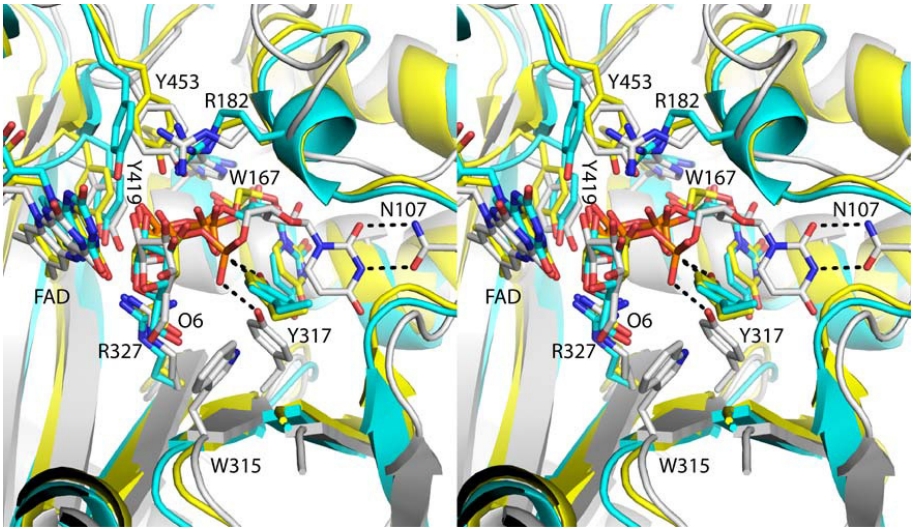

Figure 7.10 UDP-Gal*p* recognition by eukaryotic and bacterial UGMs (stereographic view). The structures of AfUGM (white), KpUGM (cyan, 3INT), and DrUGM (yellow, 3HDY) complexed with UDP-Gal*p* are shown. Selected residues of AfUGM are noted.

4. Discussion

The core structure of UGM appears to be conserved across the bacterial and eukaryotic domains of life despite low sequence identity (~16 %). The root mean square deviation between AfUGM and bacterial UGMs is 2.4 – 2.7 Å over 279 – 322 residues. And the majority of the FAD-protein interactions are also conserved.

Curiously, protoporphyrinogen oxidase from *Myxococcus xanthus* (PPOX, (25)) rather than another UGM, is the closest structural homolog of AfUGM in PDB (Fig. 11). PPOX has FAD-

binding, membrane-binding, and substrate-binding domains, which correspond to UGM domains 1, 2, and 3, respectively. PPOX (PDB code 2IVD) and AfUGM superimpose with a root mean square deviation of 2.5 Å covering 370 residues, despite sharing only 15% sequence identity. Furthermore, PPOX has some of the extra structural features of AfUGM that are not found in bacterial UGMs, including the inserted β-sheet in domain 1 and the extra helix and strand of domain 3. The significance of the structural homology to PPOX is not obvious.

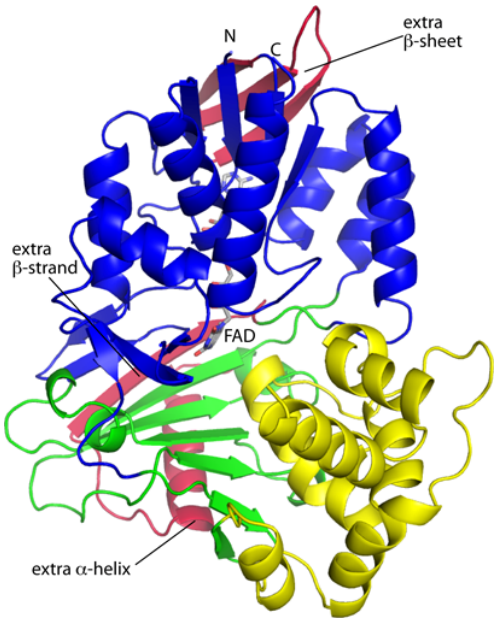

Figure 7.11 Protoporphyrinogen oxidase from *Myxococcus xanthus* (PDB code 2IVD). The FAD-binding (blue), membrane-binding (yellow), and substrate-binding (green) domains correspond to UGM domains 1, 2, and 3, respectively. Red indicates elements that are common to AfUGM and PPOX but not found in bacterial UGMs.

Neither oligomeric state nor quaternary structure is conserved in UGM. Dimers are common for bacterial UGMs, whereas AfUGM forms a tetramer in solution. UGM from *E. coli* was shown to be dimeric in solution based on dynamic light scattering (26), and the crystal structure revealed a semicircular dimer that likely represents the dimer in solution (22). This dimer is also found in the crystal lattices of KpUGM and *Mycobacterium tuberculosis* UGM (27). DrUGM appears to have a different quaternary structure, although this has not been confirmed with

solution studies. Analysis of the interfaces in the primitive orthorhombic lattice of DrUGM suggests that the enzyme forms a decamer in solution (23). The decamer is a pentamer of dimers in which the propagated dimer is unlike the semicircular dimer of the other bacterial UGMs. The DrUGM dimer is formed by interactions involving domains 1 and 3. The constituent dimers of the AfUGM tetramer are unlike any of the dimers of bacterial UGMs.

Unique structural features of AfUGM preclude the assembly of the dimers formed by bacterial UGMs. For example, if the classic UGM semicircular dimer is constructed from AfUGM protomers, several clashes across the dimer interface are evident. These clashes involve the 200s flap and the extra helix of domain 2, both of which are unique to AfUGM. Likewise, a hypothetical dimer built like DrUGM exhibits clashes in the 4-stranded sheet in domain 1 and the long inserted loop in domain 3. Thus, the protomer structure of AfUGM is incompatible with the quaternary structures of bacterial UGMs.

The observation of a tetramer raises the possibility of cooperativity between the subunits. Interestingly, previous studies have shown that 50 % of the bound flavin remains reduced under normal laboratory conditions, which suggests nonequivalence of the subunits (17). Crystal soaking populated only 50 % of the active sites with ligand, although we cannot rule out the possibility of crystal contacts near the unpopulated active sites inhibiting the large conformational changes required for ligand binding. Future studies of cooperativity in AfUGM seem warranted.

The quaternary structure of AfUGM enables conformational changes that distinguish AfUGM from bacterial UGMs. AfUGM has two flaps that move substantially upon substrate binding and product release. Bacterial UGMs have just one mobile loop that enters the active site upon substrate binding (Fig. 3B, “mobile loop”) (23,24). This loop is analogous to the 180s

flap of AfUGM. The region of bacterial UGMs corresponding to the 200s flap also participates in substrate binding (Fig. 3B, "static loop"). In particular, Tyr185 and Phe186 of KpUGM (Tyr209 and Phe210 of DrUGM) contact the pyrophosphate and Gal*p* moiety of UDP-Gal*p*, respectively. However, these residues are static because the loop is in a protein-protein interface, and a neighboring protein molecule of the oligomer restricts the motion of the loop, effectively locking it in the closed conformation. In contrast, the 200s flap of AfUGM resides on the surface of the tetramer (Fig. 4A) and is able to adopt open and closed conformations. Thus, tetramerization of AfUGM allows an additional degree of conformation freedom.

It is notable that very few of the flap residues directly interact with the substrate. (Exceptions are Arg182 and Asn207.) This observation suggests that the purpose of flap closure is not only to assemble the constellation of residues needed for substrate recognition but also to create a protected environment for catalysis. The latter role is consistent with mechanisms in which UDP is displaced during the catalytic cycle (1) because closure of the flaps presumably prevents the severed UDP from migrating out of the active site.

Finally, the AfUGM structures provide additional insight into the catalytic mechanism of UGM. Two prevailing mechanisms have been proposed based on studies of the bacterial enzymes (1). One mechanism begins with the flavin functioning as a nucleophile that attacks the anomeric carbon of galactose to form a covalent intermediate and displace UDP (28). The other mechanism involves single electron transfer from the reduced flavin to an oxocarbenium sugar intermediate followed by the formation of a flavin-sugar adduct (29, 30). Which of these mechanisms, if either, applies to eukaryotic UGMs is unknown. However, the Gal*p* moiety in the $AfUGM_r$-UDP-Gal*p* complex is poised for nucleophilic attack by the FAD N5 at the anomeric C atom (Fig. 9A). Also, the direction of the bend of the FAD isoalloxazine in AfUGM

is consistent with formation of a covalent intermediate (27). For bacterial UGMs, crystal structures, reductive trapping experiments, and studies with modified flavins support the covalent mechanism (Figure 12) (23, 24, 30). Thus, it seems likely that bacterial and eukaryotic UGMs share a common catalytic mechanism.

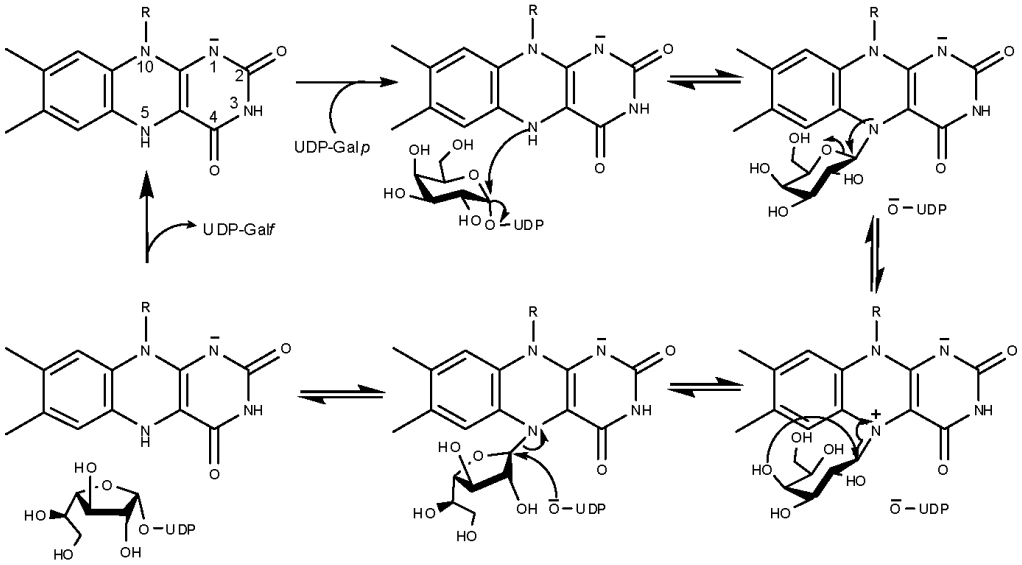

Figure 7.12 Proposed chemical mechanism of UGM. The mechanism shows the FAD acts as a nucleophile forming an iminium ion prior to the interconversion between pyranose and furanose forms.

5. Acknowledgments

We thank Dr. Norma Duke, Dr. Greg Hura, and Dr. Jonathan Schuermann for help with X-ray data collection and processing. This research was supported by NIH grant R01GM094469. Part of this work is based upon research conducted at the Northeastern Collaborative Access Team beam lines of the Advanced Photon Source, supported by award RR-15301 from the National Center for Research Resources at the National Institute of Health. Use of the Advanced Photon Source is supported by the U.S. Department of Energy, Office of Basic Energy Sciences, under contract No. W-31-109-ENG-38. The Advanced Light Source is supported by the Director, Office of Science, Office of Basic Energy Sciences, of the U.S. Department of Energy under Contract No. DE-AC02-05CH11231.

6. References

1. Richards, M. R., and Lowary, T. L. (2009) *Chembiochem* **10**, 1920-1938
2. Tefsen, B., Ram, A. F., van Die, I., and Routier, F. H. (2011) *Glycobiology*, in press
3. Pan, F., Jackson, M., Ma, Y., and McNeil, M. (2001) *J. Bacteriol.* **183**, 3991-3998
4. Schmalhorst, P. S., Krappmann, S., Vervecken, W., Rohde, M., Muller, M., Braus, G. H., Contreras, R., Braun, A., Bakker, H., and Routier, F. H. (2008) *Eukaryot. Cell.* **7**, 1268-1277
5. Kleczka, B., Lamerz, A. C., van Zandbergen, G., Wenzel, A., Gerardy-Schahn, R., Wiese, M., and Routier, F. H. (2007) *J. Biol. Chem.* **282**, 10498-10505
6. Kradin, R. L., and Mark, E. J. (2008) *Arch. Pathol. Lab. Med.* **132**, 606-614
7. Virnig, C., and Bush, R. K. (2007) *Curr. Opin. Pulm. Med.* **13**, 67-71
8. Chong, S., Lee, K. S., Yi, C. A., Chung, M. J., Kim, T. S., and Han, J. (2006) *Eur. J. Radiol.* **59**, 371-383
9. Samarakoon, P., and Soubani, A. O. (2008) *Chron. Respir. Dis.* **5**, 19-27
10. Lin, S. J., Schranz, J., and Teutsch, S. M. (2001) *Clin. Infect. Dis.* **32**, 358-366
11. Knutsen, A. P., and Slavin, R. G. (2011) *Clin. Dev. Immunol.*, in press
12. Latge, J. P. (2009) *Med. Mycol.* **47 Suppl 1**, S104-109
13. Lamarre, C., Beau, R., Balloy, V., Fontaine, T., Wong Sak Hoi, J., Guadagnini, S., Berkova, N., Chignard, M., Beauvais, A., and Latge, J. P. (2009) *Cell. Microbiol.* **11**, 1612-1623
14. Kelley, L. A., and Sternberg, M. J. (2009) *Nat Protoc* **4**, 363-371
15. Goldschmidt, L., Cooper, D. R., Derewenda, Z. S., and Eisenberg, D. (2007) *Protein Sci* **16**, 1569-1576
16. Doublie, S. (1997) *Methods Enzymol.* **276**, 523-530
17. Oppenheimer, M., Poulin, M. B., Lowary, T. L., Helm, R. F., and Sobrado, P. (2010) *Arch Biochem Biophys* **502**, 31-38
18. Dhatwalia, R., Singh, H., Oppenheimer, M., Karr, D. B., Nix, J. C., Sobrado, P., and Tanner, J. J. (2012) *J Biol Chem*
19. Krissinel, E., and Henrick, K. (2004) *Acta Crystallogr D Biol Crystallogr.* **60**, 2256-2268
20. Krissinel, E., and Henrick, K. (2007) *J. Mol. Biol.* **372**, 774-797
21. DeLano, W. L. (2002) *The PyMOL User's Manual*, DeLano Scientific, Palo Alto, CA, USA
22. Sanders, D. A., Staines, A. G., McMahon, S. A., McNeil, M. R., Whitfield, C., and Naismith, J. H. (2001) *Nat. Struct. Biol.* **8**, 858-863
23. Partha, S. K., van Straaten, K. E., and Sanders, D. A. (2009) *J. Mol. Biol.* **394**, 864-877
24. Gruber, T. D., Westler, W. M., Kiessling, L. L., and Forest, K. T. (2009) *Biochemistry* **48**, 9171-9173
25. Corradi, H. R., Corrigall, A. V., Boix, E., Mohan, C. G., Sturrock, E. D., Meissner, P. N., and Acharya, K. R. (2006) *J. Biol. Chem.* **281**, 38625-38633
26. McMahon, S. A., Leonard, G. A., Buchanan, L. V., Giraud, M. F., and Naismith, J. H. (1999) *Acta Crystallogr. D Biol. Crystallogr.* **55**, 399-402
27. Beis, K., Srikannathasan, V., Liu, H., Fullerton, S. W., Bamford, V. A., Sanders, D. A., Whitfield, C., McNeil, M. R., and Naismith, J. H. (2005) *J. Mol. Biol.* **348**, 971-982
28. Soltero-Higgin, M., Carlson, E. E., Gruber, T. D., and Kiessling, L. L. (2004) *Nat Struct. Mol. Biol.* **11**, 539-543

29. Fullerton, S. W., Daff, S., Sanders, D. A., Ingledew, W. J., Whitfield, C., Chapman, S. K., and Naismith, J. H. (2003) *Biochemistry* **42**, 2104-2109
30. Huang, Z., Zhang, Q., and Liu, H. W. (2003) *Bioorg. Chem.* **31**, 494-502

CHAPTER 8

Conclusions

UDP-galactopyranose mutase (UGM) is a unique flavin containing enzyme that has been identified as a drug target in several pathogens. This thesis presents the first recombinant expression and purification of eukaryotic UGMs from *Aspergillus fumigatus*, *Leishmania major*, and *Trypanosoma cruzi*. Detailed biochemical and biophysical analyses of these UGMs were conducted to gain insights into the chemical mechanism and the three-dimensional structure. Our studies show both similarities and differences between prokaryotic and eukaryotic UGMs, emphasizing the importance of examining eukaryotic UGMs for the development of specific inhibitors.

The kinetoplastid UGMs (TcUGM and LmUGM) have comparable k_{cat} values and both are monomeric in solution (Chapters 5, 6), while the fungal AfUGM has a 5-10 fold higher k_{cat} and is tetrameric in solution (Chapters 4, 7). AfUGM is also unique from other UGMs in that it can stabilize a half reduced state, suggesting cooperativity between the subunits (Chapter 4). These observed distinctions between these eukaryotic UGMs agree with their phylogenetic classifications based upon amino acid sequence identity (Figure 1).

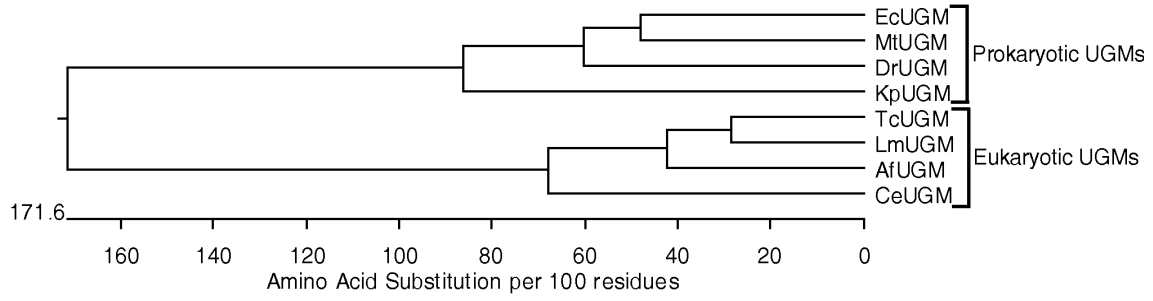

Figure 8.1 Phylogenetic tree showing the relationships of UGMs between species. The branch length of each pair signifies the percent identity (or sequence distance) between pairs and the bottom axis represents the number of amino acid subsitutions. (EcUGM, *E. coli* UGM; MtUGM, *M. tuberculosis* UGM; DrUGM, *D. radiodurans* UGM; KpUGM, *K. pneumoniae* UGM; TcUGM, *T. cruzi* UGM; LmUGM, *L. major* UGM; AfUGM, *A. fumigatus* UGM; CeUGM, *C. elegans* UGM) The figure was generated using MegAlign (DNASTAR lasergene).

Eukaryotic UGMs differ from their prokaryotic counterparts as they are able to be efficiently reduced by NAD(P)H. Our studies show eukaryotic UGMs, specifically TcUGM, are able to be reduced rapidly by NADPH and NADH, while *M. tuberculosis* UGM is unable to react with either (Chapter 6). Once reduced by NAD(P)H eukaryotic UGMs are able to stabilize the reduced state performing ~1000 isomerizations at the cost of one NAD(P)H.

The chemical mechanism of UGM is shown to be conserved across species, which is expected as each UGM requires a reduced flavin cofactor. The mechanism of eukaryotic UGMs was studied using TcUGM as a prototype and agrees with studies conducted on prokaryotic UGMs (Chapter 6). The mechanism shows the flavin acting as a nucleophile attacking the C1 of the Gal*p* by an S_N2 reaction releasing UDP. The flavin acts as a scaffold for ring opening and isomerization of galactose. Lastly, UDP attacks the newly formed Gal*f* forming UDP-Gal*f*. This mechanism is novel in that flavins are not typically nucleophilic, nor do they typically provide a scaffold for the reaction. These results suggest that the chemistry of flavoproteins is more diverse than previously thought.

Lastly, the three-dimensional structure of AfUGM was solved by X-ray crystallography (Chapter 7). While, the core structure and active site is relatively conserved between AfUGM and prokaryotic UGMs there are significant differences present in AfUGM that are important for activity and oligomerization. Unique to AfUGM, the active site has two mobile loops that close upon substrate binding, while prokaryotic UGM only has a single mobile loop. These loops are important for activity as they are proposed to trap the UDP in the active site preventing uncoupling. AfUGM also has additional helices, loops, and sheets which are important for oligomerization and perhaps play a role in cooperativity between the subunits.

This thesis presents the examination of eukaryotic UGMs, solving both the mechanism and structure. Future efforts are needed to further examine the unique features eukaryotic UGMs and to develop specific inhibitors for these proteins. In the future, works needs to be conducted to determine the NAD(P)H binding site in eukaryotic UGMs by X-ray crystallography and site-directed mutagenesis. Also, further work needs to be done to examine how UGM is able to maintain a reduced state over a series of reactions. This can be done by examining residues close to the flavin binding site and monitoring changes in oxidase and reduction activities. Also work needs to be done to identify inhibitors for eukaryotic UGMs. These can be done using both rational drug design and drug screening methods. Our lab has developed a high throughput screening assay for chemical libraries in AfUGM (see Appendix B), which can be used for screens using chemical libraries to identify potential inhibitors for eukaryotic UGMs. The idenitifed inhibitors can then be enhanced using our knowledge on the structure of eukaryotic UGMs exploiting interactions known to be important for ligand binding. Rational drug design can also be done by using both *in silico* and *in vitro* studies examining the roles of residues in the active site and designing inhibitors which mimick transition states of the reaction. Together these results will aid in the identification of inhibitors, which will hopefully lead to drugs for the treatment of aspergillosis, leishmaniasis, and Chagas' disease.

APPENDIX A

Recombinant expression, purification, and characterization of ThmD, the oxidoreductase component of tetrahydrofuran monooxygenase[†]

Reprinted from Archives of Biochemistry and Biophysics, Vol 496, Oppenheimer, M., Pierce, B.S., Crawford, J.A., Ray, K., Helm, R.F., and Sobrado, P. "Recombinant expression, purification, and characterization of ThmD, the oxidoreductase component of tetrahydrofuran monooxygenase," pp. 123-131, Copyright (2010), with permission from Elsevier.

Author Contributions:
Michelle Oppenheimer performed all the research except the experiments mentioned below.

Brad S. Pierce and Joshua A. Crawford performed the EPR studies on ThmD.

Keith Ray and Richard F. Helm performed the mass spectrometry analysis.

Pablo Sobrado oversaw and directed the research, and wrote the article.

Abstract

Tetrahydrofuran monooxygenase (Thm) catalyzes the NADH and oxygen-dependent hydroxylation of tetrahydrofuran to 2-hydroxytetrahydrofuran. Thm is composed of a hydroxylase enzyme, a regulatory subunit, and an oxidoreductase named ThmD. ThmD was expressed in *E. coli* as a fusion to maltose binding protein (MBP) and isolated to homogeneity after removal of the MBP. Purified ThmD contains covalently bound FAD, [2Fe-2S] center, and was shown to use ferricyanide, cytochrome *c*, 2,6-dichloroindophenol, and to a lesser extent, oxygen as surrogate electron acceptors. ThmD displays 160-fold preference for NADH over NADPH and functions as a monomer. The flavin-binding domain of ThmD (ThmD-FD) was purified and characterized. ThmD-FD displayed similar activity as the full-length ThmD and showed a unique flavin spectrum with a major peak at 463 nm and a small peak at 396 nm.

Computational modeling and mutagenesis analyses suggest a novel three-dimensional fold or covalent flavin attachment in ThmD.

1. Introduction

Bacterial multicomponent monooxygenases (BMM) are diiron-containing enzymes that hydroxylate a variety of hydrocarbons [1, 2]. The diiron cluster ligands are provided by the side chains of residues that make up the sequence motif (D/E)EX_2H (X)$\sim_{100}\sim EX_2H$(D/E)[3]. BMMs consist of, at least, an NADH oxidoreductase component, a hydroxylase component, which houses the diiron center, and a small protein regulatory component [2]. The BMM family has been divided into five groups based on component composition and operon organization [4]. Because these enzymes are capable of tuning the diiron center to perform C-H bond cleavage and hydroxylation in a variety of substrates, they are believed to have a potential application in bioremediation [4, 5]. There is a plethora of work regarding the mechanism of oxygen activation and several intermediates have been directly observed by using transient kinetic approaches and spectroscopy [1, 6-8]. Similarly, there are several structures of hydroxylases in the reduced and oxidized states and in the presence and absence of substrates [9-13]. More recently, structures of toluene 4-monooxygenase in complex with its regulatory protein have provided information about the mechanism of regulation in this group of enzymes. It was shown that binding of the regulatory protein causes a series of changes extending ~ 25 Å from the active site along several helices on the toluene 4- monooxygenase hydroxylase component, poising the enzyme for oxygen activation [14].

Tetrahydrofuran monooxygenase (Thm) is one of the two members of Group 5 BMM. Thm was identified from *Pseudonocardia sp*. strain K1, which is capable of growing aerobically

on tetrahydrofuran as the sole carbon source [15]. The hydroxylase enzyme of Thm is composed of only α and β subunits, which in solution are predicted to form a heterotetramer, $(\alpha\beta)_2$. In all of the BMM enzymes studied to date, the hydroxylase is composed of a dimer of three polypeptide chains, $(\alpha\beta\gamma)_2$ [2, 4]. Therefore, this novel member of the BMM family represents a "simplified" monooxygenase complex. The oxidoreductase component, ThmD, is composed of an NADH-and FAD-binding domain and a [2Fe-2S] domain. ThmD is responsible for transferring electrons from NADH to the diiron center via the FAD and the [2Fe-2S] center (Figure 1). The amino acid sequence between ThmD and other oxidoreductases is moderately conserved (30%-60%) and the cofactor-binding motifs for the various domains are strictly conserved (Figure 2). However, ThmD is the only member of this family of enzymes that contains a covalently bound flavin cofactor. Here we present the cloning, expression, purification, and characterization of the full-length ThmD enzyme and its flavin domain (ThmD-FD) and computational and mutagenesis studies that suggest that the mode of flavin attachment in ThmD appears to be novel.

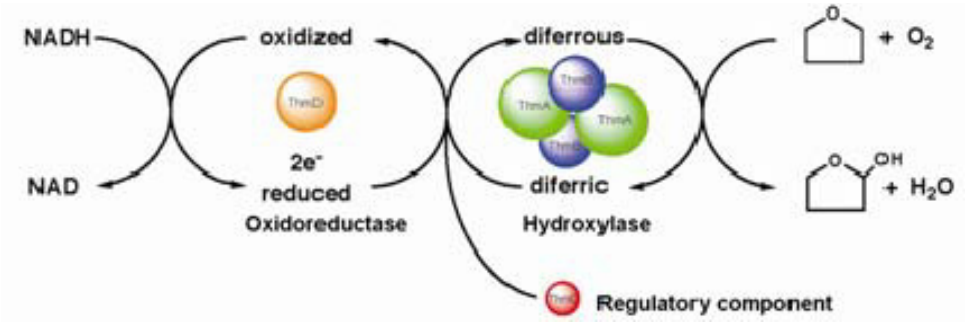

Figure A.1 Catalytic cycle of tetrahydrofuran monooxygenase. In the first step, reducing equivalents are transferred from NADH to the oxidoreductase, ThmD. ThmD reduces the diiron center housed in the ThmA subunit of the hydroxylase enzyme, ThmH. ThmH then reacts with molecular oxygen to hydroxylate tetrahydrofuran (THF). ThmH is predicted to be activated by the regulatory component, ThmC.

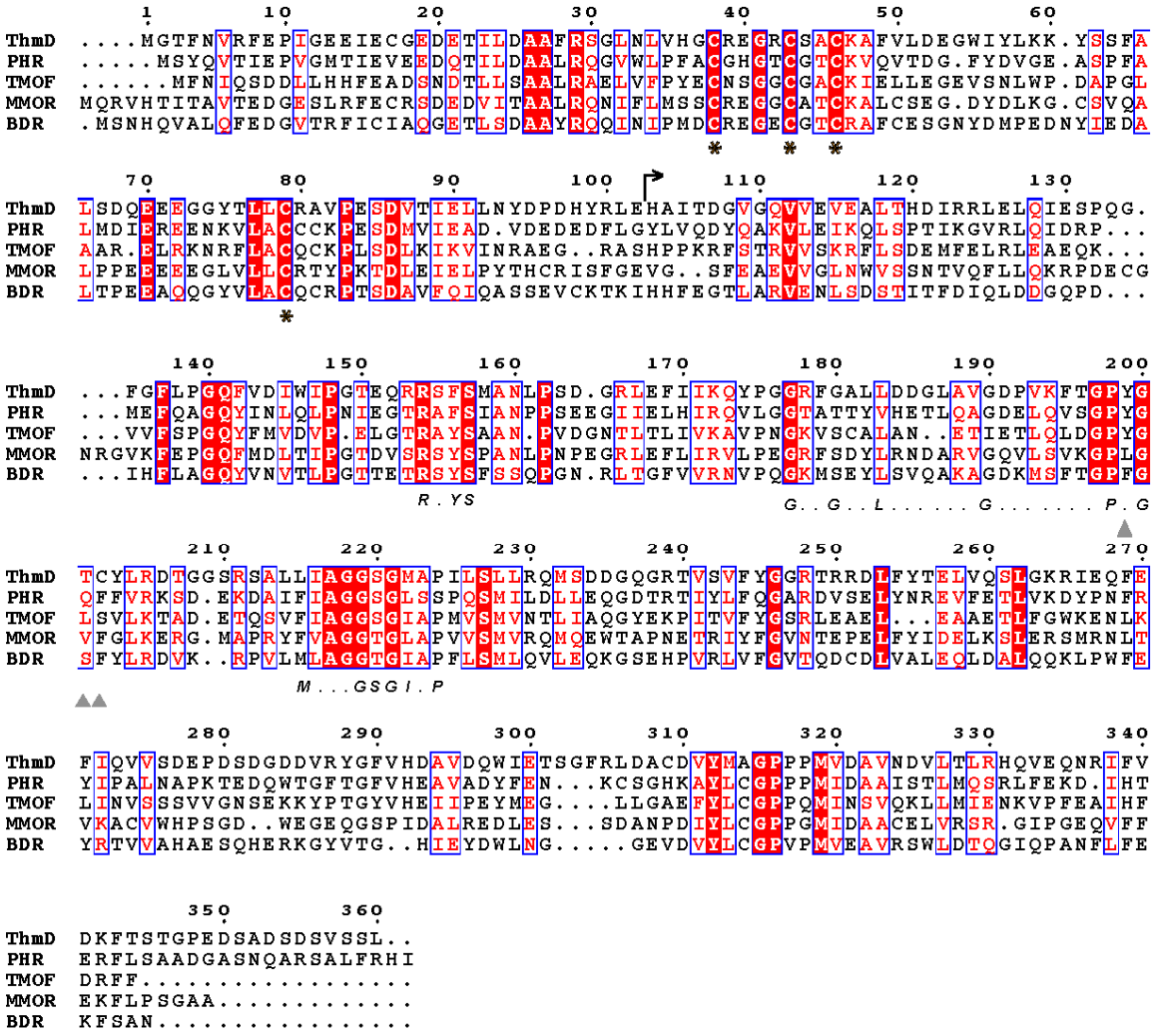

Figure A.2 Multiple sequence alignment of various oxidoreductase enzymes. Including, tetrahydrofuran monooxygenase (ThmD), phenol hydroxylase reductase (PHR), toluene-4-monooxygenase (TMOF), methane monooxygenase (MMO), benzoate 1, 2-dioxygenase reductase (BDR). Conserved residues are shown in the red box, and similar residues in red color. The four conserved cysteines that make up the [2Fe-2S] center are labeled with an asterisk (*). The predicted dinucleotide-binding regions; RxYS, GxxL(x)$_6$G(x)$_7$PxG, and M(x)$_3$GSGIxP are shown below the alignment [40]. Start of the Thm flavin domain is indicated by an arrow. Grey triangles indicate residues selected for mutagenesis studies.

2. Materials and Methods

2.1 Material. All buffers and media components were obtained from Fisher Scientific (Pittsburgh, PA). BL21T1^R chemical competent cells, NADH, NADPH, and cytochrome *c* (cyt *c*) were obtained from Sigma-Aldrich (St. Louis, MO). DNA primers were synthesized by

Integrated DNA Technologies (Coralville, IA). Isopropyl β-thio-galactopyranoside (IPTG) was obtained from Gold biotechnology (Saint Louis, MO) and DNA gel extraction and plasmid DNA purification kits were from Qiagen (Valencia, CA). *Escherichia coli* TOP-10 chemically competent cells were from Invitrogen (Carlsbad, CA). *Pme*I/*Sgf*I enzyme blend was from Promega (Madison, WI). Chromatographic columns were obtained from GE Healthcare.

2.2 Bioinformatics Analysis. Amino acid sequence alignment was done using the Clustal W program included in the DNAstar program package (Madison, WI). Figure 2 was created using the program Espript 2.2 (http://espript.ibcp.fr/ESPript/ESPript/). The program Phyre (http://www.sbg.bio.ic.ac.uk/phyre/) was used to create the threading-based 3-dimensional model of ThmD [16].

2.3 Cloning the full-length ThmD. The gene coding for ThmD was amplified by polymerase chain reaction (PCR) directly from *Pseudonocardia sp*. strain K1 genomic DNA (generous gift of Prof. B. Theimer) using the ThmD (F) and ThmD (R) primers (Table 1). A single PCR product of ~1300 bp was observed on a 0.8% agarose gel, corresponding to the expected size of the ThmD gene (1355 bp). The DNA band was excised from the gel, purified, and digested with *Pme*I/*Sgf*I restriction enzyme blend at 37 °C for 40 min. The reaction was stopped by heat denaturation at 65 °C for 30 min. This sample was ligated into the pVP56K plasmid, which was previously digested with *Pme*I and *Sgf*I using T4 ligase. This plasmid allows the expression of ThmD as a fusion to an 8xHis-maltose binding protein (8x-His-MBP) and carries a kanamycin resistant marker. A ligation reaction was also performed with the pVP55A plasmid for the expression of ThmD as a fusion with an 8x-His tag. This plasmid carries an ampicillin resistant

marker (both plasmids where obtained from the Center for Eukaryotic Structural Genomics, University of Wisconsin, Madison) [17]. Ligation reactions were transformed into chemically competent TOP-10 cells and plated in Luria-Bertani (LB) agar supplemented with the corresponding antibiotic and incubated overnight at 37 ºC. Five colonies from each ligation reaction were used to inoculate five 10 ml LB cultures supplemented with the appropriate antibiotic and grown overnight at 37 ºC. Plasmids were isolated using a Qiagen Kit and those plasmids containing the ThmD gene were identified by PCR using gene specific primers. The complete coding region was sequenced to ensure that no unwanted mutations were incorporated during the PCR reactions.

Table A.1 Primers used for cloning ThmD and its truncated forms containing the flavin domain and [2Fe-2S] centers[a].

Primer	Restriction site	Amino acids	Sequence
ThmD (F)	*Sgf*I	1-360	5'- GGTTGCGATCGCATGGGAACCTTCAACGTAAGGTTCG-3'
ThmD (R)	*Pme*I	1-360	5'- AAAAGTTTAAACAAGCGACGATACAGAATCGG-3'
ThmD-FD (F)	*Sgf*I	102-360	5'- TTCGGCGATCGCCCATGCAATTACCGATGGAGTTGGCC-3'
ThmD-[2Fe-2S] (R)	*Pme*I	1-101	5'-AGCAGTTTAAACTGCATGCTCTAGCCGATAGTGGTCAGG-3'

[a] F and R are the forward and reverse primers, respectively.

2.4 Engineering of ThmD-FD and ThmD-[2Fe-2S] domain. Amino acid sequence alignment of several members of the BMM oxidoreductase family was used to delineate the various domains in ThmD (Figure 2). The [2Fe-2S] binding domain corresponded to the first ~100 amino acids of the N-terminus. This region contains all four essential cysteine residues that bind the irons [18-20]. To clone this domain, the ThmD-[2Fe-2S] (R) and ThmD (F) primers were used in a PCR reaction using the wild-type ThmD gene as a template (Table 1). Primers ThmD-FD (F) and ThmD (R) were used to obtain the DNA fragment coding for residues 102 to 360, which correspond to the flavin and the NADH binding domains. The truncated forms of ThmD were

cloned into the pVP55A plasmid in frame with an N-terminus 8x-His tag as described above for the ThmD full-length protein.

2.5 Site directed mutagenesis. Site directed mutagenesis was performed using the QuikChange protocol (Stratagene, CA). Residues were selected for mutagenesis studies based of their proximity to the flavin cofactor in the model structure of ThmD (Figure 8).

2.6 Expression of ThmD. Expression of ThmD fused to an 8x-His tag (in the pVP55A plasmid) was performed in LB medium supplemented with 200 μg mL^{-1} of ampicillin and incubated at 37 °C with agitation set at 250 rpm. Clones were transformed into $BL21T1^{R}$ cells and grown on LB agar plates. After 24 hr incubation, a single colony was used to inoculate a 50 ml LB starter culture and incubated overnight. Four cultures each of 1.5 L of LB media were inoculated with 10 ml of the overnight culture and incubated until the optical density measured at 600 nm (OD_{600}) reached a value of ~0.8, at which point protein expression was induced by addition of 0.5 mM IPTG. After 4 hr induction, the cultures were harvested by centrifugation at 5,000g for 20 min and the cell pellet stored at -80 °C. ThmD expressed well as a fusion to an N-terminal 8x-His tag; however, this protein was completely insoluble. After modifying the expression and purification procedures, we were unable to obtain soluble enzyme in this form. ThmD was obtained in a partially soluble form when expressed as a fusion to MBP using the pVP56K plasmid. Throughout the expression of ThmD in pVP56K, the LB media was supplemented with 50 μg mL^{-1} kanamycin with agitation set at 250 rpm. A single colony of $BL21T1^{R}$ transformed with pVP56K ThmD was used to inoculate a 50 mL LB culture. This culture was incubated at 37 °C. The next day, 6 culture flasks containing 1.5 L of LB supplemented with 0. 5 M NaCl were

each inoculated with 7 mL of the overnight culture. These cultures were grown at 37 °C until the OD_{600} reached a value of ~ 0.6. The incubation temperature was increased to 47 °C for 30 min. After this heat shock period, protein expression was induced by addition of 300 μM IPTG and the media was supplemented with 150 mg ferric citrate, 150 mg ammonium ferric citrate, and 363 mg L-cysteine [21]. The cultures were incubated overnight at 10 °C. Cells were harvested by centrifugation at 5,000g for 20 min and the cell pellet stored at -80 °C. This procedure regularly yielded 20 g of cell paste.

2.7 Expression of ThmD-FD and ThmD-[2Fe-2S] domain. ThmD-FD and ThmD-[2Fe-2S] domains were expressed using the plasmid pVP55A, which produced the recombinant protein as an N-terminal fusion to an 8x-His tag. Recombinant ThmD-[2Fe-2S] domain was found to be completely insoluble. Thus, no further experiments were performed with this truncated form of ThmD. For the ThmD-FD, a single colony of BL21T1^{R} containing the pVP55A ThmD-FD plasmid was used to inoculate a 50 ml LB culture and incubated at 37 °C. The next day, 4 flasks, each containing 1.5 L of LB medium were inoculated with 10 mL of overnight culture. These cultures were incubated at 37 °C until the OD_{600} reached a value of 0.6. Protein expression was induced by addition of 0.5 mM IPTG. After 4 h of incubation at 37 °C, the cells were harvested by centrifugation at 5,000g for 20 min. This protocol normally yielded ~30 g of cell paste. All mutants of ThmD-FD were expressed following the same procedure as wild-type ThmD-FD.

2.8 Purification of ThmD. Cell pellets (~20 g) were resuspended in 90 mL 25 mM HEPES, pH 6.5, 420 μM tris(2-carboxyethyl)phosphine (TCEP), 0.75 mM phenylmethyl sulfonylfluoride (PMSF), 15 μg/mL DNase, 15 μg/mL RNase, and 15 μg/mL lysozyme, and stirred at 4 ^{o}C for 20

min. Cells were lysed by sonication for 5 min (5 s on, 10 s off). Insoluble fractions and unlysed cells were precipitated by centrifugation at 30,000g for 1 hour at 4 °C. The resulting supernatant was loaded onto a diethyl amino ethyl (DEAE) column previously equilibrated in 25 mM HEPES, pH 6.5. After washing the column with 100 mL of 25 mM HEPES, pH 6.5 containing 140 mM NaCl, a 125 mL gradient of 140 mM-400 mM NaCl was used to elute the MBP-ThmD fusion protein from the column. Fractions containing MBP-ThmD were identified by sodium dodecyl sulfate polyacrylamide gel electrophoresis (SDS-PAGE) and only those with the spectrum characteristic of a [2Fe-2S] cluster were pooled. Tobacco etch virus (Tev) protease was added (1:10) to liberate ThmD from MBP. The reaction was incubated at 4 °C overnight and the solution was centrifuged at 30,000g for 20 min to remove precipitated proteins before being loaded onto an nickel immobilized metal affinity chromatography (IMAC) column. Since both MBP and Tev proteins have an 8x-His tag these proteins remained bound, and the flow through containing free ThmD was collected. This sample was diluted 10-fold and loaded onto a second DEAE column. The column was washed with 50 mL of 25 mM HEPES, 150 mM NaCl, pH 7.5, followed by a 350 mL gradient from 150 to 400 mM NaCl in the same buffer. Fractions containing ThmD were identified by SDS-PAGE and by spectra analyses. Those fractions that were brown in color and showed spectra similar to Figure 4 were pooled concentrated and loaded onto a S-200 Sephadex column previously equilibrated in 25 mM HEPES, 125 mM NaCL, pH 7.5. This step separated ThmD from some high molecular weight contaminants yielding more than 95% pure protein. The final sample was stored at -80 °C.

2.9 Purification of ThmD-FD wild-type and mutant enzymes. Cell paste (~30 g) was resuspended in 150 mL 25 mM HEPES, 300 mM NaCl, 20 mM imidazole, 1 mM PMSF, and 25 μg/ml each

of lysozyme, DNase, and RNase, at pH 7.5 and sonicated and centrifuged as described above for ThmD. Supernatant containing Thm-FD was loaded onto a 5 mL nickel IMAC previously equilibrated with 25 mM HEPES, 300 mM NaCl, and 20 mM imidazole, at pH 7.5. The column was washed with the same buffer until the absorbance at 280 nm was near zero, at which point the bound yellow protein was eluted with buffer containing 25 mM HEPES, 300 mM imidazole, and 300 mM NaCl, pH 7.5. At this step, the ThmD-FD was ~90 % pure. The 8x-His tag was removed by addition of Tev protease (at a 1:20 ratio) and incubating overnight at 4 °C. To separate the Tev and 8x-His peptide from ThmD-FD, the solution was concentrated and diluted 10-fold to decrease the amount of imidazole and loaded onto a nickel IMAC. ThmD-FD no longer had affinity for the IMAC column and the Tev and 8x-His peptide remained bound. The flow through, containing ThmD-FD, was collected and concentrated for a final purification step on Superdex S-75 size exclusion chromatography equilibrated with 25 mM HEPES, 125 mM NaCl, pH 7.5. The final sample was more than 95% pure and was stored at -80 °C (Figure 3B).

2.10 Determination of covalent flavin binding in recombinant ThmD. To determine if the flavin cofactor in the recombinant ThmD was covalently attached, we denatured the protein and precipitated the protein by centrifugation. Both ThmD full-length and ThmD-FD wild-type and mutant proteins were denatured either by heating the protein samples at 95 °C for 5 min or by adding 1 % SDS or 10% trichloroacetic acid followed by centrifugation at 18,000g for 10 min. If the pellets remained yellow, it indicated that the flavin remained covalently attached. Western blot using a flavin specific antibody (generous gift from Dr. Dale Edmonson) was also used to determine if the flavin was covalently attached to the various proteins.

2.11 Activity Assay. The activity of ThmD was determined using cyt *c*, 2,6-dichoroindophenol (DCIP), ferricyanide, and oxygen as electron acceptors. Assays were done at 25 °C in 1 mL 25 mM HEPES, 125mM NaCl, pH 7.5, and the activity was determined by measuring the change in absorbance at 550 nm for cyt *c*, 420 nm for ferricyanide, or 600 nm for DCIP. Rates were then calculated using the extinction coefficients of 21.1 cm^{-1} mM^{-1}, 1.04 mM^{-1} cm^{-1}, and 6.2 mM^{-1} cm^{-1} for cyt *c*, ferricyanide and DCIP, respectively. The reactivity with molecular oxygen was measured directly by determining the amount of oxygen consumed is air-saturated buffer using an oxygen monitoring system from Hansatech (Norfolk, England). Protein concentration was determined using Bradford reagent [22]. Assays with varying concentrations of NADH or NADPH were done with 100 μM cyt *c*. Assays with varying concentrations of cyt *c*, ferricyaninde, DCIP, and oxygen were done with 400 μM NADH. The software KaleidaGraph (Synergy Software, Reading, PA) was used to fit the data shown in Figure 5. The steady-state parameters k_{cat} and K_M were determined by fitting of the initial velocity and substrate concentration data to the Michaelis-Menten (Equation 1). The apparent substrate inhibition constant for cyt *c* (K_{ai}) was determined by fitting the data to (Equation 2).

$$v = \frac{k_{cat} A}{K_M + A} \qquad (1)$$

$$v = \frac{k_{cat} A}{K_M + A + A^2 / K_{ai}} \qquad (2)$$

2.12 Size Exclusion Chromatography. The solution molecular weight of ThmD was determined using a Superdex 200 10/300 GL column on an Äkta Prime system. Using a set of protein standards aproprotein (6.5 kDa), ribonuclease (13 kDa), carbonic anhydrase (29 kDa), ovalbumin (43 kDa), canolbumin (75 kDa), aldolase (158 kDa), and ferritin (440 kDa)), we obtained a

standard curve. Samples from four different preparations were loaded onto the column and the elution volumes calculated. The solution molecular weight was calculated using the method described by Andrews [23].

2.13 Metal Analysis. ThmD samples were prepared at a final concentration of 3- 4 μM (according to the Bradford assay) in 4 mL of 25 mM HEPES, 125 mM NaCl, pH 7.5. Samples were analyzed to determine iron content at the Virginia Tech Soil Testing Laboratory using an inductively coupled plasma (ICP) emission spectrophotometer.

2.14 Electron Paramagnetic Resonance (EPR) Spectroscopy. X-band (9 GHz) EPR spectra were recorded on a Bruker EMX Plus spectrometer equipped with a bimodal resonator (Bruker model 4116DM). Low-temperature measurements were made using an Oxford ESR900 cryostat and an Oxford ITC503S temperature controller. A modulation frequency of 100 kHz was used for all EPR spectra. All experimental data used for spin-quantitation were collected under nonsaturating conditions. EPR spectra were simulated and quantified using Spin Count (ver.3.0.0), created by Professor M.P. Hendrich at Carnegie Mellon University. The spectral line width is dominated by *g*-strain. Therefore, simulations employ a Gaussian distribution in *g*-values to give the correct line width, specified as $\mu g_{x,y,z}$. Least squares and deconvolution analysis of the spectra were combined to allow relevant parameters to vary while maintaining a sum of multiple species that best fit the experimental data. The simulations were generated with consideration of all intensity factors, both theoretical and experimental, to allow concentration determination of species. The only unknown factor relating the spin concentration to signal intensity was an instrumental factor that depended on the microwave detection system.

However, this was determined by the spin standard, Cu(EDTA), prepared from a copper atomic absorption standard solution purchased from Sigma-Aldrich.

3. Results and Discussion

3.1 Expression and purification of ThmD. Expression of ThmD in *E. coli* yields high amounts of recombinant protein; however, the ThmD fused to an N-terminus 8x-His tag was completely insoluble. Partially soluble protein was only obtained when ThmD was expressed as a fusion to MBP (Figure 3A). MBP has been shown to increase the solubility of many proteins that are recombinantly expressed in *E. coli* [24-26]. Although expression of MBP-ThmD yielded partially soluble protein, only when the cells were subjected to heat-shock and the media was supplemented with iron and sulfur were we able to isolate ThmD with high levels of [2Fe-2S] cluster (Figure 4). Heat-shock induces the expression of chaperone proteins that presumably help in the biogenesis of the [2Fe-2S] cluster in ThmD. To purify holo ThmD, a series of chromatographic steps were required. First the MBP-ThmD fusion was loaded onto a DEAE column at pH 6.5. Only fractions that were brown in color and showed a spectrum characteristic of a [2Fe-2S] contain protein were collected. A significant amount (>50%) of the fractions containing MBP-ThmD lacked the [2Fe-2S] center but were highly active since they contained the covalently bound FAD. After cleavage of the MBP, the sample was passed onto an IMAC to isolate the free ThmD from MBP, Tev and the 8x-His tag. A second DEAE column at pH 7.5 was necessary to separate holo ThmD from apo ThmD that only contained the flavin cofactor. A final size exclusion chromatographic step yielded homogeneous holo ThmD (Figure 3A). Expression of recombinant proteins that contain [Fe-S] centers in *E. coli* commonly suffer from low solubility and low cofactor incorporation [21, 27]. This is particularly true within the family

of bacterial multicomponent monooxygenases. Only recently reports of expression and purification of the oxidoreductase component of methane monooxygenase (MMOR), toluene monooxygenase (T4MOF), and phenol hydroxylase (PHR) have been published [19, 27, 28]. Most of the recombinant proteins produced were insoluble and a large portion of the soluble fraction did not contain the [2Fe-2S] cluster or flavin cofactor. For some enzymes such as TomoF, the oxidoreductase component of toluene/*o*-xylene monooxyegenase, expression of soluble and active enzyme has not been accomplished. This enzyme was purified only after solubilization from inclusion bodies, refolding, and reconstitution of the cofactors [29]. The expression and purification procedures described here produced ~5-10 mg of pure ThmD from 20 g cell paste (Table 2). The combination of the expression of this enzyme with MBP, heat-shock expression method, and addition of iron and sulfur additives might be used to improve the solubility, stability, and cofactor incorporation of other oxidoreductases.

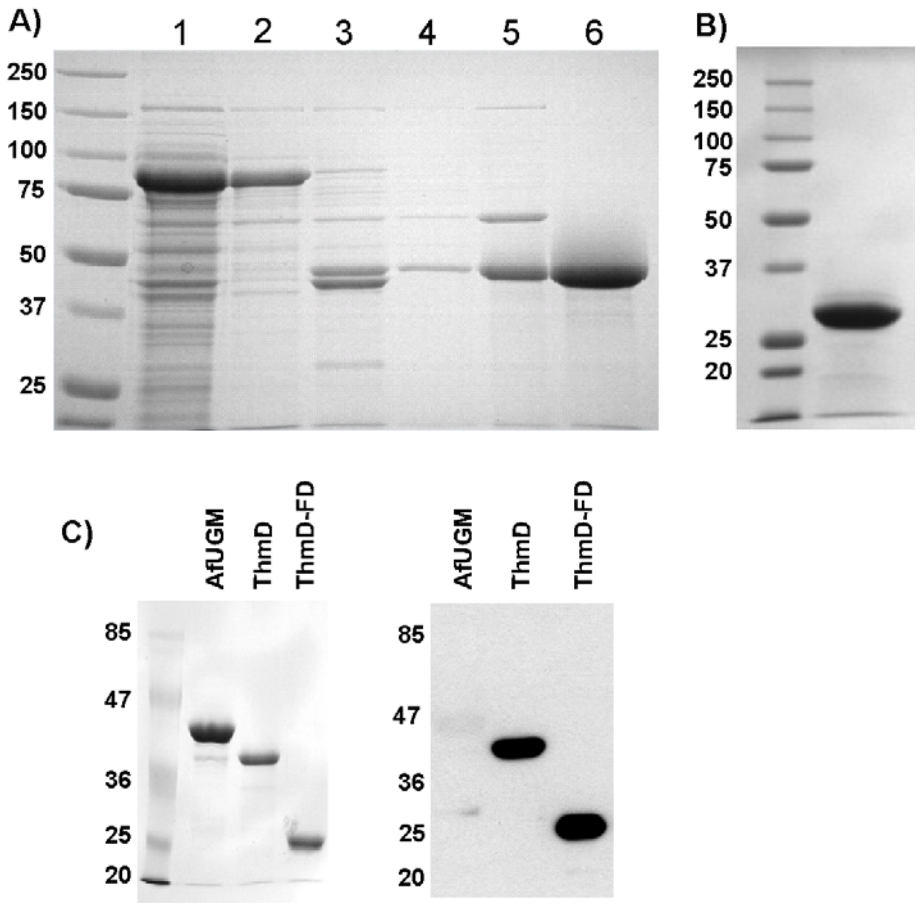

Figure A.3 SDS-PAGE and Western Blot Analysis of ThmD and ThmD-FD. A) Coomassie stained SDS-PAGE analysis of ThmD from different steps of purification. Lane 1, lysate supernatant; Lane 2, after DEAE chromatography at pH 6.5; Lane 3, after treatment with Tev protease; Lane 4, after nickel IMAC; Lane 5, after second DEAE chromatography at pH 7.5; Lane 6, after size exclusion chromatography. B) Coomassie stained SDS-PAGE showing ThmD-FD after size exclusion chromatography. C) Right panel shows the SDS-PAGE of the flavoenzyme UDP-galactopyranose mutase from *Aspergillus fumigatus* (AfUGM), ThmD, and ThmD-FD. Left panel shows the western-blot using anti-flavin antibody. Recombinant ThmD and ThmD-FD contain covalently attached flavin. The negative control, AfUGM, does not. The numbers on the left are the molecular weight standards.

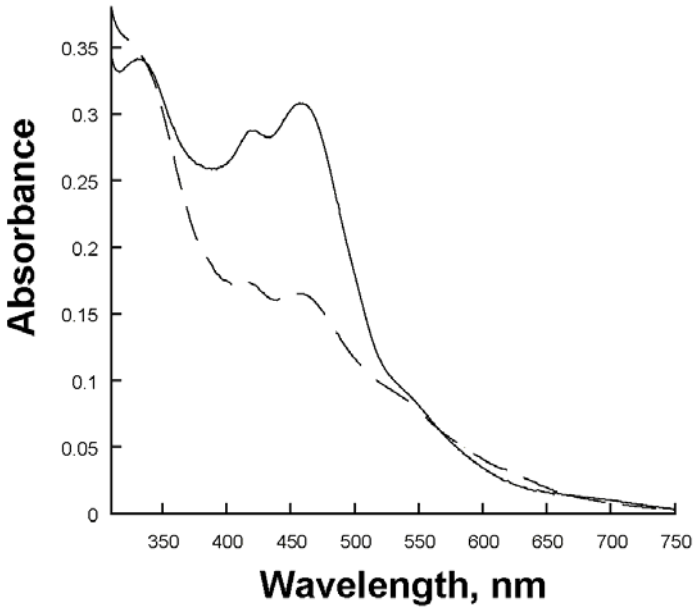

Figure A.4 Spectrum of the oxidized (solid line) and reduced (broken line) recombinant ThmD. The enzyme was reduced by addition of stoichiometric amounts of NADH.

Table A.2 Purification of recombinant ThmD.

Step [a]	Total protein (mg)	Total activity (U)[b]	Activity recovered (%)	Specific activity (U/mg)	Fold purification
CL sup	3100	2290	100	0.73	1
DEAE1	200	116	5.0	0.58	0.78
DEAE2	10	9.5	8.2	0.95	1.25
SE	5.6	7	73	1.25	1.71

[a] CL sup: complete lysate supernatant, DEAE: diethylaminoethyl chromatography, SE: size exclusion chromatography.
[b] Unit is defined as 1 μmol of cytochrome *c* reduced/min at 25 °C.

3.2 Expression and purification of ThmD domains. Previous work on the oxidoreductase component of methane monooxygenase has shown that the [2Fe-2S] and the flavin binding domains can fold independently from each other and are functional. Furthermore, the expression and purification of MMOR components has led to the structural characterization of this enzyme using NMR and X-ray crystallography and has permitted the detailed characterization of the electron transfer processes using rapid-reaction kinetic analysis [19, 30, 31]. The amino acid

sequence corresponding to the flavin- and NADH-binding domain was expressed and purified for the ThmD enzyme. The ThmD-FD protein was highly stable and contained covalently bound FAD. In contrast, the ThmD-[2Fe-2S] domain was not soluble in *E. coli*. This is surprising since domains within the oxidoreductases have been well characterized. This represents another difference between ThmD and the other oxidoreductases.

3.3 Enzyme Activity. The activity of ThmD in the Thm complex could not be assessed due to the absence of recombinant monooxygenase component. Instead, we measured the activity of the recombinant ThmD enzyme and its flavin domain variants using cyt *c* as an artificial electron acceptor. A k_{cat} value of 42 min^{-1}, K_M of 9 ± 2 μM and a k_{cat} / K_M value of 4.7 ± 1.0 μM^{-1} min^{-1} were determined for ThmD with cyt *c* as the substrate (Table 3). There are no published data of the kinetic parameters with cyt *c* for the native ThmD enzyme purified from *Pseudonocardia sp.* strain K1, however, the a specific activity of 1.6 U/mg was reported for the native ThmD, this value is very close to the specific activity determined here for recombinant ThmD [33]. We can compare the activity of ThmD to the reported activity of phenol hydroxylase reductase with cyt *c* as substrate. For this enzyme a K_M value of 1.6 μM was calculated. This value is similar to that of ThmD. In contrast, a k_{cat} value of 4020 min^{-1} was reported, which is ~100-fold higher than for ThmD [28]. The activity of the ThmD-FD was also determined with cyt *c* (Table 3). A less than 2-fold decrease in the k_{cat}/K_M for this substrate was observed for the ThmD-FD as compared to ThmD. This change originated from a 2-fold increase in the K_M value for cyt *c* in ThmD-FD, suggesting that cyt *c* binds better to ThmD when the [2Fe-2S] domain is present.

For ThmD, a K_M value for NADH of 24 ± 4 μM was calculated which is similar to the K_M values reported for phenol hydroxylase reductase (36 μM) and benzoate 1,2-dioxygenase

reductase (29 μM)[28, 34]. ThmD displays reduced dinucleotide selectivity for NADH, as indicated by a 160-fold higher catalytic efficiency for NADH as compared to NADPH (Table 3 and Figure 5). The activity of ThmD-FD with NADH is almost unchanged. With NADPH both k_{cat} and K_M increase by less than 2-fold, resulting in no change in the catalytic efficiency (Table 3).

The kinetic parameters with DCIP, ferricyanide, and molecular oxygen were also determined. With DCIP, ThmD and ThmD-FD have k_{cat} values around 30 min^{-1}, similar to the values with cyt *c*. With ferricyanide ThmD and ThmD-FD display higher k_{cat} values as compared to DCIP and cyt *c* (Table 4), however, the K_M value is more than 15-fold higher resulting in a k_{cat}/K_M value of ~6 μM^{-1} min^{-1}, which is very similar to the values with DCIP and cyt *c*. The k_{cat} values of phenol hydroxylase reductase with DCIP and ferricyanide as substrate are 780 min^{-1} and 1920 min^{-1}, respectively [28]. The lower activity of ThmD with cyt *c*, ferricyanide and DCIP as compared to phenol hydroxylase reductase, might be explained by the differences in the amino acid sequences between the two enzymes, which are only 34% identical. Furthermore, the redox potential of the FAD in ThmD might be modulated by its covalent attachment in such a way that it is not optimal for reaction with cyt *c*.

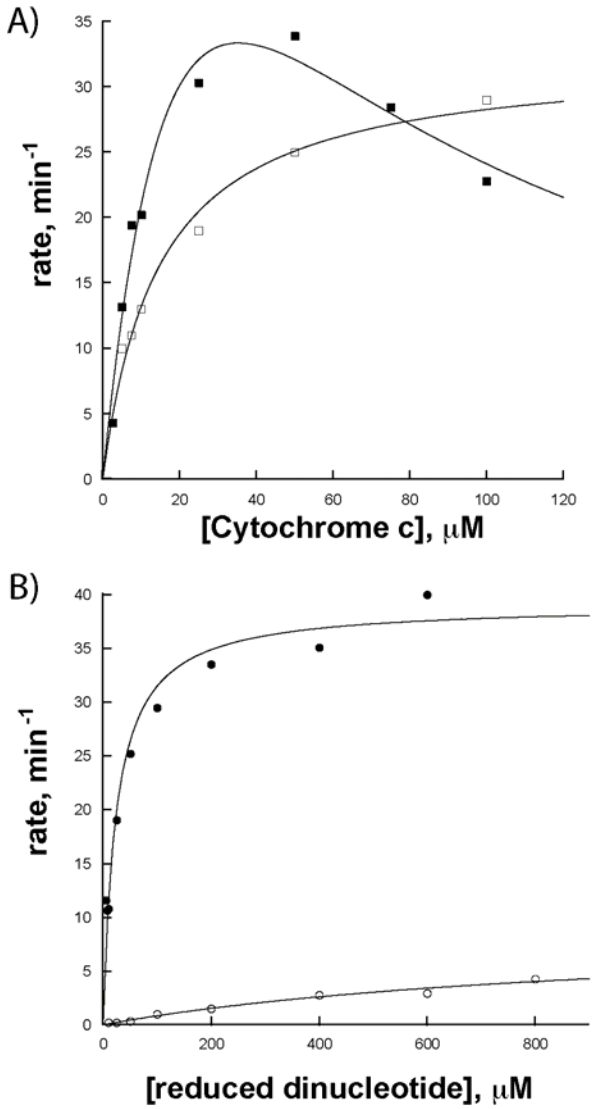

Figure A.5 Steady-state kinetics of ThmD and ThmD-FD T201A. A) Steady-state kinetic analysis of ThmD (open square) and ThmD-FD T201A (close square) varying cytochrome c at saturating concentration of NADH (400 μM). B) Kinetics of ThmD at various concentrations of NADH (solid circles) or NADPH (open circles).

Table A.3 Steady-state kinetic parameters for ThmD and ThmD-FD[a].

Substrate	Kinetic parameters	ThmD	ThmD-FD
Cytochrome *c* [b]	k_{cat} (min^{-1})	42 ± 2	50 ± 5
	K_M (μM)	9 ± 2	18 ± 5
	k_{cat} / K_M (μM^{-1} min^{-1})	4.7 ± 1.0	2.8 ± 0.6
NADH [c]	k_{cat} (min^{-1})	39 ± 1	36 ± 2
	K_M (μM)	24 ± 4	15 ± 4
	k_{cat} / K_M (μM^{-1} min^{-1})	1.6 ± 0.3	2.4 ± 0.8
NADPH [c]	k_{cat} (min^{-1})	7.1 ± 1	13 ±1
	K_M (μM)	692 ± 193	1092 ± 131
	k_{cat} / K_M (μM^{-1} min^{-1})	0.01 ± 0.0008	0.01 ± 0.002

[a] All the reactions were done in 1 mL 25 mM HEPES, pH 7.4 at 25 °C.
[b] Cyt *c* was varied while maintaining NADH saturation at 400 μM.
[c] These experiments were done with 100 μM cyt *c*.

Table A.4 Steady-state kinetic parameters for ThmD and ThmD-FD with other electron acceptors[a].

Electron acceptor	Kinetic parameter	ThmD	ThmD-FD
DCIP	k_{cat} (min^{-1})	26 ± 1	35 ± 1
	K_M, (μM)	7 ± 1	4.3 ± 0.7
	k_{cat}/K_M, ($min^{-1}\mu M^{-1}$)	3.7 ± 0.5	8 ± 1
FeCN	k_{cat}(min^{-1})	490 ± 30	600 ± 40
	K_M(μM)	70 ± 20	120 ± 30
	k_{cat}/K_M ($min^{-1}\mu M^{-1}$)	7 ± 1	5 ± 0.9
Oxygen [b]	${}_{app}k_{cat}$ (min^{-1})	10 ± 2	1.6 ± 0.1

[a] These reactions were done in 25 mM HEPES and 125mM NaCl, pH 7.5, at 25 ºC, containing 400 μM NADH.
[b] In air-saturated buffer.

3.4 UV-visible spectroscopy. The UV/Vis-spectra of the oxidized ThmD shows absorbance maxima at 457, 419, and 330 nm, consistent with other known NADH oxidoreductases (Figure

4) [19, 21, 27]. ThmD-FD shows significant differences in the spectrum of the bound flavin. There is a shift in the λ_{max} to 463 and only a small absorbance peak is observed at 396 nm. Spectra of oxidized flavins normally have two major absorbance peaks around 350 nm and 450 nm [19, 27]. In ThmD-FD, the 350 nm peak is almost absent (Figure 6). This difference in the spectra of the flavin might originate from a novel covalent attachment of the flavin or to a different active-site architecture in ThmD as compared to other known oxidoreductases.

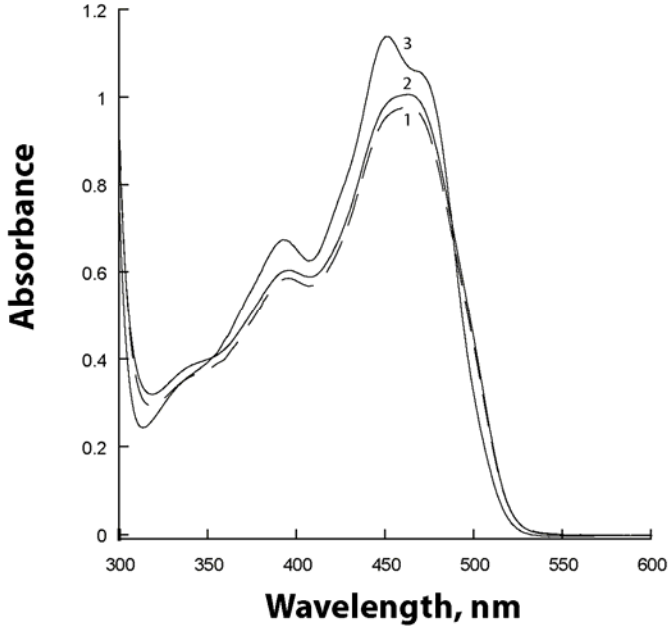

Figure A.6 Spectra of ThmD-FD (1) and the mutant variants T201A (2) and C202A (3). The spectrum of the Y199A mutant was identical to ThmD-FD (not shown).

3.5 EPR Spectroscopy. As isolated, no appreciable EPR signals were observed in samples of ThmD. The lack of an isotropic signal at $g = 4.3$ indicates the absence of adventitiously bound ferric iron. However, as shown in Figure 7 (solid line), treatment with excess sodium dithionite and methyl viologen followed by anaerobic gel filtration resulted in the formation of two spectroscopically distinct $S = 1/2$ species termed A and B. The individual contribution of each was determined by quantitative simulation (dashed line) and least squares fitting. Species A exhibits an isotropic g-value ($g_{iso} = 2.00$) and inhomogeneous saturation with a half-saturation

power ($P^{1/2}$) of 10 μW. Spin quantitation of A under nonsaturating conditions represents < 2 μM, which represents 5% of the total protein concentration. Given that both dithionite and methyl viologen were removed by gel-filtration, species A can likely be attributed to the protein-bound neutral FADH-semiquinone radical. Both the saturation behavior at this temperature and the isotropic *g*-value are consistent with this assignment.

Species B exhibits rhombic EPR spectra with *g*-values of 2.05, 1.95, and 1.87. The observed *g*-anisotropy, and the fact that the average *g*-value (g_{ave} = 1.96) is less than the free electron *g*-value (g_e = 2.0023) is diagnostic of an antiferromagnetically spin-coupled $Fe^{II}Fe^{III}$-cluster. When taken together with the saturation behavior ($P^{1/2}$ = 0.22 mW) of species B at 10 K, the observed *g*-values clearly identify the presence of an intact $[2Fe\text{-}2S]^{1+}$ cluster within [32]. A concentration of 34 ± 5 μM was determined for the $[2Fe\text{-}2S]^{1+}$ cluster by quantitative simulation under non-saturation conditions. This represents approximately 1.7 Fe atoms per protein.

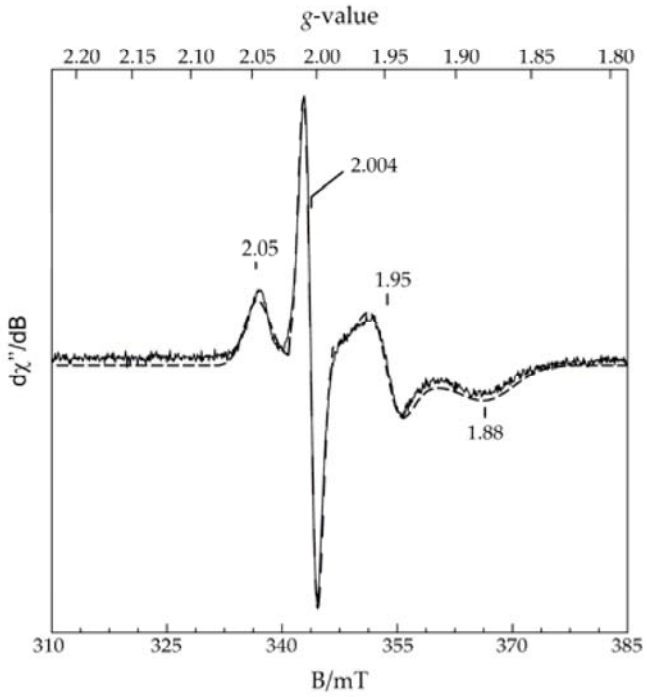

Figure A.7 X-band EPR spectrum of reduced ThmD (solid line). The ThmD sample was reduced with excess sodium dithionite in the presence of methyl viologen and then desalted anaerobically in a glove box to remove excess reductant. The resulting anaerobic protein concentration was ~ 40 μM. Instrumental parameters: microwave frequency, 9.64 GHz; microwave power, 20 μW; modulation amplitude, 9 mT; temperature, 10 K. Simulation parameters: spectrum **A**; $S = 1/2$; $g_{x,y,z} = 2.00$; $\mu_B = 0.9$ mT. Spectrum **B**; $S = 1/2$; $g_{x,y,z} = 2.047$, 1.95, 1.875; $\mu g_{x,y,z} = 0.009$, 0.009, 0.018; $\mu_B = 0.9$ mT. A quantitative component sum simulation (dashed line) for the spectra associated with species **A** and **B** was utilized to generate the simulation for this Figure. Using this technique, the respective concentration for each species was determined by least-squares analysis to be 2 μM and 34 μM, respectively.

3.6 Molecular weight determination. Purified recombinant ThmD migration on an SDS-PAGE gives an apparent molecular mass of ~40,000 Da. This value closely matches the predicted molecular weight that was calculated based on the amino acid sequence (39,845 Da). The molecular weight in solution was determined by size exclusion chromatography analysis and was calculated to be 52,000 ± 9,000 Da, indicating that in solution the protein is present as a monomer, which is consistent with the other oxidoreductases.

3.7 Cofactor incorporation. Expression of 8x-His-ThmD resulted in insoluble protein. Only when the enzyme was expressed as a fusion to MBP did approximately 50% of the total recombinant enzyme remain in the soluble form. Metal analysis by ICP, indicated that isolated ThmD contains 1.7 ± 0.3 irons per subunit of enzyme. This was supported by quantitative EPR determination of total iron content in ThmD. Similarly, determination of the flavin content indicated stoichiometric amounts of FAD. The protein engineering and expression procedures described here might be used to improve the solubility and cofactor incorporation in other members of the oxidoreductase family of enzymes.

3.8 Site of covalent flavin attachment. ThmD is the only member among the oxidoreductase components from the BMM family that has been shown to contain a covalently bound flavin cofactor. Covalently bound flavins are found in only ~10% of all flavin containing proteins, and they are bound to the side chains of histidine, tyrosine, or cysteine. The site of attachment to the flavin has mainly been observed at the C6 and Cα8-methyl group of the isoalloxazine ring. Only recently was a covalent attachment between the terminal phosphate of FMN in Na-translocating NADH-quinone reductase and a threonine residue been reported [35]. We analyzed the trypsin digest of ThmD using MALDI-TOF and LC-MS and were unable to conclusively identify a peptide containing a covalently bound flavin. Furthermore, we analyzed peptides resulting from the trypsin digest of ThmD-FD but were unable to identify the site of covalent attachment (not shown). To help us identify the site of flavin binding in ThmD, we created a three-dimensional model by threading the amino acid sequence of ThmD onto the structure of benzoate 1, 2-dioxygenase from *Acinetobacter* sp. strain ADP1 (Figure 8) [36]. This enzyme is 30% identical to ThmD. We also modeled the FAD cofactor to identify residues that are predicted to be in close

proximity to the C6α- and C8α-methyl positions of the flavin. This analysis led us to mutate T201 and C202, because they are close to the C8α-methyl, and are not strictly conserved (Figure 2). Mutagenesis of this residue to alanine produced soluble proteins that contained bound flavin. The spectra of the flavin in ThmD-FD T201A was identical to the ThmD-FD while the spectra of ThmD-FD C202A was different, suggesting that the protein microenvironment around the flavin had been changed (Figure 6). Using heat, chemical and acid denaturation, and western blot, it was determined that the flavin remained covalently attached to these mutants. Thus, T201 and C202 are not involved in covalent flavin attachment in ThmD. Steady-state kinetic analysis indicated that the mutant enzymes were able to utilize NADH with efficiencies similar to the wild-type enzyme (Table 5). Surprisingly, analysis of the activity with cyt *c* indicates that replacement of T201 and C201 with alanine induces substrate inhibition. However, the kinetic parameters were similar to wild-type ThmD-FD (Figure 5 and Table 5). Close examination of the model structure showed that Y199 is in close proximity to the Cα8-methyl group of the flavin. Thus, this amino acid was also mutated to phenylalanine. Protein denaturation, spectrum and kinetic parameters with NADH showed that this residue is also not involved in flavin attachment or catalysis (Table 5).

We also searched for cysteines, tyrosines, threonines, or histidines that might be close to the C6α-methyl position, but none were found. The fact that the 3-dimensional model of ThmD does not allow the identification of amino acids involved in flavinylation suggests that the 3-dimensional fold of ThmD might be different than other members of the oxidoreductase family of enzymes. It might also be possible that the site of covalent attachment is novel or perhaps there is a bi-covalent attachment of the FAD in ThmD. Recently, attachment of FAD cofactors at positions C6 and C8-alpha have been reported for the berberine bridge and chito-oligosaccharide

oxidase enzymes [37, 38]. Ultimately, the three-dimensional structure of ThmD or ThmD-FD will provide clear evidence of the mode of covalent flavin attachment in this novel enzyme. Our protein expression and purification efforts will allow for the screening of conditions for crystallization of ThmD and this work is currently in progress.

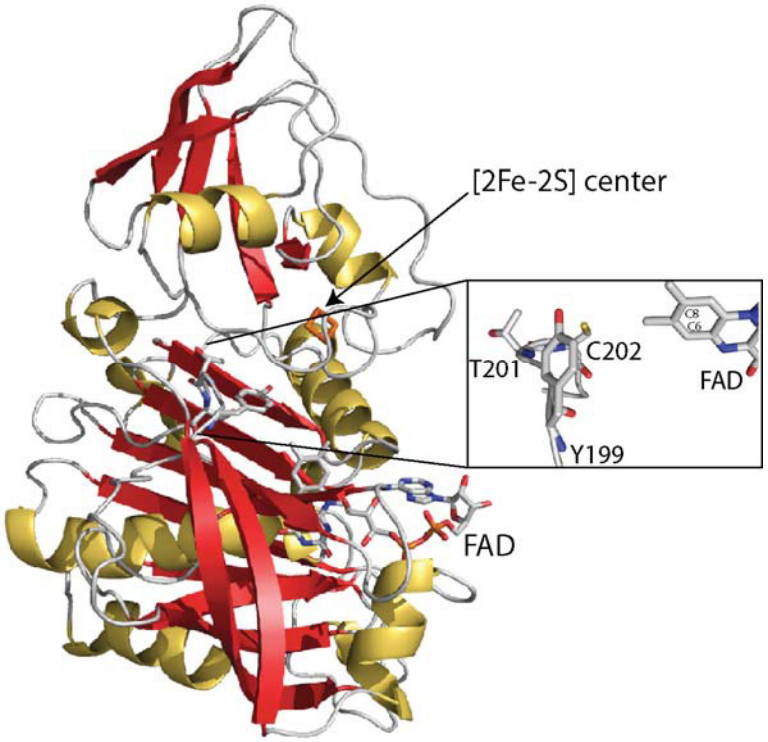

Figure A.8 Three-dimensional model of ThmD. The structure was obtained as described in Materials and Methods. The flavin cofactor (FAD) and [2Fe-2S] center area also shown. The inset shows the location of the residues selected for mutagenesis.

Table A.5 Steady-state kinetic parameters for ThmD-FD mutant enzymes[a].

Substrate	Kinetic parameters	Y199F	T201A	C202A
Cyt *c* [b]	k_{cat} (min^{-1})	51 ± 14	94 ± 38	106 ±68
	K_M (μM)	15 ± 6	32 ± 7	44 ± 35
	k_{cat}/K_M (μM^{-1} min^{-1})	3.4 ± 0.6	3.2 ± 0.6	3.1 ± 0.9
	K_i (μM)	104 ± 65	38 ± 23	25 ± 22
NADH [c]	k_{cat} (min^{-1})	31 ± 2	32 ± 1	29 ± 1
	K_M (μM)	9 ± 2	10 ± 2	4 ± 1
	k_{cat}/K_M (μM^{-1} min^{-1})	3.6 ± 0.9	3.2 ± 0.6	6 ± 1

[a] All the reactions were done in 1 ml 25 mM HEPES, pH 7.4 at 25 C.
[b] Cyt *c* was varied while maintaining NADH saturation at 400 μM.
[c] These experiments were done at 50 μM cyt *c* to prevent substrate inhibition.

4. Conclusions

Thm is a recently identified member of the BMM family of enzymes and the enzymes in this enzyme complex are different from other well-characterized systems such as methane monooxygenase and toluene 4-monooxygenase [14, 39]. In the Thm operon, ThmA and ThmB, code for the hydroxylase component. These proteins are homologous to the α and β subunits of all other BMO hydroxylases, however, Thm does not contain a γ subunit like the other proteins. The oxidoreductase component in Thm also differs from all other BMOs. Among the members of the BMO oxidoreductases, ThmD is the only enzyme with a covalently bound flavin. In this work, we presented the cloning, expression, and purification of the recombinant form of ThmD. We showed that by expressing this enzyme as a fusion to MBP and in the presence of extra iron and sulfur in the growth medium, a soluble holo enzyme could be isolated. Heat-shock of the *E. coli* cells was also necessary, which suggests that chaperones might be necessary for the proper folding of recombinant ThmD. The resulting enzyme contained full cofactor incorporation, was

active, and very stable. The flavin binding domain containing covalently bound flavin was also cloned and isolated. This domain retained wild-type ThmD NADH oxidase and cyt *c* reductase activities. Modeling studies combined with site-directed mutagenesis failed to identify the site of covalent flavin attachment in ThmD-FD suggesting that the three-dimensional structure or the nature of the residue(s) involved in covalent attachment might be novel. This hypothesis is supported by the very peculiar flavin spectrum observed in the ThmD-FD enzyme. The work presented here sets the stage for future *in vitro* studies of the role of covalent flavin attachment in this unique enzyme by rapid kinetic analysis and X-ray structural determination.

5. Acknowledgements

We thank Dr. Dale Edmonson (Emory University, Atlanta, GA) for providing the anti-flavin antibody and Dr. Barbara Theimer (Martin-Luther-Universität Halle, Germany) for providing the *Pseudonocardia sp*. strain K1 genomic DNA. The authors also thanks Dr. M.P. Hendrich (Carnegie Mellon University) for providing the EPR analysis and simulation software (Spin Count) and the UTA Center for Nanostructured Materials (http://www.uta.edu/cos/cnm) for the use of the EPR instrumentation.

6. References

[1] B.J. Wallar, J.D. Lipscomb, Chem Rev 96 (1996) 2625-2658.
[2] J.G. Leahy, P.J. Batchelor, S.M. Morcomb, FEMS Microbiol. Rev. 27 (2003) 449-479.
[3] B.G. Fox, J. Shanklin, J. Ai, T.M. Loehr, J. Sanders-Loehr, Biochemistry 33 (1994) 12776-12786.
[4] E. Notomista, A. Lahm, A. Di Donato, A. Tramontano, J. Mol. Evol. 56 (2003) 435-445.
[5] M.H. Sazinsky, J. Bard, A. Di Donato, S.J. Lippard, J. Biol. Chem. 279 (2004) 30600-30610.
[6] E.Y. Tshuva, D. Lee, W. Bu, S.J. Lippard, J. Am. Chem. Soc. 124 (2002) 2416-2417.
[7] V. Guallar, B.F. Gherman, W.H. Miller, S.J. Lippard, R.A. Friesner, J. Am. Chem. Soc. 124 (2002) 3377-3384.
[8] J.A. Broadwater, C. Achim, E. Munck, B.G. Fox, Biochemistry 38 (1999) 12197-12204.
[9] A.C. Rosenzweig, P. Nordlund, P.M. Takahara, C.A. Frederick, S.J. Lippard, Chem. Biol. 2 (1995) 409-418.
[10] L.J. Murray, S.J. Lippard, Accounts of Chemical Research 40 (2007) 466-474.
[11] M.H. Sazinsky, P.W. Dunten, M.S. McCormick, A. Didonato, S.J. Lippard, Biochemistry 45 (2006) 15392-15404.
[12] L.J. Bailey, B.G. Fox, Biochemistry 48 (2009) 8932-8939.
[13] N.L. Elsen, L.J. Bailey, A.D. Hauser, B.G. Fox, Biochemistry 48 (2009) 3838-3846.
[14] L.J. Bailey, J.G. McCoy, G.N. Phillips, Jr., B.G. Fox, Proc. Natl. Acad. Sci. U. S. A. 105 (2008) 19194-19198.
[15] B. Thiemer, J.R. Andreesen, T. Schrader, Arch. Microbiol. 179 (2003) 266-277.
[16] L. Kelly, and Sternberg, MJE, Nat. Protoc. 4 (2009) 363-371.
[17] P.G. Blommel, P.A. Martin, K.D. Seder, R.L. Wrobel, B.G. Fox, Methods Mol. Biol. (Clifton, N.J 498 (2009) 55-73.
[18] J. Muller, A.A. Lugovskoy, G. Wagner, S.J. Lippard, Biochemistry 41 (2002) 42-51.
[19] J.L. Blazyk, S.J. Lippard, Biochemistry 41 (2002) 15780-15794.
[20] J.L. Blazyk, S.J. Lippard, J. Biol. Chem. 279 (2004) 5630-5640.
[21] S. Jaganaman, A. Pinto, M. Tarasev, D.P. Ballou, Protein Expression & Purif. 52 (2007) 273-279.
[22] M.M. Bradford, Anal. Biochem. 72 (1976) 248-254.
[23] P. Andrews, The Biochemical journal 91 (1964) 222-233.
[24] P. Sobrado, M.A. Goren, D. James, C.K. Amundson, B.G. Fox, Protein Expression & Purif. 58 (2008) 229-241.
[25] W.B. Jeon, D.J. Aceti, C.A. Bingman, F.C. Vojtik, A.C. Olson, J.M. Ellefson, J.E. McCombs, H.K. Sreenath, P.G. Blommel, K.D. Seder, B.T. Burns, H.V. Geetha, A.C. Harms, G. Sabat, M.R. Sussman, B.G. Fox, G.N. Phillips, Jr., J. Struct. Func. Genomics 6 (2005) 143-147.
[26] B.P. Austin, S. Nallamsetty, D.S. Waugh, Methods Mol. Biol. (Clifton, N.J 498 (2009) 157-172.
[27] L.J. Bailey, N.L. Elsen, B.S. Pierce, B.G. Fox, Protein Expression & Purif. 57 (2008) 9-16.
[28] E. Pessione, S. Divari, E. Griva, M. Cavaletto, G.L. Rossi, G. Gilardi, C. Giunta, FEBS 265 (1999) 549-555.

[29] V. Cafaro, R. Scognamiglio, A. Viggiani, V. Izzo, I. Passaro, E. Notomista, F.D. Piaz, A. Amoresano, A. Casbarra, P. Pucci, A. Di Donato, FEBS 269 (2002) 5689-5699.
[30] L.L. Chatwood, J. Muller, J.D. Gross, G. Wagner, S.J. Lippard, Biochemistry 43 (2004) 11983-11991.
[31] D.A. Kopp, G.T. Gassner, J.L. Blazyk, S.J. Lippard, Biochemistry 40 (2001) 14932-14941.
[32] S.J.a.B. Lippard, J.M., Principles of Bioinorganic Chemistry University Science Books, 1994.
[33] B. Thiemer, J.R. Andreesen, T. Schrader, FEBS 268 (2001) 3774-3782.
[34] M. Yamaguchi, H. Fujisawa, J. Biol. Chem. 253 (1978) 8848-8853.
[35] M. Hayashi, Y. Nakayama, M. Yasui, M. Maeda, K. Furuishi, T. Unemoto, FEBS Lett. 488 (2001) 5-8.
[36] G.T. Gassner, M.L. Ludwig, D.L. Gatti, C.C. Correll, D.P. Ballou, FASEB J 9 (1995) 1411-1418.
[37] A. Winkler, F. Hartner, T.M. Kutchan, A. Glieder, P. Macheroux, J. Biol. Chem. 281 (2006) 21276-21285.
[38] C.H. Huang, W.L. Lai, M.H. Lee, C.J. Chen, A. Vasella, Y.C. Tsai, S.H. Liaw, J. Biol. Chem. 280 (2005) 38831-38838.
[39] M. Merkx, D.A. Kopp, M.H. Sazinsky, J.L. Blazyk, J. Muller, S.J. Lippard, Angew. Chem. Int. Ed. Engl. 40 (2001) 2782-2807.
[40] O. Dym, D. Eisenberg, Protein Sci. 10 (2001) 1712-1728.

APPENDIX B

Fluorescence polarization binding assay for *Aspergillus fumigatus* virulence factor UDP-galactopyranose mutase

Author Contributions:
Jun Qi performed the research except for the experiments mentioned below and wrote the article.

Michelle Oppenheimer expressed and purified the protein and helped edit the paper.

Pablo Sobrado oversaw, edited, and directed the research and writing of the article.

Abstract

Aspergillus fumigatus is an opportunistic human pathogenic fungus responsible for deadly lung infections in immunocompromised individuals. Galactofuranose (Gal*f*) residues are essential components of the cell wall and play an important role in *A. fumigatus* virulence. The flavoenzyme UDP-galactopyranose mutase (UGM) catalyzes the isomerization of UDP-galactopyranose to UDP-galactofuranose, the biosynthetic precursor of Gal*f*. Thus, inhibitors of UGM that block the biosynthesis of Gal*f* can lead to novel chemotherapeutics for treating *A. fumigatus*-related diseases. Here, we describe the synthesis of fluorescently labeled UDP analogs and the development of a fluorescence polarization (FP) binding assay for *A. fumigatus* UGM (AfUGM). High affinity binding to AfUGM was only obtained with the chromophore TAMRA, linked to UDP by either 2 or 6 carbons with K_d values of 2.6 ± 0.2 and 3.0 ± 0.7 μM, respectively. These values were ~6 times lower than when UDP was linked to fluorescein. The FP assay was validated against several known ligands and displayed an excellent Z′ factor (0.79 ± 0.02) and good tolerance to dimethyl sulfoxide.

1. Introduction

Aspergillus fumigatus is an opportunistic human pathogen responsible for diseases such as allergic reactions and lung infections, including allergic bronchopulmonary aspergillosis (ABPA) and invasive pulmonary aspergillosis (IPA) [1, 2]. This fungus is a significant health threat to immunocompromised patients, such as organ transplant recipients and people with AIDS or leukemia [3, 4]. It has been reported that IPA infections are typically accompanied by a mortality rate of 50-70% [5]. Thus, identification of novel and effective drug targets is essential in the fight against fungal infections.

Recently, the biosynthetic pathway of galactofuranose (Gal*f*), the 5-membered ring form of galactose, has been described in *A. fumigatus*. Gal*f* is a component of the cell wall of *A. fumigatus* and plays an important role in virulence [6-8]. In *A. fumigatus*, Gal*f* was first identified as a component of galactomannan by immunodetection in IPA patients [9]. Later, it was found that Gal*f* is also a major component of saccharide structures in membrane lipids and glycosyl phosphoinositol (GPI)-anchored lipophospholipids [10, 11]. UDP-galactopyranose mutase (UGM) is a flavoenzyme that catalyzes the conversion of UDP-galactopyranose (UDP-Gal*p*) to UDP-galactofuranose (UDP-Gal*f*, Figure 1), the biosynthetic precursor of Gal*f* [7, 12]. Deletion of the *A. fumigatus* UGM (AfUGM) gene results in mutant fungi with attenuated virulence, a decrease in cell wall thickness, and an increase in the sensitivity to antifungal agents [8, 13]. Moreover, Gal*f* is absent in humans [12]. Thus, inhibitors of AfUGM that block the biosynthesis of Gal*f* represent attractive drug targets for the identification of novel therapeutics against *A. fumigatus*.

Here, we describe the development of a fluorescence polarization (FP) binding assay to identify specific AfUGM inhibitors. Four fluorescently labeled UDP derivatives including two

known UDP-fluorescein analogs (**1** and **2**, Fig. 2) and two novel UDP-TAMRA analogs (**3** and **4**, Fig. 2) were synthesized to be used as fluorescent probes in the FP assay. Their concentrations were optimized to obtain a stable FP signal with minimal standard deviation, and their K_d values were determined by measuring the anisotropy changes as a function of AfUGM concentration. We found that the UDP-TAMRA analogs bind to AfUGM 6 fold tighter than the UDP-fluorescein analogs, suggesting that UDP-TAMRA analogs are better fluorescent probes for this enzyme. UDP-TAMRA probes could be competed out by UDP, a known ligand of UGMs, and the K_d value of UDP was in good agreement with the value determined previously in a fluorescence assay [7]. Furthermore, the FP assay was validated using several known ligands, and displayed an excellent Z′ factor (0.79 ± 0.02) and good tolerance to DMSO. Therefore, this fast convenient one-step FP assay is suitable for a high-throughput screening to identify AfUGM inhibitors.

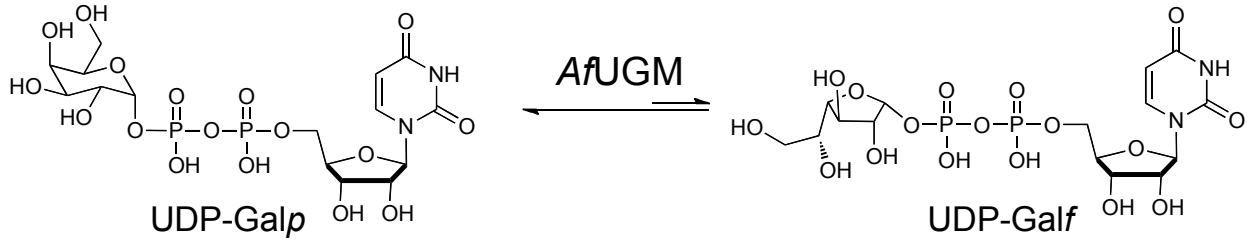

Figure B.1 Reaction catalyzed by AfUGM.

2. Materials and Methods

2.1 Materials. All chemicals were obtained from commercial sources and were used without further purification. Anhydrous reactions were performed under argon. All solvents were either reagent grade or HPLC grade. NMR spectral data were obtained using a JEOL Eclipse spectrometer at 500 MHz, or a Varian Inova spectrometer at 400 MHz. Chemical shifts were reported as *δ*-values relative to known solvent residue peaks. High-resolution mass spectra (HRMS) were obtained in the Mass Spec Incubator, Department of Biochemistry, Virginia Tech.

High performance liquid chromatography (HPLC) was performed on a C18 reverse phase column (Phenomenex Luna C18 column, 250 x 21.20 mm, 5 micron) using water and acetonitrile as the elution solvents. All compounds were more than 95% pure as judged by HPLC and ^{1}H NMR.

2.2 Protein expression and purification. AfUGM and MtUGM were expressed and purified with the same protocol as described by Oppenheimer et al [7]. A large quantity of highly pure AfUGM was obtained, which was confirmed by UV-visible spectrophotometry and SDS-PAGE (Fig. S1, [14]).

2.3 Synthesis of UDP-fluorescein chromophore 1 and 2. The synthesis of chromophore **1** was accomplished by reacting 4 mg of compound **5**, which was synthesized following a previously published procedure [15], with 6 mg of fluorescein-5-isothiocyanate (FITC) in 0.1 M pH 9.0 $NaHCO_3$ buffer (50 μL) and DMF (100 μL) (Fig. 2). After stirring at room temperature for 2 hours, the yellow solution was concentrated and loaded onto a preparative silica gel TLC plate. The isolated crude product was dissolved in water, injected onto reverse-phase HPLC (Phenomenex Luna C18 column, 250 x 21.20 mm, 5 micron), and purified at a flow rate of 5.0 mL/min with linear gradient elution of 5% to 95% acetonitrile in H_2O over 20 min to afford chromophore **1** (4 mg, 52%). ^{1}H NMR (500 MHz, 6:1 D_2O: d_7-DMF): δ 7.96 (d, J = 8.2, 1H), 7.78 (s, 1H), 7.70 (d, J = 8.1, 1H), 7.30 (dd, J = 8.2, 1.5, 1H), 7.27-7.27 (m, 2H) (t, J = 8.7, 2H), 6.65 – 6.61 (m, 2H), 6.61 – 6.58 (m, 2H), 5.91 (s, 1H), 5.91 (s, 1H), 4.36 – 4.30 (m, 2H), 4.24 – 4.21 (m, 3H), 4.19 – 4.16 (m, 2H), 3.88 (s, 2H); HRMS (MALDI) calcd for $C_{32}H_{29}N_4O_{17}P_2S$ $(M-H)^-$: 835.0729, found 835.0759 (Fig. S2, [14]).

Chromophore **2** (7.1 mg, 55%) was synthesized from the reaction of compound **6** and FITC by the same procedure as above (Fig. 2), and was purified by preparative TLC and reverse-phase HPLC (Phenomenex Luna C18 column, 250 x 21.20 mm, 5 micron). ^{1}H NMR (500 MHz, 6:1 D_2O: d_7-DMF): δ 8.00 (d, J = 8.0, 1H), 7.73 (s, 1H), 7.61 (d, J = 8.3, 1H), 7.31 (d, J = 8.3, 1H), 7.27 – 7.27 (m, 2H), 6.66 – 6.60 (m, 4H), 5.96 (s, 1H), 4.38 – 4.34 (m, 2H), 4.27 – 4.23 (m, 2H), 4.23 – 4.18 (m, 2H), 3.97 – 3.92 (m, 2H), 3.58 (s, 1H), 1.66 – 1.61 (m, 4H), 1.42 – 1.36 (m, 4H); HRMS (MALDI) calcd for $C_{36}H_{37}N_4O_{17}P_2S$ $(M-H)^-$: 891.1350, found 891.1348 (Fig. S3, [14]).

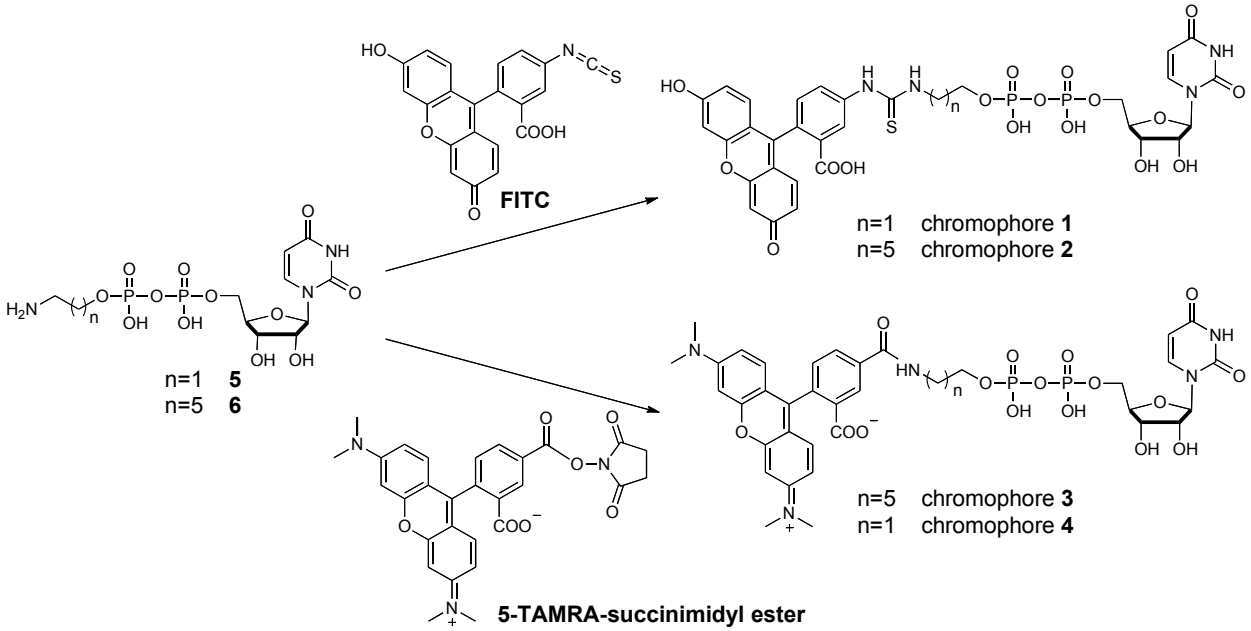

Figure B.2 Synthetic scheme of the chromophores used as ligands to AfUGM for application in FP assays.

2.4 Synthesis of UDP-TAMRA chromophore 3 and 4. The synthesis of chromophore **3** was accomplished by a reaction of 4 mg of compound **6**, which was synthesized following a previously published procedure [15], with 0.8 mg of 5-carboxytetramethylrhodamine, succinimidyl ester (5-TAMRA, SE) in 0.1 M pH 8.3 $NaHCO_3$ buffer (50 µL) and DMF (50 µL) (Fig. 2). After stirring at room temperature for 2 hours, the pink solution was concentrated and loaded onto a preparative TLC plate. The isolated crude product was dissolved in water, injected

onto reverse-phase HPLC (Phenomenex Luna C18 column, 250 x 21.20 mm, 5 micron), and purified at a flow rate of 5.0 mL/min with linear gradient elution of 5% to 95% acetonitrile in H_2O over 20 min to afford chromophore **3** (1.1 mg, 80%). ^{1}H NMR (500 MHz, D_2O) δ 8.22 (s, 1H), 8.08 (d, J = 7.7, 1H), 7.89 (d, J = 7.3, 1H), 7.60 (d, J = 8.8, 1H), 7.28 – 7.22 (m, 1H), 6.91–6.88 (m, 2H), 6.61 (s, 1H), 6.59 (s, 1H), 5.89 – 5.83 (m, 2H), 4.35 – 4.31 (m, 1H), 4.30 – 4.26 (m, 1H), 4.18 – 4.15 (m, 3H), 4.00 (dd, J = 13.3, 6.4, 2H), 3.49 (t, J = 6.8, 2H), 3.19 (s, 3H), 3.18 (s, 3H), 1.75 – 1.67 (m, 4H), 1.51 – 1.45 (m, 4H), 1.34 (s, 3H), 1.32 (s, 3H); HRMS (MALDI) calcd for $C_{40}H_{46}N_5O_{16}P_2$ $(M-H)^-$: 914.2415, found 914.2431 (Fig. S4, [14]). The above synthetic approach was also used to synthesize and purify chromophore **4** (1.5 mg, 77%). HRMS (MALDI) calcd for $C_{36}H_{38}N_5O_{16}P_2$ $(M-H)^-$: 858.1789, found 858.1851 (Fig. S5, [14]).

2.5 Optimization of chromophore concentration. Solutions containing various concentrations of chromophore in 0.05 M sodium phosphate buffer (pH 7.0) were added to 12 wells in a 96-well half area black bottom plate (Corning) with final volumes of 25 μL. FP was analyzed by a SpectraMax M5 plate reader (Molecular Devices). The parallel fluorescence emission ($F_=$) and perpendicular fluorescence emission ($F_\perp$) at 524 nm (for compounds **1** and **2**, excitation at 492 nm) or at 584 nm (for compounds **3** and **4**, excitation at 545 nm) were measured by a SpectraMax M5 plate reader (Molecular Devices), and the anisotropy (r) was calculated using Eq. 1. The minimal concentration at which stable FP signals with minimal standard deviations was chosen as the optimal concentration for the chromophore.

$$r = \frac{F_= - G \cdot F_\perp}{F_= + 2G \cdot F_\perp} \tag{1}$$

$$y = m_1 + (m_2 - m_1)\frac{(x + C_t + m_3) - \sqrt{(x + C_t + m_3)^2 - 4xC_t}}{2C_t} \tag{2}$$

2.6 FP binding assay to determine the chromophore binding affinities. Solutions containing serially diluted AfUGM and 15 nM of chromophore in 0.05 M sodium phosphate buffer (pH 7.0) were incubated at room temperature for 5 minutes. Each experiment was done in triplicate in a 96-well half area black bottom plate (Corning) at final volumes of 25 μL. Fluorescence anisotropy was measured as indicated above and the K_d values were obtained by fitting the anisotropy data to Eq. 2, where m_1 and m_2 are the minimum and maximum anisotropy values, respectively; m_3 is the K_d value, and the total concentration of UDP-chromophore is represented by C_t.

2.7 Determination of the assay Z' factor. Solutions containing 2 μM of AfUGM and 15 nM of chromophore **3** in the absence (negative control) and presence (positive control) of 300 μM of UDP were incubated at room temperature for 5 minutes. Each solution was added to octuplicate wells in a 96-well half area black bottom plate (Corning) with final volumes of 25 μL. FP was analyzed by a SpectraMax M5 plate reader (Molecular Devices). The Z′ factors were calculated using Eq. 3, where μ_- represents the mean anisotropy value of the negative control, and μ_+, the mean anisotropy value of the positive control; σ_- represents the standard deviation of the negative control, and σ_+ the standard deviation of the positive control. A Z′ factor of 0.79 ± 0.02 was obtained for chromophore **3**.

$$Z' = 1 - \frac{3(\sigma_- + \sigma_+)}{\mu_- - \mu_+} \qquad (3)$$

2.8 Optimization of AfUGM concentration. To determine the optimal concentration of AfUGM in the FP assay, solutions containing 15 nM of chromophore **3** and AfUGM at various concentrations in the absence (negative control) and presence (positive control) of 300 μM of

UDP were incubated at room temperature for 5 minutes. Each was added to octuplicate wells at a final volume of 25 μL. FP was analyzed as indicated previously, and Z′ factors were calculated from Eq. 3.

2.9 Competitive binding experiments using FP inhibition assay. Solutions (25 μL) containing 2 μM of AfUGM and 15 nM of chromophore **3** in 0.05 M sodium phosphate buffer (pH 7.0) were mixed with various concentrations of UDP, UDP-Gal*p*, **7**, or **8**, and the reactions incubated at room temperature for 5 minutes. Each solution was done in triplicate. Anisotropy values were measured and the IC_{50} values obtained by fitting the data to Eq. 4, where m_1 and m_2 are the minimum and maximum anisotropy, respectively; m_3 is the slope, and m_4 is the IC_{50}. The K_d values were obtained using Eq. 5, where K_i is the binding affinity of chromophore **3** on AfUGM (2.6 ± 0.6 μM).

$$y = m_1 + \frac{(m_2 - m_1)x^{m_3}}{{m_4}^{m_3} + x^{m_3}} \qquad (4)$$

$$K_d = \frac{IC_{50}}{1 + \frac{I}{K_i}} \qquad (5)$$

2.10 AfUGM activity assay. The AfUGM activity assay was performed by monitoring the formation of UDP-Gal*p* from UDP-Gal*f* by HPLC. A 20 μL reaction, containing 20 mM dithiothreitol, 0.5 mM UDP-Gal*f* in 25 mM HEPES, 125 mM NaCl buffer, pH 7.5 in the absence of **7** or **8** was initiated by addition of AfUGM at a final concentration of 50 nM. After incubation at 37 ^{o}C for 10 min, the reaction was quenched by heat denaturation (95 ^{o}C for 5 min) in a DNA engine thermo cycler (BioRad, Hercules, CA). The same reaction was also performed in the

presence of **7** (500 μM) or **8** (50 μM). The suspension was centrifuged and the supernatant injected onto a CarboPac PA100 (Dionex) anion-exchange column. The sample was eluted isocratically with 75 mM KH_2PO_4 (pH 4.5), and the absorbance at 262 nm was monitored to identify fractions of substrate and product. The substrate, UDP-Gal*f* eluted at 36.5 min, and the product, UDP-Gal*p* eluted at 28.3 min. The inhibition of AfUGM activity was indicated by the extent of conversion of UDP-Gal*f* to UDP-Gal*p*.

2.11 Tolerance to DMSO. To determine the tolerance of the assay to DMSO, solutions containing 2 μM of AfUGM, 15 nM of chromophore **3**, and DMSO at various concentrations in the absence (negative control) and presence (positive control) of 300 μM of UDP were incubated at room temperature for 5 minutes. Fluorescence anisotropy values and Z′ factors were calculated as indicated previously.

3. Results and Discussion

3.1 Assay design and optimization. In this study, we report the development of an FP assay that can be used for high-throughput screening of inhibitors for AfUGM, which we believe will lead to the development of new therapeutics against *A. fumigatus*-related diseases. The FP assay was designed as shown in Fig. 3. If the UDP fluorescent probe binds to AfUGM and is excited with plane-polarized light, the resulting enzyme-ligand complex tumbles slowly in solution and, thus, the fluorescence emission remains polarized (Fig. 3a). Otherwise, the emission will be depolarized as the free chromophore will rotate rapidly. The change in the rotational motion between the bound and free chromophore can be used as a signal for detection of the binding of small molecules to the active site of AfUGM because, as the small molecule replaces the bound

fluorescent probe, the free probe will rapidly rotate increasing the amount of depolarized fluorescence (Fig. 3b).

An essential component of an FP assay is a fluorescent probe that specifically binds to the enzyme or protein of interest. To design the fluorescent probe, we rationalized that the incorporation of the UDP moiety into the structure would target binding to the AfUGM active site since it is a major part of the UGM substrate. The fluorophore we first selected was fluorescein because UDP-fluorescein derivatives have been found to bind to prokaryotic UGMs from *Klebsiella pneumoniae* and *Mycobacterium tuberculosis* [15]. To minimize the steric hindrance of fluorescein with AfUGM binding site residues, UDP and fluorescein were connected with alkyl linkers of different lengths, which resulted in two UDP-fluorescein analogs (**1** and **2**, Fig. 2). We also designed a UDP bound to the chromophore, commercially known as TAMRA (Fig. 2). This chromophore offers several advantages over fluorescein. First, TAMRA is more resistant to photobleaching compared to fluorescein [16]. Second, the fluorescence emission of TAMRA does not overlap with that of the flavin cofactor in AfUGM. Fluorescein is typically excited at 494 nm and emits at 520 nm, which significanlty overlaps with the absorbance and fluorescence emission of the flavin. In contrast, TAMRA's absorbance and fluorescence maxima is at 546 nm and 580 nm, respectively [16]. This is significantly different from the flavin absorbance/emission properties, and improves signal-to-noise ratio. Finally, in comparison with fluorescein, TAMRA has one extra positive charge, which we believe increases the interaction between TAMRA and flavin and helps improve binding of the probe to AfUGM. Alkyl linkers of different lengths were also included to minimize the steric interaction of TAMRA with the binding site residues, giving two novel UDP-TAMRA analogs (**3** and **4**, Fig. 2)

In order to increase the signal-to-noise ratio, stable FP values are necessary. Therefore, we varied the concentration of UDP-chromophores to determine the optimal concentration (Fig. 4). Stable FP values with minimal standard deviation were obtained at concentrations higher than 15 nM. Therefore, we chose the 15 nM UDP-chromophore as the minimal concentration to use for further characterization.

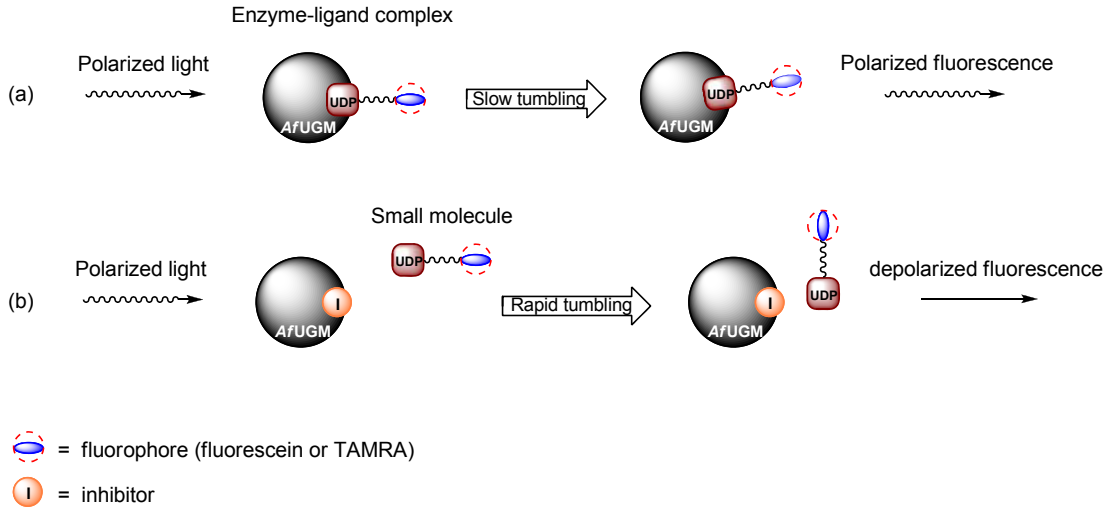

Figure B.3 FP assay design. (a) Binding of the FP probe to AfUGM leads to polarized fluorescence. (b) Displacement of the FP probe from AfUGM by inhibitor results in depolarized fluorescence.

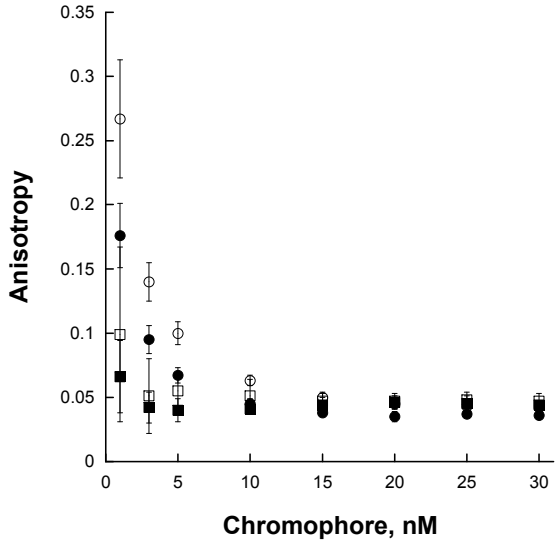

Figure B.4 Determination of optimal concentration of fluorescent probe for FP binding assay. Conditions are described in Material and Methods sections. Chromophore **1** (○), **2** (●) (excitation at 492 nm and emission at 524 nm), **3** (■), and **4** (□) (excitation at 544 nm and emission at 584 nm)

3.2 AfUGM specific UDP-chromophore for HTS assay application. Binding of the UDP-chromophore to AfUGM was determined by varying the concentration of the enzyme at a constant concentration of the UDP-chromophores (15 nM) (Fig. 5). Binding assays with the UDP-fluorescein probes (chromophores **1** and **2**) show that these ligands bind weakly to AfUGM, with K_d values of ~15 μM (Fig. 5A). This relatively low affinity impedes the utilization of these chromophores for a high-throughput FP binding assay, as it will require high quantities of enzyme. Interestingly, we tested the binding of these chromophores to bacterial UGM from *M. tuberculosis* and the K_d value of chromophore **2** was 0.10 ± 0.01 μM, consistent with previously published values (Table 1) [15]. This tighter binding suggests differences in the active site architecture between the prokaryotic and *A. fumigatus* UGM enzymes. This is also consistent with our recent report on binding assays monitoring flavin fluorescence that showed that AfUGM binds UDP-glucose 5 times tighter than *K. pneumoniae* UGM. Similarly, binding of UDP-Gal*p* to AfUGM was not detected, although UDP-Gal*p* binds to the bacterial enzyme with

a K_d value of 220 μM [7, 17]. These differences in ligand binding might originate from the low amino acid identity between the bacterial and eukaryotic UGMs (<18%). Furthermore, we have shown that the quaternary structure between these enzymes is not conserved as the bacterial enzymes have been shown to function as homodimers, while AfUGM functions as a homotetramer [7].

With the UDP-TAMRA analogs (chromophores **3** and **4**), the binding to AfUGM was ~ 6 times better than with the UDP-fluorescein analogs, and a significant anisotropy change was measured (Fig. 5B). Interestingly, the length of the linker had little or no effect on the binding affinities (Table 1), suggesting that with AfUGM the interaction between the chromophore and some components of the active site or perhaps directly with the flavin cofactor play a major role in binding. Compound **3** and **4** bound to MtUGM with similar affinities as chromophores **1** and **2**, respectively. In contrast to AfUGM, in the bacterial enzymes the length of the linker play a major role in binding with longer linkers increasing the affinity, further demonstrating that the active site architecture is varied among the UGM enzymes. We selected **3** as the FP probe for further characterization of the binding assay.

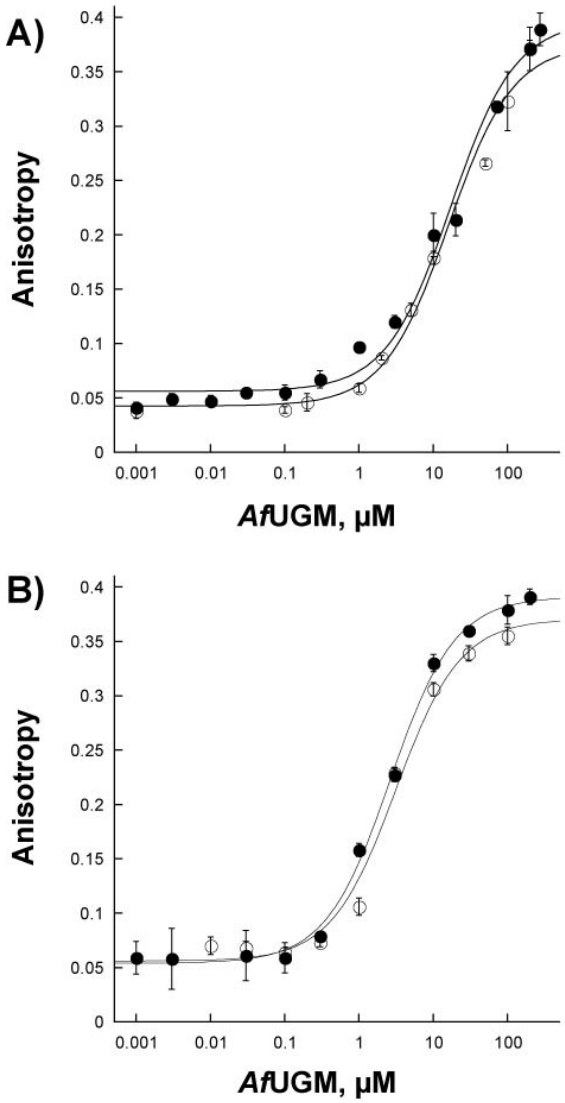

Figure B.5 FP binding assay to determine K_d of the chromophores. (a) Chromophores **1** (○) and **2** (●) (excitation at 492 nm and emission at 524 nm). (b) Chromophores **3** (●) and **4** (○) (excitation at 544 nm and emission at 584 nm).

Table B.1 K_d of the UDP-fluorescent probes on AfUGM.

Chromophore	K_d on AfUGM (μM)	K_d on MtUGM (μM)
1	17 ± 3	> 30
2	16 ± 3	0.10 ± 0.01
3	2.6 ± 0.2	0.73 ± 0.07
4	3.0 ± 0.7	> 30

3.3 Determination of competitive binding using FP assay. FP competitive inhibition binding assay was conducted to confirm that the FP probes bind to the active site on AfUGM. First, the Z′ factor as a function of AfUGM was determined to establish the proper enzyme concentration to be used in the assay. The Z′ factor is a statistical parameter that reports on the quality of the assay [18]. As shown in Fig. 6, the FP assay exhibits excellent quality at an AfUGM concentration higher than 2 μM with a Z′ factor above 0.8. The minimum value (2 μM) in this range was selected as the optimal assay concentration.

The K_d for UDP was determined using the FP assay by titrating AfUGM with serial dilutions of UDP. A value of 9.0 ± 1.7 μM was obtained, which is in good agreement with the K_d (33 ± 9 μM) previously determined by directly monitoring the flavin fluorescence (Fig. 7A) [7].

UDP-Gal*p* was the second ligand tested in the FP inhibition assay, and a K_d value of 495 ± 66 μM was calculated (Fig. 7B), indicating that UDP-Gal*p* is a poor ligand for AfUGM, which agrees well with the observation previously reported by Oppenheimer *et al* [7].

Recently, a series of prokaryotic UGM inhibitors were identified from chemical libraries by high-throughput screening (HTS) [19]. In our FP assay, we tested two of the best prokaryotic UGM inhibitors, compound **7** and compound **8** (Fig. 8). Interestingly, they behaved differently on AfUGM. Compound **7** turned out to be a poor ligand for AfUGM with a K_d of 140 ± 9 μM (Fig. 9A). In contrast, compound **8** exhibits much better binding to AfUGM (Fig. 9B) and its K_d was found to be 11 ± 0.4 μM (Table 2). We also tested these two compounds in a secondary assay, directly monitoring the activity of AfUGM to see if these molecules function as inhibitors. The HPLC chromatograms (Fig. 10) indicated that both of the compounds inhibit the activity of AfUGM. These results confirm that the FP assay identifies ligands that bind to the active site of

AfUGM and that these molecules inhibit the activity of the enzyme in a secondary assay that directly measures product formation.

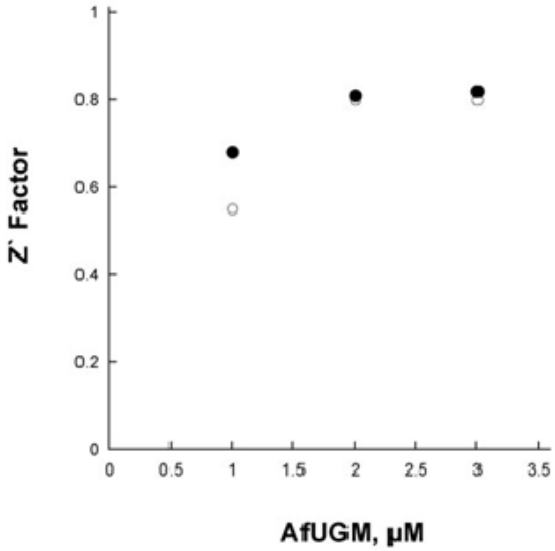

Figure B.6 Determination of optimal AfUGM concentration to use in the FP assay with chromophore **3** (●) and chromophore **4** (○).

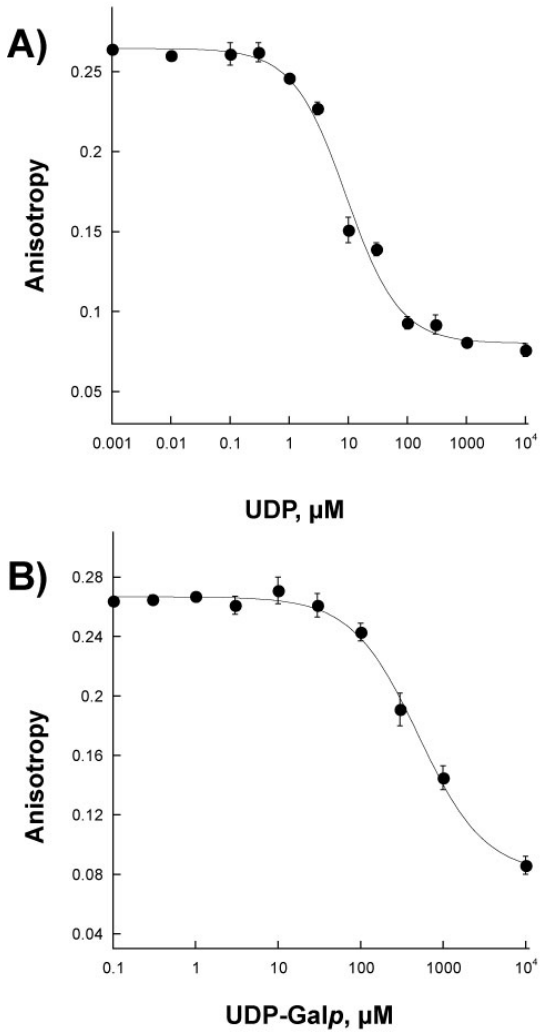

Figure B.7 FP competitive binding assay with UDP (A) and UDP-Gal*p* (B).

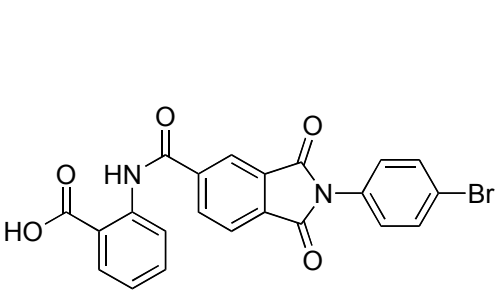

2-(2-(4-bromophenyl)-1,3-dioxoisoindoline-5-carboxamido)benzoic acid

(**7**)

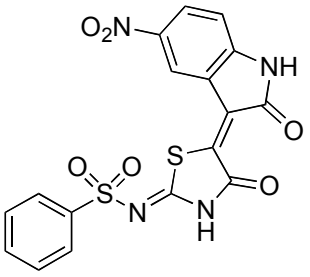

(*Z*)-*N*-((*E*)-5-(5-nitro-2-oxoindolin-3-ylidene)-4-oxothiazolidin-2-ylidene)benzenesulfonamide

(8)

Figure B.8 Structures of known inhibitors of bacterial UGM [18].

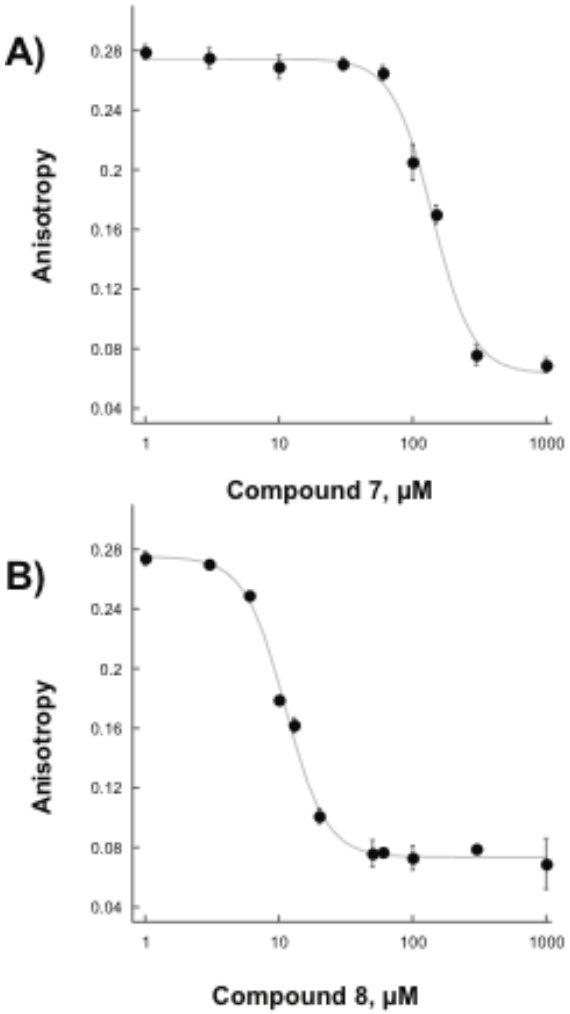

Figure B.9 FP inhibition assay with compounds **7** (A) and **8** (B).

Table B.2 K_d values of AfUGM ligands.

Ligand	K_d on AfUGM (µM)	K_d on MtUGM (µM)
UDP	9.0 ± 1.7	15 ± 2
UDP-Gal*p*	495 ± 66	563 ± 75
7	140 ± 9	21 ± 1
8	11 ± 0.4	25 ± 2

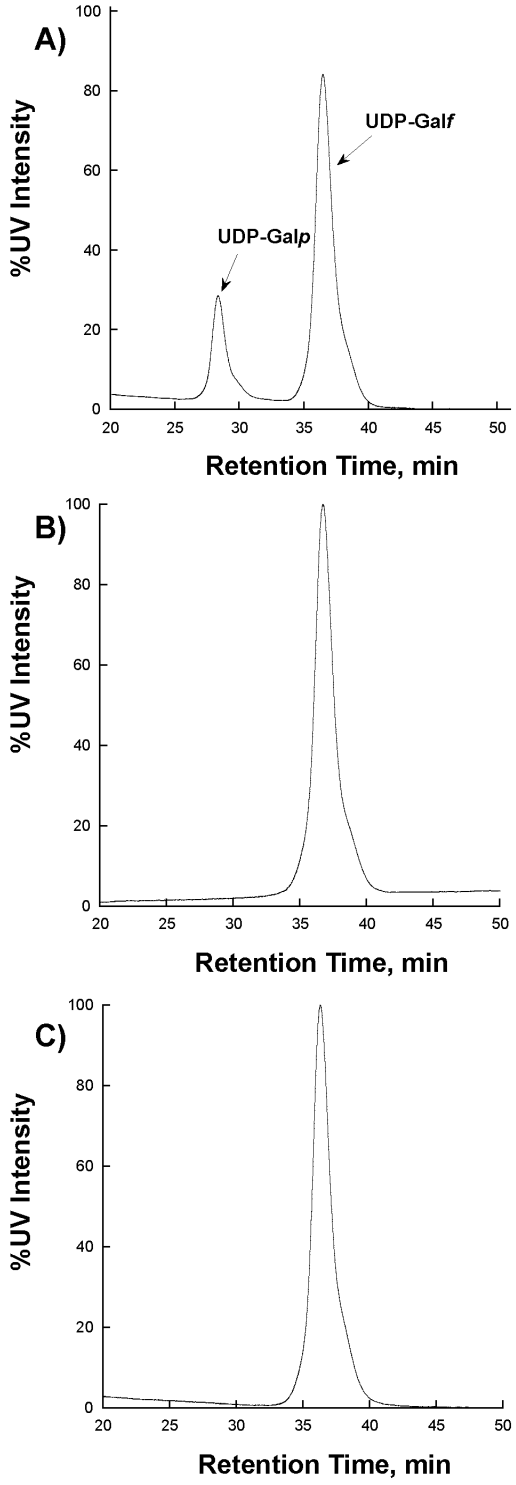

Figure B.10 AfUGM activity assay. The HPLC chromatograms at 262 nm are shown. A) AfUGM activity in the absence of inhibitor. B) In the presence of **7** (500 μM). C) In the presence of **8** (50 μM).

3.4 FP assay quality. The Z′ factor value using chromophore **3** was calculated to be 0.79 ± 0.02. An assay with a Z′ factor greater than 0.5 is considered a good assay, therefore, our FP assay is suitable for HTS (Fig. 6). We also estimated the tolerance of the FP assay to DMSO by calculating the Z′ factors at various DMSO concentrations, because a majority of compounds in HTS libraries are dissolved in DMSO. The Z′ factors were plotted against DMSO concentrations to generate a DMSO calibration curve (Fig. 11), and our assay maintains excellent quality with DMSO concentration up to 5% (v/v).

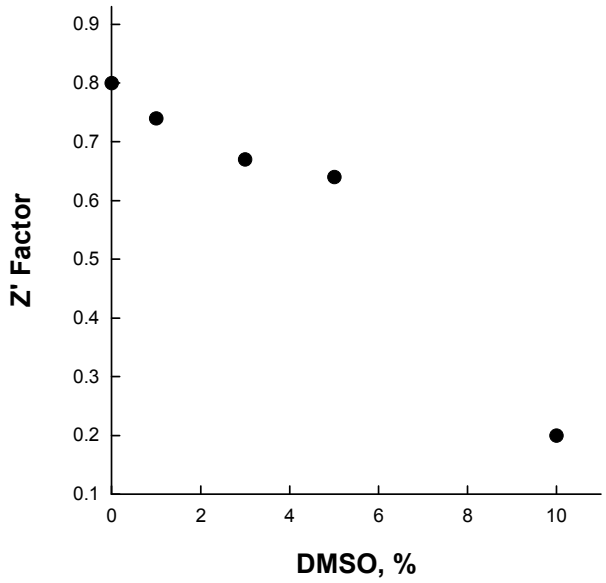

Figure B.11 Tolerance to DMSO.

4. Conclusion

In conclusion, four fluorescently labeled UDP derivatives (**1**-**4**) were synthesized and tested for binding to AfUGM. Different from the bacterial UGM, the nature of the chromophore enhanced binding to AfUGM while the length of the linkers did not. UDP-TAMRA analogs (**3** and **4**) bind to AfUGM with high affinities. Binding of chromophore **3** to the active site of AfUGM was demonstrated by a competition experiment using UDP and UDP-Galp. Furthermore, binding of known inhibitors of bacterial UGM were tested against AfUGM and it

was found that these compounds bound AfUGM, however, with lower affinities. Inhibition of AfUGM, measuring product formation by HPLC, was demonstrated with compounds **7** and **8**. A Z' factor of 0.79 was calculated and the assay was shown to exhibit good tolerance to DMSO. We expect the FP assay described here will allow fast identification of AfUGM inhibitors from chemical libraries. We believe that inhibitors of AfUGM that block the biosynthesis of Gal*f* could lead to novel therapeutics against *A. fumigatus* related diseases.

5. Acknowledgment

This work was supported in part by NIH grants RO1 GM094469 (P. Sobrado, PI) and RO1 AI082542 (R. Tarleton, PI). M.O. was supported by a fellowship from the American Heart Association.

6. References

[1]. R.J. Trof, A. Beishuizen, Y.J. Debets-Ossenkopp, A.R. Girbes, A.B. Groeneveld, "Management of invasive pulmonary aspergillosis in non-neutropenic critically ill patients," *Intensive Care Med*, vol.33, pp. 1694-1703, 2007.

[2]. R.L. Kradin, E.J. Mark, "The pathology of pulmonary disorders due to *Aspergillus* spp," *Arch Pathol Lab Med*, vol.132, pp. 606-614, 2008.

[3]. S. Chong, T.S. Kim, W.J. Koh, E.Y. Cho, K. Kim, "Case report: Invasive pulmonary aspergillosis complicated by pulmonary artery occlusion in an immunocompetent patient," *Clin Radiol*, vol.61, pp. 287-290, 2006.

[4]. C. Virnig, R.K. Bush, "Allergic bronchopulmonary aspergillosis: A US perspective," *Curr Opin Pulm Med*, vol.13, pp. 67-71, 2007.

[5]. G. Chamilos, M. Luna, R.E. Lewis, G.P. Bodey, R. Chemaly, J.J. Tarrand, A. Safdar, Raad, II, D.P. Kontoyiannis, "Invasive fungal infections in patients with hematologic malignancies in a tertiary care cancer center: An autopsy study over a 15-year period (1989-2003)," *Haematologica*, vol.91, pp. 986-989, 2006.

[6]. J.P. Latge, "Galactofuranose containing molecules in *Aspergillus fumigatus*," *Med Mycol*, vol.47 Suppl 1, pp. S104-109, 2009.

[7]. M. Oppenheimer, M.B. Poulin, T.L. Lowary, R.F. Helm, P. Sobrado, "Characterization of recombinant UDP-galactopyranose mutase from *Aspergillus fumigatus*," *Arch Biochem Biophys*, vol.502, pp. 31-38, 2010.

[8]. P.S. Schmalhorst, S. Krappmann, W. Vervecken, M. Rohde, M. Muller, G.H. Braus, R. Contreras, A. Braun, H. Bakker, F.H. Routier, "Contribution of galactofuranose to the virulence of the opportunistic pathogen *Aspergillus fumigatus*," *Eukaryot Cell*, vol.7, pp. 1268-1277, 2008.

[9]. D. Stynen, A. Goris, J. Sarfati, J.P. Latge, "A new sensitive sandwich enzyme-linked immunosorbent assay to detect galactofuran in patients with invasive aspergillosis," *J Clin Microbiol*, vol.33, pp. 497-500, 1995.

[10]. C. Costachel, B. Coddeville, J.P. Latge, T. Fontaine, "Glycosylphosphatidylinositol-anchored fungal polysaccharide in *Aspergillus fumigatus*," *J Biol Chem*, vol.280, pp. 39835-39842, 2005.

[11]. C. Simenel, B. Coddeville, M. Delepierre, J.P. Latge, T. Fontaine, "Glycosylinositolphosphoceramides in *Aspergillus fumigatus*," *Glycobiology*, vol.18, pp. 84-96, 2008.

[12]. P.M. Nassau, S.L. Martin, R.E. Brown, A. Weston, D. Monsey, M.R. McNeil, K. Duncan, "Galactofuranose biosynthesis in *Escherichia coli* K-12: Identification and cloning of UDP-galactopyranose mutase," *J Bacteriol*, vol.178, pp. 1047-1052, 1996.

[13]. J. Engel, P.S. Schmalhorst, T. Dork-Bousset, V. Ferrieres, F.H. Routier, "A single UDP-galactofuranose transporter is required for galactofuranosylation in *Aspergillus fumigatus*," *J Biol Chem*, pp., 2009.

[14]. J. Qi, M. Oppenheimer, P. Sobrado, "Fluorescence polarization binding assay for *Aspergillus fumigatus* virulence factor UDP-galactopyranose mutase," *Enzyme Res*, vol.2011, pp. 513905, 2011.

[15]. E.C. Dykhuizen, L.L. Kiessling, "Potent ligands for prokaryotic UDP-galactopyranose mutase that exploit an enzyme subsite," *Org Lett*, vol.11, pp. 193-196, 2009.

[16]. R.P. Haugland, Handbook of fluorescent probes and research chemicals, Molecular Probes, Inc., Eugene, OR, 1996.
[17]. X. Yao, D.W. Bleile, Y. Yuan, J. Chao, K.P. Sarathy, D.A. Sanders, B.M. Pinto, M.A. O'Neill, "Substrate directs enzyme dynamics by bridging distal sites: UDP-galactopyranose mutase," *Proteins*, vol.74, pp. 972-979, 2009.
[18]. J. Zhang, T.D.Y. Chung, K.R. Oldenburg, "A simple statistical parameter for use in evaluation and validation of high throughput screening assays," *J. Biomol. Screening*, vol.4, pp. 67-73, 1999.
[19]. E.E. Carlson, J.F. May, L.L. Kiessling, "Chemical probes of UDP-galactopyranose mutase," *Chem Biol*, vol.13, pp. 825-837, 2006.